

The University of Nottingham

UNITED KINGDOM · CHINA · MALAYSIA

CONTINUOUS PHOTOCHEMISTRY

Inès Geerte Thea Maria Penders, MSc (cum laude), BSc

Thesis submitted to The University of Nottingham

for the degree of Doctor of Philosophy

August 2017

Abstract

In this Thesis, several reactions are outlined, exploiting the diversity of photochemical substrates with both visible and UV light. The background of photochemistry and how it fits into the need for sustainable and selective synthesis routes is presented in Chapter 1. The Thesis is then divided into two parts, of which the first part focusses on the use of visible light for photochemical transformations. Chapter 2 describes the hydroxylation of aryl mono- and diboronic acids to their corresponding aryl alcohols employing white light LEDs. A 90-fold increase in productivity was achieved for the hydroxylation of phenylboronic acid to phenol by performing it in a continuous flow fashion as opposed to a more traditional batch fashion. Moreover, strategies for a more sustainable process were investigated such as (i) the use of a non-metal based photocatalyst (Rose Bengal), (ii) the use of supercritical carbon dioxide ($scCO_2$) as the main solvent for phototransformations and (iii) the use of immobilised $[Ru(bpy)_3]Cl_2$ as the photocatalyst. A series of studies into reaction selectivity yielded moderate to high selectivities for the mono-hydroxylation of *para/meta/ortho*-substituted aryl diboronic acids demonstrating the use of the reactors built in-house for desymmetrisation reactions. To show the scope of photochemical reactors, the use of a high-pressure reactor indicated that highly efficient reactions can be obtained in this manner.

The second part of the Thesis presents the use of UV light for photochemical transformations. Chapter 3 reports the formation of long-chain methyl ketones by the coupling of a ketone and an olefin. A recently developed excimer lamp based continuous flow photoreactor was utilised for this purpose and excimer lamps emitting at either 308, 282 or 222 nm were employed. Extensive investigation into the reaction parameters led to the selective formation of 2-undecanone *via* the coupling of 1-octene and acetone. Moreover, other sets of reaction conditions were identified to direct the product selectivity to several different reaction products. Chapter 4 describes the use of UV light for the dimerisation of ketones, primarily focussing on the dimerisation of acetone to acetonylacetone. This transformation is an example of an atom efficient and valuable reaction, but product yield was low. Several methods were explored to increase this yield, including (i) the use of a surfactant (sodium dodecyl sulfate) to create micellar

solutions, (ii) the use of alternative photo absorbers such as sodium acetate or phthalimido acetate, and (iii) recirculating the reaction mixture. Preliminary studies were carried out on the dimerisation of several ketones other than acetone (2-butanone, acetophenone, pinacolone) as well. The work in this Thesis is summarised in Chapter 5 and suggestions for future work are presented. Chapter 6 describes details of the experimental procedures while Chapter 7 is the appendix containing the standard operating procedures for the equipment used in this Thesis.

Acknowledgements

First and foremost, I would like to thank my supervisors Professor Mike W. George and Professor Sir Martyn Poliakoff for providing me with the opportunity to carry out this research as well as all their guidance and advice throughout my development. I am extremely grateful for the funding of my project by Sanofi-Aventis and I would like to thank Dr. Kai Rossen in particular for his interesting and 'out of the box' ideas and the energetic discussions.

My sincere gratitude goes to the postdocs (in alphabetical order because I love you all the same), Dr. Zahra Abada, Dr. Zacharias Amara, Dr. Jess Bellamy, Dr. Charlotte Clark, Dr. Raphael Horvath and Dr. Darren Lee for all their knowledge in organic chemistry, photochemistry, flow chemistry and essentially everything. The discussions have been very helpful to understand the underlying processes and to help me decide which way to go in my project. Of course the other members of both the George and Poliakoff research groups cannot be missed in these acknowledgements as they made me feel at home right from the start. I enjoyed our travel adventures very much as well, Dr. Stéphanie Foltran, Dr. Emilia Streng and (soon to be Dr. as well) Jing Jin! Thanks to all of you for the great time I have had during and outside office hours and I have so many amazing memories to look back on. A special shout out to Erica DeLaney; you designed the UV photoreactor and together we managed to tackle and conquer both the actinometry puzzle and Tough Mudder. I also want to thank Charlotte Pearson for being my buddy in all my crazy fitness adventures and always being there for support. You are such a loyal and generous friend! Thanks go to Jack Humby, my project student during my first year of PhD. It was great to work with you and all the best for your future.

I would also like to thank Peter Fields, Richard Wilson, James Warren, Mark Guyler and David Lichfield as part of the technical and support staff at the University of Nottingham for their expertise and amazing skill set.

Special thanks must also be given to all my dear friends from Trent Vineyard church in Nottingham. I will miss you all dearly but have so many wonderful

memories from spending time with you all. Thank you Claire Lancefield for being the best housemate ever, loved our chats and there was no problem you could not give excellent advice on.

Last but certainly not least, I cannot thank my parents and my sister Géraldine enough for always being there for me and sending lovely cards and messages for encouragement. They made a world of difference to me!

Declaration

I declare that the work presented in this Thesis is a record of my own work for the period of October 2013 to August 2017. Where any work has been carried out in collaboration, the relevant researchers have been acknowledged. This Thesis has not been accepted in partial or complete fulfilment of any other degree or personal qualification.

Inès G. T. M. Penders, 24th of August 2017

Table of Contents

Table of Contents vii

Nomenclature xiii

List of Compounds xvii

Chapter 1 Introduction 1

1.1 Background of Photochemistry 1

1.2 Introduction to Sustainable Chemistry 3

1.3 Background of Photophysics 5

1.3.1 Laws of Photochemistry 5

1.3.2 Lambert-Beer Law 6

1.3.3 Photophysical Processes 7

1.4 Photosensitisation 11

1.5 Photocatalysis 11

1.5.1 Photocatalysts 13

1.6 Photochemistry in Organic Chemistry 16

1.6.1 The Use of Solvents in Synthetic Photochemistry 21

1.6.2 Quantum Chemical Calculations 24

1.7 Reactor Set-up and Reactor Design 26

1.7.1 Light Sources for Photochemical Reactions 26

1.7.2 Continuous Photochemistry 35

1.8 Thesis Aims 38

1.9 References 39

Chapter 2 Hydroxylation of Boronic Acids 45
2.1 Mechanism of Boronic Acid Hydroxylation 49
2.1.1 Mechanisms in Literature 49
2.1.2 Quantum Chemical Computations 52
2.2 Phenol Synthesis in Batch 57
2.3 Continuous Flow Visible Light Photoreactor 62
2.4 Phenol Synthesis in Flow 64
2.5 Desymmetrisation Studies 67
2.5.1 1,4-Benzenediboronic Acid 68
2.5.2 1,3-Benzenediboronic Acid 71
2.5.3 1,2-Benzenediboronic Acid 74
2.5.4 Calculations on the Desymmetrisation of Aryl Diboronic Acids 75
2.6 Immobilisation of the Photocatalyst 79
2.6.1 Immobilisation of $[Ru(bpy)_3]Cl_2$ on Solid Support 82
2.6.2 Amberlyst 15 as a Solid Support for the Photocatalyst 84
2.6.3 Poly(ethylene oxide) as a Solid Support for the Photocatalyst 85
2.6.4 Method of Immobilisation 86
2.6.5 Characterisation of the Immobilised Photocatalyst Complexes 87
2.6.6 Leaching of the Photocatalyst out of the Solid Support 88
2.6.7 Hydroxylation of Phenylboronic acid in Batch with Immobilised Photocatalyst 89
2.6.8 Recycling of the Immobilised Photocatalyst 91
2.7 Photoredox Catalysis in Flow Using $scCO_2$ 91
2.7.1 Experimental Apparatus: Batch View Cell 92
2.7.2 Solubility of Phenylboronic Acid in $scCO_2$ 93
2.7.3 Monitoring the Hydroxylation of Phenylboronic Acid in $scCO_2$ 94
2.7.4 Hydroxylation of Phenylboronic Acid in $scCO_2$/EtOAc in Batch 95
2.7.5 Performing Photoredox Catalysis in Flow 95

2.8 Conclusions and Future Work 102
2.9 References 104

Chapter 3 Olefin and Ketone Coupling 109
3.1 Continuous Flow UV Excimer Photoreactor 111
3.1.1 Chemical Actinometry Experiments 112
3.2 Background on Acetone Excitation 113
3.3 Initial Coupling 1-Octene and Acetone 116
3.4 Optimising the Concentration of 1-Octene 120
3.5 Optimising the Concentration of Reactants 123
3.6 Adding Water as Co-solvent 128
3.7 Monitoring the Coupling of 1-Octene and Acetone in Batch 130
3.8 Coupling of 1-Octene and Acetone with Different Irradiation Wavelengths 135
3.9 Coupling of Olefins and Ketones in Micellar Media 147
3.10 Conclusions and Future Work 153
3.11 References 154

Chapter 4 Ketone Dimerisation 157
4.1 Initial Dimerisation of Acetone 159
4.2 The Addition of Water as a Co-solvent 163
4.3 Formation of Acetonylacetone in Batch 167
4.4 Formation of Acetonylacetone at Different Temperatures 169
4.5 Formation of Acetonylacetone at Different Flow Rates 172
4.6 Formation of Acetonylacetone with Different Irradiation Wavelengths ... 177
4.7 Formation of Acetonylacetone in Different Co-solvents 182
4.8 Improving the Yield of Acetonylacetone Formation 185

4.8.1 Variation of Photo Absorbers 185
4.8.2 The Use of Micellar Media 189
4.8.3 Recirculation of the Reaction Mixture 191
4.9 Scope of Ketone Dimerisation 196
4.9.1 Dimerisation of 2-Butanone 196
4.9.2 Dimerisation of Acetophenone 198
4.9.3 Dimerisation of Pinacolone 199
4.10 Cyclisation of 1,4-Diketones 202
4.10.1 Synthesis of Pyrrole Derivatives 204
4.10.2 Synthesis of Furan Derivative 207
4.11 Conclusions and Future Work 210
4.12 References 211

Chapter 5 Conclusions and Future Directions 215

Chapter 6 Experimental 231
6.1 Materials and General Procedures 231
6.1.1 Quantum Chemical Calculations 232
6.2 Visible Light Photochemistry 233
6.2.1 Visible Light Sources 233
6.2.2 Batch Experiments at Ambient Pressure 236
6.2.3 High-pressure Equipment 240
6.3 UV light Photochemistry 247
6.3.1 UV Light Sources 247
6.3.2 UV Photochemical Reactor Design 250
6.3.3 Chemical Actinometry Experiments 254
6.3.4 Procedure for UV Photochemistry in Continuous Flow 267

6.4 Cyclisation of 1,4-Diketones 273
6.4.1 Formation of Pyrrole Derivatives 273
6.4.2 Procedure for the Formation of 2,5-Dimethylfuran 275
6.5 Synthesis of Phthalimido Acetate 276
6.6 References 277

Chapter 7 Appendix 279
7.1 Procedures of the Visible Light High-pressure Batch Reactor 279
7.1.1 Standard Operating Procedure 280
7.1.2 Standard Shut-down Procedure 282
7.1.3 Emergency Shut-down Procedure 282
7.1.4 Cleaning of the Reactor 282
7.2 Procedures of the Visible Light High-pressure Flow Reactor 283
7.2.1 Standard Operating Procedure 285
7.2.2 Standard Shut-down Procedure 286
7.2.3 Emergency Shut-down Procedure 286
7.2.4 Cleaning of the Reactor 287
7.3 Procedures of the UV Light Flow Reactor 288
7.3.1 Standard Operating Procedure 289
7.3.2 Standard Shut-down Procedure 289
7.3.3 Emergency Shut-down Procedure 290
7.3.4 Cleaning of the Reactor and Changing Excimer Lamp 290
7.3.5 Safety 290

Nomenclature

BPR	back pressure regulator
bpy	2,2’-bipyridine
CD	capacitive discharge
cmc	critical micelle concentration
DBD	dielectric barrier discharge
DFT	density functional theory
DI	deionised
DMF	*N*,*N*-dimetylformamide
DMSO	dimethyl sulfoxide
DMSO-d_6	deuterated dimethyl sulfoxide
DIPEA	*N*,*N*-diisopropylethylamine
DR	diffuse reflectance
g	gram
h	hour(s)
HA^-	ascorbate ion
H_2A	ascorbic acid
HP	high-pressure

hv	light
Hz	Hertz
ID	inner diameter
IEF PCM	integral equation formalism, polarisable continuum model
IPA	isopropanol, 2-propanol
IR	infrared
L	litre
LED	light emitting diode
LP	low-pressure
M	molar
min.	minute(s)
MLCT	metal to ligand charge transfer
mM	millimolar
mmol	millimole
mol	mole
MP	medium-pressure
NBO	natural bond order
nm	nanometer
NMR	nuclear magnetic resonance spectroscopy

OD	outer diameter
PC	photocatalyst
PEO	poly(ethylene oxide)
ppm	parts per million
RB	Rose Bengal
[RB]-Amberlite	Rose Bengal immobilised on Amberlite IRA 900
RE	reaction efficiency
RQ	reductive quencher
r.t.	room temperature
$[Ru^{II}]$	$[Ru(bpy)_3]^{2+}$
$[Ru^{I}]$	$[Ru^{II}(bpy)_3^{-\bullet}]^{+}$
[Ru]-Amberlyst 15	$[Ru(bpy)_3]^{2+}$ immobilised on Amberlyst 15
[Ru]-PEO	$[Ru(bpy)_3]^{2+}$ immobilised on poly(ethylene oxide)
$scCO_2$	supercritical carbon dioxide
SDS	sodium dodecyl sulfate
SET	single electron transfer
SOP	standard operating procedure
TD DFT	time dependent density functional theory

TEA	trimethylamine
TOF	turnover frequency
TON	turnover number
UV	ultra violet
Vis	visible
VUV	vacuum ultra violet

List of Compounds

1	phenylboronic acid
2	phenol
tris-**1**	triphenylboroxine
3a	1,4-benzenediboronic acid
3b	1,3-benzenediboronic acid
3c	1,2-benzenediboronic acid
4a	4-hydroxyphenylboronic acid
4b	3-hydroxyphenylboronic acid
4c	2-hydroxyphenylboronic acid
5a	1,4-dihydroxybenzene
5b	1,3-dihydroxybenzene
5c	1,2-dihydroxybenzene
6	benzoxadiborole
7	1-octene
8	acetone
9	2-undecanone
10	3-hexyl-2,2-dimethyloxetane

11	4-hexyl-2,2-dimethyloxetane
12	4-hydroxy-4-methylpentan-2-one
13	2,5-hexanedione
14	2,3-dimethyl-2,3-butanediol
15	2-propanol
16	6,7-divinyldodecane
17	2-methyl-3-vinyloctan-2-ol
18	2-methyldecan-2-ol
19	4-methyl-3-penten-2-one
20	2-methyltridec-2-en-4-one
21	prop-1-en-2-ol
22	2,2,3-trimethyl-3-oxetanol
23	2,4,4-trimethyl-2-oxetanol
24	phthalimido acetate
25	2-methylisoindoline-1,3-dione
26	2-butanone
27	octane-3,6-dione
28	3,4-dimethylhexane-2,5-dione
29	4-acetyl-3,6-dimethyloctane-2,7-dione
30	acetophenone

31	1,4-diphenylbutane-1,4-dione
32	1-phenylethan-1-ol
33	2,3-diphenylbutane-2,3-diol
34	3,3-dimethyl-2-butanone
35	2,2,7,7-tetramethyloctane-3,6-dione
36a	2-aminopropane
36b	aniline
36c	benzylamine
36d	4-(aminomethyl)pyridine
36e	4-methoxyaniline
37a	1-isopropyl-2,5-dimethyl-1*H*-pyrrole
37b	2,5-dimethyl-1-phenyl-1*H*-pyrrole
37c	1-benzyl-2,5-dimethyl-1*H*-pyrrole
37d	4-((2,5-dimethyl-1*H*-pyrrol-1-yl)methyl)pyridine
37e	1-(4-methoxyphenyl)-2,5-dimethyl-1*H*-pyrrole
38	2,5-dimethylfuran
39	1-β-D-ribofuranosyluracil
40	photohydrate of 1-β-D-ribofuranosyluracil

41	*trans*-azobenzene
42	*cis*-azobenzene

Chapter 1 Introduction

1.1 Background of Photochemistry

The utilisation of sunlight for chemical processes is not a recent technology as ancient Egyptians used sunlight curing to waterproof papyrus boats over 4000 years ago.[1] However, the understanding of the underlying photochemical processes and therefore the photochemistry that is known nowadays started to develop in the 18th century.[2] Modern photochemistry is defined as the physical and chemical processes induced by the absorption of photons.[3] Joseph Priestly, one of the first contributors to modern photochemistry, considered light as a chemical principle and made important contributions to the recognition of photosynthesis. However, Ciamician is generally regarded as the father of photochemistry and with his contributions and visions, the use of light in compound synthesis was launched. He discovered the photochemical transformation of benzoquinone in ethanol to hydroquinone and acetaldehyde in the 19th century,[2] but is mostly well-known for his extensive study into the photoreactivity of the carbonyl group and olefins regarding intramolecular isomerisations, cycloadditions, reductions and cleavages.[4] Together with his colleague Paul Silber, he published 33 papers on 'the chemical action of light', presenting a vast amount of photochemical transformations.[5]

In a time that only the synthetic target was of interest and not the route towards it, Ciamician held a lecture before the French Chemical Society in 1908 in Paris addressing the issues of using 'brute force' in the chemical lab:

'It has often been a reproach to the great successes of modern organic chemistry that victory has been obtained with too great a show of strength. Indeed, one has to admit that such an objection is not deprived of some ground. Using aggressive reagents and high temperatures is almost always unavoidable when carrying out an organic synthesis in the laboratory. Deploying energy would, on the other hand, not be so frustrating for modern organic chemistry, were it not that the living world, in particular plants, gives us the marvelous example of great results obtained, at least from what appears, by using minimal means. Chemistry in the laboratory differs from chemistry of organisms not in the materials, but in the reagents used. It is thus apparent that the further advancement of biology requires that all of the compounds present in nature can be produced by using only reagents present in nature, rather than agents that do not belong to the living world.' [6]

His solution to circumvent harsh conditions in synthesis was the use of enzymes or solar radiation. These strategies are also outlined in Ciamician's publication in the Science journal from 1912, entitled 'The photochemistry of the future'.[7] In here, the clean and mild transformations in plants are named as an inspiration for modern synthesis in a chemical lab. Moreover, the depletion of fossil fuels is recognised, stating that solar radiation could provide a suitable alternative.

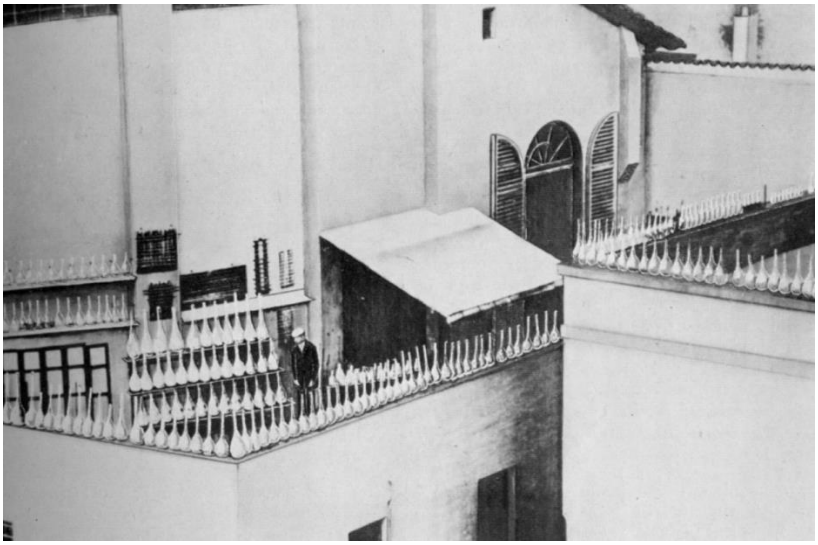


Figure 1-1 Giacomo Ciamician on the roof of the Chemical Institute in Bologna among the flasks he is exposing to solar light.[8]

1.2 Introduction to Sustainable Chemistry

As outlined by Ciamician, the burden of chemistry on the environment is significant and needs to be addressed. Non-renewable resources are getting scarce and human development is placing an enormous burden on the environment. Greenhouse gases and toxic waste are increasingly released into the environment evidenced by the fact that there was a 13 % increase in chemical waste between 2004 and 2010 in the European Union.[9] These concerns for the environment are shared globally as shown by organisations such as the EPA (United States Environmental Protection Agency) and UNEP (United Nations Environment Program) which are monitoring and taking initiatives to protect the environment. They encourage more environmentally acceptable processes in the chemical industry.[10] Since the 1990s, the terms 'Green Chemistry' and 'sustainable chemistry' have been introduced to help describe how those needs might be met. While sustainable chemistry mostly focusses on performing chemistry without sacrificing the capability to meet the needs of future generations,[11] Green Chemistry changes processes by design to make chemistry as environmentally benign as possible. Therefore, it can be suggested that Green Chemistry is a means to achieve sustainability.[12]

The principles of Green Chemistry were first introduced by Anastas and colleagues[13] and emphasise the elimination of (toxic) waste and hazardous substances. Due to the 'benign by design' motto, the focus is on the prevention of waste rather than waste remediation.[12] Summarised in the mnemonic 'PRODUCTIVELY' as developed by Poliakoff and co-workers,[14] Green Chemistry encourages the use of catalytic reagents, the prevention of waste, low toxicity of chemicals and processes carried out at ambient temperature and pressures.

P - Prevent wastes

R - Renewable materials

O - Omit derivatisation steps

D - Degradable chemical products

U - Use safe synthetic methods

C - Catalytic reagents

T - Temperature, Pressure ambient

I - In-Process monitoring

V - Very few auxiliary substances

E - E-factor, maximise feed in product

L - Low toxicity of chemical products

Y - Yes, it is safe

In order to compare chemical processes in terms of environmental impact, Sheldon developed the E-factor.[13] The E-factor is defined as the mass ratio of waste to desired product; therefore, the ideal E-factor is zero. Table 1-1 shows typical E-factors for the different industries, in which water is excluded from this calculation.

Table 1-1 E-factors in the chemical industry.[10]

Industry segment	**Volume (tons/annum)**	**E-factor (kg waste/kg product)**
Bulk chemicals	10^4-10^6	< 1-5
Fine chemicals	10^2-10^4	5 - > 50
Pharmaceutical industry	10-10^3	25 - > 100

It is clear that the pharmaceutical industry has the biggest environmental impact in terms of E-factor. Although the production of bulk chemicals happens on a large scale, the use of stoichiometric reagents is generally prohibited for economic reasons.[13] As the chemical structures of pharmaceutical compounds is frequently more complicated, multiple step syntheses are generally needed which often requires a large amount of solvents and additional reagents.

Although the E-factor considers the amount of waste produced, it does not contain information about the toxicity of waste. For example, sodium chloride will have a lower environmental impact than the same weight of a transition metal containing compound. Therefore, Sheldon introduced the term 'environmental quotient', EQ.[15] This value is obtained by multiplying the E-factor with Q, an assigned unfriendliness quotient. Q will depend on the ease of recycling and toxicity of a compound. Although the magnitude of Q is difficult to quantify, the environmental impact assessment can give an indication for the value of Q.

Arbitrarily, sodium chloride can be given a Q value of 1. Heavy metal salts like chromium would get a Q value of 100-1000. It is important to note that product disposal and recycling also depends on volume, as tons of sodium chloride will

have a larger impact on the environment than a kilogram, leading to a higher Q value.[16] Related to the E-factor is the term atom economy, developed by Trost in 1991.[17] This parameter is defined as the molecular weight of the desired product divided by the sum the molecular weights of all reagents present in the reaction, expressed as a percentage.

The use of photochemistry itself is generally able to eliminate harsh conditions and chemicals and can therefore be considered a green approach to chemical synthesis.[18] Light is a traceless reagent, leaving no waste. And even when an additional reagent is needed to absorb the light instead of the starting material, this reagent is often catalytic in nature, avoiding the use of stoichiometric compounds.

Moreover, reaction selectivity can be increased due to different reaction parameters (e.g. different reaction pathways, or ambient reaction temperatures). Low or ambient process temperatures and the use of solar radiation also lead to less energy intensive processes.[19]

1.3 Background of Photophysics

In order to grasp photochemical processes and the challenges and opportunities related to it, an understanding of photophysics is necessary. The Sections below will give a brief outline of some of the fundamentals.

1.3.1 Laws of Photochemistry

Accompanying the progression in understanding photochemical principles, the Grotthuss–Draper law (1842) and the Stark–Einstein law (1913) were acknowledged early on. The Grotthuss–Draper law, seen as the first law of photochemistry, states that 'only the light which is absorbed by a molecule can be effective in producing photochemical change in that molecule'. The second photochemistry law, formulated by Stark and Einstein states that 'the absorption of light by a molecule is a one-quantum process so that the sum of the primary process quantum yield must be unity'.[20] This is expressed in an integral quantum

yield of one.[21] Equation 1-1 shows the quantum yield (Φ) for a photochemical reaction as defined by IUPAC.[21]

$$\Phi\ (\lambda) = \frac{number\ of\ reactants\ consumed\ or\ product\ formed}{number\ of\ photons\ absorbed} \qquad 1\text{-}1$$

However, not all absorbed photons will result in the desired chemical transformation as non-radiative decay processes are likely to happen. Therefore, photochemical reactions with a quantum yield greater than 0.3 are generally considered efficient.[22]

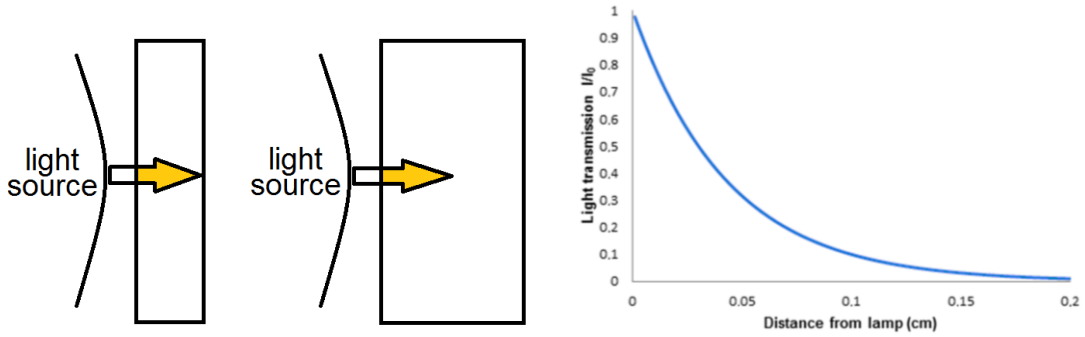
Nowadays, multiple photon-induced processes are known, but when viewing these transformations as a result of a sum of individual one-photon interactions, the photochemistry law is still obeyed. An exception on this law is radical chain reactions in which a quantum yield greater than one can be obtained.

1.3.2 Lambert-Beer Law

The absorption of light by the desired reactant is crucially important when performing photochemical reactions. The Lambert-Beer law (Equation 1-2) can give insight in how to achieve the most efficient irradiation in the reaction process. The path length (L) of light penetration into the reaction vessel at a given wavelength depends on the absorbance (A), molar extinction coefficient (ε) and concentration (c) of the compound that absorbs the light, called a chromophore.

$$A = \varepsilon c L \qquad 1\text{-}2$$

In practical terms, the Lambert-Beer law presents photochemistry with the challenge of scale-up since using a large reaction vessel while maintaining the same reaction conditions can mean that not the whole reaction vessel is irradiated (Figure 1-2a), causing an inefficient reaction. Efficient mixing can help overcome this issue as chromophores and reagents are brought close to the light source.



(a) (b)

Figure 1-2 a) Scheme of light penetration in a reaction vessel in which the yellow arrow represents the depth of substrate that can absorb the light, b) transmission profile of benzene (0.05 M, ε = 200 L/mol·cm).[23]

Lowering the concentration of the absorbing species or choosing a chromophore with a lower molar extinction coefficient ensures that light penetrates a larger area of the reaction vessel, as less absorbing molecules are present per area. It is important to calculate the path length of irradiation at the chosen reaction conditions to ensure optimum irradiation of the whole reaction mixture. Another parameter for efficient light absorption is the distance between the light source and solution mixture as shown in Figure 1-2b. The light transmission decreases rapidly when the distance from the lamp increases.

1.3.3 Photophysical Processes

Basic photophysics lies at the base of understanding the interactions between matter and light used in photochemical reactions. In order for light to react with matter, it must possess the right energy. The Planck-Einstein equation describes the energy (E) of a photon (a single measure of light) by its frequency as displayed in Equation 1-3; where *h* is the Plancks constant and *v* is the frequency of light.

$$E = hv \qquad 1\text{-}3$$

In the same way, matter has quantised energy levels, divided in rotational, vibrational and electronic energy levels. The lowest energy state of a molecule is

named the ground state, whereas any higher energy states are termed excited states. Figure 1-3 shows the possible photophysical processes in the form of a Jablonski diagram, assuming a singlet ground state molecule. The straight vertical lines represent radiative transitions while the wavy arrows represent non-radiative transitions. The thick lines are the electronic energy states, either singlet (S) or triplet (T), while the thin lines are the vibrational energy states (v_0-v_n).

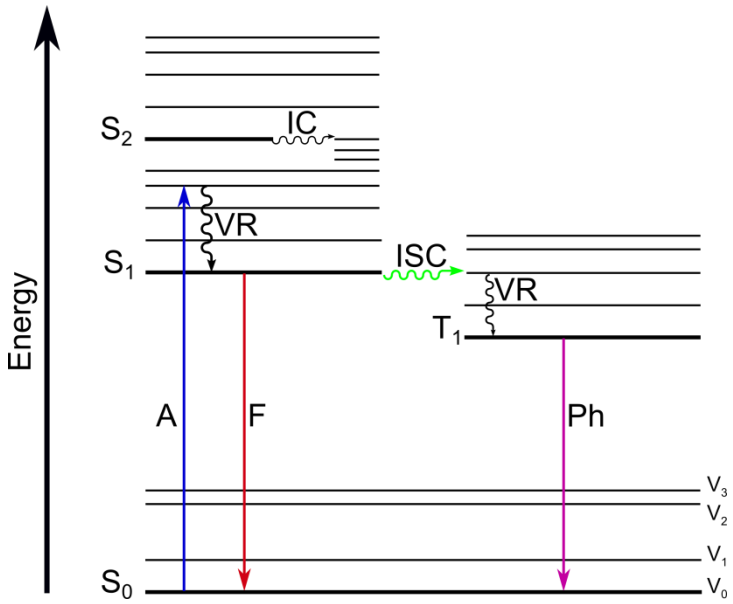


Figure 1-3 Jablonski diagram showing A) absorption, F) fluorescence, IC) internal conversion, ISC) intersystem crossing, VR) vibrational relaxation, Ph) phosphorescence.

For most molecules, the ground state is a singlet state, exhibiting two electrons with opposite spins in the lowest vibrational energy state (v_0). Some molecules like dioxygen have a triplet ground state (T_0), in which two electrons with the same spin multiplicity are in the two lowest vibrational states (v_0 and v_1).

When the energy of the photon matches the energy gap between two energy levels in the molecule, the molecule can absorb the photon. Absorption (A) means the promotion of an electron from the ground state of the molecule (S_0) to an excited state ($S_{1\text{-}n}$). When the electron is excited to a vibrational state higher than v_0, vibrational relaxation (VR) to a lower vibrational energy state can occur. Fluorescence (F) is a radiative transition from the lowest singlet excited state to the ground state. Non-radiative decay from the singlet excited state to the corresponding ground state can also occur, which causes loss of energy as heat.

Internal conversion (IC) can also follow excitation. In this case, there is a transition between two rotational states of the same energy. In Figure 1-3, this is displayed by the transition between S_2,v_0 and S_1,v_7, but internal conversion can also occur between energy levels in the triplet state.

Another phenomenon that can occur after excitation is intersystem crossing (ISC). Although spin forbidden, this transition is either from a singlet to a triplet excited state or the reverse transition. Magnetic interactions can facilitate the spin flip. This transition is much slower than internal conversion, but becomes faster when there is a change in orbital type (e.g. ^{1}n,π* to ^{3}π,π*).[24] The spin- and orbital interactions in metals and heavy atoms is also high, explaining why transition metal containing compounds undergo intersystem crossing more favourably. Once in the triplet excited state, phosphorescence (Ph) can occur which is a radiative transition back to the singlet ground state. Since this is a spin forbidden process, the lifetime of the triplet excited state before returning to the ground state is longer than that of the singlet excited state. This increase in lifetime means that the molecule has a longer time to react *via* the desired photochemical reaction pathway. Non-radiative decay back to the ground state which generates heat can occur as well.

The timescale of the different processes described above differs per molecule, but Table 1-2 shows the typical range of timescales on which the processes occur.

Table 1-2 Timescale of photophysical processes.[24]

Process	**Name**	**Time scale (s)**
A	Absorption	10^{-15}
F	Fluorescence	10^{-9}-10^{-7}
IC	Internal conversion	10^{-12}-10^{-6}
ISC	Intersystem crossing	10^{-12}-10^{-6}
VR	Vibrational relaxation	10^{-13}-10^{-12}
Ph	Phosphorescence	10^{-6}-10^{-3}

Apart from the processes described in Figure 1-3, the compound in the excited state can be quenched by another compound, undergoing a photochemical reaction. Figure 1-4 shows the different pathways of compound AB. Pathway vi, which can be either fluorescence or phosphorescence, pathway vii and pathway v are of low interest for synthetic photochemistry.

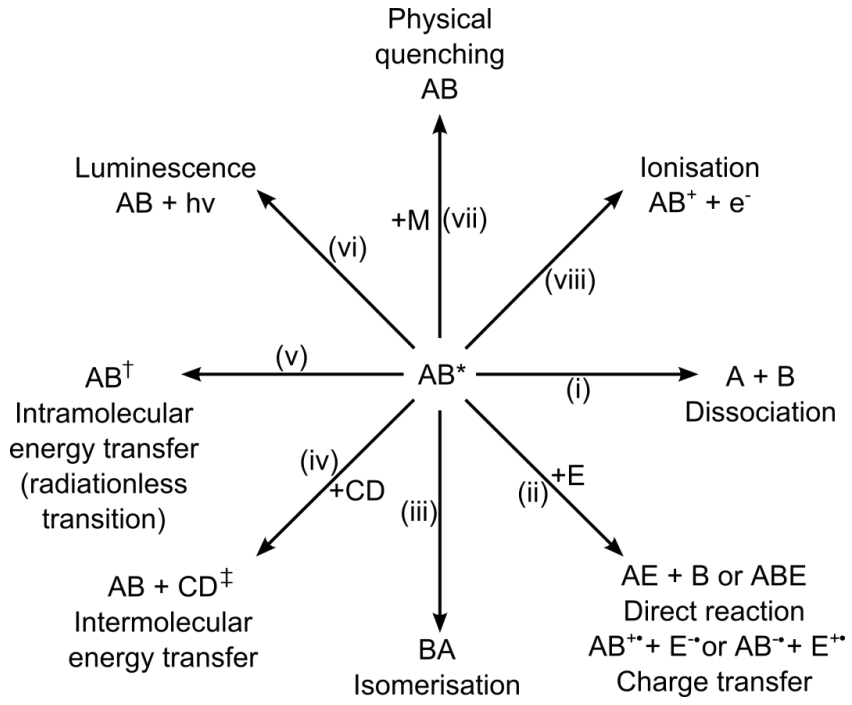


Figure 1-4 Processes after excitation of compound AB.[25]

In synthetic photochemistry, two types of light absorption are possible. The first pathway is the direct excitation of the reaction substrate, leading to the product. The second pathway involves the excitation of an additional compound, which can transfer either its excess of energy or an electron to the reaction substrate to initiate the photochemical reaction. Most organic substrates cannot absorb photons directly from visible light and must react *via* the second pathway and therefore, require a photosensitiser or a photocatalyst to absorb the photon. Although this generally enlarges the carbon footprint of the photochemical reaction, reaction selectivity could be improved or tuned. This is because the only accessible pathway is the reaction of the photosensitiser or photocatalyst with the substrate, eliminating side reactions from light interacting with the substrate. Sections 1.4 and 1.5 will describe these different processes.

1.4 Photosensitisation

If direct excitation of the starting material is not possible, a photosensitiser could be employed to absorb the incoming light after which it can transfer this excess of energy to the substrate. This is depicted in Figure 1-4 as route (iv). In order for intermolecular energy transfer to occur between the photosensitiser and the reaction substrate, the emission of the photosensitiser must overlap spectrally with the excitation of the desired substrate. Moreover, a long excited state lifetime, high photostability and a strong absorption in the desired light region are important parameters for efficient photosensitisers.

In that case, energy transfer between the excited photosensitiser and the substrate can take place and subsequently, the chemical transformation towards the reaction product proceeds.

Common photosensitisers for synthetic photochemistry include acetone, benzophenone, Rose Bengal and Methylene Blue. Processes that involve photosensitisation include photodynamic therapy to treat tumours, and purification processes by destroying any impurities. The latter two applications are based on the photochemical generation of reactive oxygen species which are destructive for cell materials.[26]

1.5 Photocatalysis

Another way of initiating a photochemical reaction is by way of electron transfer between the excited state photocatalyst and an electron donor or accepter (Figure 1-4, route ii). These excited state redox reactions can occur at room temperature and eliminate the need for reactive and possibly toxic radical mediator such as tributyltin hydride.[27] In contrast to photosensitisation, photocatalysis is based on catalytic electron transfer to and from the photocatalyst instead of energy transfer as is the case in photosensitisation.

The presence of a photocatalyst introduces more advantages since radical ion intermediates are formed following electron transfer which exhibit different reactivity compared to ground- or excited states which gives access to unique

reaction pathways otherwise unaccessible. Moreover, photocatalysts are often selected for their relatively long excited state lifetimes, increasing the quantum yield of the photoreaction and therefore facilitating efficient reaction processes.

Photon absorption by the chromophore of the photocatalyst will induce the promotion of an electron in the HOMO to the LUMO, generating an excited state. This generation of an electron-hole pair leads to the opportunity for the excited photocatalyst to act both as a reductant and an oxidant.[28] If the photocatalyst has strong enough reduction (or oxidation) potentials, single electron transfer (SET) between the excited photocatalyst and an oxidative (or reductive) quencher (respectively OQ, RQ) occurs (Figure 1-5). These quenchers can be either a sacrificial compound which subsequently reacts with the reaction substrate to form the desired product, or the substrate directly. The chemical reaction of the substrate to form the product happens therefore on the lowest potential ground state surface.[29]

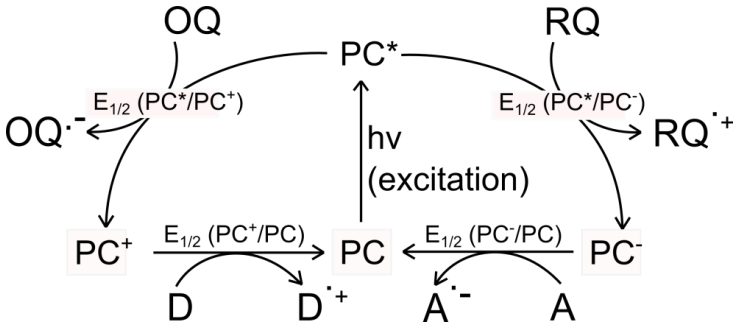


Figure 1-5 Photo excitation and quenching processes of a photocatalyst (PC) by an oxidative quencher (OQ) or reductive quencher (RQ) with the use of an electron donor (D) or acceptor (A) to complete the catalytic circle.[30]

Three main categories of photocatalysts exist, namely compounds based on semiconductor materials, compounds containing transition metals or solely organic components. The next Section will elaborate on the metal and organic based photocatalysts as these were employed during this work.

1.5.1 Photocatalysts

Most visible light photocatalysts contain conjugated aromatic moieties in order to absorb visible light. Other than this characteristic, the chemical structure of photocatalysts can be very diverse in terms of functional groups, charge and size. Due to this variety, the redox potentials of the photocatalyst and the substrate can be matched. Figure 1-6 shows common photocatalysts, both transition metal based compounds and organic compounds, but is far from a comprehensive list.

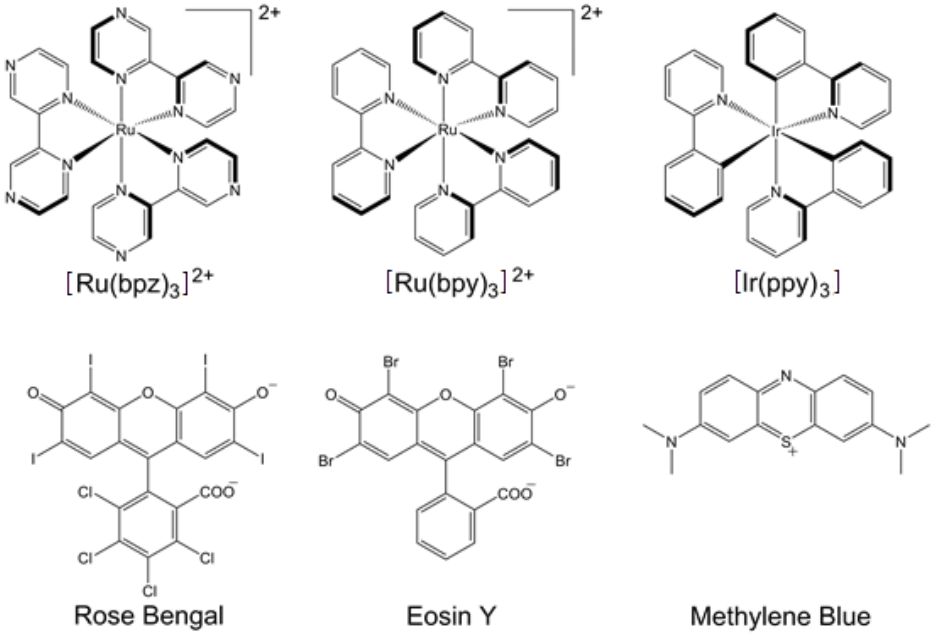


Figure 1-6 Structures of common transition metal and organic photocatalysts.

Transition metal based photocatalysts generally exhibit a very high molar extinction coefficient, combined with long (triplet) excited state lifetimes. Moreover, their redox potentials are relatively easy accessible, meaning that the excited state quencher does not need to exhibit strong potentials. The accessibility of multiple oxidation states of the metal means that both oxidative and reductive quenching can occur. Especially the opportunity to tune the properties and therefore strength of the photocatalyst by varying the ligands on the metal core makes metallic photocatalysts attractive.[30b, 31] However, transition metals are often scarce and toxic which impedes the sustainable character of using catalysts. Table 1-3 shows the most important properties of some photocatalysts.

Table 1-3 Overview of the properties of common metal and organic photocatalysts.

Photo-catalyst (PC)	**$E_{1/2}$ (PC^*/PC^+)**	**$E_{1/2}$ (PC^*/PC^-)**	**$E_{1/2}$ (PC^+/PC)**	**$E_{1/2}$ (PC^-/PC)**	**ES lifetime (ns)**	**$\lambda_{max,\ exc}$ (nm)**	**$\varepsilon/10^3$ (L/mol·cm)**	**ref**
$[Ru(bpy)_3]^{2+}$	-0.81	+0.77	+1.29	-1.33	$1.1x10^3$	452	13	32
$[Ru(bpz)_3]^{2+}$	-0.26	+1.45	+1.86	-0.80	740	443		33
fac-$[Ir(ppy)_3]$	-1.73	+0.31	+0.77	-2.19	$1.9x10^3$	375	7.2	34
Rose Bengal	-0.68[a]	+0.99[a]	+0.78	-1.11	0.5	558	135[a]	35
Methylene Blue	-1.15	+0.83	+1.13	-0.30	1.0	656	76[a]	35c, 36
Eosin Y	-0.95	+0.75	+0.89	-1.09	2.1	539	31	35c, 37

Redox potential measurements were performed in acetonitrile at room temperature unless stated otherwise. $E_{1/2}$ half potential in volts versus the saturated calomel electrode (SCE); ES = excited state; PC = photocatalyst; $\lambda_{max,\ exc}$ = maximum excitation wavelength; [a]Measured in aqueous solution.

Although $[Ru(bpy)_3]^{2+}$ has less strong redox potentials than the other two transition metal based photocatalysts in Table 1-3, this catalyst was chosen for the research described in this Thesis. Most investigated reductive quenchers were able to quench the excited state of $[Ru(bpy)_3]^{2+}$ and this catalyst is one of the cheapest transition metal based photocatalyst commercially available, making a strong economic argument for its use. It has also been widely investigated and the main absorption area has the best overlap with the emission output of the light sources used in this project out of the three transition metal based photocatalysts.

Another disadvantage of using homogeneous photocatalysts is the need for separation of the photocatalyst from the product mixture. This often requires the use of additional solvents and creates more waste. Recycling or immobilisation of transition metal photocatalysts make these complexes more economically and environmentally sustainable. Another way to reduce costs further and to reduce the environmental impact of the reactions studied, is to employ organic photocatalysts. Rose Bengal was chosen for this work due to its strong absorption in the emission region of the light sources. Moreover, the photodegradation (photobleaching) was less problematic compared to other studied organic photocatalysts. Immobilisation of this organic photocatalyst could remove the need for additional separation steps after the chemical transformation. The two chosen photocatalysts will be described in detail below.

1.5.1.1 $[Ru(bpy)_3]Cl_2.6H_2O$

Transition metal complexes are proven to be efficient as photoredox catalysts.[38] Tris(2,2′-bipyridyl)dichlororuthenium(II) hexahydrate $[Ru(bpy)_3]Cl_2.6H_2O$ (Figure 1-6) absorbs visible light,[39] has almost quantitative formation of the long lived triplet state and relatively easy accessible redox potentials. Upon excitation of the metal complex, an electron from the metal dπ orbitals is excited to a π* orbital of the ligand,[30b] resulting in a singlet metal to ligand charge transfer (MLCT) state, $[Ru^{III}(bpy)_3^{-\bullet}]^{2+*}$. This singlet MLCT excited state can undergo intersystem crossing to a triplet MLCT excited state, which in the case of $[Ru(bpy)_3]^{2+}$ is extremely efficient ($\Phi \sim 1$). Moreover, this triplet MLCT state is long lived, as the transition back to the singlet ground state is spin-forbidden.[40] Ligand centered charge transfer (LC) can also occur upon excitation and possesses an absorption maximum around 300 nm, and involves a π to π* transition within a single bpy ligand.[41] After excitation of the complex, quenching of the excited MLCT state can take place *via* SET between the photocatalyst and the quencher. When the photoexcited catalyst is reductively quenched, the strong electron donor, which can be the substrate or an external electron donor like a tertiary amine, can donate an electron to the metal complex, which results in ground state $[Ru^{II}(bpy)_3^{-\bullet}]^{+}$, abbreviated as the $[Ru^{I}]$ complex and a cationic radical donor species. $[Ru^{I}]$ is a strong reductant which can reduce a (weak) electron acceptor. Again the acceptor can be the substrate, but also an external acceptor. On the other hand, oxidative quenching of the metal complex can be accomplished using an electron acceptor to yield ground state $[Ru^{III}]$ and an anionic radical acceptor species. After oxidation of a (sacrificial) electron donor, $[Ru^{II}]$ is regenerated. Differentiation between photo oxidation and photo reduction can be achieved by tuning the electronic properties of the reductive- or oxidative quencher for a particular photocatalyst.[40b]

1.5.1.2 Rose Bengal

Rose Bengal (Figure 1-6) has a high intersystem crossing yield (Φ 0.76-0.98).[35b] Its maximum absorption shifts depending on the hydrogen-bonding ability of the solvent. A strong hydrogen-bond between Rose Bengal and the solvent will result

in a maximum absorption at a shorter wavelength compared to a weak hydrogen-bond.

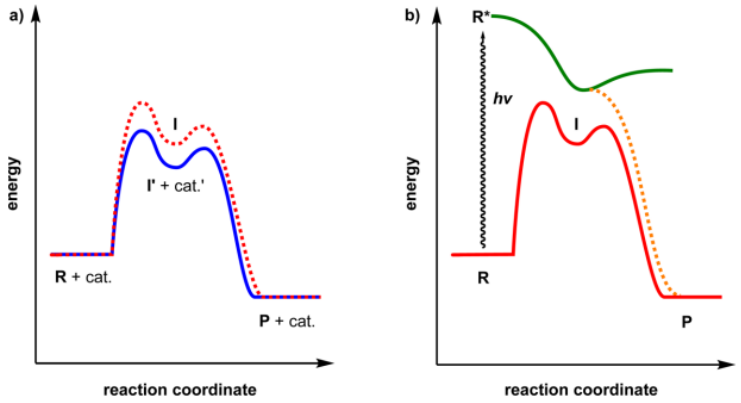
The triplet excited state of Rose Bengal is quenched by oxygen at a rate approximately 1/9 the diffusion-controlled limit under air atmosphere, leaving enough time for other quenchers to react if needed. Although superoxide radicals can be formed after electron transfer, this process is bimolecular with Rose Bengal as the triplet excited state of Rose Bengal undergoes electron transfer with a ground state Rose Bengal molecule. Subsequently, the semireduced Rose Bengal radical can transfer an electron to dioxygen to form the superoxide radical.[42]

As Rose Bengal can also undergo photosensitisation, quenching of the Rose Bengal excited state by an electron donor or acceptor must be more efficient than energy transfer between Rose Bengal and the substrate in order to access the photocatalytic properties of Rose Bengal.

1.6 Photochemistry in Organic Chemistry

Having discussed the fundamentals of photochemistry, Section 1.6 will describe the use of photochemistry as a synthetic method. The utilisation of photochemistry in organic reactions first became an active area of research in the 1970s, but began receiving a tremendous amount of attention after 2008.[43] There has been a large increase in the use of organic photochemistry particularly photocatalysis and groups including those of Yoon, Stephenson and MacMillan have made important contributions to the selectivity improvement of these types of reactions.[40b, 44] Many recent review articles have been published in this area.[27-28, 35c, 45]

By using photochemistry, not only can existing reactions be carried out, but also novel chemistry can be developed as now, new reactions pathways are available in the form of the excited singlet state and the triplet state.[30b, 40a, 45f, 46] This is pictured in Scheme 1-1 in which the green coloured reaction path is the photochemically induced reaction pathway.[45f]

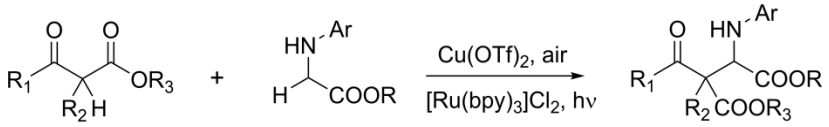


(a) (b)

Scheme 1-1 Reaction pathways in a) a thermal reaction with reagent R yielding product P, catalysed by catalyst 'cat' via intermediate I' and b) in a photochemically induced reaction where the chemical reaction proceeds from the excited state of the reagent (R).*[45f]

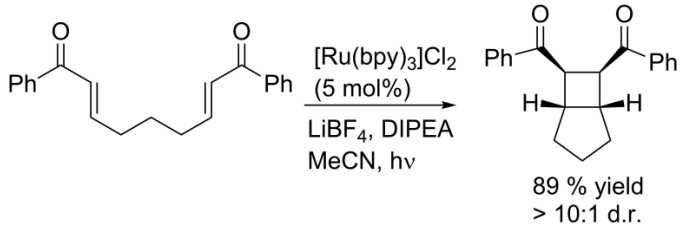
From a sustainability point of view, the use of traceless photons as the activation source for chemical reactions provides an alternative to the use of harsh chemicals or extensive heating for activation purposes. The generally mild reaction conditions associated with photochemistry fits in with the requirements of diminishing the burden organic chemistry has on the environment.[45d]

Photochemistry has proven to have broad applicability in the field of organic synthesis, and the scope of reaction types is fast expanding. The most common reactions carried out include dehalogenations, cycloadditions, rearrangements, isomerisations, oxygenations and C-H activation to perform hydrogen atom abstraction. Excellent reviews on these different reactions have been reported[30, 35c, 40, 45d, 45h, 47] and therefore, only a few examples will be highlighted below. C-H bond formation is a standard procedure in organic chemistry and photochemical routes are widely available as described in the reviews mentioned above. An example was published by Gao *et al.* in which C_{sp3}-C_{sp3} bonds were formed between secondary amines and β-keto esters (Scheme 1-2). The functionalisation of secondary amines can be challenging due to its relatively high oxidation potential, but by combining copper catalysis and transition metal photoredox catalysis, the alkylation of secondary amines was accomplished.[48]



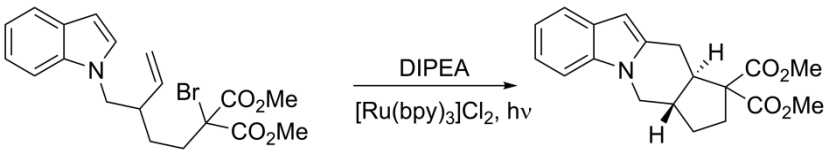
Scheme 1-2 The alkylation of secondary amines via visible light catalysis and transition metal catalysis.

Photochemistry can also be utilised to introduce ring structures into large motifs and thereby introducing stereocentres and increasing the functionality of the structure often in a single step. Cycloadditions are a good example of these cyclisation reactions and Yoon *et al.* described a [2+2] cycloaddition which provided good diastereoselectivity (>10:1) (Scheme 1-3).[49] The same group has reported [3+2] and [4:2] cycloadditions as well, and even a [2+2+2] aerobic cycloaddition to form endoperoxides.[44d, 50]



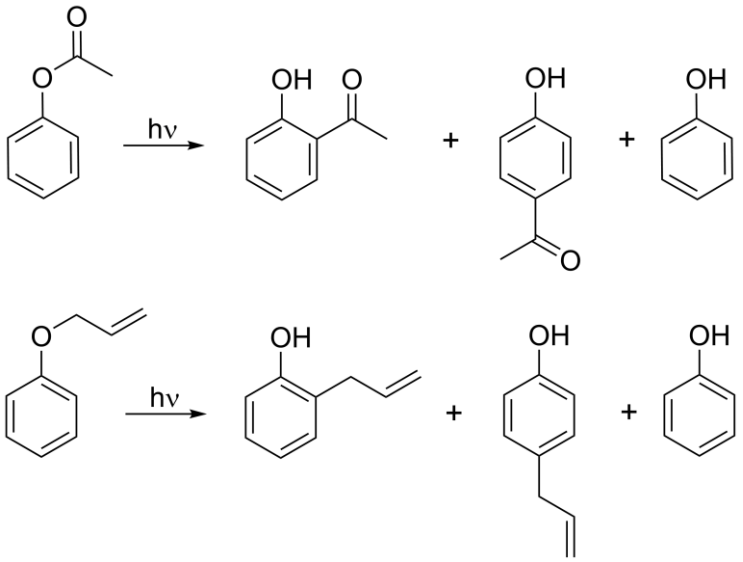
Scheme 1-3 The photo-induced [2+2] cycloaddition of an aromatic bis(enone).

Other cyclisation reactions often occur *via* alkylradical formation after photo-induced reduction of an activated carbon-halogen bond. An example is the cyclisation reported by Tucker *et al.* in which an array of functionalised indoles was cyclised. To show the versatility of this transformation, a cascade cyclisation was carried out, yielding the product as a single diastereoisomer in 79 % (Scheme 1-4).[51]



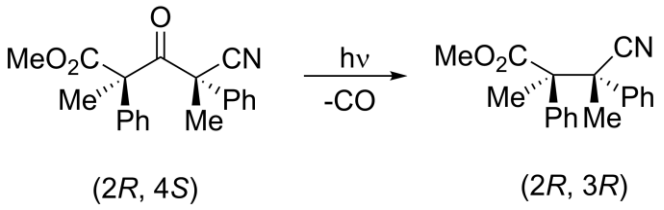
Scheme 1-4 The photo-induced cascade cyclisation of a functionalised indole, obtaining the product in high diastereoselectivity.

Knowledge of photo-induced rearrangements can become valuable when considering the reactivity of substrates to determine all accessible reaction pathways and when explaining reaction products. Photo-induced analogues of rearrangement reactions have been reported since the 1950s, like the Fries (1960s) and Claisen (1950s) rearrangements (Scheme 1-5).[52]



Scheme 1-5 Top: Photo-Fries rearrangement; Bottom: Photo-Claisen rearrangement.

When substrates are less reactive, they can potentially be activated by means of dual-catalysis.[28] To name just one example, MacMillan and co-workers combined photoredox catalysis and organocatalysis for both the alkylation and α-benzylation of aldehydes.[44f, 44g] By combining photoredox catalysis and transition-metal catalysis, aryl-aryl bonds can be formed *via* the generation of an arylradical, for example following photodehalogenation or photo-induced degradation of aryldiazonium salts.[53] Recently, Hernández-Linares *et al*. described a solid state, enantiospecific photodecarbonylation of nanocrystalline hexasubstituted ketones in near 100 % yield, with quantitative diastereoselectivity and enantiomeric excess (Scheme 1-6).[54] Aqueous suspensions of nanocrystalline ketones were flowed through a continuous flow photoreactor. This control over stereo- and regiochemistry during radical chemistry is remarkable and important in synthetic transformations, especially in the synthesis of natural products and pharmaceuticals. The scale-up of this process to multigram scale was achieved as well.



Scheme 1-6 Solid state continuous flow photodecarbonylation of nanocrystalline ketones with quantitative diastereoselectivity and enantiomeric excess.

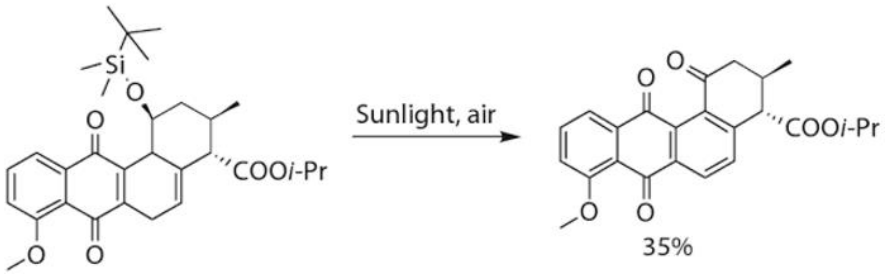
To emphasise the potential of organic photochemistry, several reports on the viability of large scale photochemistry have been presented.[55] Examples include the synthesis of ε-caprolactam for nylon production which was started by Toray, and also a photochemical ring opening in the synthesis of vitamin D3 has been reported.[55-56] Moreover, Sanofi developed a production plant for artimisinin synthesis in which semi-synthetic artimisisin was obtained *via* a singlet oxygen based photo-oxidation step.[57] The synthesis of Rose Oxide has been demonstrated on a large scale by Scharf and co-workers, producing over a 100 tonnes per year.[58]

However, the use of synthetic photochemistry also introduces challenges. For example, these new substrate reactivities mentioned above require an understanding of photophysics in synthetic organic chemistry, a skill that might not be commonly available. On a larger scale, other challenges arise as well; such as the large investment in equipment and the large operational costs of lamps on a large scale. The latter might deplete the 'sustainable character' of the photochemical reaction and increase the operating cost of the reaction above a viable level.[58] Therefore, a better understanding of photophysics and the scope of possible photochemical transitions are desirable to develop the use of photochemistry in organic synthesis. When this is accomplished, smart reactor design might tackle the scale-up challenges.

Solvent scope could also be limited compared to conventional synthetic methods due to the requirement of light transparency.[59] Reactant solubility and light transparency are essential for appropriate solvents in organic photochemical reactions, but possible solvent toxicity might interfere with the effort to accomplish a sustainable process. The following Section will touch on the use and selection of solvents for photochemical processes.

1.6.1 The Use of Solvents in Synthetic Photochemistry

All the reactions carried out for this Thesis employed a reaction solvent. Both the amount and toxicity of solvents are a great aspect in the environmental impact of chemical reactions. GlaxoSmithKline (GSK) estimated that *ca* 85 % of the total mass of chemicals involved in the pharmaceutical manufacture is from the use of solvents and that the recovery efficiencies of those are 50-80 %.[60] Solvent-free reactions would therefore be ideal in order to minimise (toxic) waste, but are hard to accomplish. Photochemical reactions involving a liquid starting material, could potentially be carried out solvent-free, although light penetration can be problematic due to the high concentration of absorber. An example of a successful photochemical solvent-free reaction was reported in the synthesis of Rubiginone C_2, a potential drug for the treatment of AIDS and Alzheimer's diseases (Scheme 1-7).[61] The desilylation and subsequent oxidation and aromatisation were accomplished in a 35 % yield in 4 hours.



Scheme 1-7 Solvent-free photochemical step in the synthesis of Rubiginone C_2.

In cases where a reaction solvent is necessary, large pharmaceutical companies such as AstraZeneca, GlaxoSmithKline (GSK) and Sanofi have published guides and information on the choice of solvents for chemists.[62] The use of 'green' solvents can decrease the toxicity of chemical waste substantially. To date, solvents are the biggest source of waste in the chemical industry[63] and key issues are containment, recovery and reuse. Therefore, when considering solvents 'green', they should provide easy and efficient separation from the reaction mixture and exhibit high solubility of the reactants.[12] However, many volatile organic compounds, often used as solvents for their easy separation from the products, are a serious health issue.[10] Therefore, in addition to ease of separation and high solubility of reactants, the desired solvent should exhibit low toxicity, and preferably be biodegradable and non-flammable.

To help with this judgment, the GSK solvent guide provides an overview of solvents which put a strain on the environment and ranks solvents in terms of waste, separability and life cycle assessment.[62b] Among the alternative and greener solvents are water, aqueous mixtures, ionic liquids, lower alcohols (like ethanol), esters and supercritical carbon dioxide ($scCO_2$), while ketones, aromatics and ethers exhibit multiple environmental concerns.[12, 62b]

Using aqueous mixtures, the cyclisation of phthalimide derivatives after decarboxylation was described,[64] as well as the formation of arylated compounds.[65] Visible light-induced brominations, as well as oxidations,[66] and the synthesis of γ-lactones and γ-lactols have been carried out in water.[67]

1.6.1.1 The Use of $scCO_2$ as a Solvent in Synthesis

A reaction solvent that is less of an environmental burden is CO_2. Due to its non-flammable, non-toxic properties, and very importantly, its easy separation from the reaction mixture, $scCO_2$ is a promising solvent for replacing conventional solvents.[68] Although energy is required to generate CO_2 in the supercritical phase, its critical temperature and pressure are relatively low (T_c = 31.2 °C, P_c = 73.8 bar, Figure 1-7) compared to other solvents.[69]

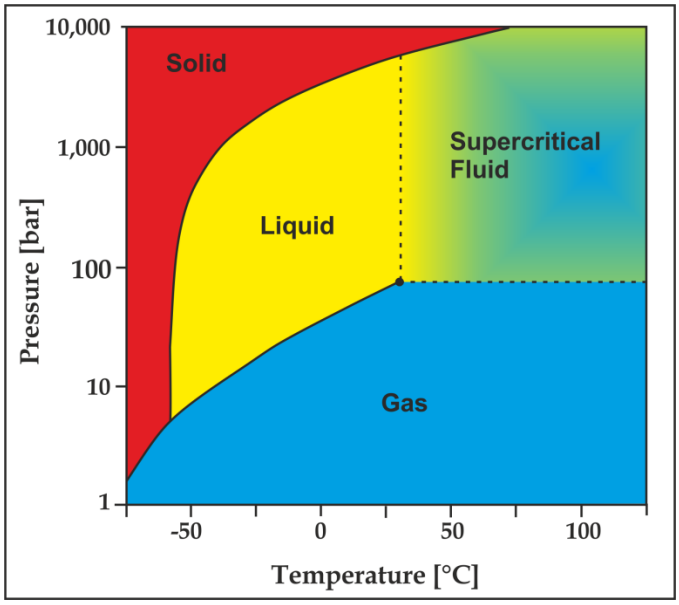


Figure 1-7 Phase diagram of CO_2 showing the supercritical fluid region and the transition points between the different phases.

Supercritical fluids exhibit mixed gaseous and liquid phase physical properties such as an enhanced diffusion rate of solutes over liquid phase solvents, and greater solubility of reagents compared to the gas phase. Although CO_2 is a non-polar molecule, it has a larger affinity for polar solutes than, for example, pentane due to its large molecular quadrupole.[69] Moreover, it is fully miscible with gases, resulting in homogeneous reaction mixtures with reactants that could be in different phases at ambient conditions. A large research area involves hydrogenation reactions using H_2, in which enantioselectivity can be retained or even improved upon the use of $scCO_2$ as opposed to conventional solvents.[69]

Photochemistry in combination with $scCO_2$ has potential benefits for radical reactions due to the low viscosity and low density of $scCO_2$ resulting in a higher diffusion rate of reactants compared to reactions carried out in the gas phase.[69] Johnston *et al*. reported a photochemical [2+2] cycloaddition in $scCO_2$ in 1989 in which product selectivity was accomplished by pressure variations.[70]

A different class of reactions that can be carried out more advantageously in $scCO_2$ is synthetic transformations exploiting singlet oxygen ($^1O_2$) due to the extended lifetime of $^1O_2$ in $scCO_2$. Singlet oxygen can be generated efficiently in $scCO_2$ with a photosensitiser present and the singlet oxygen can be used subsequently for photochemical transformations.[68] For example, the reaction of α-terpinene with $^1O_2$ to ascaridole proceeded rapidly and quantitatively (Figure 1-8) with a 2-fold increase in reaction rate compared to the use of tetrachloromethane as solvent.[71]

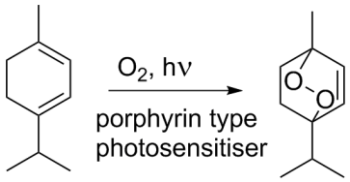


Figure 1-8 Photochemical oxidation of α-terpinene to ascaridole.

Co-solvents are often required when employing $scCO_2$ as the main solvent to dissolve more polar protic reactants. This was demonstrated in the oxidation of 1-naphthol to naphthalene-1,4-dione.[71] However, in this instance, lower turnover frequencies were reached compared to the reaction carried out in conventional

solvents, probably due to quenching effects $^1O_2$ by the co-solvent and lower initial concentration of reactants.

1.6.2 Quantum Chemical Calculations

Predicting the reactivity of molecules and the most feasible reaction pathway in a photochemical reaction can help in the reaction design, and reduce time spend on reaction optimisation. Quantum chemical calculations can help model these phenomena and have been used as part of this Thesis.

The way to elucidate the energy and electronic structure of compounds is to solve the Schrödinger equation. However, this equation is too complex to solve for multielectronic systems and therefore, approximations are often used. The Born-Oppenheimer approximation[72] is an often-used approximation in which nuclei are considered static due to their slow movement as they are about 2000 times heavier than electrons. Calculating only the energy of electrons, two methods of solving the approximate Schrödinger equation exist. The first one is a wave function based method of which the Hartree-Fock model is the most well-known. Each electron is represented by its wave function, generating an n-dimensional equation (where n is the number of electrons in a system).

The second method utilises electron density instead of wave functions and is called density functional theory (DFT). By definition, the density is 3-dimensional, reducing the dimensionality of the equation, making it more suitable for larger compounds. The electron density is displayed in Kohn-Sham orbitals and DFT calculations solve the corresponding Kohn-Sham equations which is a derivative of the classical Schrödinger equation. An important part of the Kohn-Sham equations is the exchange and correlation energy. As the exact electron-electron interaction and the kinetic interaction cannot be calculated, the deviation of these interactions can be described in respectively the exchange and correlation energies. Many methods to approximate the exchange and correlation energies exist, but hybrid functionals are often used. In these functionals, the exact exchange energy from the Hartree-Fock theory is combined with the correlation term obtained *ab initio* or empirical. This way, molecular properties such as atomisation energies, bond lengths and vibration frequencies can be described more accurately.[73]

The partly empirical method called Becke 3 Lee-Yang-Parr, abbreviated to B3LYP, is an example of such a hybrid functional[74] and is the function used for the work described in this Thesis. Next to a method to approximate exchange and correlation energies for the Kohn-Sham equations, a basis set is needed to describe the radial electron distribution, represented in the orbitals. The basis set used in this work is 6-311+G(d,p). As valence electrons, in contrast to core electrons, primarily take part in the bonding of atoms, these orbitals are represented by multiple basis functions. The combination of the different orbitals can adjust the spatial extent of the electron density depending on molecular environment. In the basis set 6-311+G(d,p), the description of core atomic orbitals is represented by the first number of the basis set. In this case, 6 primitive Gaussians are present in each core atomic orbital basis function. The valence electrons in this basis set are split in three sets of functions, represented by the presence of three numbers: 311. The numbers itself represent how many functions describe this set of valence electrons. The '+' sign notes the presence of diffuse functions. This way, the orbitals distant from the atomic nuclei can be described more accurately. Another way of increasing the accuracy is to add empty orbitals to the basis to enlarge the area in which the electron can be positioned. This concept is called polarisation and allows for an asymmetric electron environment which is most often the case for bonded atoms.[75] In the work presented in this Thesis, empty d and p orbitals were added to the basis set.

A polarisable continuum solvent model was used to better mimic reaction conditions. The solvent is modelled as spheres of uniform dielectric constant.[76] Interlocking atomic spheres, which represent this dielectric constant, are positioned around the molecule of interest to model solvent contribution (Figure 1-9). The optimisation of the molecule of interest can change the structure of these solvent spheres.

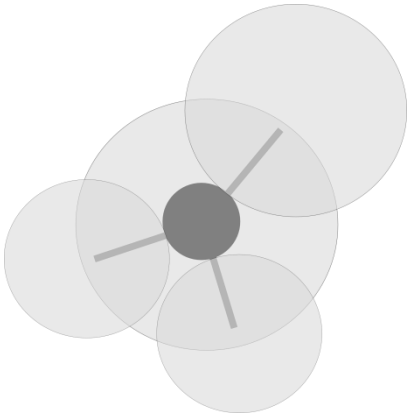


Figure 1-9 Representation of a polarised continuum solvent model for quantum chemical calculations containing a molecule (dark grey) surrounded by interlocking solvent spheres (light grey).

However, rendering the solvent as a collection of dielectric constants instead of individual solvent molecules cannot accurately describe the interactions between solvent and substrate molecules. These interactions can change reaction kinetics by altering the energy of certain compounds due to stabilisation or destabilisation as a result of these solvent-solute interactions.

1.7 Reactor Set-up and Reactor Design

The reaction set-up is crucial in achieving efficient photochemical reactions. The need for sufficient light penetration has been mentioned in Section 1.3.2 and choosing the most suitable light source contributes to this. Moreover, the use of a continuous flow reaction set-up can overcome light penetration issues often present in batch experiments.

1.7.1 Light Sources for Photochemical Reactions

In order to accomplish efficient photochemical reactions, the emission characteristics and geometry of the light source are vital, since they determine the efficiency of excitation of the molecules in the reactor. For example, the light penetration must be optimal as discussed *vide supra* and the emission spectrum

of the light source must overlap as much as possible with the absorption spectrum of the absorber (which can be the substrate or either a photosensitiser or photocatalyst). Photochemistry can be carried out using visible light bringing advantages such as its benign nature and high availability; or ultra-violet (UV) light which often offers spectral overlap with substrate absorption. Multiple examples from both categories will be discussed below.

1.7.1.1 The Use of Sunlight for Photochemical Reactions

The sun is the most abundant light source on earth with a total irradiance of 1.361 kW/m^2 hitting the Earth's atmosphere every second.[77] Nature utilises this by performing many sunlight-induced transformations with photosynthesis being the most well-known example. Solar radiance as an energy source is promising since the global energy consumption in 2014 was 5.4x10^{20} J, which could be provided by solar energy within 2 hours of irradiation.[78] However, solar energy as a renewable energy source for our daily use is still in development, with a growth of around 7 % per year.[79]

Ciamician: *'It may also happen that the problem of using solar energy becomes interesting under another respect. When oil will have been all burned in our prodigal industries, it may become necessary, even on social grounds, to come to exploit solar energy.'*[6b]

Therefore, solar radiation could be viewed as the ideal energy source since it is highly abundant and cheap. Moreover, photons do not leave any trace after the photochemical reaction, rendering it a clean energy source.

An important point that must be considered for using solar radiation for photochemically driven chemistry is the ability of the desired reactants to absorb the sunlight. Sunlight consists mostly of infrared (IR) and visible light (Figure 1-10). The presence of infrared light from solar radiation will contribute to heating of the reaction mixture which makes temperature control crucial.

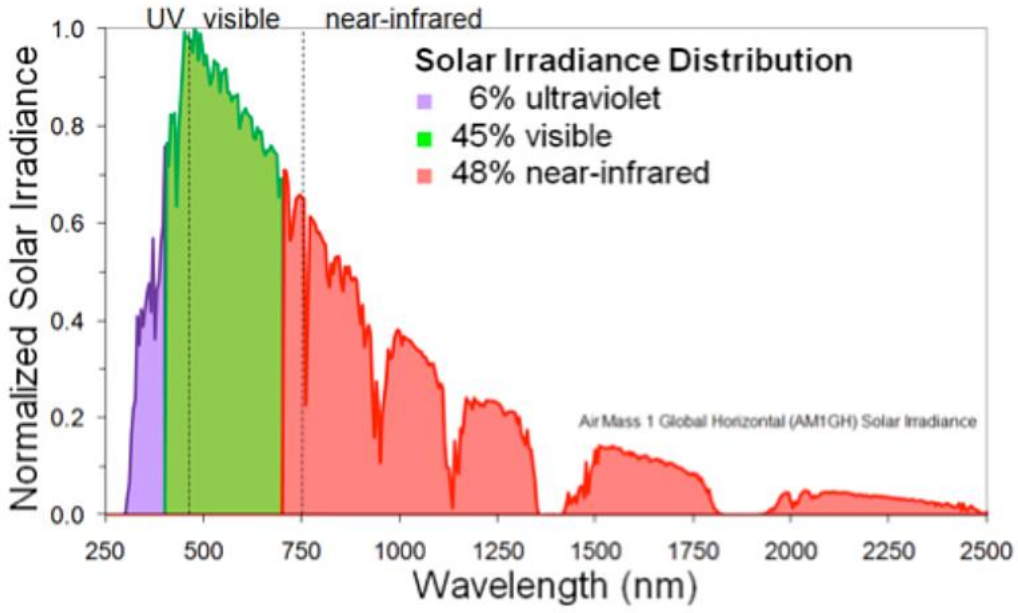


Figure 1-10 Solar radiation distribution.[80]

Because of the broad emission spectrum of sunlight, reactants will be irradiated with photons containing a range of energies and therefore, selectively irradiating a specific moiety in the substrate can be challenging.

However, most organic substrates do not absorb visible or infrared light. Therefore, a photosensitiser or photocatalyst is necessary in order to absorb the visible solar radiation and consequently transfer energy or electrons to the substrate to perform the photochemical transformation. As therefore only a specific band of energy will reach the reagent solution, control over which molecule participates in the photochemical reaction can be achieved.

Utilising this light as an energy source for synthetic reactions has received increasing attention from synthetic chemists.[29a, 30b, 40a, 47a, 49] Most frequently reported are photocatalysed functionalisation of electrophilic olefins,[81] cycloadditions,[49] photo-Friedel-Crafts type reactions,[47a] amidations, dimerisations, oxidations, reductions, decarboxylations[82] and halogenations.[5]

Modern solar radiation reactors have moved away from the set-up of a flask in the sun and moved towards concentrated sunlight reactors in order to increase its efficiency. These reactors concentrate sunlight onto the reaction mixture, intensifying the irradiation power which often increases reactant conversion which leads to a higher space-time yield of the reaction. In this way, multiple

compounds have been synthesised up to kilogram scale.[5] Examples include oxygenations, oxidations,[83] cycloadditions, acylations and isomerisations.[5]

Importantly, large scale photochemical transformations using solar radiation have been demonstrated. The large scale photochemical production of (-)-*cis*-rose oxide has been demonstrated with the PROPHIS reactor in Cologne, Germany.[84]

The photosensitised oxygenation of β-citronellol to synthetically produce (-)-*cis*-rose oxide is widely studied and an industrially relevant compound for its rose fragrance. Both thermal and photochemical procedures have been published, although, all studied photochemical routes were superior to thermal routes in terms of yield. The reactor PROPHIS consists of 4 parabolic troughs in order to concentrate sunlight and the reactants flow through the middle (Figure 1-11). Depending on how many of these sheets are in operation, up to 120 L can be irradiated at once, with 30-32 times the sunlight by the light concentration abilities.[84] With a similar reaction yield as the other photochemical routes to produce (-)-*cis*-rose oxide, this is an industrially viable reaction route.[58, 85]

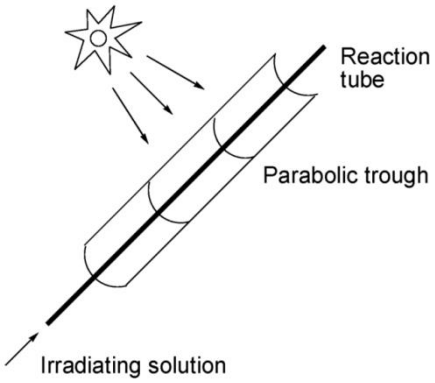


Figure 1-11 Schematic representation of a parabolic trough reactor.[5]

1.7.1.2 The Use of Visible Light LEDs for Photochemical Reactions

Although the sun is a very green light source, reaction selectivity can be lower due to the broad output of energy photons by the sun as mentioned before. Moreover, artificial light sources are not dependent on the weather and position on the earth. An example of a rapidly developing artificial visible light source is light emitting diodes (LEDs). After a voltage is applied to the LED, these

semiconductors emit incoherent electroluminescence by the recombination of a hole and an electron within the device.[46] This process results in a constant source of photons being emitted, generally over a short wavelength range (typically 20 nm). As different materials can be used in the LED, the recombination energy of the hole and the electron can be tuned to specific wavelengths. However, the conversion of absorbed power (typically around 100 mW) to light depends on the wavelength of the LED, generating less efficient devices at shorter wavelengths.[46] Besides altering the semiconductor material in the LED, another way of changing the output emission spectrum of a LED is to apply a phosphor coating. This phosphor coating absorbs the initial incoming LED light, and emits light with a longer wavelength upon relaxation to its ground state. White light generation can benefit from this phosphor coating technique as this method is more efficient than producing white light by combining three different LEDs (red, green and blue). Commercial LEDs are generally cheap and long-lived ($>10^4$ h), making them ideal for photochemical applications. However, most often an array of LEDs is required to acquire sufficient radiation intensity.

These light sources have become more widespread due to their long lifetime and brightness; and have uses in many household applications such as street-, car- and house lights. In chemistry, they are employed abundantly for water purification by photocatalytic degradation of pollutants, dye degradation, bacteria inactivation and hydrogen production.[86] More recently, LEDs have attracted the attention of synthetic chemists as the light source for photochemical reactions. Meyer *et al.* published the oxidation of β-citronellol *via* singlet oxygen using blue LEDs in 2007. Multiple designs of the LED arrays were constructed to fit the different reactors.[87]

As mentioned earlier, most reaction substrates cannot absorb visible light which makes the addition of a photocatalyst necessary. The use of UV light provides an interesting alternative as a light source for synthetic photochemistry as no additional photo-absorbers are required since most substrates are able to absorb UV light directly. Multiple options are available and the most frequently used UV light sources are outlined below.

1.7.1.3 The Use of Mercury Arc Lamps for Photochemical Reactions

The most commonly used UV light sources are mercury vapour arc lamps of which most are low-pressure (LP) mercury lamps. They consist of evacuated glass tubes containing mercury vapour. A spark induced by an arc discharge heats the mercury and an electrical discharge subsequently excites the mercury atoms which results in emission of UV radiation.[23]

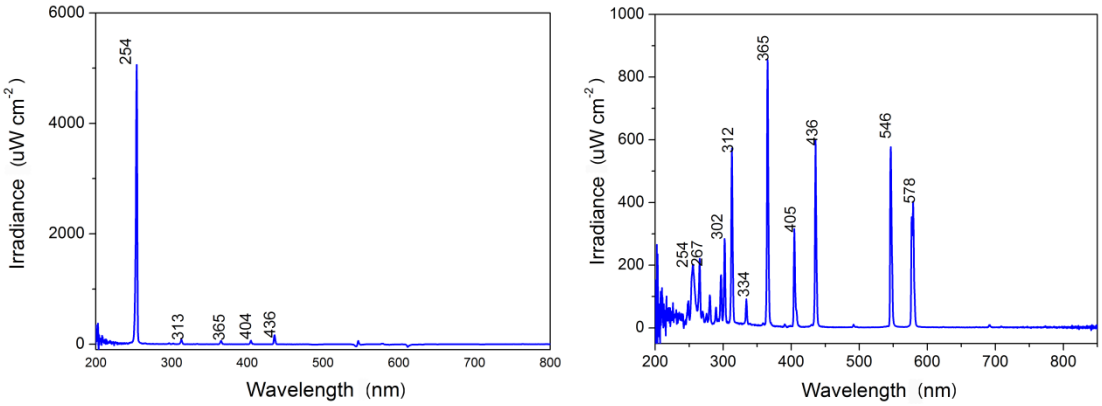


Figure 1-12 Emission spectra of a) 6 W LP mercury lamp (at 1 cm), b) 125 W Heraeus Noblelight MP mercury lamp (at 6 cm). Both spectra were recorded using a calibrated Ocean Optics UV-Vis USB 2000+ spectrometer and cosine probe.

In LP mercury lamps, around 30 % of the input energy (6-300 W) is converted into light[23] and over 80 % of this emission occurs at 254 nm (Figure 1-12a), although this wavelength can be changed by applying a phosphor (or a mixture of phosphors) coating.[46]

Medium- and high-pressure (respectively abbreviated as MP, HP) mercury lamps have a much higher power input (400 W for laboratory use, but up to 60 kW for industrial applications) and are broad band emitters (Figure 1-12b). The output spectrum can be altered, by applying band-filters to regions of the emission spectrum. A drawback for this approach is the loss of photon flux. Due to strong emissions in the IR light region, these lamps operate at high temperatures (up to 600 °C), requiring additional cooling.[23, 88] Despite their low cost, mercury lamps have the disadvantage of only exhibiting a limited number of emission bands which could impede efficient irradiation of photochemical reactants if they have

no strong absorbance at those wavelengths. Moreover, the presence of mercury is a strong argument against these light sources for environmental reasons.

1.7.1.4 The Use of UV - Excimer Lamps for Photochemical Reactions

An example of an almost monochromatic light source, while maintaining a high photon flux, is an excimer lamp. With a very narrow emission band at a specific wavelength, the achieved reaction selectivity can be optimal. Other features that make these lamps suitable for synthetic photochemistry are the stability of the excimer molecules in the excited electronic state and the absence of a strong bond of these excimer species in the ground state, allowing for a less energy demanding device. The relatively high radiation power density (up to 700 W/cm^2), relatively low operating temperatures due to the lack of infrared emission, the possibility of scaling and the ability to shape the radiation geometry as desired make these lamps attractive for photochemistry.

Excimer lamps are based on one of three main mechanisms. In each case an exciplex (heteronuclear dimer) or excimer (homonuclear dimer) is formed by the release of energy after a discharge mechanism (*vide infra*). These exciplexes or excimers relax back to their ground state within nanoseconds producing an intense emission band and dissociation of the excimer or exciplex. The wavelength of this emission is determined by the energy gap between the excited- and ground state of the exciplex or excimer. The term excimer lamp is generally used for lamps based on both types of excited state complexes. Excimers are formed by the association reaction depicted in Equation 1-4 in which R and R* are rare gas atoms in their ground- and excited state respectively. Short lived rare gas dimers are formed in the excited state.

$$R^* + R + R \rightarrow R_2^* + R \qquad 1\text{-}4$$

To access other emission wavelengths, excimer lamps containing exciplexes can be employed. These exciplexes are produced *via* the so-called harpoon reaction in which a rare gas atom (R) and a halogen (Y)-containing molecule (MY or Y_2) (Equation 1-5, with a second, alternative route in brackets).

$$R^* + Y_2\,(MY) \rightarrow RY^* + Y(M) \qquad 1\text{-}5$$

The recombination of a positive atomic (R^+) or molecular rare gas ion (R_2^+) with a negative ion (Y^-) can also produce an exciplex. This mechanism is shown in Equation 1-6 in which P is a third particle able to carry away the excess energy.[89]

$$R^+(R_2^+) + Y^- + P \rightarrow RY^* + P + (R) \qquad 1\text{-}6$$

In order to create these excimers and exciplexes, a discharge mechanism is needed to provide the necessary excitation energy. The main discharge mechanisms are capacitive and dielectric barrier (silent) discharge (CD and DBD respectively) due to their prolonged service life, but other mechanisms exist.[90] The dielectric barrier discharge mechanism is self-sustained, the simplest and the most accessible way and therefore most widely used.[90b] Moreover, due to the higher gas pressure in the lamp, DBD has a smaller spectral bandwidth than CD lamps while maintaining its radiant power, providing another advantage of DBD lamps.[91]

In DBD lamps, the electrodes are insulated by a dielectric layer. A high voltage (7 to 10 kV) combined with a high frequency (100 to 500 kHz) pulse is applied, generating an arc discharge. At the surface of the dielectric, multiple arcs can be formed semi-simultaneously. These micro-discharges are short lived (a few nanoseconds) but are able to excite the rare gas atoms, resulting in bursts of light pulses with a repetition frequency of about 100 kHz.[42, 92] Table 1-4 shows a selection of peak wavelengths that can be obtained by combining both rare gases and halogens for the generation of either excimer or exciplexes.

Table 1-4 Peak wavelengths of excimer light sources.[42]

Gas	**Peak wavelength (nm)**
Ar_2*	126
Kr_2*	146
Xe_2*	172
KrBr*	207
KrCl*	222
XeBr*	283
XeCl*	308
Hg_2*	334
HgBr*	503
HgCl*	558

Figure 1-13 exhibits some of the typical emission spectra of both rare gas dimers and rare gas halogen exciplex light sources, including their main transition bands. For the exciplex molecules, the B-X transition is the strongest, but both weaker transitions (e.g. D-X, D-A, C-A) and halogen dimer molecules are present in the emission spectrum.[91] In order to supress the formation of rare gas dimers in gas halogen exciplex lamps, the pressure of the halogen is higher than that of the rare gas. As shown in Figure 1-13, the emission of the rare gas dimer lamps is broader than the gas halogen exciplex lamps. In the case of the excimer species, the different vibrational transitions are close to the main B-X, resulting in a broad emission spectrum.

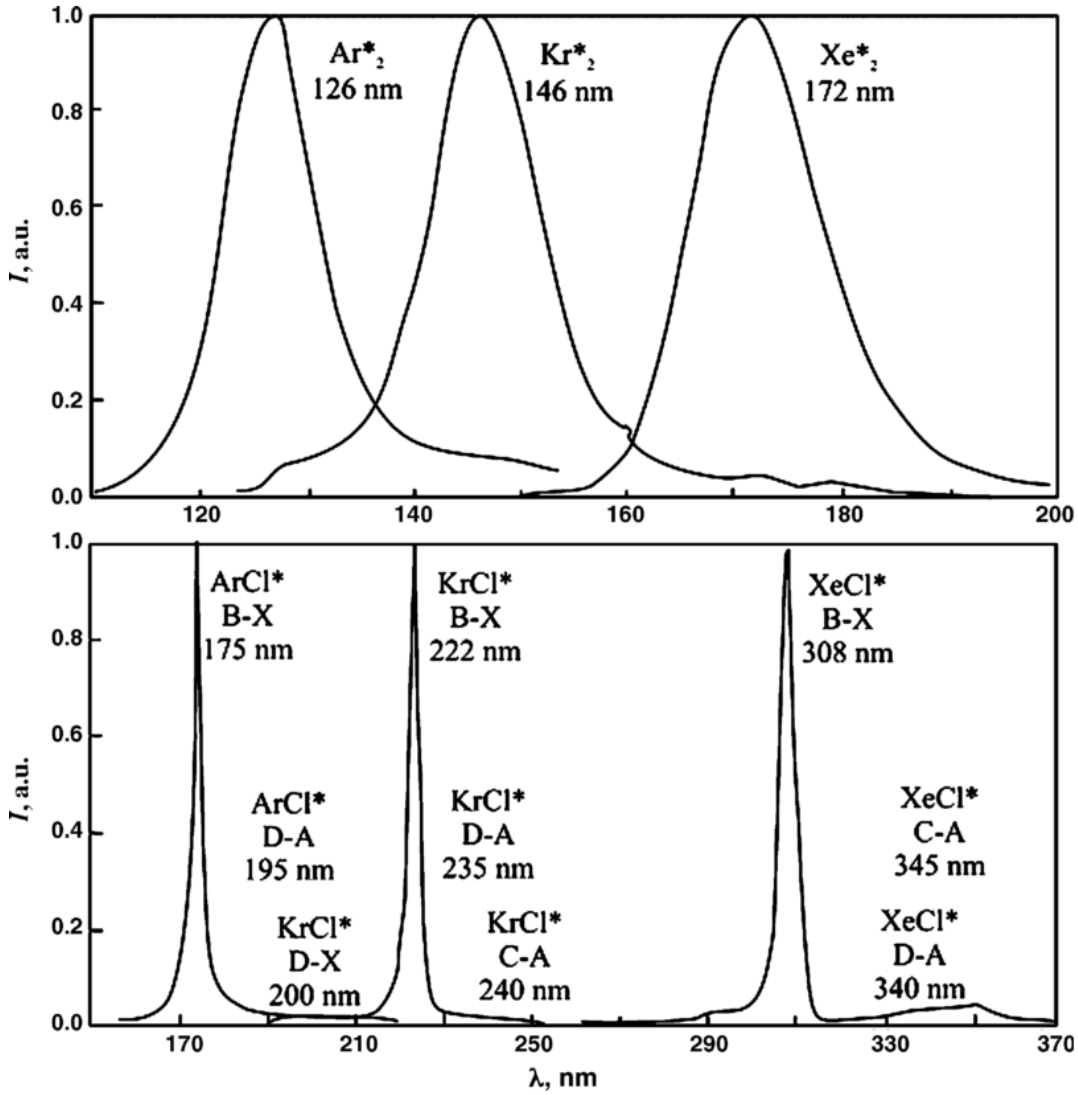


Figure 1-13 Typical emission spectra of both excimer and exciplex light sources, obtained in barrier discharge at high pressures.[91]

Excimer lamps have found applications in for example UV curing and actinometry.[90, 93] On an industrial scale, these lamps have been utilised for surface cleaning, photomedicine (e.g. skin disease treatment[90b]), artificial lighting and plasma displays.[90a] Water purification has been accomplished by for example advanced oxidation processes, in which reactive radicals induce the degradation of pollutant molecules.[94] The irradiation of water with VUV light (wavelengths between 100-200 nm) has been shown to cause photosplitting of water.[94a] Excimer lamps have also been recognised to exhibit bactericidal character, shown by the irradiation of E. coli bacteria among others, with both XeBr* and KrCl* excimer lamps.[90b] More recently, excimer lamps have been utilised to decrease the water content in natural gas. The irradiation of water with a Xe^*_2 excimer lamp caused water homolysis and therefore depleted the water vapour concentration 1.7 times. This is important for preventing corrosion of pipelines during gas transport and has been applied and patented on large scale.[93]

In synthetic photochemistry, Griesbeck and Oelgemöller have pioneered the use of excimer lamps as they performed photodecarboxylations, photocycloadditions and Type III photo-oxygenations with high yields using a XeCl* excimer lamp. A simple falling film reactor with water cooling was used as the reaction set-up.[64a, 88] An industrial application came to light with the use of a XeBr* excimer lamp for the partial synthesis of Vitamin D3 by performing photolysis of 7-dehydrocholesterol.[42] An example indicating its biological applications is the photosynthesis of aspartic acid in trace amounts by irradiation (172 nm) of an aqueous solution of urea and maleic acid. This can shed light on the formation of biomolecules on the primitive earth and the origin of life.[42] Despite their advantageous photophysical properties, the use of excimer lamps as a light source for synthetic photochemistry might only increase slowly due to the high cost of excimer lamps at present.

1.7.2 Continuous Photochemistry

When considering a reactor set-up, not only selecting the correct the light source is important, the way in which the light source is positioned is crucial as well. Traditionally, organic synthesis reactions are performed in standardised glassware in a batchwise fashion and this has been the case since the time of Justus Liebig, the founder of organic chemistry. Although industry is driven by

automation and high-throughput syntheses, flow chemistry was only used for production processes until recently.[95] This shift allowed for the utilisation of continuous processing in organic synthesis. The main advantages of a continuous reaction include improvement in reaction efficiency, increase in yields and the reduction of reaction times due to rapid heat transfer and mixing of the reactants.[96]

For small scale reactions, flow chemistry provides the tools for efficient optimisation processes and reaction screening so that less starting material is wasted. This is especially important for the pharmaceutical sector in its early stages of drug discovery. As the reaction mixture exits the flow system, the inclusion of inline analysis in the form of IR/UV-Vis/GC-MS/HPLC can give fast information about the reaction efficiency. Moreover, when a feedback loop connects this analysis output with the control over the parameters of the reaction system (e.g. pump speed, temperature, reactant ratios), automated reaction optimisation can be accomplished. [69a, 70]

Continuous chemistry is also very beneficial for multi-step synthesis as the reactants for consequent steps can be added *via* pumps down-stream, removing the need for product isolation, purification and changing reaction vessels in between each step. This method provides an uninterrupted reaction network, which is less time-consuming and both increases synthetic efficiency and reduces waste.[97] Moreover, the handling of possible toxic or highly reactive intermediates is prevented which is a clear safety argument.[98] Examples can involve the generation of a gas, the handling of toxic substances or rapid degradation of starting materials, such as diazonium salts and phosgene.[99] Not only is there less contact between the toxic chemicals and the chemists, less of the toxic or reactive compounds are in the reactor system due to the narrow flow channels, providing another advantage from a safety point of view.

Flow chemistry also provides an accessible way to scale-up reactions, building bridges between chemistry in a laboratory and the large scale production process. Large scale reactions do not require large reactors anymore, leading to a positive impact on the safety considerations and lowering the carbon footprint. Without expensive apparatus, flow set-ups can be built and it could find great applications in industry as higher control over the reaction parameters can be obtained.[100] Moreover, it provides secured reproducibility, and process reliability.[98b]

All these advantages remain valid regarding the use of photochemistry in flow, but even more positive considerations can be made. Light penetration is an enormous problem for large scale photochemical batch reactors.[45d] Due to the higher surface area to volume ratio in the reactor, light penetration to initiate photocatalytic reactions is more efficient, resulting in shorter reaction times compared to batch experiments. The reliable scale-up is extra important for continuous photochemistry as narrow light pathways can be maintained when scaling-up. Moreover, products are moving away from the light source in flow, which impedes the generation of side products.[23, 100b]

In the last 20 years, flow photochemistry has gained interest for synthetic transformations and complex organic molecules can be synthesised in precise and controllable multi-reactor flow systems.[23, 101] Now, almost any batch reaction can be performed in flow.[23] Figure 1-14 shows an example of a simple flow set-up for organic transformations developed by Booker-Milburn and co-workers in 2005, which is now widely used in photoredox chemistry by many groups. The reagents flow through transparent tubing which is wrapped around a lamp.[102]

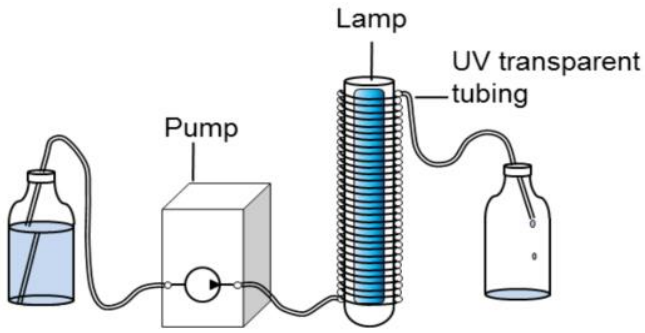


Figure 1-14 Diagram of a photochemical flow reactor as developed by Booker-Milburn and co-workers.[102]

Stephenson and co-workers also developed a visible light based photochemical application for synthesis in flow in which up to 50-fold rate enhancements were obtained over corresponding batch methods.[100a] Moreover, lower catalyst loading was required in order to obtain products in excellent yield. Among the developed reactions were the bromination of alcohols, reductive opening of an epoxide and the reduction of a halogen acetate. A drawback to using flow chemistry is the lack of familiarity with it for most organic chemists while the correct reactor set-up is imperative to efficient reactions. Reactor blockages can form an additional challenge to flow chemistry.

Next to conventional solvents, processes in $scCO_2$ and continuous flow have been explored for photoredox catalysis. In 2008, our group published the first $^1O_2$ continuous flow photo-oxidation in $scCO_2$.[103] A scale-up of 3000-fold in terms of throughput was reached compared to the original batch reactor.[104] This work was extended by the development of greener ways of performing this reaction by using immobilised photocatalyst or fluorous phase extraction and recycling of the photocatalyst.[105] Moreover, important progress was made on the development of a sustainable route for the photochemical step in the synthesis of artemisinin, by performing the reaction in continuous flow, using CO_2 as the reaction solvent.[106]

1.8 Thesis Aims

Organic photochemistry has a high potential to add value to the organic synthesis toolbox since it introduces new reaction pathways by utilising the excited state of the reactants.[107] The work presented in this Thesis aims to further demonstrate the versatility of continuous flow photochemistry and to show its ability to easily tune reaction conditions to guide product selectivity. More specifically, the goals of the work presented in this Thesis were:

1. To demonstrate that visible light photochemistry can contribute to sustainable chemical production while maintaining high productivity and product selectivity.

2. To deepen the understanding of the mechanism of the hydroxylation of aryl boronic acids by performing quantum chemical calculations in order to investigate which reaction parameters would influence reaction productivity and selectivity most.

3. To achieve a mild and clean synthetic route to extended methyl ketones by employing a recently developed excimer lamp UV continuous flow reactor.

4. To optimise reaction parameters for the formation of 1,4-diketones by the photochemical dimerisation of several ketones.

5. To employ 1,4-diketones in the Paal-Knorr synthesis to form 2,5-dimethylfuran and several pyrrole derivatives.

1.9 References

1. Decker, C.; Bendaikha, T., *J. Appl. Polym. Sci.* **1998,** *70* (11), 2269-2282.
2. Roth, H. D., *Angew. Chem. Int. Ed.* **1989,** *28* (9), 1193-1207.
3. Turro, N. J., Modern Molecular Photochemistry. University Science Books: Sausalito, California, 1991.
4. Albini, A.; Dichiarante, V., *Photochem. Photobiol. Sci.* **2009,** *8* (2), 248-254.
5. Protti, S.; Fagnoni, M., *Photochem. Photobiol. Sci.* **2009,** *8* (11), 1499-1516.
6. (a) *Photochem. Photobiol. Sci.* **2010,** *9* (12), 1533-1534; (b) Albini, A.; Fagnoni, M., *Green Chem.* **2004,** *6* (1), 1-6.
7. Ciamician, G., *Science* **1912,** *36* (926), 385-394.
8. *Green Chem.* **2004,** *6* (1), G13.
9. European Union, Eurostat: Generation of waste by waste category http://epp.eurostat.ec.europa.eu/tgm/table.do?tab=table&init=1&language=en&pcode=ten00108&plugin=1 (accessed March 2014).
10. Sheldon, R. A., *Green Chem.* **2005,** *7* (5), 267-278.
11. Anastas, P. T.; Lankey, R. L., *Green Chem.* **2000,** *2* (6), 289-295.
12. Sheldon, R. A., *Chem. Commun.* **2008,** (29), 3352-3365.
13. Sheldon, R. A., *Chem. Soc. Rev.* **2012,** *41* (4), 1437-1451.
14. (a) Anastas, P.; Eghbali, N., *Chem. Soc. Rev.* **2010,** *39* (1), 301-312; (b) Tang, S. L. Y.; Smith, R. L.; Poliakoff, M., *Green Chem.* **2005,** *7* (11), 761-762.
15. Sheldon, R. A., *Chem. Tech.* **1994,** *24* (3).
16. Sheldon, R. A., *Green Chem.* **2007,** *9* (12), 1273-1283.
17. Trost, B. M., *Science* **1991,** *254*, 1471-1477.
18. Zeitler, K., *Angew. Chem. Int. Ed.* **2009,** *48* (52), 9785-9789.
19. Stankiewicz, A., *Chem. Eng. Res. Des.* **2006,** *84* (7), 511-521.
20. Guillet, J., *Polymer photophysics and photochemistry: an introduction to the study of photoprocesses in macromolecules*. CUP Archive: 1985.
21. Braslavsky, S. E., *Pure Appl. Chem.* **2007,** *79* (3), 293-465.
22. Coyle, E. PhD Thesis. Dublin City University, 2010.
23. Knowles, J. P.; Elliott, L. D.; Booker-Milburn, K. I., *Beilstein J. Org. Chem.* **2012,** *8*, 2025–2052.
24. Klán, P.; Wirz, J., *Photochemistry of Organic Compounds: From Concepts to Practice*. John Wiley & Sons: Hoboken, 2009.
25. Wayne, C. E.; Wayne, R. P., *Photochemistry*. Oxford University Press: New York, 1996.

26. (a) Yanyan, G.; Snezna, R.; Peng, Z., *Nanotechnology* **2010,** *21* (6), 065102; (b) Thandu, M.; Comuzzi, C.; Goi, D., *Int. J. Photoenergy* **2015,** *2015*, 22.

27. Balzani, V.; Bergamini, G.; Ceroni, P., *Angew. Chem. Int. Ed.* **2015,** *54* (39), 11320-11337.

28. Skubi, K. L.; Blum, T. R.; Yoon, T. P., *Chem. Rev.* **2016,** *116* (17), 10035-10074.

29. (a) Fagnoni, M.; Dondi, D.; Ravelli, D.; Albini, A., *Chem. Rev.* **2007,** *107* (6), 2725-2756; (b) Ravelli, D.; Dondi, D.; Fagnoni, M.; Albini, A., *Chem. Soc. Rev.* **2009,** *38* (7), 1999-2011.

30. (a) Shi, L.; Xia, W., *Chem. Soc. Rev.* **2012,** *41* (23), 7687-7697; (b) Xi, Y.; Yi, H.; Lei, A., *Org. Biomol. Chem.* **2013,** *11* (15), 2387-2403.

31. Nguyen, J. D.; D'Amato, E. M.; Narayanam, J. M. R.; Stephenson, C. R. J., *Nat. Chem.* **2012,** *4* (10), 854-859.

32. (a) Bock, C. R.; Connor, J. A.; Gutierrez, A. R.; Meyer, T. J.; Whitten, D. G.; Sullivan, B. P.; Nagle, J. K., *J. Am. Chem. Soc.* **1979,** *101* (17), 4815-4824; (b) Juris, A.; Balzani, V.; Belser, P.; von Zelewsky, A., *Helv. Chim. Acta* **1981,** *64* (7), 2175-2182.

33. Crutchley, R. J.; Lever, A. B. P., *J. Am. Chem. Soc.* **1980,** *102* (23), 7128-7129.

34. Flamigni, L.; Barbieri, A.; Sabatini, C.; Ventura, B.; Barigelletti, F., Photochemistry and Photophysics of Coordination Compounds: Iridium. In *Photochemistry and Photophysics of Coordination Compounds II*, Balzani, V.; Campagna, S., Eds. Springer Berlin Heidelberg: Berlin, Heidelberg, 2007; pp 143-203.

35. (a) Lambert, C. R.; Kochevar, I. E., *Photochem. Photobiol.* **1997,** *66* (1), 15-25; (b) Marin, M. L.; Santos-Juanes, L.; Arques, A.; Amat, A. M.; Miranda, M. A., *Chem. Rev.* **2012,** *112* (3), 1710-1750; (c) Romero, N. A.; Nicewicz, D. A., *Chem. Rev.* **2016,** *116* (17), 10075-10166; (d) Rauf, M. A.; Graham, J. P.; Bukallah, S. B.; Al-Saedi, M. A. S., *Spectrochim. Acta, Part A* **2009,** *72* (1), 133-137.

36. (a) Scholz, M.; Dedic, R.; Breitenbach, T.; Hala, J., *Photochem. Photobiol. Sci.* **2013,** *12* (10), 1873-1884; (b) Antony, T.; Atreyi, M.; Rao, M. V. R., *Chem. Biol. Interact.* **1995,** *97* (3), 199-214.

37. (a) Neumann, M.; Füldner, S.; König, B.; Zeitler, K., *Angew. Chem. Int. Ed.* **2011,** *50* (4), 951-954; (b) Seely, G. R., *Photochem. Photobiol.* **1978,** *27* (5), 639-654; (c) Aleksandr, K. C., *Russ. Chem. Rev.* **1981,** *50* (7), 615; (d) Al-Omair, N. A.; Reda, S. M.; Al-Hajri, F. M., *Advances in Nanoparticles* **2014,** *3* (1), 5.

38. Wang, X.-y.; Del Guerzo, A.; Schmehl, R. H., *J. Photoch. Photobio. C.* **2004,** *5*, 55-77.

39. Tucker, J. W.; Stephenson, C. R. J., *J. Org. Chem.* **2012,** *77* (4), 1617-1622.

40. (a) Prier, C. K.; Rankic, D. A.; MacMillan, D. W. C., *Chem. Rev.* **2013,** *113* (7), 5322-5363; (b) Teplý, F., *Collect. Czech. Chem. Commun.* **2011,** *76* (7), 859-917.

41. Kulkarni, S. S.; Santra, B. K.; Munshi, P.; Lahiri, G. K., *Polyhedron* **1998,** *17* (25–26), 4365-4377.

42. Volman, D.; Hammond, G., *Advances in photochemistry, volume 18*. John Wiley & Sons, Inc: New York, 1993; Vol. 18.

43. (a) Xuan, J.; Xiao, W.-J., *Angew. Chem. Int. Ed.* **2012,** *51* (28), 6828-6838; (b) Hedstrand, D. M.; Kruizinga, W. H.; Kellogg, R. M., *Tetrahedron Lett.* **1978,** *19* (14), 1255-1258.

44. (a) Du, J.; Espelt, L. R.; Guzei, I. A.; Yoon, T. P., *Chem. Sci.* **2011,** *2* (11), 2115-2119; (b) Du, J.; Yoon, T. P., *J. Am. Chem. Soc.* **2009,** *131* (41), 14604-14605; (c) Furst, L.; Narayanam, J. M. R.; Stephenson, C. R. J., *Angew. Chem. Int. Ed.* **2011,** *50* (41), 9655-9659; (d) Hurtley, A. E.; Cismesia, M. A.; Ischay, M. A.; Yoon, T. P., *Tetrahedron* **2011,** *67* (24), 4442-4448; (e) Nagib, D. A.; Scott, M. E.; MacMillan, D. W. C., *J. Am. Chem. Soc.* **2009,** *131* (31), 10875-10877; (f) Nicewicz, D. A.; MacMillan, D. W. C., *Science* **2008,** *322* (5898), 77-80; (g) Shih, H.-W.; Vander Wal, M. N.; Grange, R. L.; MacMillan, D. W. C., *J. Am. Chem. Soc.* **2010,** *132* (39), 13600-13603; (h) Tucker, J. W.; Narayanam, J. M. R.; Shah, P. S.; Stephenson, C. R. J., *Chem. Commun.* **2011,** *47* (17), 5040-5042; (i) Yoon, H.-S.; Ho, X.-H.; Jang, J.; Lee, H.-J.; Kim, S.-J.; Jang, H.-Y., *Org. Lett.* **2012,** *14* (13), 3272-3275.

45. (a) Remy, R.; Bochet, C. G., *Chem. Rev.* **2016,** *116* (17), 9816-9849; (b) Ramamurthy, V.; Sivaguru, J., *Chem. Rev.* **2016,** *116* (17), 9914-9993; (c) Ghogare, A. A.; Greer, A., *Chem. Rev.* **2016,** *116* (17), 9994-10034; (d) Cambié, D.; Bottecchia, C.; Straathof, N. J. W.; Hessel, V.; Noël, T., *Chem. Rev.* **2016,** *116* (17), 10276-10341; (e) Poplata, S.; Tröster, A.; Zou, Y.-Q.; Bach, T., *Chem. Rev.* **2016,** *116* (17), 9748-9815; (f) Kärkäs, M. D.; Porco, J. A.; Stephenson, C. R. J., *Chem. Rev.* **2016,** *116* (17), 9683-9747; (g) Arias-Rotondo, D. M.; McCusker, J. K., *Chem. Soc. Rev.* **2016,** *45* (21), 5803-5820; (h) Oelgemöller, M.; Hoffmann, N., *Org. Biomol. Chem.* **2016,** *14*; (i) Oelgemöller, M., *Chem. Rev.* **2016,** *116* (17), 9664-9682.

46. Albini, A.; Fagnoni, M., *Handbook of synthetic photochemistry*. WILEY-VCH Verlag GmbH & Co. KGaA: Weinheim, 2010.

47. (a) Hoffmann, N., *Chem. Rev.* **2008,** *108* (3), 1052-1103; (b) Yoon, T. P., *ACS Catal.* **2013,** *3* (5), 895-902; (c) Teegardin, K.; Day, J. I.; Chan, J.; Weaver, J., *Org. Process Res. Dev.* **2016,** *20* (7), 1156-1163; (d) Staveness, D.; Bosque, I.; Stephenson, C. R. J., *Acc. Chem. Res.* **2016,** *49* (10), 2295-2306; (e) Ravelli, D.; Protti, S.; Fagnoni, M., *Chem. Rev.* **2016,** *116* (17), 9850-9913.

48. Gao, X.-W.; Meng, Q.-Y.; Xiang, M.; Chen, B.; Feng, K.; Tung, C.-H.; Wu, L.-Z., *Adv. Synth. Catal.* **2013,** *355* (11-12), 2158-2164.

49. Yoon, T. P.; Ischay, M. A.; Du, J., *Nat. Chem.* **2010,** *2* (7), 527 - 532.

50. (a) Lu, Z.; Shen, M.; Yoon, T. P., *J. Am. Chem. Soc.* **2011,** *133* (5), 1162-1164; (b) Lin, S.; Ischay, M. A.; Fry, C. G.; Yoon, T. P., *J. Am. Chem. Soc.* **2011,** *133* (48), 19350-19353; (c) Parrish, J. D.; Ischay, M. A.; Lu, Z.; Guo, S.; Peters, N. R.; Yoon, T. P., *Org. Lett.* **2012,** *14* (6), 1640-1643.

51. Tucker, J. W.; Narayanam, J. M. R.; Krabbe, S. W.; Stephenson, C. R. J., *Org. Lett.* **2010,** *12* (2), 368-371.

52. (a) Galindo, F., *J. Photochem. Photobiol. C Photochem. Rev.* **2005,** *6* (2-3), 123-138; (b) Coppinger, G. M.; Bell, E. R., *J. Phys. Chem.* **1966,**

70 (11), 3479-3489; (c) Belluč, D.; Hrdlovič, P., *Chem. Rev.* **1967,** *67* (6), 599-609.

53. (a) Neufeldt, S. R.; Sanford, M. S., *Adv. Synth. Catal.* **2012,** *354* (18), 3517-3522; (b) Kalyani, D.; McMurtrey, K. B.; Neufeldt, S. R.; Sanford, M. S., *J. Am. Chem. Soc.* **2011,** *133* (46), 18566-18569.

54. Hernández-Linares, M. G.; Guerrero-Luna, G.; Pérez-Estrada, S.; Ellison, M.; Ortin, M.-M.; Garcia-Garibay, M. A., *J. Am. Chem. Soc.* **2015,** *137* (4), 1679-1684.

55. Fischer, M., *Angew. Chem. Int. Ed.* **1978,** *17* (1), 16-26.

56. (a) Aillet, T.; Loubiere, K.; Dechy-Cabaret, O.; Prat, L., *Chem. Eng. Process.: Process Intensification* **2013,** *64*, 38-47; (b) Funken, K.-H.; Müller, F.-J.; Ortner, J.; Riffelmann, K.-J.; Sattler, C., *Energy* **1999,** *24* (8), 681-687.

57. Turconi, J.; Griolet, F.; Guevel, R.; Oddon, G.; Villa, R.; Geatti, A.; Hvala, M.; Rossen, K.; Göller, R.; Burgard, A., *Org. Process Res. Dev.* **2014,** *18* (3), 417-422.

58. Ravelli, D.; Protti, S.; Neri, P.; Fagnoni, M.; Albini, A., *Green Chem.* **2011,** *13* (7), 1876-1884.

59. Su, Y.; Straathof, N. J. W.; Hessel, V.; Noël, T., *Chem. Eur. J.* **2014,** *20* (34), 10562-10589.

60. Constable, D. J. C.; Curzons, A. D.; Cunningham, V. L., *Green Chem.* **2002,** *4* (6), 521-527.

61. Carreño, M. C.; Somoza, Á.; Ribagorda, M.; Urbano, A., *Chem. Eur. J.* **2007,** *13* (3), 879-890.

62. (a) Diorazio, L. J.; Hose, D. R. J.; Adlington, N. K., *Org. Process Res. Dev.* **2016,** *20* (4), 760-773; (b) Henderson, R. K.; Jimenez-Gonzalez, C.; Constable, D. J. C.; Alston, S. R.; Inglis, G. G. A.; Fisher, G.; Sherwood, J.; Binks, S. P.; Curzons, A. D., *Green Chem.* **2011,** *13* (4), 854-862; (c) Prat, D.; Pardigon, O.; Flemming, H.-W.; Letestu, S.; Ducandas, V.; Isnard, P.; Guntrum, E.; Senac, T.; Ruisseau, S.; Cruciani, P.; Hosek, P., *Org. Process Res. Dev.* **2013,** *17* (12), 1517-1525.

63. Curzons, A. D.; Constable, D. J. C.; Mortimer, D. N.; Cunningham, V. L., *Green Chem.* **2001,** *3* (1), 1-6.

64. (a) G. Griesbeck, A.; Kramer, W.; Oelgemöller, M., *Green Chem.* **1999,** *1* (4), 205-208; (b) DeLaney, E. N.; Lee, D. S.; Elliott, L. D.; Jin, J.; Booker-Milburn, K. I.; Poliakoff, M.; George, M. W., *Green Chem.* **2017,** *19* (6), 1431-1438.

65. Dichiarante, V.; Fagnoni, M., *Synlett* **2008,** *2008* (6), 787-800.

66. Palmisano, G.; Yurdakal, S.; Augugliaro, V.; Loddo, V.; Palmisano, L., *Adv. Synth. Catal.* **2007,** *349* (6), 964-970.

67. Dondi, D.; Caprioli, I.; Fagnoni, M.; Mella, M.; Albini, A., *Tetrahedron* **2003,** *59* (7), 947-957.

68. Han, X.; Bourne, R. A.; Poliakoff, M.; George, M. W., *Chem. Sci.* **2011,** *2* (6), 1059-1067.

69. Oakes, R. S.; Clifford, A. A.; Rayner, C. M., *J. Chem. Soc. Perk. T. 1* **2001,** (9), 917-941.

70. Hrnjez, B. J.; Mehta, A. J.; Fox, M. A.; Johnston, K. P., *J. Am. Chem. Soc.* **1989,** *111* (7), 2662-2666.

71. Han, X.; Bourne, R. A.; Poliakoff, M.; George, M. W., *Green Chem.* **2009,** *11* (11), 1787-1792.

72. Born, M.; Oppenheimer, R., *Ann. d. Phys.* **1927,** *389* (20), 457-484.

73. Perdew, J. P.; Ernzerhof, M.; Burke, K., *J. Chem. Phys.* **1996,** *105* (22), 9982-9985.

74. (a) Becke, A. D., *J. Chem. Phys.* **1993,** *98* (2), 1372-1377; (b) Becke, A. D., *J. Chem. Phys.* **1993,** *98* (7), 5648-5652; (c) Lee, C.; Yang, W.; Parr, R. G., *Phys. Rev. B.* **1988,** *37* (2), 785-789.

75. Koch, W.; Holthausen, M. C., *A Chemist's Guide to Density Functional Theory*. Second ed.; Wiley-VCH Verlag GmbH: Weinheim, 2001.

76. Foresman, J. B.; Frisch, Æ., *Exploring chemistry with electronic structure methods*. second ed.; Gaussian: Pittsburgh, Pa., 1996.

77. Kopp, G.; Lean, J. L., *Geophys. Res. Lett.* **2011,** *38* (1).

78. (a) BP *Statistical review of world energy June 2015*; 2015; (b) Navarro, R. M.; Sanchez-Sanchez, M. C.; Alvarez-Galvan, M. C.; Valle, F. d.; Fierro, J. L. G., *Energy Environ. Sci.* **2009,** *2* (1), 35-54.

79. Administration, U. S. E. I., **2015**.

80. http://coolcalifornia.org/science-of-cool-roofs (accessed March 2014).

81. Protti, S.; Ravelli, D.; Fagnoni, M.; Albini, A., *Chem. Commun.* **2009**, 7351-7353.

82. Yoshimi, Y.; Nishio, A.; Hayashi, M.; Morita, T., *J. Photoch. Photobio. A.* **2016,** *331*, 17-21.

83. Oelgemöller, M.; Jung, C.; Ortner, J.; Mattay, J.; Zimmermann, E., *Green Chem.* **2005,** *7* (1), 35-38.

84. Oelgemöller, M., *J. Chin. Chem. Soc.* **2014,** *61* (7), 743-748.

85. Monnerie, N.; Ortner, J. r., *J. Sol. Energy Eng.* **2001,** *123* (2), 171-174.

86. Jo, W.-K.; Tayade, R. J., *Ind. Eng. Chem. Res.* **2014,** *53* (6), 2073-2084.

87. Meyer, S.; Tietze, D.; Rau, S.; Schäfer, B.; Kreisel, G., *J. Photoch. Photobio. A.* **2007,** *186* (2–3), 248-253.

88. Griesbeck, A. G.; Maptue, N.; Bondock, S.; Oelgemöller, M., *Photochem. Photobiol. Sci.* **2003,** *2* (4), 450-451.

89. Lomaev, M., I.; Skakun, V. S.; Sosnin, E. A.; Tarasenko, V., F.; Shitts, D. V.; Erofeev, M. V., *Physics-Uspekhi* **2003,** *46* (2), 193.

90. (a) *CRC Handbook of Organic Photochemistry and Photobiology*. Third edition ed.; CRC Press, Taylor and Francis Group: Boca Raton, Florida, 2012; Vol. 1; (b) Lomaev, M. I.; Sosnin, E. A.; Tarasenko, V. F., *Prog. Quantum Electron.* **2012,** *36* (1), 51-97.

91. Sosnin, E. A.; Oppenländer, T.; Tarasenko, V. F., *J. Photochem. Photobiol. C Photochem. Rev.* **2006,** *7* (4), 145-163.

92. Boyd, I. W.; Zhang, J. Y., *Nucl. Instrum. Methods Phys. Res. B* **1997,** *121* (1–4), 349-356.

93. Lomaev, M. I.; Sosnin, E. A.; Tarasenko, V. F., *Chem. Eng. Technol.* **2016,** *39* (1), 39-50.

94. (a) Al-Gharabli, S.; Engeßer, P.; Gera, D.; Klein, S.; Oppenländer, T., *Chemosphere* **2016,** *144*, 811-815; (b) Arany, E.; Láng, J.; Somogyvári, D.; Láng, O.; Alapi, T.; Ilisz, I.; Gajda-Schrantz, K.; Dombi, A.; Kőhidai, L.; Hernádi, K., *Sci. Total Environ.* **2014,** *468–469*, 996-1006.

95. Jas, G.; Kirschning, A., *Chem. Eur. J.* **2003,** *9* (23), 5708-5723.

96. (a) Mason, B. P.; Price, K. E.; Steinbacher, J. L.; Bogdan, A. R.; McQuade, D. T., *Chem. Rev.* **2007,** *107* (6), 2300-2318; (b) Plutschack, M. B.; Pieber, B.; Gilmore, K.; Seeberger, P. H., *Chem. Rev.* **2017,** *117* (18), 11796-11893.

97. (a) Webb, D.; Jamison, T. F., *Chem. Sci.* **2010,** *1* (6), 675-680; (b) Lange, H.; Carter, C. F.; Hopkin, M. D.; Burke, A.; Goode, J. G.; Baxendale, I. R.; Ley, S. V., *Chem. Sci.* **2011,** *2* (4), 765-769; (c) Chernyak, N.; Buchwald, S. L., *J. Am. Chem. Soc.* **2012,** *134* (30), 12466-12469.

98. (a) Oger, N.; Le Grognec, E.; Felpin, F.-X., *Org. Chem. Front.* **2015,** *2* (5), 590-614; (b) Wegner, J.; Ceylan, S.; Kirschning, A., *Chem. Commun.* **2011,** *47* (16), 4583-4592.

99. Anderson, N. G., *Org. Process. Res. Dev.* **2012,** *16* (5), 852-869.

100. (a) Bou-Hamdan, F. R.; Seeberger, P. H., *Chem. Sci.* **2012,** *3* (5), 1612-1616; (b) Tucker, J. W.; Zhang, Y.; Jamison, T. F.; Stephenson, C. R. J., *Angew. Chem. Int. Ed.* **2012,** *51* (17), 4144-4147; (c) Neumann, M.; Zeitler, K., *Org. Lett.* **2012,** *14* (11), 2658-2661; (d) Nguyen, J. D.; Rei; Dai, C.; Stephenson, C. R. J., *Chem. Commun.* **2013,** *49* (39), 4352-4354.

101. (a) Elliott, L. D.; Knowles, J. P.; Koovits, P. J.; Maskill, K. G.; Ralph, M. J.; Lejeune, G.; Edwards, L. J.; Robinson, R. I.; Clemens, I. R.; Cox, B.; Pascoe, D. D.; Koch, G.; Eberle, M.; Berry, M. B.; Booker-Milburn, K. I., *Chem. Eur. J.* **2014,** *20* (46), 15226-15232; (b) McQuade, D. T.; Seeberger, P. H., *J. Org. Chem.* **2013,** *78* (13), 6384-6389.

102. Hook, B. D. A.; Dohle, W.; Hirst, P. R.; Pickworth, M.; Berry, M. B.; Booker-Milburn, K. I., *J. Org. Chem.* **2005,** *70* (19), 7558-7564.

103. Bourne, R. A.; Han, X.; Chapman, A. O.; Arrowsmith, N. J.; Kawanami, H.; Poliakoff, M.; George, M. W., *Chem. Commun.* **2008**, 4457-4459.

104. Han, X. PhD Thesis. University of Nottingham, Nottingham, 2010.

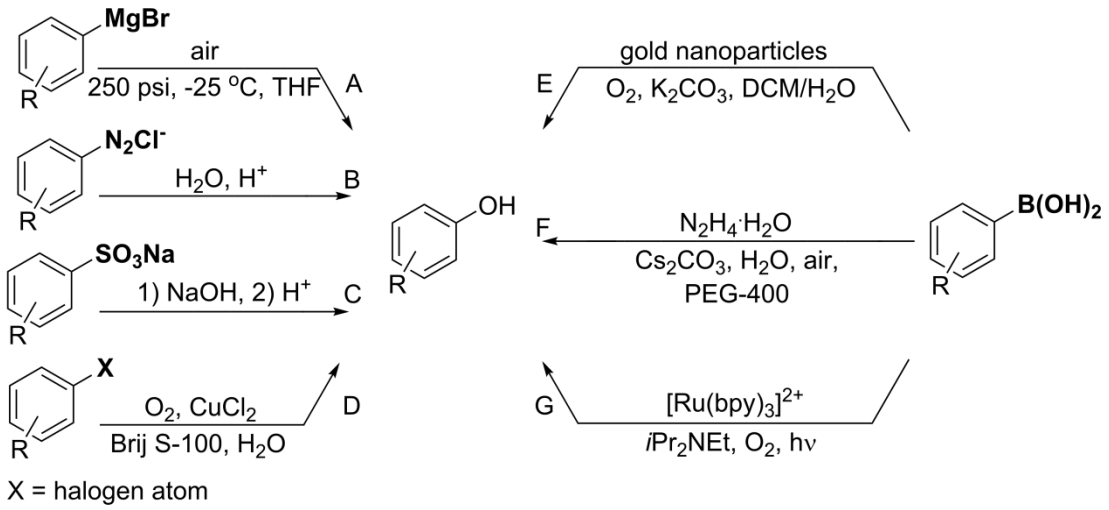
105. Hall, J. F. B.; Han, X.; Poliakoff, M.; Bourne, R. A.; George, M. W., *Chem. Commun.* **2012,** *48* (25), 3073-3075.

106. (a) Amara, Z.; Bellamy, J., F. B.; Horvath, R.; Miller, S. J.; Beeby, A.; Burgard, A.; Rossen, K.; Poliakoff, M.; George, M. W., *Nat. Chem.* **2015,** *7* (6), 489-495; (b) Hall, J. F. B.; Bourne, R. A.; Han, X.; Earley, J. H.; Poliakoff, M.; George, M. W., *Green Chem.* **2013,** *15* (1), 177-180.

107. Griesbeck, A. G.; Meierhenrich, U. J., *Angew. Chem. Int. Ed.* **2002,** *41* (17), 3147-3154.

Chapter 2 Hydroxylation of Boronic Acids

As stated in Chapter 1, visible light photoredox catalysis is a rapidly expanding field of research.[1] One of the main focus points of previous work at the University of Nottingham has been the incorporation of oxygen into compounds *via* the generation of singlet oxygen,[2] both in conventional solvents and in $scCO_2$. A continuous flow visible light photoreactor was built for continuous flow photochemical reactions in $scCO_2$ and the details of this reactor can be found in the Experimental Chapter. The work carried out for this Chapter utilises visible light for the efficient formation of aryl alcohols. The introduction of an aromatic alcohol moiety in compounds is a desirable transformation as they are versatile synthetic intermediates[3] with many pharmaceuticals containing these moieties as they exhibit antibacterial, antiviral, cardioprotective and antimutagenicity activities.[4] New and more efficient methodologies to generate this functional group are highly desirable. Reactions producing aryl alcohols have been studied widely and many different methods have been developed as shown in Scheme 2-1.



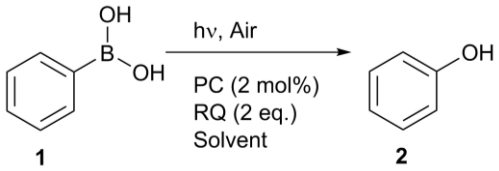
Scheme 2-1 Various reported synthetic routes to aryl alcohols, showing a range of starting materials and corresponding conditions to transform aryl compounds to aryl alcohols. Abbreviations used are POF = porous organic framework, MOF = metal organic framework, MB = methylene blue, QN = quinone, EY = Eosin Y.

He *et al.* reported the oxidation of aryl Grignard compounds towards a range of aryl alcohols using compressed air (Scheme 2-1, route A).[4b] Aryl alcohols have also been synthesised *via* the hydrolysis of aryl diazonium salts (Scheme 2-1, route B) or the pyrolysis of the sodium salt of benzenesulfonic acid (Scheme 2-1, route C).[3a-c, 4b] However, these methods require harsh oxidants and often suffer from poor functional group compatibility and a narrow substrate scope.[3b] In addition, aryl diazonium salts are potentially explosive and introduce an additional safety concern into process design. Nucleophilic aromatic substitution reactions *via* the hydroxylation of aromatic halides (Scheme 2-1, route D) potentially offer a larger substrate scope, but the metal catalysts that are being used are often toxic and more expensive than organic photocatalysts.[3b]

Aryl boronic acids have been recognised as valuable alternative starting materials for the synthesis of aryl alcohols since they are widely available, non-toxic and stable.[4a] Although aryl boronic acids often react under mild conditions, numerous literature examples still employ transition metals (Scheme 2-1, route E).[3b, 3d, 5] Organic oxidants can be used as an alternative to transition metal oxidants (Scheme 2-1, route F), but these organic reagents can be corrosive or toxic.[6] More benign organic oxidants have been used, but these reactions generally require elevated temperatures (80 °C),[7] or the use of chlorinated solvents like

dichloromethane and trifluoroethanol, or prolonged reaction times (up to 48 h).[8] Electrochemical routes have also been employed as well for the conversion of aryl boronic acids to aryl alcohols.[9]

Molecular oxygen has been recognised as an attractive oxidation source since it is environmentally benign and is abundant in the atmosphere.[10] However, molecular oxygen often requires activation in order for it to react with organic substrates. Traditionally, transition metals have been utilised to activate molecular oxygen in order for it to react,[3b, 11] but a more sustainable route involves the use of visible light to activate molecular oxygen.[10a, 12] In 2012, Zou *et al*. published the first visible light photocatalytic pathway towards aryl alcohols (Scheme 2-1, route G) using mild conditions such as air as the green oxidant source without elevated temperatures.[13] However, the use of scarce and toxic transition metal catalysts containing either ruthenium or iridium prevents this method from being a green route. Employing this method, even electron-rich aryl alcohols, which are generally difficult to generate *via* nucleophilic substitution of aryl halides, were easily obtained.[13] This aerobic oxidative hydroxylation reaction of aryl boronic acids was carried out using $[Ru(bpy)_3]Cl_2.6H_2O$ as the photocatalyst (Scheme 2-2).



*Scheme 2-2 Visible light photoredox catalysed hydroxylation of phenylboronic acid (**1**) to phenol (**2**), employing visible light (hv), air, a photocatalyst (PC) and a reductive quencher (RQ).[13]*

High yields of aryl alcohol were obtained (77-93 %) using moderate to long reaction times (28-96 h). The reaction was found to be most efficient when carried out in DMF as it went to completion in either 28 and 48 hours, using respectively *N,N*-diisopropylethylamine (DIPEA) or triethylamine (TEA) as the sacrificial reductive quencher. Section 2.1 will give more details of the mechanism proposed for this reaction. The effect of carrying out this reaction in a range of solvents including water and ethanol was examined, but longer reaction

times were required to reach full conversion to the aryl alcohol.[13] In water, the maximum yield was only 60 %.

Since this publication of Zou *et al.*'s photochemical route for the transformation of aryl boronic acids to aryl alcohols in 2012, multiple alternative photochemical routes have been reported, using both transition metal and organic photocatalysts.[14] Recently, a one-pot synthesis was reported to transform aryl halides into aryl alcohols where the aryl halides were reacted photochemically with diboron species to provide aryl boronic esters and subsequent photochemical hydroxylation of these aryl boronic esters yielded aryl alcohols.[15]

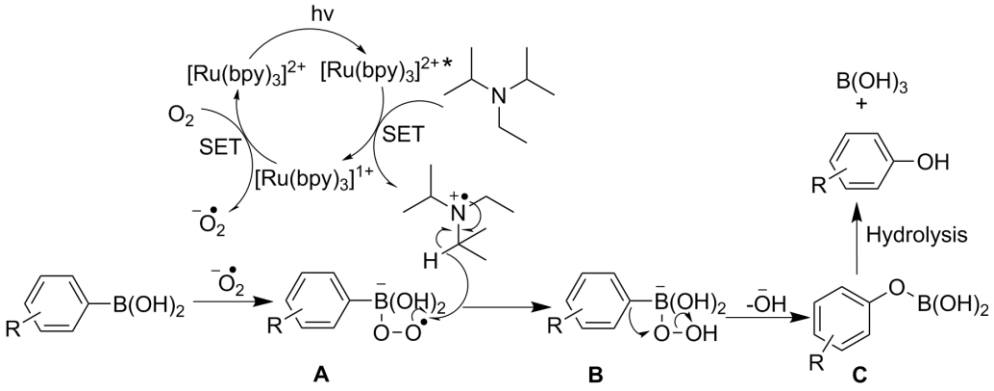
Organic photocatalysts are desirable alternatives to transition metal catalysts, as they are often less toxic and utilise more abundantly available elements. Methylene blue,[14d] Eosin Y,[14a] a flavin derivative,[14f] an acridinium salt,[14f] anthraquinone,[14c] porphyrin[16] and carbazole[14b] derivatives have all been employed to catalyse the hydroxylation of aryl boronic acids. However, relatively long reaction times (6-24 h) were needed to achieve full conversion of the aryl boronic acid to the corresponding aryl alcohol. In an attempt to further limit the generation of waste from photocatalytic reactions, porous organic frameworks (POFs) and metal organic frameworks (MOFs) have been designed to encapsulate the photocatalyst,[14b, 14e, 16] and recycling was possible over a number of cycles. However, long reaction times up to 48 hours were required to achieve high yields using these catalysts.

Ideally, short reaction times and mild conditions are present in the synthesis of aryl alcohols because long reaction times present a limitation in the scale-up of batch photochemical processes.[17] Therefore, this Chapter describes the use of continuous flow photochemistry for the hydroxylation of boronic acids, exploring faster reactions and potentially better processes. Furthermore, the safety aspects for this reaction considering the presence of oxygen in a scaled-up reaction are potentially reduced by carrying out the reaction in continuous flow. This is because a smaller reaction volume is used and therefore less of the potentially explosive mixture is in close proximity to the light. The Sections below describe the proposed mechanisms for the conversion of **1** to **2** and the results of using a flow photoreactor built in-house, air rather than pure oxygen, and organic photocatalysts for this specific synthetic transformation. Some modifications to the previously developed equipment are highlighted.

2.1 Mechanism of Boronic Acid Hydroxylation

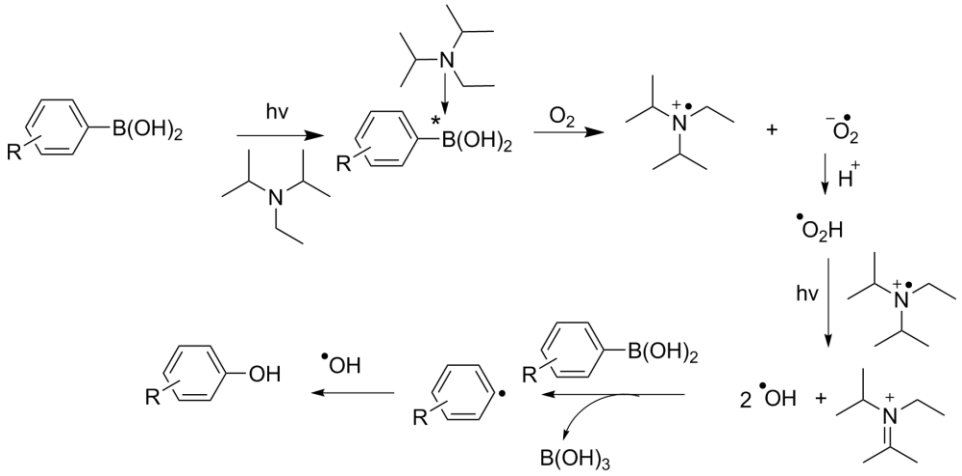
2.1.1 Mechanisms in Literature

The hydroxylation of boronic acids to form aryl alcohols is part of the work presented in this Thesis. An initial mechanism for this transformation was proposed by Zou *et al.*[13] and is depicted in Scheme 2-3. After excitation of the photocatalyst, *N*,*N*-diisopropylethylamine (DIPEA) reductively quenches the excited state of the photocatalyst *via* a single electron transfer (SET) process, forming a cationic amine radical and $[Ru^{II}(bpy)_3^{-\bullet}]^+$, abbreviated as the $[Ru^I]$ complex. SET between molecular oxygen and this $[Ru^I]$ complex forms a superoxide radical anion ($O_2^{-\bullet}$) and regenerates the ground state photocatalyst. Then $O_2^{-\bullet}$ undergoes nucleophilic addition to the empty p_z orbital of the boron atom in the aryl boronic acid to form peroxy borate **A**. Suggested by the authors, this complex then abstracts a hydrogen atom from the radical cationic amine to form hydroperoxy borate (**B**). However, as both radical complex **A** and the cationic amine radical are believed to be short lived, it might be possible that complex **A** abstracts a hydrogen atom from DIPEA instead. Subsequently, the benzene ring inserts into the peroxygen moiety forming complex **C**, followed by hydrolysis, generating the aryl alcohol and boric acid. Similar mechanisms have been reported for the formation of aryl alcohols from boronate complexes.[18]



Scheme 2-3 Mechanism of hydroxylation of aryl boronic acids as proposed by Zou et al.[13] involving the photocatalytic generation of superoxide which subsequently inserts into the aryl boronic acid, followed by insertion of aryl moiety into a peroxygen moiety and hydrolysis to form aryl alcohols.

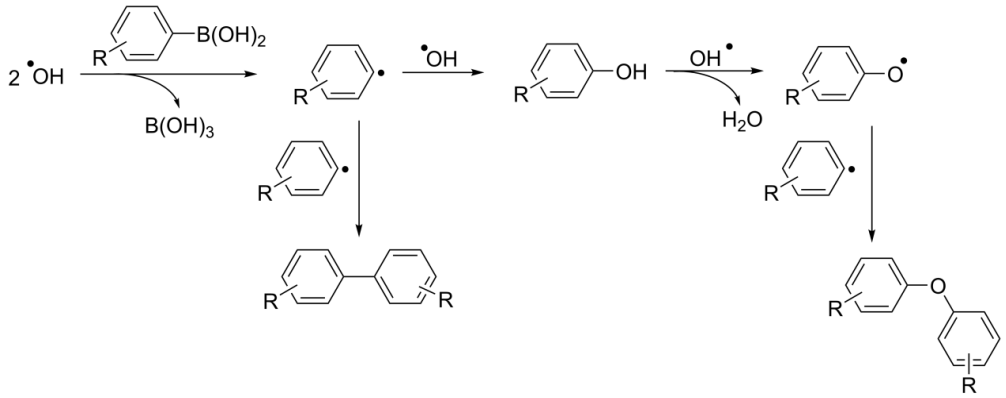
Zou *et al.* performed quantum chemical calculations on the transition from complex **B** to **C** and their results suggested that it is not the carbon-boron σ bond but the benzene ring that attacks the peroxygen atom in complex **B**; this rearrangement is believed to be concerted. In 2014, Jiang *et al.* reported the hydroxylation of aryl boronic acids to form aryl alcohols using a tertiary amine, air and light, omitting the photocatalyst.[19] However, prolonged reaction times were required for the conversion of aryl boronic acids to aryl alcohols. They obtained biphenyl and diphenyl ether as by-products which could not be explained by the mechanism originally proposed by Zou *et al*. These researchers undertook electron paramagnetic resonance (EPR) experiments to investigate the mechanism of this reaction further.[19] These experiments revealed the presence of both hydroxyl free radicals and carbon-centred free radicals and this led to the proposal of an alternative mechanism as shown in Scheme 2-4.



Scheme 2-4 Proposed mechanism for the hydroxylation of aryl boronic acids as reported by Jiang et al.[19] involving the formation of an aryl boronic acid-amine exciplex, the reaction of a hydroxyl radical with the aryl boronic acid to form an aryl radical to which another hydroxyl radical can add to form the aryl alcohol.

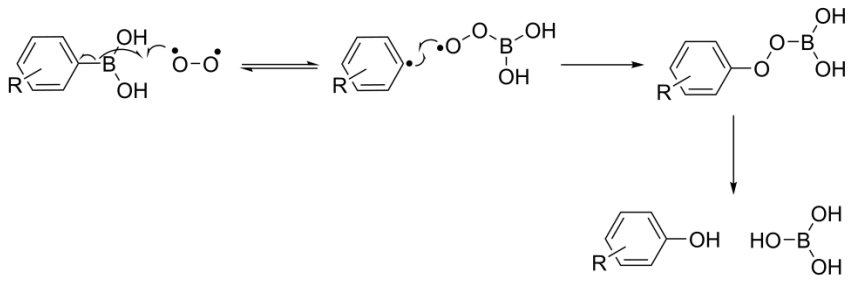
In this mechanism, no photocatalyst is required as the light directly interacts with the aryl boronic acid-amine complex and an exciplex is formed consisting of DIPEA and the aryl boronic acid. This excited state complex then interacts with ground state dioxygen to form both a superoxide and a DIPEA radical. After protonation of the superoxide radical by water, a second photochemical step takes place involving the DIPEA radical cation to generate two hydroxyl radicals and a cationic amine by-product. Subsequently, the hydroxyl radical can react

with the aryl boronic acid to generate an aryl radical and boric acid. Another hydroxyl radical adds to the aryl radical to form the aryl alcohol. The formation of biphenyl was explained by the coupling of two aryl radicals as shown in Scheme 2-5. Diaryl ether was formed by the reaction of the aryl alcohol with a hydroxyl radical, and subsequent coupling with an aryl radical.



Scheme 2-5 Mechanism of by-product formation in the hydroxylation of aryl boronic acids as proposed by Jiang et al.[19] involving the coupling of two aryl radicals and the formation of a diaryl ether.

Although the existence of a hydroxyl free radical was found by Jiang *et al.* during EPR experiments, this does not necessarily result in participation in the hydroxylation mechanism. The hydroxyl free radical is believed to be very reactive and able to rapidly abstract a hydrogen atom from an amine species. As a result, the likelihood that the hydroxyl free radical and the aryl radical meet to form the aryl alcohol is low. It could be proposed that the formation of an aryl radical originates from a S_H2 reaction between molecular oxygen and an aryl boronic acid (Scheme 2-6).[20] The two formed radicals can recombine to form a peroxide species, followed by the formation of the aryl alcohol and boric acid. This alternative mechanism would also explain the formation of both the biaryl compound and the diaryl ether by-product.



Scheme 2-6 Alternative proposed mechanism for the findings by Jiang et al. in the hydroxylation of aryl boronic acid.

Before undertaking experimental work, quantum chemical calculations were carried out to investigate the mechanistic aspects of this reaction further and to shed light on which of the two mechanisms is more thermodynamically favourable. The results will be discussed in the next Section. Moreover, rate-determining steps can possibly be identified by performing these calculations which was thought to be helpful in the process of reaction optimisation.

2.1.2 Quantum Chemical Computations

DFT calculations have been used by Zou *et al.* to investigate the mechanism of the hydroxylation of phenylboronic acid (**1**) to phenol (**2**).[13] As part of this Thesis, it was attempted to extend this previously reported DFT work, starting with the mechanism described by Zou *et al*.[13] All computations were carried out with Gaussian version 03 using the B3LYP functional, and 6-311+G(d,p) as the basis set.[21] The energy of each molecule involved in the reaction and its most stable orientation was calculated, initially without solvent correction, in vacuum. In order to mimic the experimental reaction environment better, a polarisable continuum solvent model was introduced into the DFT calculations. The reactants and intermediates involved in the hydroxylation of **1** are highly polarised and therefore, the energy of the molecules involved may change in a polarised environment; hence the addition of a solvent field might prove more accurate in calculating reaction mechanisms. Only the results using the solvent field are outlined in this Section. Figure 2-1 shows the calculated free energy of the

complexes involved in the hydroxylation of **1** to **2**. Overall, the reaction has a negative free energy (-111.6 kcal/mol), indicating a thermodynamically favourable reaction. Moreover, the insertion of superoxide into **1** appeared to be the rate-determining step with an energy barrier of 14.7 kcal/mol to the corresponding transition state.

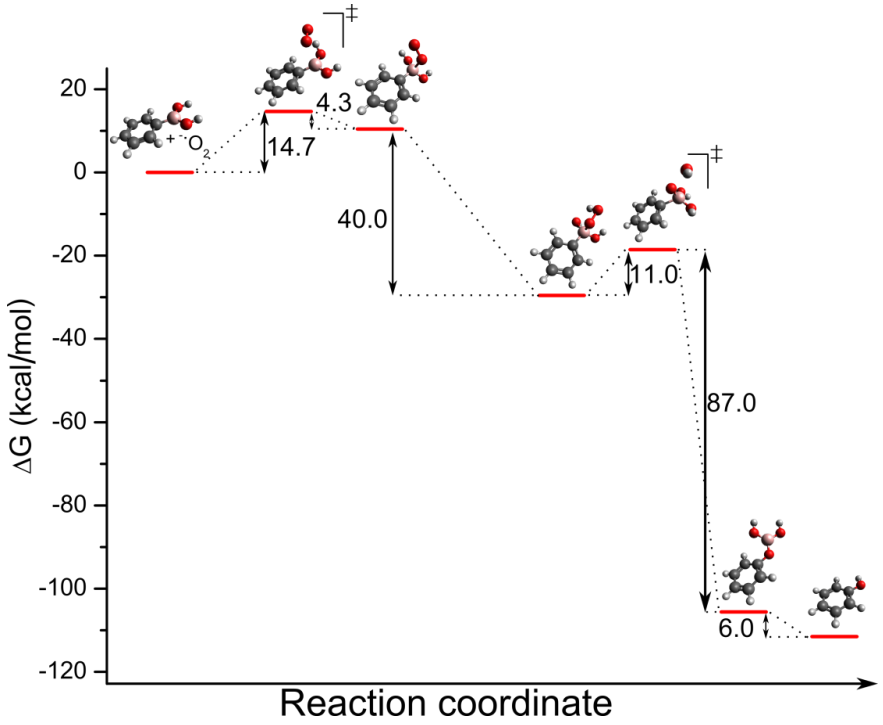
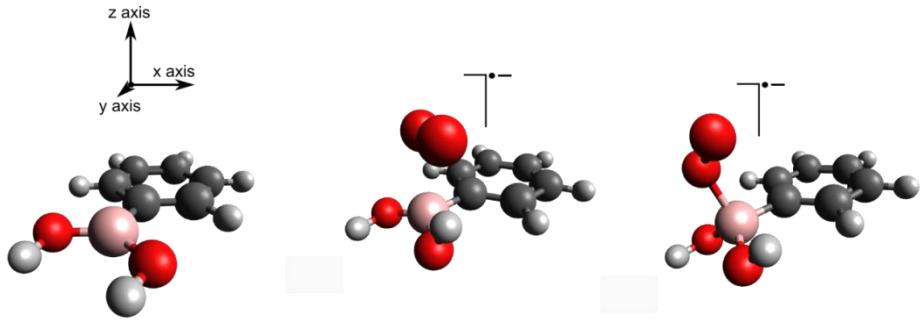


*Figure 2-1 DFT calculations of the hydroxylation of **1** based on the mechanism proposed by Zou et al. using the solvent field parameters of DMF, showing that the insertion of superoxide into **1** exhibits the highest energy barrier. Changes in free energy are relative to the free energy of **1**. Transition state complexes are labelled with the ‡ notation.*

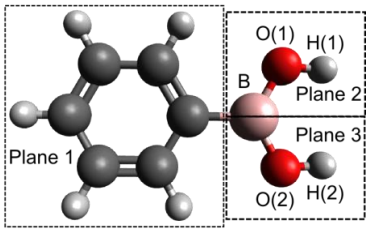
Figure 2-2 shows the view along the y axis of **1** and a superoxide molecule through the insertion of superoxide into **1** as calculated with DFT. The bending of the atoms during this insertion is reflected in torsion angles. Table 2-1 shows the torsion angles in each of the structures represented in Figure 2-2. Phenylboronic acid is an almost planar molecule (P1-2 and P1-3 are close to zero), but the proximity of superoxide forces the boronic acid moiety to bend out of plane, with one hydrogen atom of the hydroxyl group interacting with the superoxide radical. After insertion of the superoxide, the hydroxyl groups in the boronic acid moiety are bent further out of the benzene ring plane, allowing space for the dioxygen moiety.



(a) (b) (c)

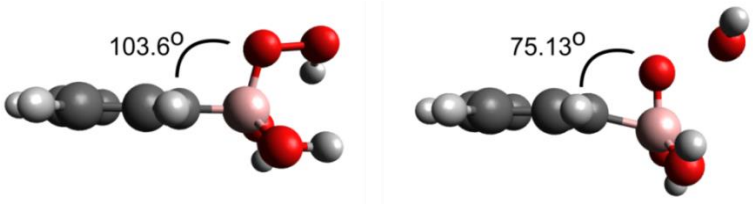
*Figure 2-2 The orientation of **1** as viewed along the y axis during the insertion of superoxide as calculated with DFT. a) ground state **1** (pink = boron, red = oxygen, light grey = hydrogen, dark grey = carbon), b) first transition state, superoxide inserts into **1**, c) superoxide inserted into **1**.*

*Table 2-1 View along the z axis of **1**; plane 1 is the x-y plane of **1**, plane 2 consists of atoms B, O(1) and H(1) while plane 3 consists of atoms B, O(2) and H(2). Torsion angles between planes 1 and 2 (P1-2) and planes 1 and 3 (P1-3) are outlined.*



	P1-2 (°)	P1-3 (°)
Figure 2-2a	0.233	0.258
Figure 2-2b	-3.99	13.9
Figure 2-2c	-13.2	36.5

Another transition state represents the attack of the peroxygen moiety by the benzene ring as depicted in Figure 2-3 (view along x axis of molecule). The C-B-O bond angle changes significantly towards that of an equilateral triangle in this transition state (Figure 2-3b). The boron atom bends out of the plane of the benzene ring and the O-O bond of the peroxygen moiety is extended. This is in good agreement with the calculations performed by Zou *et al.* who proposed a concerted mechanism.[13] The energy of the transition state calculated for this Thesis was found 12.6 kcal/mol lower than the energy of the transition state calculated by Zou *et al*. As expected, there is also a corresponding difference in bond length and angles between the two sets of calculations.



(a) (b)

Figure 2-3 View along the x axis of the compound showing the change in conformation a) before insertion of the benzylic π system into the peroxygen moiety and b) the transitions state of this insertion, showing the near equilateral triangle shape in the transition state.

As experimental work on the hydroxylation of **1** will be conducted in different solvents, all the calculations were repeated with both water and ethanol solvent field parameters. Little difference was observed between solvent polarity and the degree of stabilisation of the charged compounds. The difference in energy between the structures calculated in the different solvent fields was <2.0 kcal/mol and no significant changes in geometry were observed when using the different solvent field parameters.

No quantum chemical calculations were performed by Jiang *et al.* on their proposed mechanism. Therefore, the calculations of this route were attempted as part of this Thesis but were only successful for the addition of the hydroxyl radical to **1** and subsequent steps. Computations were performed to find the optimised ground state and excited state structures of the DIPEA-**1** complex, but no complex formation between the two compounds could be identified using the B3LYP functional. Compared to B3LYP, M06 has more complete correlation and includes dispersion in the functional. Therefore, this functional was utilised next to improve on the calculation of the long distance interactions between DIPEA and **1**. Although the optimised complex was closer in space (3.071 Å instead of the 4.679 Å found previously with the B3LYP functional), this is still too far away for any plausible non-covalent interactions.

From the reaction steps computed, the rate-determining step was calculated to be the insertion of the hydroxyl radical into **1**, with an activation barrier of 17.1 kcal/mol to the corresponding transition state (Figure 2-4).

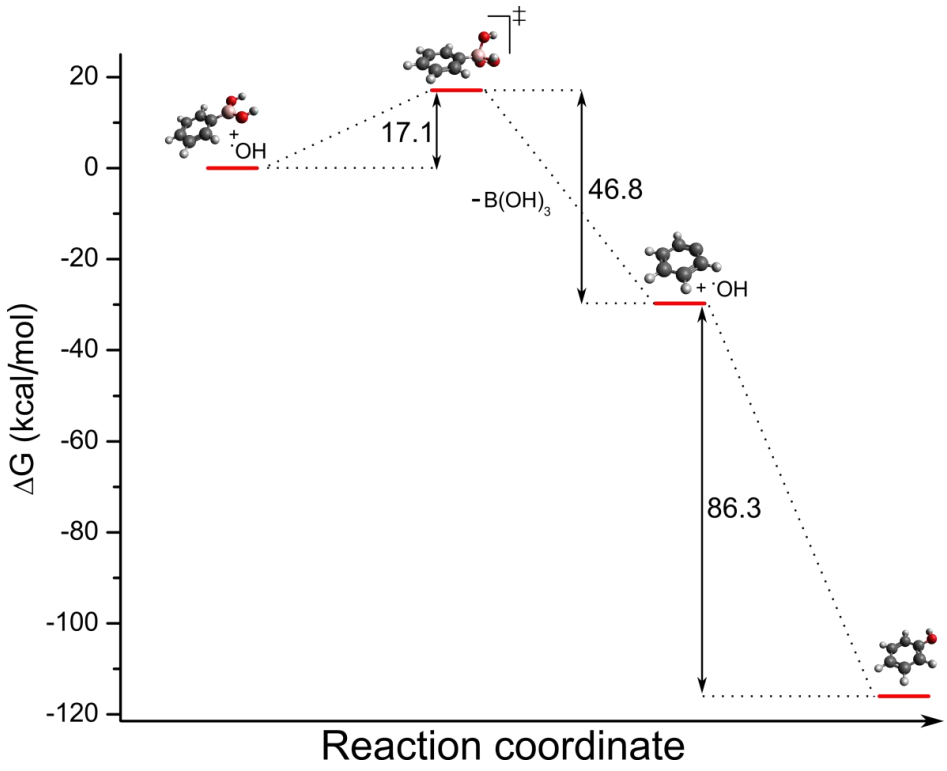
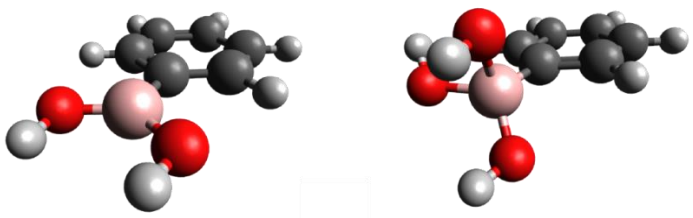


*Figure 2-4 DFT calculations of the insertion of a hydroxyl radical into **1** and subsequent steps in the hydroxylation of **1** based on the mechanism proposed by Jiang et al. using the solvent field parameters of DMF showing that the reaction between **1** and the hydroxyl radical exhibits the highest energy barrier.*

In the transition state of the insertion of the hydroxyl radical into **1**, the boron atom and one of the two oxygen atoms remain in the plane of the benzene ring (Figure 2-5b). The other oxygen atom bends out of the plane of the benzene ring.



(a) (b)

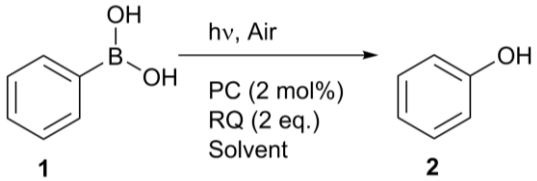
*Figure 2-5 View along the y axis of a) ground state **1** and b) the transition state of the insertion of a hydroxyl radical into **1**, showing the distortion of the almost planar structure of **1** during the insertion of the hydroxyl radical.*

No transition state was found in the addition of the hydroxyl radical and the aryl radical which is intuitive as the combination of two radicals is very favourable.

Comparing the two proposed mechanisms, the activation energy for the calculated rate-determining step is lower for the mechanism proposed by Zou *et al.* compared to the mechanism proposed by Jiang *et al.*, suggesting a more easily accessible route. It is important to note that the calculated rate-determining steps may not be the true rate-determining step as the initial excitation of the reactant and the excited state lifetime of the subsequently formed species need to be considered. Although these were not calculated for this Thesis, the calculations provided more detail on various steps in the reaction compared to the two literature precedents by Zou *et al.* and Jiang *et al.*

2.2 Phenol Synthesis in Batch

The first reaction that was studied was the hydroxylation of phenylboronic acid (**1**) to form phenol (**2**) (Scheme 2-7).[13, 14d] This transformation was chosen to study and optimise reaction parameters both in batch and flow in order to provide insight into the reaction mechanism. This was envisioned to help with further hydroxylation studies as presented in Section 2.5. The hydroxylation of **1** was carried out initially in batch in order to screen reaction conditions. The reaction set-up consisted of one LED light bank irradiating the reaction mixture inside a round bottom flask. The reaction mixture was cooled in a water bath. Details of the set-up can be found in the Experimental Chapter.



*Scheme 2-7 Aerobic hydroxylation of phenylboronic acid (**1**) to phenol (**2**) in batch, employing visible light (hv), air as the oxygen source, a photocatalyst (PC) and a reductive quencher (RQ).*

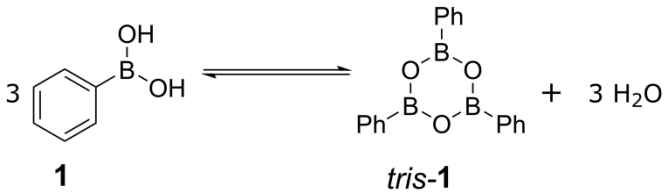
Initially, conditions as described by Zou *et al.* were replicated for the conversion of phenylboronic acid to phenol,[13] using $[Ru(bpy)_3]Cl_2$ as the photocatalyst, using both triethylamine (TEA) and *N*,*N*-diisopropylethylamine (DIPEA) as the reductive quencher, with **1** (0.1 M) in DMF. Later experiments were carried out using Rose Bengal (RB) as a photocatalyst and ascorbic acid (H_2A) as the reductive quencher. All reactants were added together in a round bottom flask, equipped with a condenser open to air. The mixture was stirred and irradiated with a fan cooled array of visible light LEDs until full conversion of the starting material. Aliquots taken during this time were quenched with brine and extracted using diethyl ether before analysis by ^{1}H NMR spectroscopy.

*Table 2-2 Initial screening of reaction conditions for the conversion of phenylboronic acid (**1**) to phenol (**2**).*

Entry	Solvent	Photocatalyst (PC)	Reductive quencher (RQ)	Maximum conversion	Time
1	DMF	$[Ru(bpy)_3]Cl_2$	TEA	87 %	47 h
2	DMF	$[Ru(bpy)_3]Cl_2$	DIPEA	92 %	30 h
3	DMF	$[Ru(bpy)_3]Cl_2$	H_2A	> 99 %	6 h
4	MeOH	$[Ru(bpy)_3]Cl_2$	H_2A	> 99 %	6 h
5	MeOH	RB	H_2A	24 %	5 h
6	MeOH	RB	DIPEA	98 %	5 h

*Reaction conditions: **1** (0.41 mmol, 0.1 M), PC (2 mol%), RQ (2 eq.), solvent (4 mL), 5x 1000 lumen visible light LEDs, r.t.; RB = Rose Bengal, TEA = trimethylamine, DIPEA = N,N-diisopropylethylamine, H_2A = ascorbic acid*

The improved yield and shorter reaction times obtained when using DIPEA as opposed to TEA (Table 2-2, entries 1,2) most likely originated from the stronger redox potentials of DIPEA, increasing its effectiveness in quenching the excited state photocatalyst. Upon ^{1}H NMR analysis of the starting material mixture in $CDCl_3$, 6 % of triphenylboroxine (*tris*-**1**) was observed next to the signals of **1**. Reversible condensation of **1** can occur towards the formation of a six-membered boroxine complex, driven by the elimination of water (Scheme 2-8).[22]



*Scheme 2-8 The formation of triphenylboroxine (tris-**1**) by condensation of phenylboronic acid (**1**).*

Typical ^{1}H NMR spectra obtained during the reaction after work-up contained aromatic protons in the range of 6.8-8.3 ppm (Figure 2-6). The main components during the reaction are **1** (H_a, H_b, H_c), **2** ($H_{a'}$, $H_{b'}$, $H_{c'}$) and *tris*-**1** ($H_{a''}$, $H_{b''}$, $H_{c''}$). When the aromatic substituent changes from boronic acid to the more electron donating phenol, the protons in the *ortho*- and *para*-position of the aromatic ring are affected mostly by the higher electron density due to resonance structures. Therefore, these protons will shift largely upfield during the hydroxylation process while the protons in the *meta*-position on the aromatic ring only slightly move upfield. The conversion of **1** to **2** was monitored by ^{1}H NMR by taking aliquots at regular intervals and calculated by the ratio of the doublet of phenol to the sum of the doublets of both **1** and *tris*-**1** (Figure 2-6).

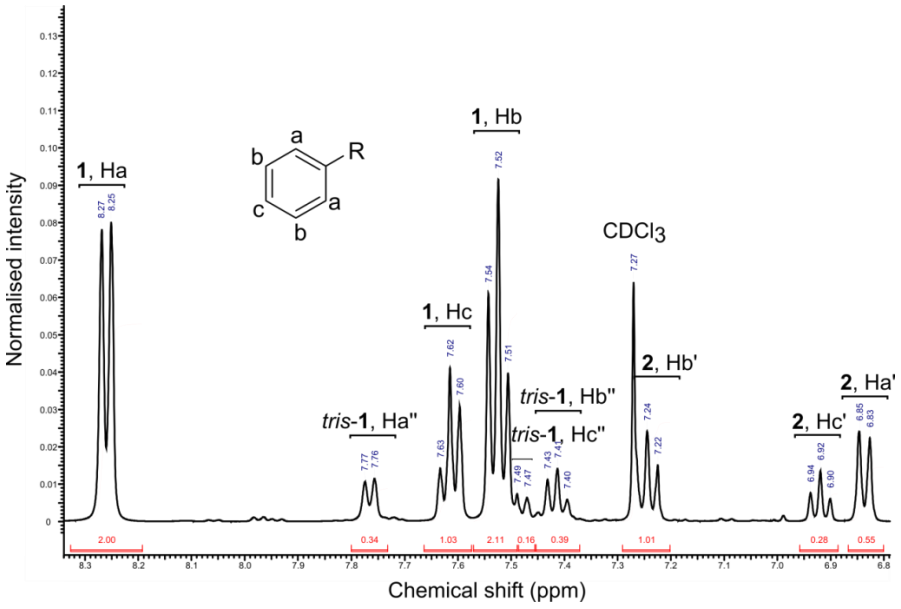


*Figure 2-6 Expanded ^{1}H NMR spectrum (400 MHz, $CDCl_3$) of the oxidative hydroxylation of **1** to **2** in DMF with TEA after 4 h, showing signals of phenylboronic acid (**1**), triphenylboroxine (tris-**1**) and phenol (**2**); R = $B(OH)_2$, $B(O_3B_2Ph_2)$ or OH.*

When the reaction was followed by ^{1}H NMR, data analysis suggested the role of *tris*-**1** as a reaction intermediate (Figure 2-7). While the amount of **1** decreased immediately after irradiation was started, the phenol concentration did not increase at the same rate. Instead, *tris*-**1** was formed more quickly than **2** in the beginning; and as the concentration of *tris*-**1** decreased after 23 hours, the concentration of **2** increased. It might be suggested that the boroxine complex is more reactive to oxidation than the boronic acid complex.[23]

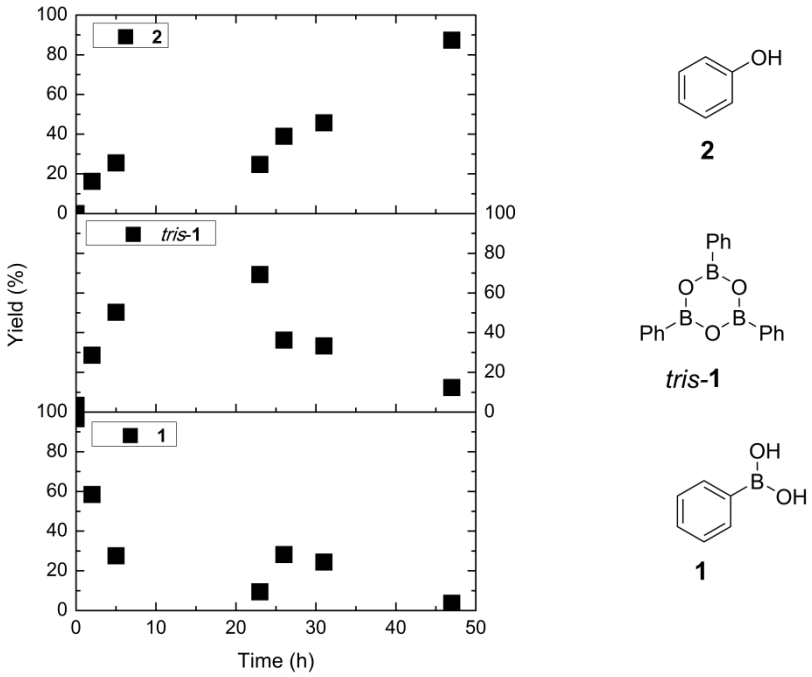
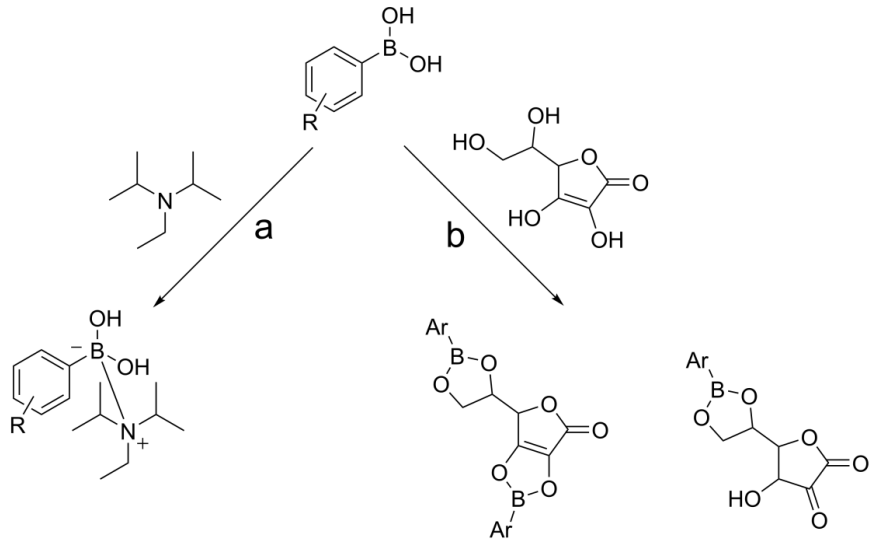


*Figure 2-7 Conversion data of the oxidative hydroxylation of phenylboronic acid (**1**) to phenol (**2**) in DMF with TEA and $[Ru(bpy)_3]^{2+}$ which may suggest that triphenylboroxine (tris-**1**) behaved like an intermediate as its yield initially increased but decreased later during the reaction.*

After these successful batch reactions, reaction conditions were screened to find optimum conditions in terms of yield and reaction time to take forward into flow chemistry. The use of ascorbic acid (H_2A) as an alternative reductive quencher was investigated since ascorbic acid is a non-toxic and an environmentally benign electron donor. Both ascorbic acid and the tertiary amines are hydrogen donors which is a requirement for the reaction to proceed (Schemes 2-3,2-4) and ascorbic acid has been used previously as a sacrificial electron donor[24] to quench excited state $[Ru(bpy)_3]^{2+}$. The active species to interact with the excited state photocatalyst is the ascorbate ion (HA^-), the anion of ascorbic acid.[24-25] Due to

the Lewis acidity of the aryl boronic acid, ascorbic acid can form complexes with it as shown in Scheme 2-9. As explained by Bull *et al.*, boronic acids form dynamic complexes with several different compounds.[22] The alcohol moieties in ascorbic acid can undergo boronate esterification (Scheme 2-9b). In the presence of a Lewis base, such as a tertiary amine, a highly polarised coordination complex can be formed (Scheme 2-9a).



Scheme 2-9 Complexes of aryl boronic acids with reductive quenchers DIPEA (route a) and H_2A (route b) which can be formed in solution.

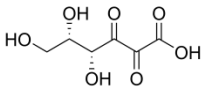
Although superoxide is required in the hydroxylation of the aryl boronic acid, it has been reported that ascorbic acid can be oxidised by superoxide to form the ascorbate ion HA^- (Equation 2-1), the species that can quench the excited state photocatalyst.[26]

$$O_2^{-\cdot} + H_2A \rightarrow HA^- + HO_2^{\cdot} \qquad 2\text{-}1$$

$$HO_2^{\cdot} + O_2^{-\cdot} \rightarrow O_2 + HO_2^- \qquad 2\text{-}2$$

$$O_2 + HA^- \rightarrow A + HO_2^- \qquad 2\text{-}3$$

$$A + OH^- \rightarrow 2{,}3-diketogulonic\ acid \qquad 2\text{-}4$$



Various other side reactions may occur (Equations 2-2 to 2-4), for example the generation of the fully oxidised form of ascorbic acid, dehydroascorbic acid (A), as described in Equation 2-3. Neither dehydroascorbic acid nor 2,3-diketogulconic acid were observed in the product mixture. Another route for superoxide consumption is the regeneration of oxygen (Equation 2-2) after which the molecular oxygen is available for participation in the hydroxylation of the aryl boronic acid. Although these reactions can interfere with the mechanism of the hydroxylation of boronic acid, it was found that the reaction proceeded much faster in the presence of ascorbic acid compared to the use of tertiary amines as reductive quenchers, reducing reaction times from 30 to 6 hours (Table 2-2, entries 1-3). The strong oxidation potential of the ascorbate ion (+0.12 V *vs* SCE)[26] might account for this difference as the tertiary amines have an oxidation potential around 1 V *vs* SCE.[27] When Rose Bengal was employed in combination with ascorbic acid, only low conversion of **1** was observed (Table 2-2, entry 5). This was probably due to the deactivation of the Rose Bengal by the acidic ascorbic acid or the ascorbate radical ($HA^{\bullet}$). Rose Bengal was effective as a photocatalyst in this reaction when using DIPEA as the reductive quencher and full conversion from **1** to **2** was observed after 5 hours. Finally, in an effort to steer away from toxic solvents such as DMF, MeOH was used as a solvent for this reaction. Despite the increase in polarity, the reaction in MeOH proceeded at the same rate as in DMF (Table 2-2, entries 3,4) which is an encouraging result from a sustainability perspective. As stated above, screening reaction conditions allowed for faster hydroxylation of **1** to **2** as the reaction times in batch were reduced from 30 to 5 hours. However, in order to make this reaction more attractive for scale-up, reaction times needed to be reduced further, allowing for higher substrate throughput and a less energy intense process. Therefore, the hydroxylation of **1** to form **2** was investigated in continuous flow for the first time, using a continuous photoreactor which is described in Section 2.3.

2.3 Continuous Flow Visible Light Photoreactor

A continuous visible light photoreactor has been used previously by our group in Nottingham. It was originally designed for oxidations with $^1O_2$ in $scCO_2$ and it is a

high-pressure rated reactor system (250 bar) with multiple safety features.[2b, 2d, 28] The reactor has been redesigned multiple times to ensure ever more efficient irradiation of the substrates and has been used for the photo-oxidation of dihydroartemisinic acid, α-terpinene and β-citronellol.[2e, 2g, 29] The initial experiments described in this Thesis examined the hydroxylation of aryl boronic acids and were not undertaken in $scCO_2$. Therefore, the photoreactor was altered to avoid dead head space in the reactor (Figure 2-8) where large amounts of flammable mixture could potentially accumulate, increasing the explosion risk.

The reactor itself consisted of a stainless steel frame holding three banks, each bank equipped with 5 high-power (1000 lumen) white light emitting diodes (LEDs) providing visible irradiation. A visible light transparent sapphire tube (8.1 mm inner diameter, 119.4 mm in length) was positioned in the centre of these LEDs through which the reactants flowed. The sapphire tube was filled with glass beads (6 mm in diameter) to promote mixing and to minimise inner filter effects. Surrounding this sapphire tube was a concentric transparent Lexan™ cooling jacket, which was cooled *via* a recirculating bath.

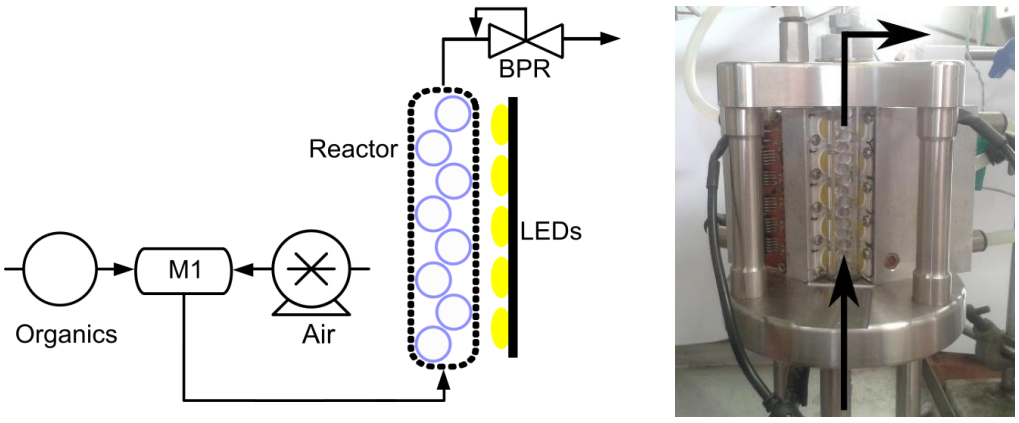


Figure 2-8 The continuous flow sapphire tubular photoreactor in upflow configuration (direction of flow is indicated by the black arrows in the picture on the right). The organic feed is pumped using a HPLC piston pump and air is dosed via a dosing valve (Rheodyne®). Both the liquids and gas are mixed in a static micro-mixer (M1) before entering the reactor which contained glass beads. The desired pressure is generated by the setting on the back pressure regulator (BPR).

The reaction solution containing the dissolved substrate, photocatalyst and reductive quencher was held in a flask open to the air. Additional air was dosed into the reactor system under pressure using a Rheodyne® unit. The reagents

were mixed with the air in a micro-mixer (M1) prior to entering the reactor *via* the lower end. A back pressure regulator (BPR) was situated after the reactor to hold the desired pressure. Further details of this reactor can be found in the Experimental Chapter.

2.4 Phenol Synthesis in Flow

In the hydroxylation of phenylboronic acid, as in batch, 2 molar equivalents of reductive quencher and 2 mol% of photocatalyst were used. The concentration of **1** in solvent was 0.05 M, which is half the concentration compared to the batch experiment, to ensure better light penetration in the flow experiments. Air was chosen as the oxygen source and the results are summarised in Table 2-3.

*Table 2-3 Conversion of phenylboronic acid (**1**) to phenol (**2**) in continuous flow in MeOH with various reductive quencher and photocatalyst combinations to find optimum conditions.*

Entry	Flow rate[a] (mL/min)	Photocatalyst (PC)	Reductive quencher (RQ)	Conversion
1	0.1	$[Ru(bpy)_3]Cl_2$	DIPEA	> 99 %
2	0.4	$[Ru(bpy)_3]Cl_2$	DIPEA	27 %
3	0.1	$[Ru(bpy)_3]Cl_2$	H_2A	95 %
4[b]	0.1	$[Ru(bpy)_3]Cl_2$	H_2A	43 %
5	0.1	RB	DIPEA	> 99 %
6	0.4	RB	DIPEA	> 99 %
7	0.8	RB	DIPEA	54 %
8	0.1	RB	H_2A	42 %
9	0.8	RB	H_2A	9 %

*Reaction conditions: **1** (0.26 mmol, 0.05 M), PC (2 mol%), RQ (2 eq.), methanol, 3x5 1000 lumen visible light LEDs, 25 °C, 0.1 MPa; [a]Air:**1** was 67:1 molar ratio; [b]In contrast to all other experiments, the reactor was not filled with glass beads*

As the reaction in batch proceeded at the same rate in MeOH and DMF, MeOH was used as the reaction solvent in flow and air was dosed in at a 67-fold excess to **1**. In a larger reactor volume, low mass transfer may turn out to be the bottleneck for reaction conversion. To minimise this problem, the reactor was filled with glass beads. Although this reduced the irradiated volume by *ca* 35 %, the conversion increased 2-fold at a constant flow rate (Table 2-3, entries 3,4). This can probably be contributed to improved mixing resulting from the presence of glass beads and the reduction of the irradiation path length, resulting in more efficient irradiation of the reaction mixture inside the reactor.

Since shorter reaction times were required to reach full conversion of **1** in flow compared to batch, the reaction mixture has less contact with the LED light compared to batch experiments. Due to this reduced irradiation time, ascorbic acid was tested again as the reductive quencher with Rose Bengal (RB) in the hope that the reaction would be complete before the Rose Bengal had degraded. However, ascorbic acid still performed less well than DIPEA (Table 2-3, entries 5,8) suggesting a fast deactivation of the Rose Bengal catalyst. This was supported by the brown colour of the reaction output in contrast to the pink substrate solution of fresh Rose Bengal. Increasing the flow rate did not improve this parameter (Table 2-3, entry 9). Interestingly, ascorbic acid was found less effective as a reductive quencher of $[Ru(bpy)_3]^{2+}$ than DIPEA (Table 2-3, entries 1,3) which is the opposite result obtained from the batch experiment. As ascorbic acid is sensitive to light and oxygen, the increase in light intensity reaching the reactant solution in flow could have degraded ascorbic acid. Moreover, the amount of air present in the flow experiments was presumed to be higher than in batch experiments and therefore, the degradation of ascorbic acid by oxygen would have been potentially higher in flow.

When comparing photocatalysts, Rose Bengal appeared to be a more suitable photocatalyst compared to $[Ru(bpy)_3]Cl_2$. Although the ruthenium based photocatalyst has a longer excited state lifetime, the spectral overlap between the LED emission and the photocatalyst absorption is better in the case of Rose Bengal. The strongest absorbance band of Rose Bengal around 558 nm overlaps well with the LED emission band centred around 560 nm. This enables for more efficient catalyst excitation which could potentially result in higher reaction rates. A control experiment without photocatalyst was conducted but resulted in only traces of phenol. This corresponds to the work by Jiang *et al*., who needed

prolonged irradiation of the reaction mixture without photocatalyst to reach high yields.[19]

Next, the solvents, pressure, and air concentration were varied to establish the optimum conditions for the reaction in continuous flow. In all experiments, Rose Bengal was employed as the photocatalyst and DIPEA as the reductive quencher. The results are displayed in Table 2-4.

*Table 2-4 Screening of reaction conditions in the hydroxylation of **1** to **2** in continuous flow to optimise for oxygen to substrate ratio and solvent.*

Entry	Flow rate (mL/min)	Solvent	Air:1 (O_2:1)[a]	Pressure (MPa)	Conversion
1	0.8	MeOH	67:1 (13:1)	0.1	54 %
2	0.8	EtOH	67:1 (13:1)	0.1	62 %
3	0.8	H_2O/EtOH[c]	67:1 (13:1)	0.1	67 %
4	0.8	H_2O/EtOH[c]	134:1 (26:1)	0.1	32 %
5	0.8	H_2O/EtOH[c]	33:1 (6:1)	0.1	13 %
6	0.8	H_2O/EtOH[c]	--[b]	0.1	6 %
7	0.8	H_2O/EtOH[c]	67:1 (13:1)	2	> 99 %
8	2.4	H_2O/EtOH[c]	67:1 (13:1)	2	> 99 %
9	2.8	H_2O/EtOH[c]	67:1 (13:1)	2	80 %
10	3.2	H_2O/EtOH[c]	67:1 (13:1)	2	54 %

*Reaction conditions: **1** (0.26 mmol, 0.05 M), RB (2 mol%), DIPEA (2 eq.), solvent, 3x5 1000 lumen visible light LEDs, 25 °C; [a]Molar ratio; [b]No additional air; [c]Volume 1:1*

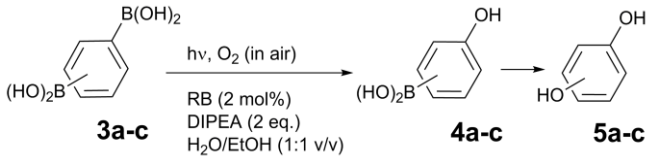
The use of an aqueous ethanol mixture instead of MeOH led to a significant increase in conversion (Table 2-4, entries 1,3). This could possibly be attributed to the quenching of singlet oxygen by water in H_2O/EtOH solvent mixtures. Singlet oxygen can be formed upon energy transfer between the photocatalyst and molecular oxygen, but it does not participate in the hydroxylation transformation and its generation is therefore best avoided.

Previous studies have shown that the use of pure oxygen should increase the reaction rate.[14d] However, in our studies we observed diminishing conversions when higher concentrations of oxygen in the reaction mixture were present (Table 2-4, entries 3,4). Again, the increased formation of singlet oxygen at these higher oxygen concentrations could be a possible explanation for this. Another reason for this lower conversion could be the force of the air pulsing through the reactor, leading to a decrease in residence time. The oxygen concentration was found to have an optimum at a 13:1 molar ratio with **1**. Increasing and decreasing the oxygen concentration from this molar ratio reduced the conversion of **1**.

In order to reduce reaction time even further, the system pressure was increased to 2 MPa. At this pressure, the flow rate could be increased to 2.4 mL/min while maintaining full conversion (Table 2-4, entry 8). This corresponds to a productivity of *ca* 3.4 g of phenol after 5 h. Employing the batch reaction set-up described in Section 2.2, only 0.125 g of phenol could be obtained after 5 h, showing a 90-fold increase in productivity in flow.

2.5 Desymmetrisation Studies

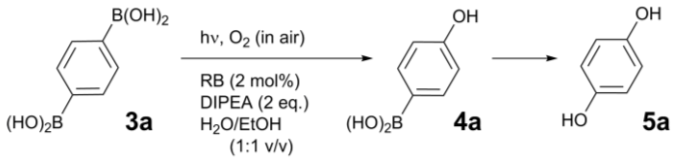
As residence times can be accurately controlled in flow chemistry, selectivity of chemical reactions can potentially be improved by performing reactions in flow fashion compared to batch synthesis. Desymmetrisation reactions are a challenging part of product selectivity and therefore, it was investigated whether our continuous flow reactor could afford improvements in terms of selectivity, by performing desymmetrisation reactions. Only a few precedents of desymmetrisation reactions in flow exist in the literature as only diol mono-hydroxylations or thiophene dissymmetric lithiation have been reported.[30] To the best of our knowledge, this Section will describe the first example of an aryl diboronic acid desymmetrisation reaction. The mono-hydroxylation of *ortho*-, *meta*- and *para*-substituted benzenediboronic acid was studied (Scheme 2-10).



*Scheme 2-10 Photochemical desymmetrisation of aryl diboronic acids **3a-c** to form mono-hydroxylated products **4a-c**.*

2.5.1 1,4-Benzenediboronic Acid

The first substrate reacted was 1,4-benzenediboronic acid (**3a**). This symmetrical substrate has a boronic acid moiety *para* to another one, in which case steric interactions are minimised and therefore are not likely to influence the reactivity of the substrate towards the second hydroxylation step. It was attempted to generate 4-hydroxyphenylboronic acid (**4a**) without performing full hydroxylation to 1,4-dihydroxybenzene, known as hydroquinone (**5a**) (Scheme 2-11).



*Scheme 2-11 Study into the mono-hydroxylation of 1,4-benzenediboronic acid (**3a**) to 4-hydroxyphenylboronic acid (**4a**) while minimising the formation of hydroquinone (**5a**).*

Initial reactions were performed at 2 MPa system pressure, at a flow rate of 0.8 mL/min. However, the reaction proceeded quickly and afforded full conversion of **3a** to **5a**, with no selectivity for **4a** (Table 2-5, entry 1). Increasing the flow rate to 2.4 mL/min did not improve the selectivity for **4a** in the reaction. Performing the reaction at atmospheric pressure however did improve the selectivity for **4a**. Without directing groups to influence the hydroxylation efficiency, the conversion of **3a** and the selectivity for **4a** are in competition.

Interestingly, reducing the light intensity by a factor 0.75 improved conversion compared to the reaction at full light intensity (Table 2-5, entries 3,4). It

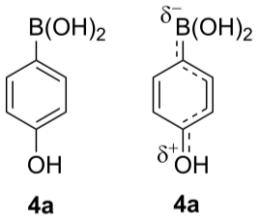
appeared that full intensity of the LED lights led to over-irradiation of the reaction mixture. As the level of oxygen is in excess compared to **3a**, the higher level of irradiation could have generated more singlet oxygen which is, as described before, best avoided.

*Table 2-5 Screening reaction conditions for the optimum desymmetrisation of **3a** to form **4a** in flow using RB and DIPEA.*

Entry	Flow rate (mL/min)	Solvent	Air:3a (O_2:3a)[a]	Pressure (MPa)	Conversion	Selectivity for 4a
1	0.8	H_2O/EtOH[c]	67:1 (13:1)	2	> 99 %	0 %
2	2.4	H_2O/EtOH[c]	67:1 (13:1)	2	> 99 %	0 %
3	0.4	H_2O/EtOH[c]	67:1 (13:1)	0.1	26 %	78 %
4[b]	0.4	H_2O/EtOH[c]	67:1 (13:1)	0.1	43 %	64 %
5	0.1	H_2O/EtOH[c]	67:1 (13:1)	0.1	78 %	38 %

*Reaction conditions: **3a** (0.26 mmol, 0.05 M), RB (2 mol%), DIPEA (2 eq.), solvent, 3x5 1000 lumen visible light LEDs, 25 °C; [a]Molar ratio; [b]Only ¼ of the light intensity was used; [c]Volume 1:1*

Initially, it was envisioned that the second hydroxylation step would be slower than the first hydroxylation step caused by the mesomeric resonance effect[31] present in structure **4a**. As illustrated in Scheme 2-12, it would be expected that the boron atom would be less electrophilic after the first hydroxylation step. From this, it could be expected that the second hydroxylation step would be slower than the first as the boron atom would be more deactivated towards insertion of the electron-rich superoxide. However, the experimental data showed that this was not the case.



4a **4a**

*Scheme 2-12 Potential mesomeric resonance effect in 4-hydroxyphenylboronic acid (**4a**), showing a partly negative charge on the boron atom.*

A tentative explanation might be that the insertion of the superoxide into the boron atom proceeds *via* a radical mechanism instead of the negative charged part of the molecule. However, this would require further investigation. Another possible explanation for the experimental results could be that the single occupied molecular orbital (SOMO) of superoxide was closer in energy to the LUMO of the aryl boronic acid as opposed to the HOMO of the aryl boronic acid. This would have been due to stabilisation of the HOMO in aryl boronic acid induced by the higher electron density (Scheme 2-12). The electrons in the orbitals after the SOMO-LUMO interaction are more stabilised than when a SOMO-HOMO interaction would have taken place. Therefore, the hydroxylation of **4a** would be favourable.

To follow the progress of the reaction over time and to see whether this competition between conversion of **3a** and selectivity for **4a** was present in batch as well, the reaction was replicated in batch, using the same batch reaction set-up as for the hydroxylation of **1**. Although the photocatalyst, reductive quencher and solvent ratios were the same in both batch and flow experiments, the concentration of oxygen might have varied. The conversion of **3a** and the selectivity for **4a** were again in competition, but a higher selectivity for **4a** was observed in these batch experiments compared to the experiments performed in flow (Figure 2-9). An explanation for the difference in results obtained from the batch and flow experiments could be the difference in irradiation of the reaction mixture. In batch, 1 LED block of 5 LED arrays was used while in flow 3 of these LED blocks were used. As less of the reaction mixture was irradiated at one time in batch, the chance of irradiating a molecule **3a** instead of **4a** is greater, leading to an increased selectivity for **4a**.

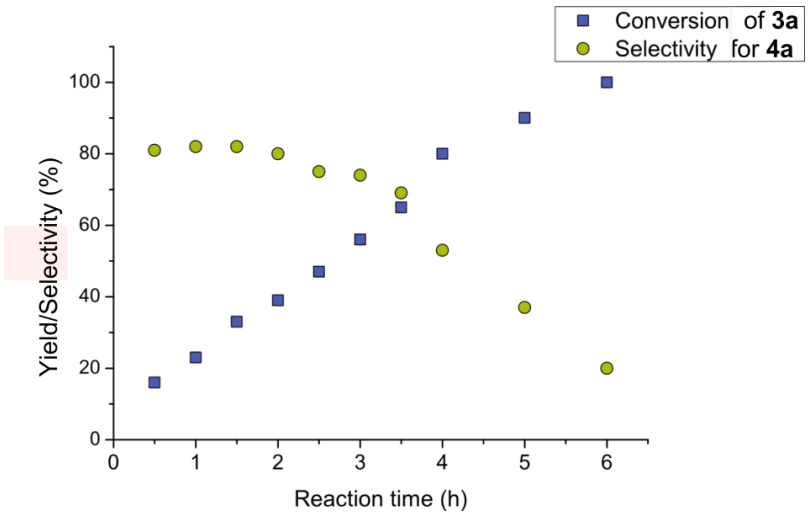
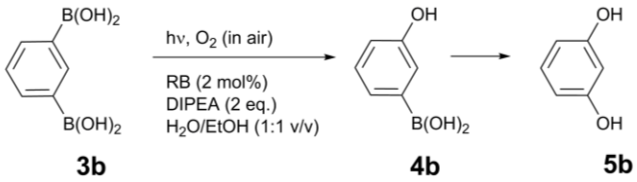


*Figure 2-9 Hydroxylation of 1,4-benzenediboronic acid (**3a**) in batch using RB and DIPEA, showing the conversion of **3a** and the selectivity for the mono-hydroxylated compound (**4a**) over time as a competing process.*

In both batch and flow, the selectivity for **4a** is modest, but it serves as a proof of principle for a substrate without any directing groups to facilitate mono-hydroxylation. To increase the viability of this process, residual starting material could be separated and recycled.

2.5.2 1,3-Benzenediboronic Acid

The next substrate tested was 1,3-benzenediboronic acid (**3b**) (Scheme 2-13). With the boronic acid groups in *meta*-positions of each other, the mesomeric effects were thought to influence the efficiency of hydroxylation of **3b** less compared to **4b**.



*Scheme 2-13 Study into the mono-hydroxylation of 1,3-benzenediboronic acid (**3b**) to 3-hydroxyphenylboronic acid (**4b**) while minimising the formation of 1,3-dihydroxy-benzene (**5b**).*

The best conditions found for the conversion of **3a** to **4a** were replicated with substrate **3b** to directly compare the substrates (Table 2-6, entry 2). It was found that the hydroxylation of **3b** was slower than in the case of substrate **3a**. While full conversion of **3a** was accomplished at 2 MPa and 2.4 mL/min, only 63 % of **3b** was converted under the same conditions (Table 2-6, entry 1). It might be possible that steric effects played a role in the conversion of substrate **3b**.

*Table 2-6 Screening reaction conditions for the optimum desymmetrisation of **3b** to form **4b** in flow using RB and DIPEA.*

Entry	Flow rate (mL/min)	Solvent	Air:3b (O_2:3b)[a]	Pressure (MPa)	Conversion	Selectivity for 4b
1	2.4	H_2O/EtOH[b]	67:1 (13:1)	2	63 %	78 %
2	0.4	H_2O/EtOH[b]	67:1 (13:1)	0.1	25 %	100 %
3	0.1	H_2O/EtOH[b]	67:1 (13:1)	0.1	71 %	80 %

*Reaction conditions: **3b** (0.26 mmol, 0.05 M), RB (2 mol%), DIPEA (2 eq.), 3x5 1000 lumen visible light LEDs, 25 °C; [a]Molar ratio; [b]Volume 1:1*

Steric effects would likely stimulate the hydroxylation of **4b** over that of **3b**, leading to a diminishing selectivity for **4b** over **5b**. Compared to the hydroxylation of *para*-substituted benzenediboronic acid (**3a**), the selectivity for the mono-hydroxylated product was higher for this *meta*-substituted substrate

(**3b**). That the presence of an electron donating moiety in the *meta*-position would inhibit efficient hydroxylation of the boronic acid moiety is in accordance with the fact that the presence of an electron withdrawing moiety in this position enhanced the hydroxylation as previously reported.[13] Therefore, it appears that in the case of **4b**, inductive effects were not the main contributing factor as the electron donating hydroxyl moiety would have increased the electron density on the boronic acid moiety in **4b** which, following the reasoning given in Section 2.5.1, would facilitate the hydroxylation mechanism and diminish the selectivity for **4b** over **5b**.

Batch experiments were carried out for comparison to the results obtained in flow and quantitative selectivity was obtained up to 75 % conversion of **3b** (Figure 2-10).

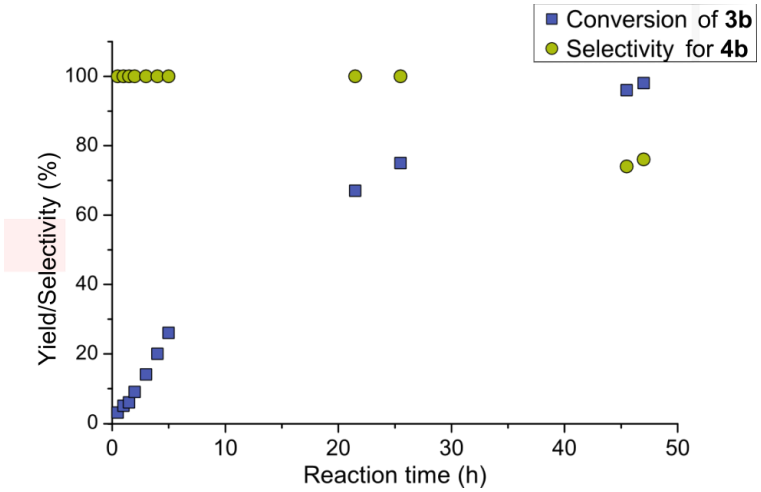
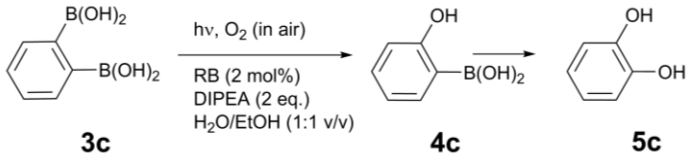


*Figure 2-10 Hydroxylation of 1,3-benzenediboronic acid (**3b**) in batch using RB and DIPEA, displaying conversion and the selectivity for the mono-hydroxylated compound (**4b**) over time. Note that quantitative selectivity for **4b** was observed up to 75 % conversion of **3b**.*

In contrast to the mono-hydroxylation of **3a**, the mono-hydroxylation of **3b** achieved high selectivity both in batch and flow. A conversion of 71 % took 28 min. in flow while the batch experiment it took 25.5 hours to achieve 75 %, achieving similar selectivity, underlining the potential of flow chemistry by showing a 52-fold increase in productivity compared to batch experiments.

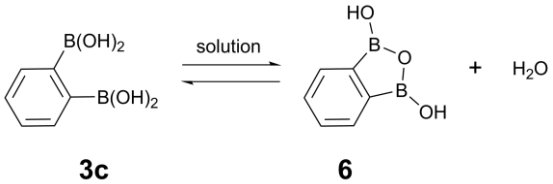
2.5.3 1,2-Benzenediboronic Acid

For 1,2-benzenediboronic acid (**3c**), steric effects will potentially play a larger role in the efficiency of mono-hydroxylation of **3c** (Scheme 2-14) compared to substrates **3a**/**b**. As a result, it was expected that the hydroxylation of **4c** would be faster than that of **3c**, which will render mono-hydroxylation of **3c** challenging. The mesomeric effects will be comparable to those in **3a**, while the inductive effects are thought to be stronger in substrate **3c** compared to **3a**.



*Scheme 2-14 Study into the mono-hydroxylation of 1,2-benzenediboronic acid (**3c**) to 2-hydroxyphenylboronic acid (**4c**) while minimising the formation of catechol (**5c**).*

1,2-Benzenediboronic acid (**3c**) was synthesised in a 2-step synthesis. Details can be found in the Experimental Chapter. Purification proved difficult and only 37.6 mg of material was obtained (0.6 % yield). It is well-known that 1,2-benzeneboronic acid is in equilibrium with its cyclic semi anhydride form called benzoxadiborole[32] (**6**) (Scheme 2-15) and additional signals to **3c** were observed in the NMR spectrum that could potentially correspond to **6**.



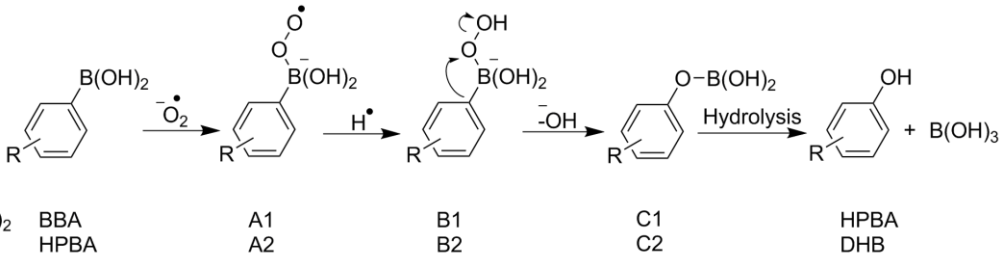
*Scheme 2-15 1,2-Benzenediboronic acid (**3c**) in equilibrium with benzoxadiborole (**6**), probably occurring in the reaction solution.*

The desymmetrisation of **3c** was attempted in batch but no continuous flow experiments were conducted due to the low availability of starting material. After

one hour of reaction time, **5c** was obtained in 2.4 % yield while no **4c** could be observed in the ^{1}H NMR spectrum of the reaction mixture. Analysis of the reaction mixture after 8 hours of irradiation time showed full conversion of **3c** to **5c**. The conversion of substrate **3c** appeared to proceed on the same timescale as substrate **3a** (within 8 hours). However, no information about the desymmetrisation of 1,2-benzenediboronic acid could be obtained.

2.5.4 Calculations on the Desymmetrisation of Aryl Diboronic Acids

To investigate the difference in reactivity of the different substituted benzenediboronic acids, quantum chemical calculations were performed to calculate the energy levels of the different compounds and the distribution of electron density in the molecule. In order to compare the previously described calculations (Section 2.1.2), DMF was chosen as the solvent field model, and the same method and basis set were used. The Gibbs free energy was calculated for all stages of the hydroxylation process, according to the mechanism described by Zou *et al.* as this appeared to be the main mechanism. It was assumed that the second hydroxylation step followed the same mechanism as the first step. The numbering of the complexes is displayed in Scheme 2-16.



Scheme 2-16 Numbering of complexes present inthe hydroxylation of aryl diboronic acids.

Figure 2-11 shows the result of these calculations on *ortho*/*para*/*meta*-substituted benzenediboronic acid. As all three of the substrates are displayed in the same Scheme, the calculated energy levels are labelled with text instead of structures. Superoxide inserts into the benzenediboronic acid (BBA),

resulting in radical anion A1. After the addition of a hydrogen atom to complex A1, intermediate B1 is formed. Then the insertion of the benzene ring into the peroxygen moiety generates intermediate C1 which leads to hydroxyphenylboronic acid (HPBA) after hydrolysis. The reaction sequence is then repeated and these intermediate complexes in the second hydroxylation steps are numbered A2-C2. Dihydroxybenzene (DHB) is the product after two hydroxylation steps.

DFT calculations suggested that the rate-determining step in all hydroxylation steps of benzenediboronic acids **3a-c** was the superoxide insertion. However, no viable transition state conformation could be determined for the insertion of superoxide into *o*-BBA. In the case of *p*-BBA, the insertion of superoxide into *p*-HPBA was found 1.0 kcal/mol more favourable than the insertion of superoxide into *p*-BBA as determined by the difference in energy of the transition states $A1^{\ddagger}$ *versus* $A2^{\ddagger}$.

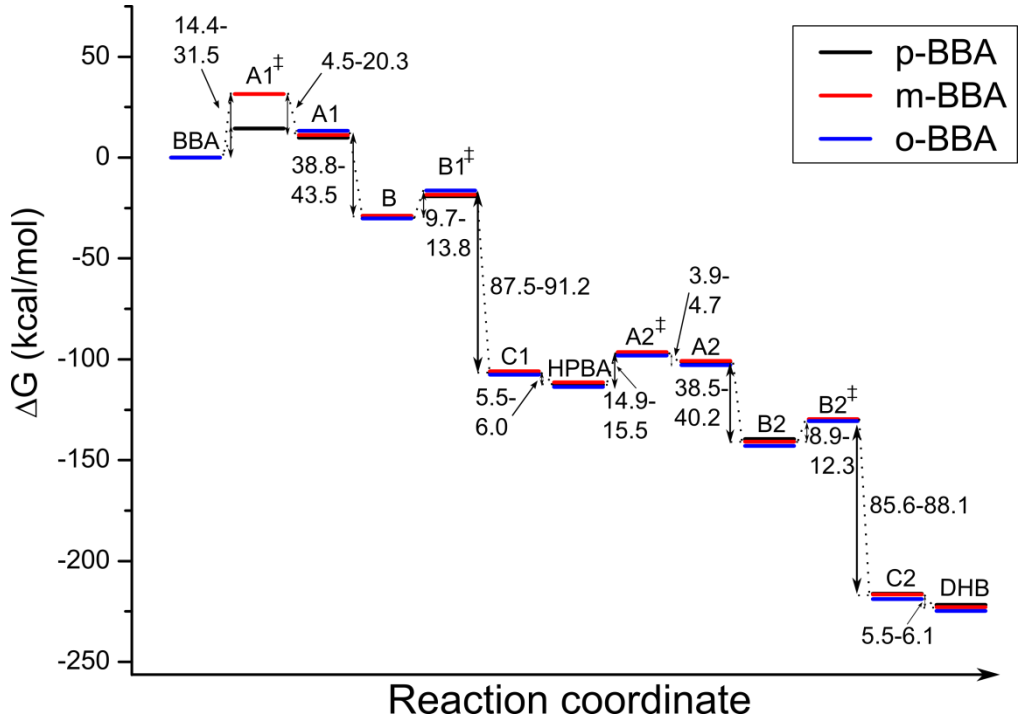
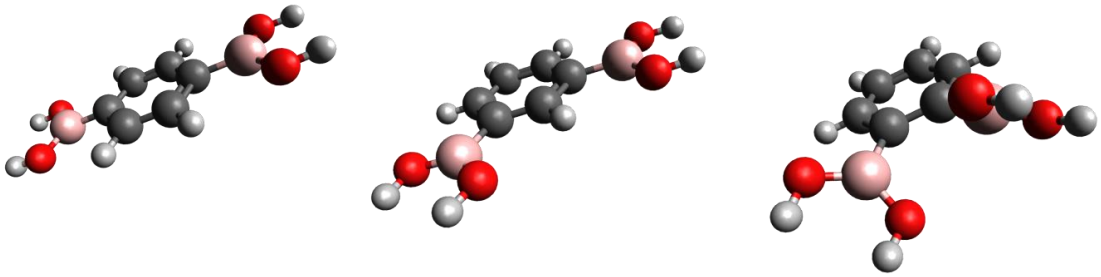


Figure 2-11 DFT calculations on the hydroxylation of ortho/para/meta-substituted benzenediboronic acids based on the mechanism proposed by Zou et al.[13] using the solvent field parameters of DMF. These results suggest little difference in energy levels between the o/m/p-substituted compounds at each step of the hydroxylation and the insertion of superoxide into BBA appeared to be the rate-determining step. Structure $A1^{\ddagger}$ for o-BBA could not be determined. Changes in free energy are relative to the free energy of BBA. Transition state complexes are labelled with the ‡ notation.

Transition state A1‡ for *m*-BBA was significantly higher in energy than transition state A2‡. This would suggest that the insertion of superoxide into *m*-HPBA proceeds more favourably than the insertion into *m*-BBA. And with this step calculated to be the rate-determining step, this would result experimentally in low selectivity for the mono-hydroxylated compound since the second hydroxylation would happen faster than the first hydroxylation step. However, experimental data showed the opposite trend.

The calculations may suggest that no steric effects were present between the two boronic acid moieties in the *meta*-substituted benzenediboronic acid (**3b**), since both boronic acid moieties are in the same plane as the benzene ring (Figure 2-12).



(a) (b) (c)

*Figure 2-12 Ground state structures of a) 1,4-benzenediboronic acid (**3a**), b) 1,3-benzenediboronic acid (**3b**), c) 1,2-benzenediboronic acid (**3c**), showing the rotation of the boronic acid moiety out of the plane of the benzene ring in **3c**.*

In both **3a** and **3b**, the second boronic acid moiety stays in the plane of the benzene ring during the first hydroxylation step despite the increase in steric effects by the superoxide addition. This boronic acid moiety bends out of the benzene ring plane when the second hydroxylation step starts. The hydroxyl moiety after the hydroxylation process was positioned in the plane of the benzene ring in all cases for the hydroxylation processes of **4a**, **4b** and **4c**. Steric effects were present in the *ortho*-substituted substrate **3c** as the boronic acid moieties were bent out of the plane of the benzene ring in **3c**. The mono-hydroxylated product **4c** had both the boronic acid and hydroxyl moiety in plane with the benzene ring, indicating the reduced steric effects of having these substituents in the *ortho*-position.

The calculations showed that in structure A1 of *o*-BBA, hydrogen-bonding between the superoxide and the second boronic acid moiety could occur (Figure 2-13a,b). The hydrogen-bonding interaction represented a 10.4 kcal/mol increase in energy compared to the non-hydrogen bonded configuration. This barrier could be overcome thermally and it is possible that the hydrogen-bonding interaction facilitates the superoxide insertion.

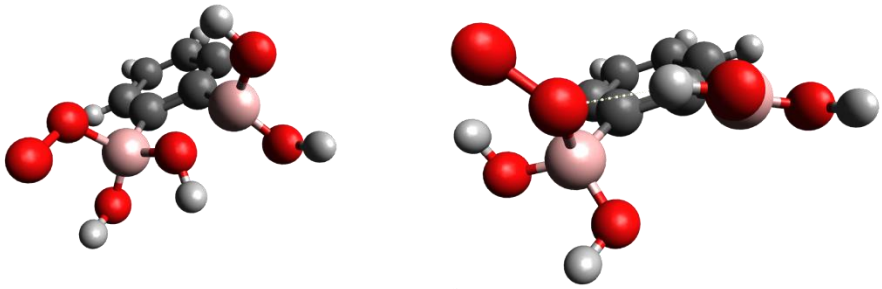


Figure 2-13 A1 complex of o-BBA displaying a) no hydrogen-bonding between the superoxide and the second boronic acid moiety and b) the presence of hydrogen-bonding between those two moieties, indicating a change in geometry of the compound dependent on whether hydrogen-bonding is present.

In an attempt to gain insight in the electron density and therefore the electrophilicity of the boron atom in the different boron containing complexes, natural bond order (NBO) charges were calculated. The charge on the boron atom during superoxide insertion was calculated to be without significant change when comparing *o*/*m*/*p*-BBA and HPBA (Figure 2-14). This would suggest that the electron density on the boron atom did not change when comparing the *o*/*m*/*p*-BBA and HPBA complexes. Moreover, no significant difference was found when comparing the charges on the boron atom between the different substituted aryl diboronic acid complexes. An exception is the A2 complex of the *ortho*-substituted diboronic acid. In this complex, the charge on the boron atom halved after insertion of the superoxide.

During the calculated transition state of the insertion of superoxide, the charge on the boron atom increased by 3 % for all BBA and HPBA complexes. Complexes A1-A2 for all BBA and HPBA compounds exhibited a 8 % reduction of charge on the boron atom compared to the transition state of the superoxide insertion. For

comparison, the NBO charges during the insertion of superoxide into phenylboronic acid are plotted in the same graph. The initial charge on the boron atom for phenylboronic acid is equal to that of the aryl diboronic acid complexes. However, after the insertion of superoxide, the charge on the boron atom was halved in the case of phenylboronic acid.

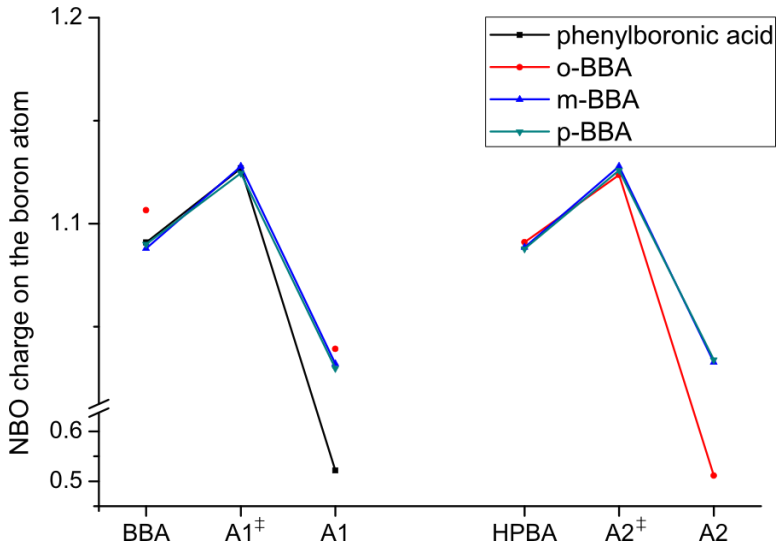


Figure 2-14 NBO charges of the boron atom in phenylboronic acid and ortho/meta/para-substituted diboronic acids involved in the insertion of superoxide, indicating the increase in charge on the boron atom in the transition state of the superoxide insertion and the similarity in charge up to this transition state when comparing all four compounds. Transition state complexes are labelled with the ‡ notation.

In conclusion, the quantum chemical calculations could not corroborate the differences in reactivity of the aryl diboronic acid complexes observed experimentally. However, a deeper understanding about the geometry of these complexes during the calculated rate-determining step was obtained.

2.6 Immobilisation of the Photocatalyst

Albini *et al.* pointed out in a critical review on visible light photocatalysis that although visible light can be used as the energy source for reactions, expensive and rare photocatalysts are generally needed for the reaction, which decreases

the green aspect of visible light photocatalysis.[33] An approach to solving this problem is to separate the photocatalyst from the reaction mixture after reactions in order to recycle and reuse it. For such needs, a heterogeneous catalyst could be prepared by immobilisation of the photocatalyst on a support. Separation of the photocatalyst from reactants and products could be accomplished by simple filtration. Moreover, immobilisation of the photocatalyst on a support often provides a greater surface area of the photocatalyst for contact with the reactants, resulting in more efficient reactions.[34]

Two main methods of catalyst immobilisation are possible, either covalent or non-covalent linkage to the support. Furthermore, both insoluble and soluble immobilisation supports can be utilised. Soluble supports have the advantage of providing a homogeneous reaction mixture, and separation of the supported catalyst after the reaction is more easily accomplished than for non-supported catalysts, for example by precipitation. Generally, the separation of photocatalysts immobilised on soluble supports from reaction products is more challenging than for photocatalysts immobilised on insoluble supports and the reusability of the catalyst on soluble support can be lower.[34a, 34b] Insoluble supports provide a heterogeneous reaction mixture which can diminish reaction yields due to the reactants being in separate phases. Despite this, these solid supports are widely used as they are easily accessible, exhibit easy separation from reactants and are well understood.[35]

Silica and poly(ethylene glycol) (PEG) are widely employed for covalent coupling of the catalyst to a support and act as either soluble or insoluble supports depending on the solvent.[36] In the case of silica, the hydroxyl moieties can be functionalised with the catalyst while for PEG, the polymer backbone must be altered. Due to this covalent bond between the catalyst and the support, catalyst leaching is often negligible. However, random packing of the support may lead to low product selectivity and it can create local environments of different polarity which makes control over the reaction harder.[37] The advantage of using PEG as opposed to silica is the ability of the polymer to swell in organic solvents. The swelling generally results in better reaction kinetics as more catalyst sites become available for the reactants.

A major disadvantage of using a covalently bound catalyst-support system is that the preparation of these systems requires additional reaction steps to attach the

catalyst to the immobilisation support. This produces more waste, makes the approach less atom efficient and is often time-consuming. Since this reduces the green aspect of catalyst immobilisation intensely, non-covalently bound catalyst-support systems are desired. However, this strategy is often reaction specific. In each case different interactions between substrates for the chemical reaction, additives and solvents are present which can influence the strength of the interaction between the catalyst and the support (Figure 2-15).

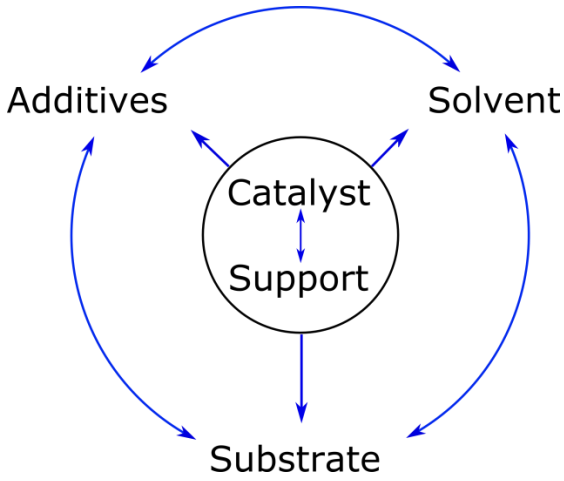


Figure 2-15 Illustration of the different interactions (blue arrows) between all the components in a reaction system with immobilised catalysts.

The supports for non-covalent binding include zeolite, ionic liquids, β-cyclodextrin, phosphotungstic acid and ion-exchange resins.[37-38] These supports exhibit inherent advantages including low cost, the availability of a wide choice of materials with different chemical and physical properties and the reasonable chemical and thermal resistance of these supports.[35] In the case of zeolites, the main contribution to catalyst immobilisation is the entrapment of the catalyst within the pores of the microporous crystalline aluminosilicate structure. Resins are employed to immobilise photocatalysts by the ion-exchange of a charged catalyst with the counter ion of the functional group of the resin. If needed, their acidic/basic properties could be used as additional catalysts in the reaction. This type of immobilisation will be discussed in the next Section which will focus on the immobilisation of $[Ru(bpy)_3]Cl_2$ as reported in literature.

2.6.1 Immobilisation of $[Ru(bpy)_3]Cl_2$ on Solid Support

In the 1980s the immobilisation of $[Ru(bpy)_3]^{2+}$ was already reported. Bard *et al*. used the ion-exchange resin Nafion, a material containing a network of perfluoronated alkyl chains with sulfonic acid functional groups, as the solid support for $[Ru(bpy)_3]^{2+}$ in electrogenerated chemiluminescence studies.[39] The interaction between Nafion and $[Ru(bpy)_3]^{2+}$ was also employed by Choi *et al.* for free radical polymerisation of methyl methacrylate and other monomers.[40] Photocatalyst $[Ru(bpy)_3]^{2+}$ was immobilised on silica particles which were coated with Nafion (Figure 2-16). Recyclability of the catalyst was achieved and even after 5 cycles, no decrease in catalyst activity was observed. The superiority in photocatalytic properties of the Nafion coated silica compared to $[Ru(bpy)_3]^{2+}$ immobilised on solely SiO_2 support was demonstrated as both catalyst leaching and degradation was prevented upon coating of the SiO_2 support.

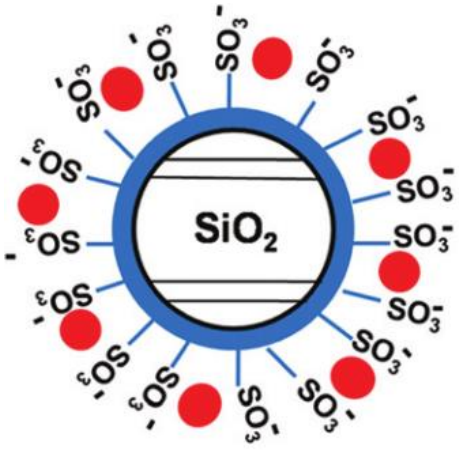


Figure 2-16 Immobilised $[Ru(bpy)_3]^{2+}$ (red) on a Nafion polymer (blue) coated silica support (the core).

Our group also tested the immobilisation of $[Ru(bpy)_3]^{2+}$ on silica aerogel.[2d] This supported photocatalyst was utilised in a flow reaction for the oxidation of citronellol. In contrast to a similar reaction using free photocatalyst, a great decrease in reaction activity was observed over 5 hours.[2d] When Ogawa *et al.* immobilised the photocatalyst on mesoporous silica, the adsorbed photocatalyst showed interactions with the support causing a blue shift of the luminescence

maxima of the photocatalyst.[41] However, hydration of the catalyst-support complexes was needed, in which $[Ru(bpy)_3]^{2+}$ was dispersed in the mesopore. Otherwise, aggregation would lead to self-quenching of the excited state of the photocatalyst.

There have been reports on the entrapment of the catalyst by the support. Recently, Grzybowski and co-workers published a metal-organic framework consisting of rubidium/caesium hydroxide, γ-cyclodextrin and $[Ru(bpy)_3]^{2+}$ (Figure 2-17).[42] The prevention of photo degradation of the photocatalyst was observed upon catalyst entrapment and its activity was retained when it was applied for the reduction of metal salts to nanoparticles.

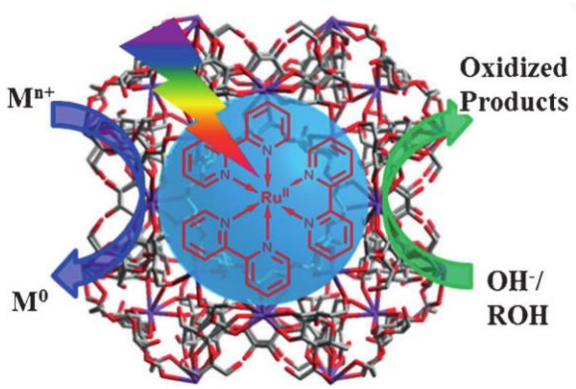
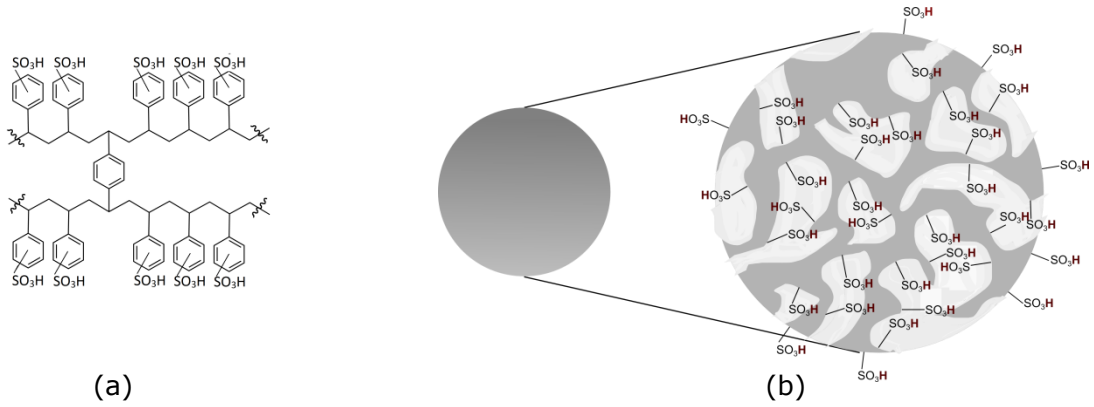


Figure 2-17 Metal-organic framework of rubidium or caesium hydroxide, γ-cyclodextrin and $[Ru(bpy)_3]^{2+}$. The blue sphere represents the volume of the cavity.[42]

More widely utilised materials for catalyst entrapment are zeolites. As early as the 1980s, Lunsford *et al*. investigated the spectral properties of $[Ru(bpy)_3]^{2+}$ entrapped in zeolite Y.[43] Although the luminescence maximum of the photocatalyst remained constant, the incorporation of $[Ru(bpy)_3]^{2+}$ in zeolite Y led to prolonged lifetime due to shielding of oxygen quenching, but only at low catalyst concentrations. At higher catalyst concentrations in zeolite Y, the lifetime was greatly decreased due to concentration quenching by other $[Ru(bpy)_3]^{2+}$ compounds.

2.6.2 Amberlyst 15 as a Solid Support for the Photocatalyst

In this project, two supports were used for initial catalyst immobilisation. The first is a strong cationic ion-exchange resin, Amberlyst 15, a porous sulfonated copolymer of styrene and divinylbenzene (Figure 2-18). Its pores are 30 nm in diameter and the polymer support has a sulfonic acid loading of 4.8 eq. per kg of Amberlyst 15. This support was chosen for its high catalyst loading capacity and its fast ion-exchange. Strong ionic interactions between the sulfonic acid groups and the charged photocatalyst complex were expected. Moreover, π-π interactions between the polymer and $[Ru(bpy)_3]^{2+}$ can occur.



(a) (b)

Figure 2-18 a) Molecular structure of Amberlyst 15, b) schematic representation of the sulfonic acid groups in Amberlyst 15.

Amberlyst 15 has been reported previously as a catalytic support for photocatalysts meso-tetraphenylporphyrin (TPP) and meso-tetrakis(penta-fluorophenyl)porphyrin (TPFPP)[2a], but Amberlyst 15 has not yet been described as a catalyst support for $[Ru(bpy)_3]Cl_2$. A related example was reported by Dal Santo *et al.* where they immobilised a rhodium catalyst on DOWEX 50WX2 (Figure 2-19).[38a] DOWEX is an ion-exchange resin consisting of sulfonated polystyrene. Asymmetric hydrogenation of methyl acetoacetate was accomplished with yields and selectivity comparable to those obtained *via* homogeneous catalysis. Moreover, catalyst leaching was negligible in each experiment (< 2 %).

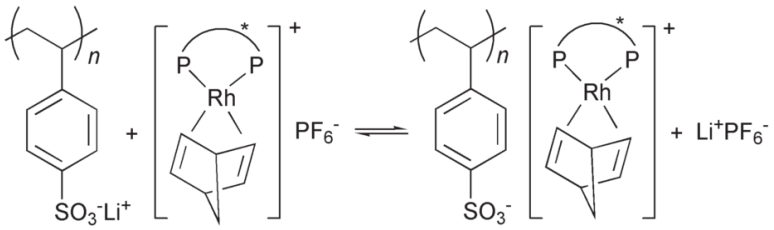
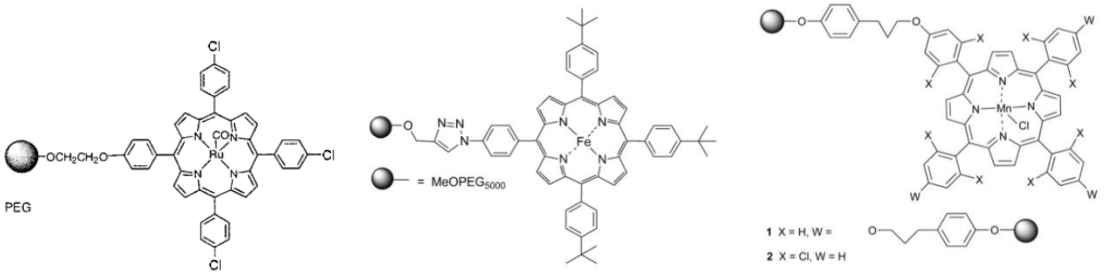


Figure 2-19 Immobilisation of the rhodium catalyst on lithiated DOWEX 50WX2 by the process of ion-exchange.[38a]

2.6.3 Poly(ethylene oxide) as a Solid Support for the Photocatalyst

As a second catalyst support, a non-acidic polymer was chosen. Poly(ethylene oxide) (PEO) exhibits an ether functionality that can facilitate non-covalent interactions with $[Ru(bpy)_3]Cl_2$. Poly(ethylene glycol), which has the same chemical structure as PEO but is formed with different monomer building block, has often been used for catalyst immobilisation. However, all the examples in literature to date are covalently linked PEG-catalyst complexes. Although mainly organic catalysts have been coupled to PEG,[44] examples of metal complexes do exist.[45] To highlight one of the catalyst types, Zhang *et al.*, Benaglia *et al.* and Chinnusamy *et al.* immobilised ruthenium, iron and manganese porphyrins on PEG (Figure 2-20).[46]



(a) (b) (c)

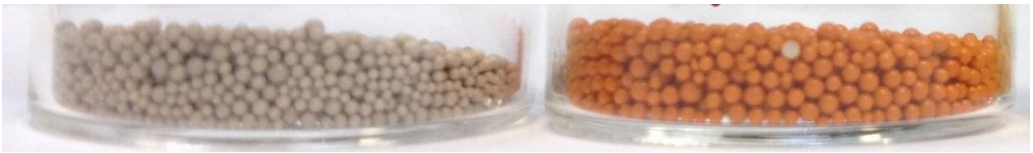
Figure 2-20 Immobilised metalloporphyrins as employed by a) Zhang et al.,[46a] *b) Chinnusamy et al.,*[46b] *c) Benaglia et al.*[46d]

Reactions carried out with the immobilised catalysts include the epoxidation, cyclopropanation and the aziridination of alkenes next to the olefination of aldehydes. [46] Products were obtained in high selectivity, and retention of catalyst activity was observed in all cases, compared to non-immobilised porphyrins. It is important to note however, that for polymers which are able to swell in contact with solvents, more catalyst leaching may occur since the pores in the support, which occlude the catalyst, expand.[47]

2.6.4 Method of Immobilisation

2.6.4.1 Process of Photocatalyst Immobilisation on Amberlyst 15

Amberlyst 15 beads were stirred in deionised water and subsequently, $[Ru(bpy)_3]Cl_2.6H_2O$ was added to the solution. After stirring for an additional 30 minutes, the beads were filtered and washed with deionised water until the pH of the filtrate was 7. Before using the immobilised catalyst in the chemical reaction, the beads (Figure 2-21b) were dried in a 80 °C oven overnight. A photocatalyst loading of 3 wt% was found to be the maximum.



(a) (b)

Figure 2-21 Pictures of a) Amberlyst 15, and b) $[Ru(bpy)_3]Cl_2.6H_2O$ immobilised on Amberlyst 15, illustrating the colour change of Amberlyst 15 from grey to red upon catalyst immobilisation.

2.6.4.2 Process of Photocatalyst Immobilisation on Poly(ethylene oxide)

The PEO and $[Ru(bpy)_3]Cl_2.6H_2O$ powders were mixed thoroughly in a 10:1 wt ratio before using a melt press at 110 °C and approximately 72 MPa to press a disc with 100 μm thickness (Figure 2-22).



Figure 2-22 Disc (100 μm thickness) of $[Ru(bpy)_3]Cl_2.6H_2O$ immobilised on poly(ethylene oxide) polymer, 10:1 wt ratio PEO to photocatalyst.

2.6.5 Characterisation of the Immobilised Photocatalyst Complexes

It is important to investigate the preservation of the photocatalytic activity of $[Ru(bpy)_3]^{2+}$ upon immobilisation. A property that is important for catalytic activity is the position of the energy levels from which the catalyst reacts with the substrate. To estimate those energy levels, the energy of the ^{3}MLCT state of both solid and immobilised $[Ru(bpy)_3]^{2+}$ was determined by emission spectroscopy. The position of the absorbance band of the immobilised $[Ru(bpy)_3]^{2+}$ was measured by diffuse reflectance (DR) UV-Vis spectroscopy. The absorbance maximum of both the ^{1}MLCT and π-π* transitions of $[Ru(bpy)_3]^{2+}$, at respectively 455 and 287 nm, did not shift upon immobilisation on Amberlyst 15 ([Ru]-Amberlyst 15) as measured by diffuse reflectance UV-Vis spectroscopy. The emission maximum was observed to red shift by 19 nm, from 592 to 611 nm. Upon immobilisation of $[Ru(bpy)_3]^{2+}$ on PEO ([Ru]-PEO), the energy of the π-π* transition did not shift and the corresponding absorbance maximum remained at 287 nm. The most intense ^{1}MLCT transition of $[Ru(bpy)_3]^{2+}$ underwent a 15 nm red shift upon immobilisation on PEO, from 455 nm to 570 nm. The ^{3}MLCT state of the photocatalyst showed a 5 nm blue shift in the emission spectrum, from

587 to 592 nm. To conclude, the position of the absorbance and emission bands of $[Ru(bpy)_3]^{2+}$ showed no large shift upon catalyst immobilisation which may be a promising indication that the immobilised catalyst can still be utilised as a photocatalyst.

2.6.6 Leaching of the Photocatalyst out of the Solid Support

Leaching can present a significant problem with immobilised metal catalysts.[48] Therefore, before investigating the reactivity of the immobilised catalyst in the synthetic reaction, catalyst leaching of the immobilised catalyst from the support was assessed. If leaching does occur, one cannot distinguish between the reaction being facilitated by the supported catalyst and by the catalyst in solution. Leaching of $[Ru(bpy)_3]^{2+}$ out of either the PEO or Amberlyst 15 support was analysed in a three step process and after each stage, the solution was assessed for leaching. (1) The immobilised catalyst was placed in the solvent for 30 minutes. The tested solvents were toluene, DMF, acetonitrile, deionised water, tetrahydrofuran, heptane/EtOAc and EtOAc. (2) 2 eq. of TEA was added and the solution was left for a further 120 minutes; (3) 1 eq. of **1** was added and the solution was left for a further 60 minutes. Under the tested conditions, no leaching of the photocatalyst from the support was observed with [Ru]-PEO in either toluene or heptane/EtOAc (5:2 v/v). In polar solvents, the photocatalyst underwent significant leaching. In the case of [Ru]-Amberlyst 15, two different reductive quenchers were tested, namely TEA and ascorbic acid. The immobilised catalyst in combination with TEA displayed no leaching in either toluene or EtOAc. In the case of [Ru]-Amberlyst 15 with ascorbic acid showed no leaching in both DMF and deionised water. These results indicate that $[Ru(bpy)_3]^{2+}$ immobilised on either PEO or Amberlyst 15 could potentially be suitable as the photocatalyst in the hydroxylation of phenylboronic acid to phenol.

2.6.7 Hydroxylation of Phenylboronic acid in Batch with Immobilised Photocatalyst

Employing the same procedure as described in Section 2.2, the hydroxylation of phenylboronic acid (**1**) to phenol (**2**) using immobilised catalyst was carried out in batch. The amount of $[Ru(bpy)_3]^{2+}$ on Amberlyst 15 was estimated to be 3 wt%, while the photocatalyst loading on PEO was 9.1 wt%.

*Table 2-7 Comparison between employing free and immobilised $[Ru(bpy)_3]Cl_2$ as the photocatalyst for the conversion of phenylboronic acid (**1**) to phenol (**2**) under different conditions.*

Entry	Solvent	Photocatalyst (PC)	Reductive quencher (RQ)	Maximum conversion
1	DMF	$[Ru(bpy)_3]Cl_2$	TEA	87 % (47 h)
2	DMF	$[Ru(bpy)_3]Cl_2$	DIPEA	92 % (30 h)
3	Heptane/EtOAc (5:2 v/v)	$[Ru(bpy)_3]Cl_2$	DIPEA	71 % (30 h)
4	EtOAc	[Ru]-Amberlyst 15	TEA	41 % (44 h)
5	Toluene	[Ru]-Amberlyst 15	TEA	trace (47 h)
6	Heptane/EtOAc (5:2 v/v)	[Ru]-PEO	DIPEA	80 % (30 h)
7	DMF	$[Ru(bpy)_3]Cl_2$	H_2A	> 99 % (6 h)
8	DMF	[Ru]-Amberlyst 15	H_2A	> 99 % (24 h)

*Reaction conditions: **1** (0.41 mmol, 0.1 M), PC (2 mol%), RQ (2 eq.), 5x 1000 lumen visible light LEDs, r.t.; [a]Reaction time in parentheses; TEA = trimethylamine, DIPEA = N,N-diisopropylethylamine, H_2A = ascorbic acid*

The hydroxylation of **1** to **2** using [Ru]-Amberlyst 15 as the photocatalyst and TEA as the reductive quencher occurred only in EtOAc (Table 2-7, entry 4), whereas in toluene, only traces of **2** were obtained (Table 2-7, entry 5). This might possibly be explained by the fact that this reaction proceeds more efficiently in polar solvents due to the presence of highly polarised, charged and radical intermediates which are stabilised by polar environments.

The direct comparison between homogeneous and heterogeneous catalysis at the most efficient conditions found for homogeneous catalysis in batch (Section 2.2) was not possible in the case of [Ru]-Amberlyst 15 and TEA due to catalyst leaching for the immobilised catalyst in DMF and MeOH. Compared to the homogeneous process with non-immobilised catalyst, the maximum conversion of **1** to **2** decreased (Table 2-7, entries 1,4). Reduced contact between the photocatalyst and the reactants due to phase separation, and therefore limited diffusion, could potentially provide an explanation.

When ascorbic acid was utilised as the reductive quencher in combination with [Ru]-Amberlyst 15, prolonged irradiation was needed compared to the use of free photocatalyst to reach full conversion (Table 2-7, entries 7,8). Compared to the other reaction conditions using immobilised catalysts, the conditions described in Table 2-7 entry 8 were the only conditions in which full conversion of **1** was achieved. Interestingly, [Ru]-PEO performed better as a photocatalyst than free $[Ru(bpy)_3]^{2+}$ in heptane/EtOAc (5:2 v/v) (Table 2-7, entries 3,6). Both processes are heterogeneous as the photocatalyst did not dissolve in the solvent mixture. It is feasible that the immobilisation process enlarged the surface area of the photocatalyst, increasing the interactions between the photocatalyst and the reactants.

The reaction with [Ru]-PEO was more than twice as efficient as with [Ru]-Amberlyst 15 (Table 2-7, entries 4,6). This could potentially be a result of the stronger reductive quencher employed with [Ru]-PEO since this increased the rate of the reaction by a factor of 2 in DMF (Table 2-7, entries 1,2).

2.6.8 Recycling of the Immobilised Photocatalyst

Using the conditions from Table 2-7, entry 8, recycling of the immobilised catalyst complex [Ru]-Amberlyst 15 was tested. After the first reaction cycle, full conversion was observed after 22 hours. The catalyst beads were filtered from the reaction solution and washed with DMF to remove the product and ascorbic acid. The catalyst beads were then added to a fresh solution of DMF, **1** and ascorbic acid and this mixture was irradiated with the LED light until all **1** was converted to **2**. After three cycles, no decrease in conversion was observed after 24 hours. This corresponds to a turnover number of 150 and a turnover frequency of 6.3 per hour. However, leaching of the photocatalyst out of the support did occur as the reaction solution gained a red colour during the reaction. UV-Vis measurements of the reaction solution were taken after 24 hours, estimating 2.6 ± 0.9 % catalyst leaching in each reaction cycle.

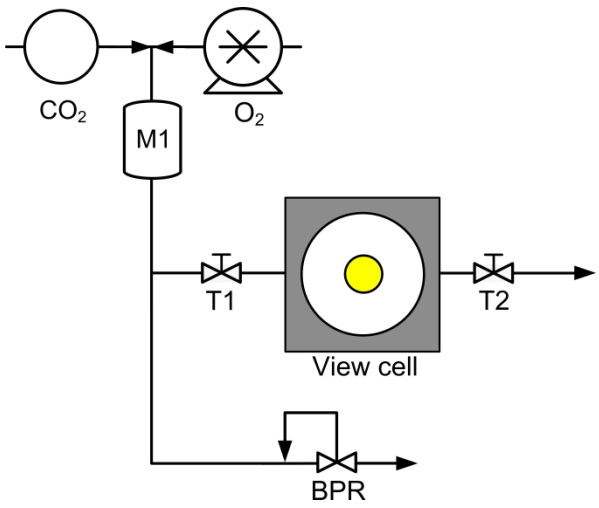
2.7 Photoredox Catalysis in Flow Using $scCO_2$

As explained in Chapter 1, $scCO_2$ is considered an attractive solvent for chemical reactions. For the oxidative hydroxylation of **1**, the miscibility of $scCO_2$ with oxygen[49] is very beneficial as this eliminates phase boundaries between oxygen and both **1** and the photocatalyst. This offers the possibility that oxygen reacts more rapidly and vigorously in $scCO_2$ compared to common organic solvents. Therefore, mass transfer limitations can be diminished and reaction rates could potentially be accelerated.[50] Moreover, the non-flammable character of $scCO_2$ reduces the explosive risk of the presence of oxygen.

2.7.1 Experimental Apparatus: Batch View Cell

Before investigating the hydroxylation of **1** in continuous flow using $scCO_2$ as the solvent, solubility tests with **1** in $scCO_2$ were performed in batch at high-pressure. This batch set-up included a view cell containing pressure rated windows, to visually monitor reactant solubility. Scheme 2-17 shows a simplified diagram of the high-pressure batch reactor set-up, further details can be found in the Experimental Chapter.

All reactants except for CO_2 and O_2 are loaded in the view cell and CO_2 and O_2 are pumped into the system with manual valves T1 and T2 closed. The system pressure would be set at 160-180 bar. By opening T1 very slowly, the CO_2/O_2 mixture enters the view cell and mixes with the reactants. With the view cell completely filled with the CO_2/O_2 mixture and reactants, T1 is then closed. This isolates the mixture in the view cell from the rest of the system. When performing photochemistry in this reactor set-up, a single LED would be placed in front of the window of the view cell to irradiate the mixture. After the experiment, T2 is opened very slowly to release pressure inside the view cell.

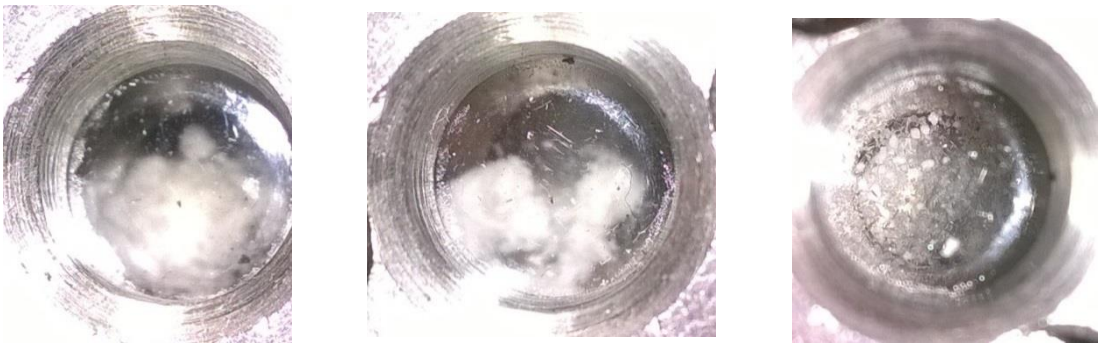


Scheme 2-17 Simplified schematic of the high-pressure batch reactor, with CO_2 and O_2 mixing in mixer M1. The view cell can be isolated by disconnecting the stainless steel tubing at manual valves 1 and 2 (T1, T2). Pressure is held in the system by setting the back pressure regulator (BPR).

2.7.2 Solubility of Phenylboronic Acid in $scCO_2$

Although $scCO_2$ is a desirable solvent from a product separation point of view, its low dielectric constant hinders the solubility of many organic compounds in it. Therefore, the solubility of **1** in $scCO_2$ was tested in a high-pressure view cell. The starting material, phenol, and the photocatalyst were not soluble in $scCO_2$. Therefore, a co-solvent was needed to dissolve the reactants.

With the aim of carrying out the reaction with an immobilised photocatalyst in the future, the co-solvent must dissolve **1** but not the photocatalyst in order to prevent catalyst leaching. EtOAc was used as a co-solvent and the solubility of **1** in $scCO_2$/EtOAc mixtures was tested at 180 bar and 40 °C. The addition of the co-solvent improved the solubility of **1**, but even at a concentration of 0.1 M of **1** in a mixture of $scCO_2$/EtOAc (5:2 mol/mol), **1** did not dissolve completely (Figure 2-23c). Decreasing the concentration of **1** to 0.03 M in a mixture of $scCO_2$/EtOAc (5:2 mol/mol) resulted in a homogeneous solution in which **1** was dissolved. Therefore, these conditions can be used in the hydroxylation of **1** in $scCO_2$/EtOAc.



(a) (b) (c)

*Figure 2-23 Pictures of the batch view cell containing a) 0.1 M **1** in $scCO_2$ (160 bar, 40 °C), b) 0.1 M **1** in $scCO_2$/EtOAc (9:1 mol/mol) (160 bar, 40 °C), c) 0.1 M **1** in $scCO_2$/EtOAc (5:2 mol/mol) (180 bar, 40 °C) for testing the solubility of **1** under different conditions. Although conditions described under a) and b) resulted in poor solubility of **1** in the solvent mixture, conditions depicted under c) provided almost full solubility of **1**.*

2.7.3 Monitoring the Hydroxylation of Phenylboronic Acid in $scCO_2$

In conventional solvents, the hydroxylation of **1** was followed by ^1H NMR. However, when using $scCO_2$ as a solvent, no samples can be taken easily during the reaction as the cell needs to be depressurised before it can be opened to take an aliquot. Therefore, different characterisation techniques were tested for their capability of determining reaction yields inside the $scCO_2$ reactor cell. As the hydroxylation of **1** will be carried out in $scCO_2$ with EtOAc as a co-solvent, EtOAc was used as the medium for these studies. Preliminary tests using Fourier transform infrared spectroscopy (FTIR) and attenuated total reflectance FTIR (ATR-FTIR) were unsuccessful.

Raman spectroscopy was investigated next in order to obtain characteristic vibrational bands of **1** and **2**. Although Raman spectroscopy on solid **1** and **2** showed a promising characteristic vibrational band for **1** at 661 cm^{-1} from the C-B-O bond, this was not observed in solution (EtOAc). In an attempt to enhance the Raman signals of **1** and **2** but not that of EtOAc, surface enhanced Raman spectroscopy (SERS) was attempted. This technique requires a substrate, for example gold or silver, on which electromagnetic enhancement occurs and on which the reagent (**1** or **2**) can adsorb. The SERS substrate was submerged in a solution containing the various reactants and solvents and the Raman probe was situated above this solution, in alignment with the SERS substrate. The greatest Raman signal enhancement will correspond to the strongest adsorption of a compound to the SERS substrate. As a gold coated surface showed no enhancement of **1** and **2** compared to the signal of EtOAc, a silver SERS substrate was tested as this has previously been shown to give signal enhancement of phenol.[51] For **1**, signal enhancement was observed showing some of the vibrational modes predicted. However, in contrast to the gold SERS substrate, no characteristic Raman signals for phenol could be distinguished from EtOAc. In-situ monitoring of the hydroxylation of **1** would require the acquirement of SERS spectra of the whole reaction mixture. To see if the Raman signals of **1** would still be distinguishable from the solvent and other compounds, SERS spectra were taken of a mixture of **1**, $[Ru(bpy)_3]Cl_2.6H_2O$ and DIPEA using a silver SERS substrate. Raman signals of $scCO_2$ are expected to occur at 1277 and 1381 cm^{-1}, obscuring these regions for comparison of the **1** and **2** signals.[52]

However, no distinguishable Raman bands for **1** and **2** could be observed during preliminary studies.

So far, no suitable method has been developed to monitor the conversion of **1** to **2** in EtOAc. As a result, no tests were undertaken to monitor this reaction in $scCO_2$/EtOAc. The most progress for reaction monitoring was obtained with SERS. Therefore, exploring different substrates might prove successful. Although gold and silver based substrates were tested in this work, the surface of the substrate could be varied greatly by the different methods of depositing these metals onto the substrate,[53] which could offer an opportunity for a varying degree of adsorption by different compounds.

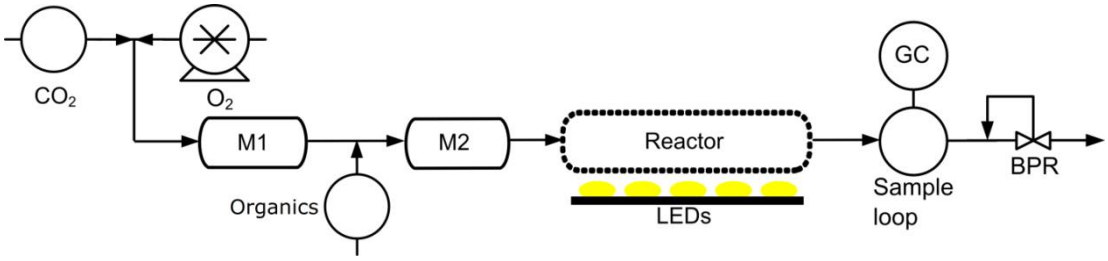
2.7.4 Hydroxylation of Phenylboronic Acid in $scCO_2$/EtOAc in Batch

The hydroxylation of **1** was initially tested in $scCO_2$/EtOAc in batch and an experiment was carried out in the batch view cell, at 40 °C and 180 bar. The batch cell was loaded with **1** (0.1 M in EtOAc), DIPEA (2 eq.) and $[Ru(bpy)_3]Cl_2.6H_2O$ (2 mol%). Before the reaction started, CO_2 and oxygen were dosed into the batch cell, achieving an oxygen concentration of 3.7 % and a 5:2 molar ratio of $scCO_2$ to EtOAc. After 4 hours of irradiation by the LED light, the batch cell was depressurised and ^1H NMR analysis of the reaction mixture showed 46 % conversion of **1**. This encouraging result showed the viability of using $scCO_2$ as the main solvent for the hydroxylation of **1**. Since the reaction proceeded in $scCO_2$ in batch, the reaction was attempted in flow in a high-pressure photoreactor next, using $scCO_2$ as the main solvent in order to scale-up the reaction and to hopefully shorten reaction times.

2.7.5 Performing Photoredox Catalysis in Flow

Details on the continuous flow high-pressure photoreactor are outlined in the Experimental Chapter. In this design, CO_2 was mixed with O_2 prior to the addition

of the organic reagent stream in order to dilute the O_2 in the system which reduces the risk of explosion (Scheme 2-18). Mesitylene acted as the internal standard in order to determine the conversion of **1**. The reactor output containing the mesitylene was analysed with in-line GC and the area of the mesitylene peak was compared to that of phenol.



Scheme 2-18 Simplified diagram of the rig developed for high-pressure continuous photochemistry, with mixers (M1/M2), a sapphire tube reactor at 40 °C illuminated by 3 banks each containing 5 LEDs and a sample loop to take a sample for gas liquid chromatograph (GC) and the back pressure regulator (BPR).

In the reactions outlined below, CO_2 and O_2 were mixed at 180 bar and 40 °C in mixer 1 (M1) after which the organic mixture containing co-solvent, **1** (0.1 M in co-solvent), $[Ru(bpy)_3]Cl_2.6H_2O$ (2 mol%), DIPEA (2 eq.) and mesitylene (1 eq.) was pumped into the reactor to mix with the $scCO_2/O_2$ mixture. The oxygen was dosed so that the concentration would be 3.7 % in the end mixture and 10 % of co-solvent (EtOAc or MeOH)/substrate mixture in $scCO_2$ was accomplished by controlling the flow rates of both CO_2 and the organic components. Due to safety concerns regarding the presence of flammable co-solvent and potentially explosive O_2, 10 % co-solvent in $scCO_2$ was used as a maximum concentration. The reactor outlet was depressurised by the settings on the back pressure regulator (BPR) and GC samples were taken *via* the sample loop.

2.7.5.1 Homogeneous Hydroxylation of Phenylboronic Acid in Flow Using $scCO_2$

Using this high-pressure flow reactor, methanol (MeOH) and ethyl acetate (EtOAc) were tested as co-solvents for $scCO_2$ in the hydroxylation of phenylboronic acid. A homogeneous solution of **1** (4.0 mmol, 0.1 M), $[Ru(bpy)_3]Cl_2.6H_2O$ (2 mol%) and DIPEA (2 eq.) in either MeOH or EtOAc was pumped through the reactor. Although multiple attempts were made, the results were identical each time. Table 2-8 shows the outcome of these reactions.

The first homogeneous hydroxylation of **1** in flow was attempted with MeOH as the co-solvent for $scCO_2$ (Table 2-8, entry 1), following the procedure described *vide supra*. Although the cooling bath was set to keep the reactor temperature at 40 °C, the inside of the reactor reached 80 °C within 20 minutes, most likely due to insufficient circulation of the cooling liquid.

Table 2-8 Reaction conditions for the continuous hydroxylation of phenylboronic acid in $scCO_2$ in the high-pressure flow reactor.

Entry	Solvent	Pressure	Temperature	O_2[a]	Result
1	10 % MeOH in $scCO_2$	180 bar	40 °C (inside the reactor reached 80 °C)	3.7 %	Precipitation of photocatalyst
2	10 % EtOAc in $scCO_2$	180 bar	40 °C	3.7 %	Blockages

*Reaction conditions: **1** (4.0 mmol, 0.1 M), $[Ru(bpy)_3]Cl_2.6H_2O$ (2 mol%), DIPEA (2 eq.), 3x5 1000 lumen visible light LEDs; [a]Molar %*

When the reactor was examined after the reaction, precipitated photocatalyst was found on the walls of the sapphire tube reactor (Figure 2-24). The liquid collected at the output of the reactor was coloured red, indicating that not all ruthenium photocatalyst precipitated out on the walls during the reaction. It appeared that the solubility of the photocatalyst in methanol was reduced under these conditions, leading to precipitation of the photocatalyst.

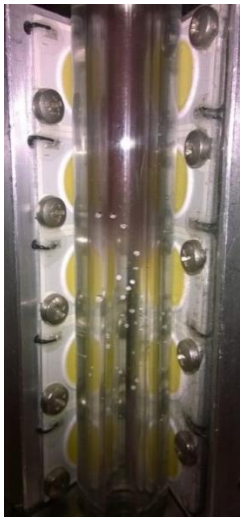


*Figure 2-24 Photo of the reactor inside the continuous flow rig after the hydroxylation of **1** via homogeneous catalysis with 10 % MeOH in $scCO_2$ showing precipitated photocatalyst on the reactor walls.*

Monitoring the reaction progress was a challenge as not all the components in the reaction were soluble in $scCO_2$ to the same degree. Therefore, the mixture coming out of the flow reactor contained very likely a higher concentration of components that were soluble in $scCO_2$. In-line GC was utilised to take aliquots under pressure. GC analysis of this run showed that no phenol was formed.

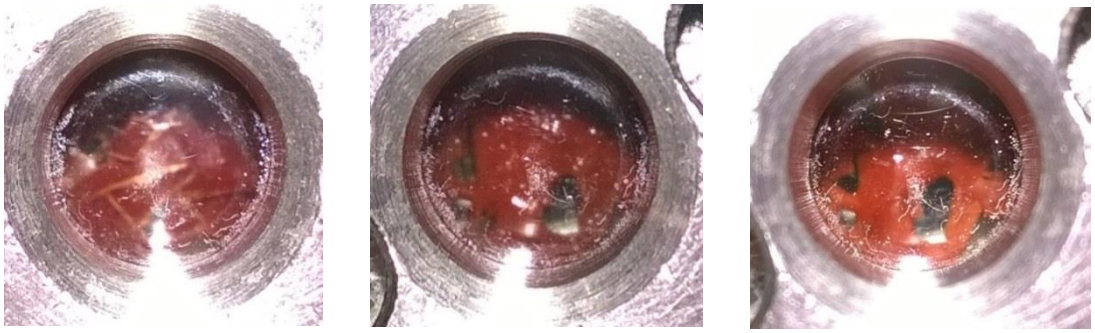
The next experiment was performed using EtOAc as co-solvent (Table 2-8, entry 2). Extensive sonication of the reaction mixture afforded a homogeneous solution. However, blockage of the system was observed when the organic mixture was pumped through the flow rig and the experiment had to be discontinued. Dilution of the reactants in EtOAc by a factor of 10 prior to reaction did not improve on this and blockages could not be prevented.

2.7.5.2 Heterogeneous Hydroxylation of Phenylboronic Acid in Flow Using $scCO_2$

Since the hydroxylation of **1** in homogeneous flow was shown to be problematic with, most likely, the photocatalyst causing the blockage of the reactor, the reaction with immobilised catalyst was attempted in the same flow reactor. In batch, leaching of the photocatalyst out of [Ru]-Amberlyst 15 was observed as described *vide supra*. Therefore, for the flow experiments described below, [Ru]-PEO was utilised as the catalyst complex. In this experiment, the sapphire tube reactor was packed with the [Ru]-PEO discs prior to starting the photochemical reaction.

Influence of $scCO_2$ on Polymer Support

Before using the supported catalyst in the conversion of **1** to **2**, the influence of $scCO_2$ on this support was investigated. Amberlyst 15 has been used in $scCO_2$ before[54] without any structural changes of Amberlyst 15. However, it has been reported that $scCO_2$ is able to plasticise PEO.[55] Therefore, the interaction between $scCO_2$ and [Ru]-PEO was investigated in the batch reactor view cell. Fragments of [Ru]-PEO discs were placed in the batch cell which was subsequently pressurised to 180 bar at a temperature of 40 °C. Upon reaching 180 bar, the PEO in the immobilised catalyst disc had plasticised (Figure 2-25). Plasticisation occurred as PEO can capture CO_2 in its structure. No further structural changes of plasticised PEO were observed after 160 minutes. As the photocatalyst on PEO did not seem affected, this polymer support was still used in further experiments.



(a) (b) (c)

Figure 2-25 Photos of the high-pressure batch cell containing [Ru]-PEO disc fragments at a) 0 bar, b) 180 bar after 0 minutes, c) 180 bar after 160 minutes; showing that plasticisation of PEO occurred at reaching 180 bar.

Conversion of 1 to 2 in 10 % EtOAc in $scCO_2$ with [Ru]-PEO discs

The high-pressure continuous flow photoreactor was used to study the hydroxylation of **1** in $scCO_2$ and EtOAc. The reactor (internal volume of 7 mL) was filled with 2 discs of [Ru]-PEO (33 mm in diameter), curled up against the walls of the sapphire tube reactor (Figure 2-26, left). Each disc had a surface area of approximately 8.6 cm^2. The total flow rate of organics and $scCO_2$ was 0.3 mL/min and the residence time for irradiation was 21 minutes. Flushing $scCO_2$ through the photoreactor filled with the [Ru]-PEO complex prior to the photochemical reaction caused minor plasticisation of PEO, resulting in swelling of the PEO. During the photochemical reaction, the reaction mixture output contained a small amount of leached photocatalyst, followed by colourless solution. This limited amount of initial leaching of the photocatalyst might have been caused by photocatalyst present on the surface of PEO as there would probably not be any further interactions between the photocatalyst and the support to hold the photocatalyst onto the support. After 30 minutes of irradiation time, the reaction was stopped. A red to black colour change of the [Ru]-PEO discs inside the sapphire tube reactor was observed, indicating degradation of the photocatalyst. Moreover, the PEO was plasticised in large areas (Figure 2-26, right). The estimated conversion from **1** to **2** was 5 %, as determined by in-line GC (aliquot after 30 min.). This low conversion could be a result of the low contact area between the reaction mixture and the

photocatalyst. Only reactants flowing near the reactor walls could have interacted with the excited state photocatalyst. Moreover, degradation of the photocatalyst most likely reduced the amount of active photocatalyst.

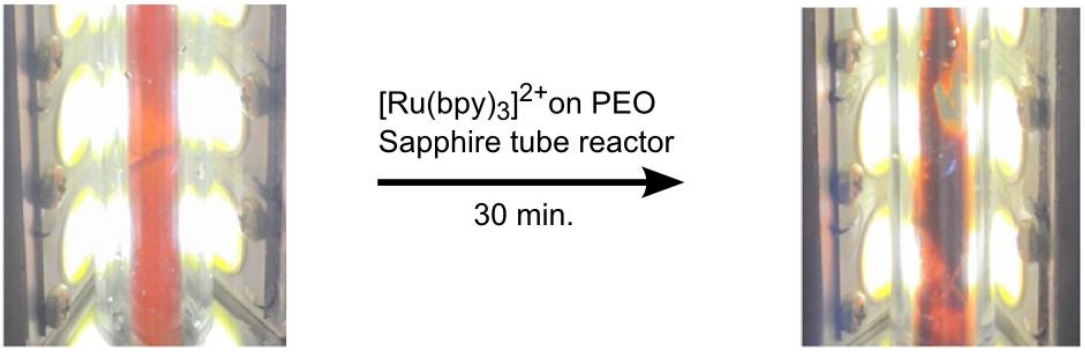


*Figure 2-26 Reactor filled with [Ru]-PEO discs before (left) and after 30 minutes of reaction time (right) in the conversion of **1** to **2** in 10 % EtOAc in $scCO_2$. Plasticisation of PEO and degradation of the photocatalyst were observed after the reaction as indicated by the dark areas on the immobilised catalyst disc and the disappearance of the original disc shape in the picture on the right.*

Conversion of 1 to 2 in 10 % EtOAc in $scCO_2$ with [Ru]-PEO discs and glass beads

After establishing the possibility of performing heterogeneous hydroxylation of **1** in flow, a new approach for the position of [Ru]-PEO inside of the reactor was developed. Glass beads (1.5-2 mm in diameter) were utilised to support the [Ru]-PEO discs. One [Ru]-PEO disc (33 mm in diameter) was cut into roughly 0.3 cm^2 sized pieces and distributed throughout the sapphire tube filled with glass beads (Figure 2-27, left). In this method, the [Ru]-PEO can plasticise onto the glass beads and remain active for irradiation instead of moving down the reactor. Moreover, the distance between the LED light and the catalyst is greater since the catalyst is now distributed throughout the whole reactor instead of placed against the walls of the reactor. This was thought to reduce the heat experienced by the photocatalyst and can hopefully prevent catalyst degradation. The presence of the catalyst in the middle of reactor also provides more of its surface area to be in contact with the flow of reactants which should result in more efficient catalysis. The disadvantage of this system is the smaller internal

reactor volume as glass beads occupied *ca* 2/3 of the reactor volume, decreasing the reactor volume to 2.3 mL. The reaction had to be stopped after 30 minutes as blockages in the flow rig caused overpressure in the system. As the few drops coming out of the flow rig were coloured, it was assumed that $[Ru(bpy)_3]^{2+}$ leached out of PEO which also explains the pale colour of the [Ru]-PEO discs after the reaction was stopped (Figure 2-27, right). It is possible that enhanced contact between the supported photocatalyst and the reaction solution led to a higher degree of leaching.

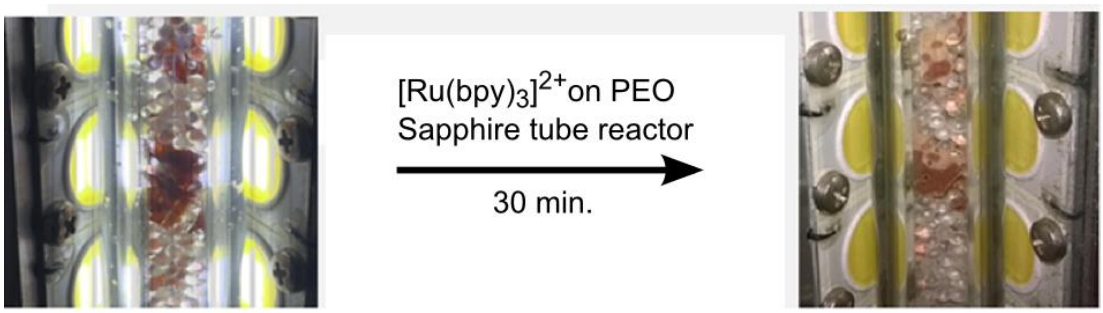


*Figure 2-27 Reactor filled with [Ru]-PEO disc fragments and glass beads (1.5-2 mm) before (left) and after 30 minutes of reaction time (right) in the conversion of **1** to **2** in 10 % EtOAc in $scCO_2$. Plasticisation of PEO and leaching of the photocatalyst out of PEO were observed after the reaction as indicated by the structural and colour change of the immobilised photocatalyst in the picture on the right.*

Aliquots analysed by GC revealed conversion from **1** to **2** to be 7 % in this 2.3 mL reactor. This was a very promising result since the amount of catalyst was reduced compared to previous experiments due to the challenge of packing the reactor. This yield was obtained after only 7 minutes of residence time. Although the issue of the blockage needs to be resolved, this set-up of the flow reactor seems very promising for improving the reaction efficiency.

2.8 Conclusions and Future Work

In this Chapter, the main focus was the utilisation of visible light photoredox catalysis for the hydroxylation of phenylboronic acid to phenol. Experiments were

conducted successfully in continuous flow and screening of reaction conditions led to a 90-fold increase in productivity compared to the reaction carried out under similar reaction conditions in batch. Quantum chemical DFT calculations suggested that the insertion of superoxide into phenylboronic acid was the rate-determining step of the reaction and the experimental results indeed indicated the crucial role of oxygen concentration on reaction conversion. To address the sustainable character of the reaction, $[Ru(bpy)_3]Cl_2$ was immobilised on both Amberlyst 15 and PEO while maintaining its photophysical properties. Immobilisation of the catalyst on Amberlyst 15 reduced the reaction rate in the hydroxylation of phenylboronic acid, but the immobilised catalyst complex was reused up to 3 times as an active photocatalyst. Preliminary results with $[Ru(bpy)_3]Cl_2$ immobilised on PEO in continuous flow showed the potential for heterogeneous photocatalysis in flow using $scCO_2$ as a co-solvent. 7 % conversion of phenylboronic acid was achieved in only 7 minutes of irradiation time in a 2.3 mL reactor. Other methods to improve the reaction in terms of Green Chemistry involved the successful use of non-metal containing photocatalyst Rose Bengal for the hydroxylation of phenylboronic acid. To investigate the control over reaction selectivity obtained by performing reactions in continuous flow as opposed to batch experiments, the desymmetrisation of aryl diboronic acids was studied. The mono-hydroxylation of these diboronic acids was achieved in moderate to high selectivities in the continuous flow reactor. DFT calculations on the different steps in these desymmetrisation reactions gave an indication on substrate orientation and the energy levels in the first and second process of hydroxylation.

Future experiments could be focussed on the development of using immobilised catalysts in flow as photobleaching and leaching present a significant problem as for now. Based on the work presented in Section 2.7.5.2, it would be interesting to coat individual glass beads with the [Ru]-PEO catalyst complex to enlarge the contact area with the reaction mixture flowing through the reactor. These coated glass beads would be situated inside the sapphire tube reactor. Another research area could be the immobilisation of Rose Bengal photocatalyst on Amberlite IRA 900 or Seralite SRA 400 and that way improve the sustainable character of this reaction even further.[56]

2.9 References

1. (a) Balzani, V.; Bergamini, G.; Ceroni, P., *Angew. Chem. Int. Ed.* **2015,** *54* (39), 11320-11337; (b) Teplý, F., *Collect. Czech. Chem. Commun.* **2011,** *76* (7), 859-917; (c) Prier, C. K.; Rankic, D. A.; MacMillan, D. W. C., *Chem. Rev.* **2013,** *113* (7), 5322-5363.

2. (a) Amara, Z.; Bellamy, J., F. B.; Horvath, R.; Miller, S. J.; Beeby, A.; Burgard, A.; Rossen, K.; Poliakoff, M.; George, M. W., *Nat. Chem.* **2015,** *7* (6), 489-495; (b) Bourne, R. A.; Han, X.; Poliakoff, M.; George, M. W., *Angew. Chem. Int. Ed.* **2009,** *48* (29), 5322-5325; (c) Bourne, R. A.; Han, X.; Chapman, A. O.; Arrowsmith, N. J.; Kawanami, H.; Poliakoff, M.; George, M. W., *Chem. Commun.* **2008**, 4457-4459; (d) Han, X.; Bourne, R. A.; Poliakoff, M.; George, M. W., *Chem. Sci.* **2011,** *2* (6), 1059-1067; (e) Hall, J. F. B.; Han, X.; Poliakoff, M.; Bourne, R. A.; George, M. W., *Chem. Commun.* **2012,** *48* (25), 3073-3075; (f) Han, X.; Bourne, R. A.; Poliakoff, M.; George, M. W., *Green Chem.* **2009,** *11* (11), 1787-1792; (g) Hall, J. F. B.; Bourne, R. A.; Han, X.; Earley, J. H.; Poliakoff, M.; George, M. W., *Green Chem.* **2013,** *15* (1), 177-180.

3. (a) Anderson, K. W.; Ikawa, T.; Tundel, R. E.; Buchwald, S. L., *J. Am. Chem. Soc.* **2006,** *128* (33), 10694-10695; (b) Inamoto, K.; Nozawa, K.; Yonemoto, M.; Kondo, Y., *Chem. Commun.* **2011,** *47* (42), 11775-11777; (c) Chen, G.; Chan, A. S. C.; Kwong, F. Y., *Tetrahedron Lett.* **2007,** *48* (3), 473-476; (d) Maleczka, R. E.; Shi, F.; Holmes, D.; Smith, M. R., *J. Am. Chem. Soc.* **2003,** *125* (26), 7792-7793.

4. (a) Gogoi, P.; Bezboruah, P.; Gogoi, J.; Boruah, R. C., *Eur. J. Org. Chem.* **2013,** *2013* (32), 7291-7294; (b) He, Z.; Jamison, T. F., *Angew. Chem.* **2014,** *126* (13), 3421-3425; (c) Tyman, J., *Synthetic and Natural Phenols*. Elsevier: New York: 1996; (d) Quideau, S.; Deffieux, D.; Douat-Casassus, C.; Pouységu, L., *Angew. Chem. Int. Ed.* **2011,** *50* (3), 586-621.

5. (a) Chowdhury, A. D.; Mobin, S. M.; Mukherjee, S.; Bhaduri, S.; Lahiri, G. K., *Eur. J. Inorg. Chem.* **2011,** *2011* (21), 3232-3239; (b) Xu, J.; Wang, X.; Shao, C.; Su, D.; Cheng, G.; Hu, Y., *Org. Lett.* **2010,** *12* (9), 1964-1967; (c) Yang, H.; Li, Y.; Jiang, M.; Wang, J.; Fu, H., *Chem. Eur. J.* **2011,** *17* (20), 5652-5660; (d) Yang, D.; An, B.; Wei, W.; Jiang, M.; You, J.; Wang, H., *Tetrahedron* **2014,** *70* (22), 3630-3634; (e) Zheng, J.; Lin, S.; Zhu, X.; Jiang, B.; Yang, Z.; Pan, Z., *Chem. Commun.* **2012,** *48* (50), 6235-6237; (f) Wang, L.; Zhang, W.; Sheng Su, D.; Meng, X.; Xiao, F.-S., *Chem. Commun.* **2012,** *48* (44), 5476-5478; (g) Affrose, A.; Azath, I. A.; Dhakshinamoorthy, A.; Pitchumani, K., *J. Mol. Catal. A: Chem.* **2014,** *395*, 500-505; (h) Gogoi, N.; Gogoi, P. K.; Borah, G.; Bora, U., *Tetrahedron Lett.* **2016,** *57* (36), 4050-4052; (i) Dhakshinamoorthy, A.; Asiri, A. M.; Garcia, H., *Tetrahedron* **2016,** *72* (22), 2895-2899; (j) Schulz, T.; Torborg, C.; Schäffner, B.; Huang, J.; Zapf, A.; Kadyrov, R.; Börner, A.; Beller, M., *Angew. Chem. Int. Ed.* **2009,** *48* (5), 918-921.

6. (a) Simon, J.; Salzbrunn, S.; Surya Prakash, G. K.; Petasis, N. A.; Olah, G. A., *J. Org. Chem.* **2000,** *66* (2), 633-634; (b) Webb, K. S.; Levy, D., *Tetrahedron Lett.* **1995,** *36* (29), 5117-5118; (c) Travis, B. R.; Ciaramitaro, B. P.; Borhan, B., *Eur. J. Org. Chem.* **2002,** *2002* (20),

3429-3434; (d) Zhong, Y.; Yuan, L.; Huang, Z.; Gu, W.; Shao, Y.; Han, W., *RSC Adv.* **2014,** *4* (63), 33164-33167; (e) Wang, L.; Dai, D.-Y.; Chen, Q.; He, M.-y., *J. Fluorine Chem.* **2014,** *158*, 44-47; (f) Mulakayala, N.; Ismail; Kumar, K. M.; Rapolu, R. K.; Kandagatla, B.; Rao, P.; Oruganti, S.; Pal, M., *Tetrahedron Lett.* **2012,** *53* (45), 6004-6007; (g) Jiang, M.; Yang, H.-J.; Li, Y.; Jia, Z.-Y.; Fu, H., *Chin. Chem. Lett.* **2014,** *25* (5), 715-719; (h) Gupta, S.; Chaudhary, P.; Srivastava, V.; Kandasamy, J., *Tetrahedron Lett.* **2016,** *57* (23), 2506-2510.

7. Contreras-Celedón, C. A.; Chacón-García, L.; Lira-Corral, N. J., *J. Chem.* **2014,** *2014*, 1-5.

8. (a) Cheng, G.; Zeng, X.; Cui, X., *Synthesis* **2014,** *46* (3), 295-300; (b) Zhu, C.; Wang, R.; Falck, J. R., *Org. Lett.* **2012,** *14* (13), 3494-3497; (c) Ding, W.; Chen, J.-R.; Zou, Y.-Q.; Duan, S.-W.; Lu, L.-Q.; Xiao, W.-J., *Org. Chem. Front.* **2014,** *1* (2), 151-154; (d) Zhong, Y.; Yuan, L.; Huang, Z.; Gu, W.; Shao, Y.; Han, W., *RSC Adv.* **2014,** *4* (63), 33164-33167; (e) Kotoučová, H.; Strnadová, I.; Kovandová, M.; Chudoba, J.; Dvořáková, H.; Cibulka, R., *Org. Biomol. Chem.* **2014,** *12* (13), 2137-2142; (f) Silveira-Dorta, G.; Monzon, D. M.; Crisostomo, F. P.; Martin, T.; Martin, V. S.; Carrillo, R., *Chem. Commun.* **2015,** *51* (32), 7027-7030.

9. (a) Qi, H.-L.; Chen, D.-S.; Ye, J.-S.; Huang, J.-M., *J. Org. Chem.* **2013,** *78* (15), 7482-7487; (b) Jiang, H.; Lykke, L.; Uttrup Pedersen, S.; Xiao, W.-J.; Anker Jorgensen, K., *Chem. Commun.* **2012,** *48* (57), 7203-7205.

10. (a) Tada, N.; Cui, L.; Ishigami, T.; Ban, K.; Miura, T.; Uno, B.; Itoh, A., *Green Chem.* **2012,** *14* (11), 3007-3009; (b) Cheng, Y.; Yang, J.; Qu, Y.; Li, P., *Org. Lett.* **2011,** *14* (1), 98-101.

11. Punniyamurthy, T.; Velusamy, S.; Iqbal, J., *Chem. Rev.* **2005,** *105* (6), 2329-2364.

12. (a) Wang, L.; Ma, Z.-G.; Wei, X.-J.; Meng, Q.-Y.; Yang, D.-T.; Du, S.-F.; Chen, Z.-F.; Wu, L.-Z.; Liu, Q., *Green Chem.* **2014,** *16* (8), 3752-3757; (b) Nagasawa, Y.; Tanba, K.; Tada, N.; Yamaguchi, E.; Itoh, A., *Synlett* **2015,** *26* (3), 412-415; (c) Cheng, X.; Yang, B.; Hu, X.; Xu, Q.; Lu, Z., *Chem. Eur. J.* **2016,** *22* (49), 17566-17570.

13. Zou, Y.-Q.; Chen, J.-R.; Liu, X.-P.; Lu, L.-Q.; Davis, R. L.; Jørgensen, K. A.; Xiao, W.-J., *Angew. Chem.* **2012,** *124* (3), 808-812.

14. (a) Paul, A.; Chatterjee, D.; Rajkamal; Halder, T.; Banerjee, S.; Yadav, S., *Tetrahedron Lett.* **2015,** *56* (19), 2496-2499; (b) Luo, J.; Zhang, X.; Zhang, J., *ACS Catal.* **2015,** *5* (4), 2250-2254; (c) Matsui, K.; Ishigami, T.; Yamaguchi, T.; Yamaguchi, E.; Tada, N.; Miura, T.; Itoh, A., *Synlett* **2014,** *25* (18), 2613-2616; (d) Pitre, S. P.; McTiernan, C. D.; Ismaili, H.; Scaiano, J. C., *J. Am. Chem. Soc.* **2013,** *135* (36), 13286-13289; (e) Yu, X.; Cohen, S. M., *Chem. Commun.* **2015,** *51* (48), 9880-9883; (f) Poznik, M.; Konig, B., *React. Chem. Eng.* **2016,** *1* (5), 494-500; (g) Sawant, S. D.; Hudwekar, A. D.; Aravinda Kumar, K. A.; Venkateswarlu, V.; Singh, P. P.; Vishwakarma, R. A., *Tetrahedron Lett.* **2014,** *55* (4), 811-814.

15. Jiang, M.; Yang, H.; Fu, H., *Org. Lett.* **2016,** *18* (20), 5248-5251.

16. (a) Johnson, J. A.; Luo, J.; Zhang, X.; Chen, Y.-S.; Morton, M. D.; Echeverría, E.; Torres, F. E.; Zhang, J., *ACS Catal.* **2015,** *5* (9), 5283-5291; (b) Toyao, T.; Ueno, N.; Miyahara, K.; Matsui, Y.; Kim, T.-H.; Horiuchi, Y.; Ikeda, H.; Matsuoka, M., *Chem. Commun.* **2015,** *51* (89), 16103-16106.

17. (a) Anderson, N. G., *Org. Proc. Res. Dev.* **2012,** *16* (5), 852-869; (b) Mason, B. P.; Price, K. E.; Steinbacher, J. L.; Bogdan, A. R.; McQuade, D. T., *Chem. Rev.* **2007,** *107* (6), 2300-2318.

18. Sikora, A.; Zielonka, J.; Lopez, M.; Joseph, J.; Kalyanaraman, B., *Free Radic. Biol. Med.* **2009,** *47* (10), 1401-1407.

19. Jiang, M.; Li, Y.; Yang, H.; Zong, R.; Jin, Y.; Fu, H., *RSC Adv.* **2014,** *4* (25), 12977-12980.

20. (a) Ollivier, C.; Renaud, P., *Chem. Rev.* **2001,** *101* (11), 3415-3434; (b) Allies, P. G.; Brindley, P. B., *J. Chem. Soc. B* **1969**, 1126-1131.

21. (a) Becke, A. D., *J. Chem. Phys.* **1993,** *98* (7), 5648-5652; (b) Becke, A. D., *J. Chem. Phys.* **1993,** *98* (2), 1372-1377; (c) Lee, C.; Yang, W.; Parr, R. G., *Phys. Rev. B.* **1988,** *37* (2), 785-789.

22. Bull, S. D.; Davidson, M. G.; van den Elsen, J. M. H.; Fossey, J. S.; Jenkins, A. T. A.; Jiang, Y.-B.; Kubo, Y.; Marken, F.; Sakurai, K.; Zhao, J.; James, T. D., *Accounts Chem. Res.* **2012,** *46* (2), 312-326.

23. Clary, J. W. PhD Thesis. University of California, California, 2012.

24. Krishnan, C. V.; Sutin, N., *J. Am. Chem. Soc.* **1981,** *103* (8), 2141-2142.

25. (a) Wang, M.; Na, Y.; Gorlov, M.; Sun, L., *Dalton Trans.* **2009,** (33), 6458-6467; (b) Creutz, C., *Inorg. Chem.* **1981,** *20* (12), 4449-4452; (c) Borak, J. B.; Falvey, D. E., *J. Org. Chem.* **2009,** *74* (10), 3894-3899; (d) Wallentin, C.-J.; Nguyen, J. D.; Finkbeiner, P.; Stephenson, C. R. J., *J. Am. Chem. Soc.* **2012,** *134* (21), 8875-8884.

26. Nanni, E. J.; Stallings, M. D.; Sawyer, D. T., *J. Am. Chem. Soc.* **1980,** *102* (13), 4481-4485.

27. (a) Ravelli, D.; Protti, S.; Fagnoni, M., *Chem. Rev.* **2016,** *116* (17), 9850-9913; (b) Arbogast, J. W.; Foote, C. S.; Kao, M., *J. Am. Chem. Soc.* **1992,** *114* (6), 2277-2279.

28. Han, X. PhD Thesis. University of Nottingham, Nottingham, 2010.

29. Bellamy, J. PhD Thesis. University of Nottingham, Nottingham, 2014.

30. (a) Patel, M. K.; Davis, B. G., *Org. Biomol. Chem.* **2010,** *8* (19), 4232-4235; (b) Licence, P.; Gray, W. K.; Sokolova, M.; Poliakoff, M., *J. Am. Chem. Soc.* **2004,** *127* (1), 293-298; (c) Seyler, H.; Haid, S.; Kwon, T.-H.; Jones, D. J.; Bäuerle, P.; Holmes, A. B.; Wong, W. W. H., *Aust. J. Chem.* **2013,** *66* (2), 151-156.

31. Hall, D. G., Structure, Properties, and Preparation of Boronic Acid Derivatives. In *Boronic Acids*, Wiley-VCH Verlag GmbH & Co. KGaA: Weinheim, 2011; pp 1-100.

32. Durka, K.; Jarzembska, K. N.; Kamiński, R.; Luliński, S.; Serwatowski, J.; Woźniak, K., *Cryst. Growth Des.* **2013,** *13* (10), 4181-4185.

33. Ravelli, D.; Protti, S.; Fagnoni, M.; Albini, A., *Curr. Org. Chem.* **2013,** *17* (21), 2366-2373.

34. (a) Reger, T. S.; Janda, K. D., *J. Am. Chem. Soc.* **2000,** *122* (29), 6929-6934; (b) Clapham, B.; Reger, T. S.; Janda, K. D., *Tetrahedron* **2001,** *57* (22), 4637-4662; (c) Anyanwu, U. K. PhD Thesis. University of Massachusetts Amherst, Massachusetts, 2005.

35. Marrodan, C. M.; Berti, D.; Liguori, F.; Barbaro, P., *Catal. Sci. Technol.* **2012,** *2* (11), 2279-2290.

36. (a) Bandini, M.; Benaglia, M.; Sinisi, R.; Tommasi, S.; Umani-Ronchi, A., *Org. Lett.* **2007,** *9* (11), 2151-2153; (b) Kirschning, A.; Solodenko, W.; Mennecke, K., *Chem. Eur. J.* **2006,** *12* (23), 5972-5990; (c) Corma, A.; Garcia, H., *Adv. Synth. Catal.* **2006,** *348* (12-13), 1391-1412.

37. Benaglia, M., *Recoverable and recyclable catalysts*. John Wiley & Sons Ltd: Chichester, 2009.

38. (a) Barbaro, P.; Bianchini, C.; Giambastiani, G.; Oberhauser, W.; Bonzi, L. M.; Rossi, F.; Dal Santo, V., *Dalton Trans.* **2004,** (12), 1783-1784; (b) Simons, C.; Hanefeld, U.; Arends, I. W. C. E.; Maschmeyer, T.; Sheldon, R. A., *J. Catal.* **2006,** *239* (1), 212-219.

39. Rubinstein, I.; Bard, A. J., *J. Am. Chem. Soc.* **1980,** *102* (21), 6641-6642.

40. Zhang, G.; Song, I. Y.; Park, T.; Choi, W., *Green Chem.* **2012,** *14* (3), 618-621.

41. Ogawa, M.; Nakamura, T.; Mori, J.-i.; Kuroda, K., *J. Phys. Chem. B* **2000,** *104* (35), 8554-8556.

42. Han, S.; Wei, Y.; Grzybowski, B. A., *Chem. Eur. J.* **2013,** *19* (34), 11194-11198.

43. DeWilde, W.; Peeters, G.; Lunsford, J. H., *J. Phys. Chem.-US* **1980,** *84* (18), 2306-2310.

44. Benaglia, M., *New J. Chem.* **2006,** *30* (11), 1525-1533.

45. (a) Yao, Q.; Rodriguez Motta, A., *Tetrahedron Lett.* **2004,** *45* (11), 2447-2451; (b) Zaman, S.; Abell, A. D., *Tetrahedron Lett.* **2009,** *50* (38), 5340-5343; (c) Guerreiro, P.; Ratovelomanana-Vidal, V.; Genêt, J.-P.; Dellis, P., *Tetrahedron Lett.* **2001,** *42* (20), 3423-3426; (d) Fan, Q.-H.; Deng, G.-J.; Lin, C.-C.; Chan, A. S. C., *Tetrahedron-Asymmetr.* **2001,** *12* (8), 1241-1247.

46. (a) Zhang, J.-L.; Che, C.-M., *Org. Lett.* **2002,** *4* (11), 1911-1914; (b) Chinnusamy, T.; Rodionov, V.; Kühn, F. E.; Reiser, O., *Adv. Synth. Catal.* **2012,** *354* (9), 1827-1831; (c) Zhang, J.-L.; Huang, J.-S.; Che, C.-M., *Chem. Eur. J.* **2006,** *12* (11), 3020-3031; (d) Benaglia, M.; Danelli, T.; Pozzi, G., *Org. Biomol. Chem.* **2003,** *1* (3), 454-456.

47. Blaser, H.-U.; Malan, C.; Pugin, B.; Spindler, F.; Steiner, H.; Studer, M., *Adv. Synth. Catal.* **2003,** *345* (1-2), 103-151.

48. McMorn, P.; Hutchings, G. J., *Chem. Soc. Rev.* **2004,** *33* (2), 108-122.

49. Seki, T.; Baiker, A., *Chem. Rev.* **2009,** *109* (6), 2409-2454.

50. Musie, G.; Wei, M.; Subramaniam, B.; Busch, D. H., *Coord. Chem. Rev.* **2001,** *219–221*, 789-820.

51. (a) Li, D.; Li, D.-W.; Fossey, J. S.; Long, Y.-T., *Anal. Chem.* **2010,** *82* (22), 9299-9305; (b) Sánchez-Cortés, S.; Garcia-Ramos, J. V., *J. Colloid Interf. Sci.* **2000,** *231* (1), 98-106.

52. Grignard, B.; Gilbert, B.; Malherbe, C.; Jérôme, C.; Detrembleur, C., *ChemPhysChem* **2012,** *13* (11), 2666-2670.

53. Fan, M.; Andrade, G. F. S.; Brolo, A. G., *Anal. Chim. Acta* **2011,** *693* (1-2), 7-25.

54. (a) Rezayat, M.; Ghaziaskar, H. S., *Green Chem.* **2009,** *11* (5), 710-715; (b) Stevens, J. G.; Bourne, R. A.; Poliakoff, M., *Green Chem.* **2009,** *11* (3), 409-416.

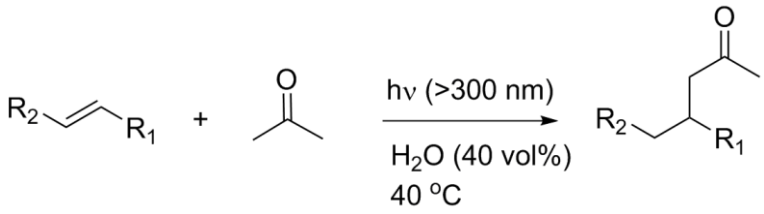
55. (a) Yang, Z.-Z.; He, L.-N.; Zhao, Y.-N.; Li, B.; Yu, B., *Energ. Environ. Sci.* **2011,** *4* (10), 3971-3975; (b) Li, J.; Ye, Y.; Chen, L.; Qi, Z., *J. Chem. Eng. Data* **2011,** *57* (2), 610-616; (c) Chen, X.; Feng, J. J.; Bertelo, C. A., *Polym. Eng. Sci.* **2006,** *46* (1), 97-107; (d) Kendall, J. L.; Canelas, D. A.; Young, J. L.; DeSimone, J. M., *Chem. Rev.* **1999,** *99* (2), 543-564.

56. Gazi, S.; Ananthakrishnan, R., *Appl. Catal., B.* **2011,** *105* (3–4), 317-325.

Chapter 3 Olefin and Ketone Coupling

The formation of ketones is important for synthesis including that of natural products since most natural products utilise this moiety either as a building block during synthesis or contain it in the end product.[1] Ketone functionality is often introduced *via* the oxidation of an alcohol. However, toxic, harsh or reactive reagents such as chromium based oxidants,[2] activated dimethyl sulfoxide[2] and hypervalent iodine complexes are often required.[3] The common use of flammable solvents on top of these harmful reagents has made the use of alcohol oxidations for large-scale production processes a challenging transformation due to safety concerns.[4] Molecular oxygen has received attention for its use as a terminal oxidant due to potential economic and environmental benefits. Transition metal free variants of this method exist, but toxic reagents such as halogen containing compounds[5] or the use of pressurised oxygen,[6] which is a safety concern, are often required. Alternative routes for ketone synthesis include the Wacker reaction in which olefin oxidation takes place and the cross-coupling of organoborons with haloarenes or acyl halides in the Suzuki-Miyaura reaction.[7] These methods still involve the use of transition metals which can be expensive. Therefore, more sustainable and efficient transformations to ketones are desirable to help in the production of clean industrial processes particularly as the disposal of undesired by-products and hazardous waste is often problematic.[8]

As a step towards a more sustainable route for the formation of ketones, Shiraishi *et al.* reported a photochemical, metal-free route to extended ketones by the intermolecular coupling of acetone with olefins (Scheme 3-1).[7] This method utilises light (from a Xe lamp) as the activation source and water as the co-solvent. Controlling reaction selectivity is crucial in this transformation as many side products can be formed. Although the reported yields and selectivities of a variety of methyl ketones were high (73-94 %), long reaction times were required to achieve this (6-72 h). The low concentrations of olefin (5-20 mM) in the reaction solution lowered the reaction productivity even further (0.030 mmol/h).



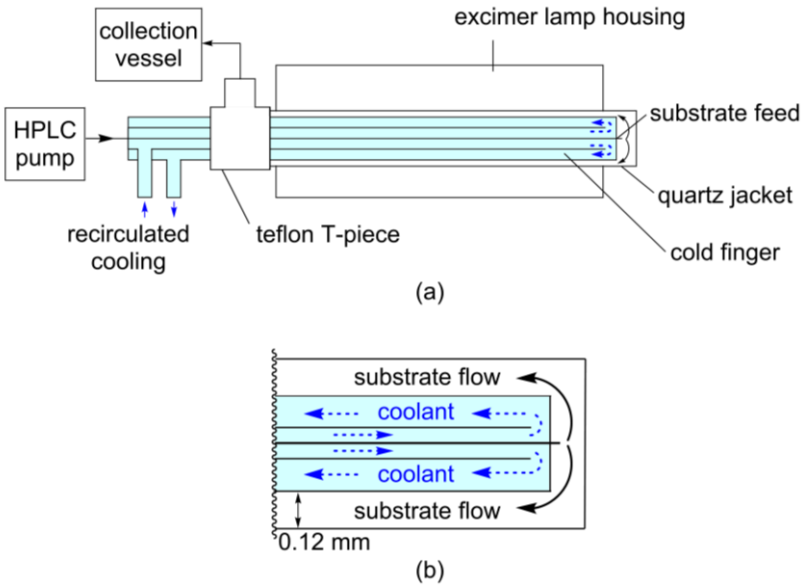
Scheme 3-1 Reaction scheme of the photo-induced coupling of acetone with an olefin to form extended methyl ketones in water as reported by Shiraishi et al.[7]

In summary, this useful reaction needs optimisation in order to give the desired productivity needed for widespread applications. For starters, reaction times need to be shortened in order to improve the productivity of this transformation. Reaction times on the order of minutes were reported by Yamashita *et al.* for this transformation by using a photochemical microreactor.[9] Improved light penetration and micromixing were the main contributing factors for these fast reactions. They reported methyl ketone formation by the photochemical coupling of pent-4-en-1-ol and acetone in aqueous solutions using a medium-pressure mercury lamp. Although short reactions times (0.25-2 min.) were required, the use of a photochemical microreactor restricts the productivity of the reaction due to limitations on material throughput dictated by the narrow channels in the reactor. Moreover, the selectivity for their desired reaction product was only moderate which highlights the need for further optimisation of this reaction.

The work presented in this Thesis aimed to further improve the productivity of this reaction to increase its potential viability for wider applications by using a different type of continuous flow UV photoreactor.

3.1 Continuous Flow UV Excimer Photoreactor

As highlighted in Chapter 1, the use of excimer lamps as the light source in UV photochemical reactions provides attractive characteristics over the use of other UV light sources. Their monochromatic light emission and the relatively low operation temperature are among the main benefits. Three different excimer lamps were employed for the work presented in this Thesis. Each lamp contained a different gas mixture, resulting in three light sources emitting at different wavelengths. The gas mixtures were KrCl*, XeBr* and XeCl*, corresponding to output spectra with narrow bands at 222, 282 and 308 nm respectively. These light sources were employed in a continuous flow UV photoreactor to ensure efficient irradiation through a narrow pathway between the light source and the reaction solution. The reactor was constructed in-house and consisted of a horizontally orientated quartz tube encasing the reactant solution and multiple stainless steel tubes. This quartz tube fitted through a hole in the middle of the excimer lamp.[10] The reactant solution was pumped through stainless steel tubes where it was released into the quartz tube (Scheme 3-2a). The solution flowed through the quartz tube from the left to the right while it was irradiated by the excimer light, followed by collection at the right end of the tube. The reaction mixture was cooled *via* heat exchange with a cooling liquid inside the stainless steel tubing. While the total system volume was approximately 10 mL, the irradiation volume was only 1.37 mL, with a narrow pathway of the reactant solution (0.12 mm) to facilitate good light penetration. A more detailed description of the reactor can be found in the Experimental Chapter.



Scheme 3-2 a) Simplified diagram of the UV photoreactor adapted from DeLaney et al.[10] showing the HPLC pump to pump the reagents through centre of the reactor into the quartz jacket, and showing the coolant (blue) and the excimer lamp housing. A Teflon T-piece holds the quartz tube in place and connects the collection pipe with the reactor, b) enhanced schematic of the tip of the cold finger inside the quartz jacket illustrating the flow of coolant and reagents.

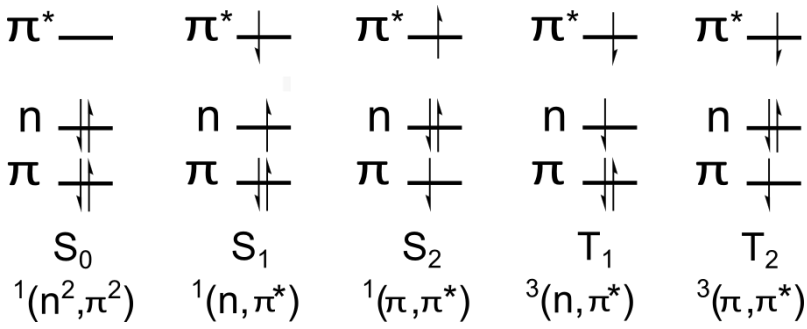
3.1.1 Chemical Actinometry Experiments

The work presented in this Thesis was based on using the light from UV excimer lamps to irradiate the reaction mixture. Ensuring the reproducibility of the reactor set-up required the experimental determination of its parameters. The number of photon emitted by the excimer lamps, the photon flux, should be determined on a biannual basis. This way, any decrease in photon flux over time can be detected and reaction yields obtained for chemical reactions over time can be compared. Chemical actinometry is an appropriate method and was chosen over radiometry measurements as the high photon flux of the excimer lamp saturated the tested radiometer. Moreover, chemical actinometry experiments do not require specialist equipment.[11] Chemical actinometry has been employed for over 70 years as a relatively simple and accurate method to measure the photon flux of light sources.[12] The Experimental Chapter describes the procedures and results of the chemical actinometry experiments.

3.2 Background on Acetone Excitation

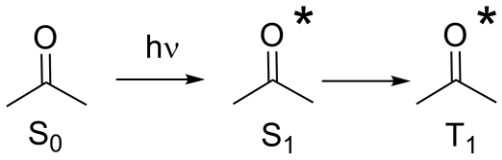
The formation of methyl ketones as depicted in Scheme 3-1 relies on the excitation of the ketone. Almost all reactions studied for this Thesis involving UV light are based on the excitation of acetone and therefore, this Section will cover the spectroscopic properties of this ketone.

Acetone in solution possesses two major absorbance bands. A π-π* transition band is present with a maximum around 187 nm depending on the solvent in which the absorbance is measured. The second transition is caused by a n-π* transition and is present with a maximum around 270 nm. As this n-π* transition is spin forbidden, the molar extinction coefficient is lower than that of the π-π* transition. The electrons in the n-orbitals of acetone are higher in energy compared to electrons in the σ- or π orbitals. Therefore, promoting electrons in n-orbitals to higher energy orbitals requires less energy compared to electrons in σ- or π orbitals. These transitions involving electrons in n-orbitals occur at longer wavelengths than transitions involving σ- or π orbitals. By population of the π* antibonding orbital after excitation, the C=O bond is weakened and therefore more reactive compared to the C=O bond in the ground state of acetone.[13] Scheme 3-3 shows simplified electron configurations of the lowest ground and excited states of acetone. S_0 represents the singlet ground state of acetone, whereas S_1 and S_2 represent the first two singlet excited states. T_1 and T_2 represent the first two triplet excited states.



Scheme 3-3 Simplified electron configuration of ground state and excited state acetone.

Lifetimes of these excited states of acetone have been reported.[14] A long excited state lifetime is desirable as this ensures more time for the excited state molecule to react inter- or intra-molecularly before returning to its unreactive ground state. This is especially important in intermolecular reactions where molecules need to diffuse into the proximity of each other before a reaction can occur. It has been reported that intersystem crossing is very efficient for acetone,[15] with a lifetime on the order of 10 ns. Fluorescence and phosphorescence lifetimes are on the order of 0.1 and 1 μs respectively.[14a] It has been reported that the intersystem crossing is a S_1 $^1(n,\pi^*)$ to T_1 $^1(n,\pi^*)$ transition.[14a, 15-16] This is generally a relatively slow transition compared to a S_1-T_2 transition as there is no change in orbital multiplicity since S_1 and T_1 are both n,π* states (El-Sayed's rule).[17] The reported lifetime for the lowest singlet excited state is 1-10 ns and the lowest triplet excited state lifetime is on the order of 10 μs.[14a] As the transition from the triplet excited state to the ground state of acetone is spin-forbidden, the lifetime of this excited state is longer compared to the singlet excited state.[14b] According to Kasha's rule, only the lowest vibrationally equilibrated excited state of a given multiplicity (singlet or triplet) is involved in the primary photophysical and photochemical processes of organic molecules in solution.[14a, 18] Therefore it is expected that the T_1 excited state of acetone will be the reactive species, instead of higher vibrationally excited triplet states such as T_2 or T_3 (Scheme 3-4).



Scheme 3-4 Excitation and subsequent intersystem crossing of ground state acetone.

Figure 3-1 shows a typical UV-Vis spectrum of acetone in water. The light sources used in this project will most likely facilitate the n-π* transition due to spectral overlap between the emission wavelength of the light source and the absorbance maximum of acetone.

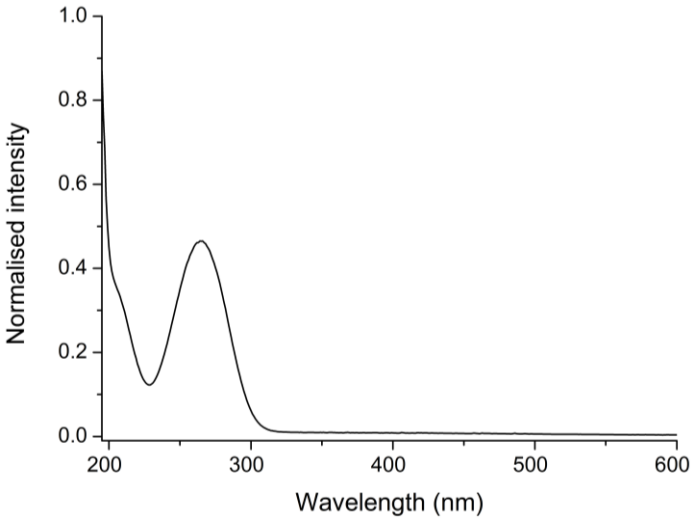


Figure 3-1 UV-Vis spectrum of acetone in water with the intensity maximum normalised to 0.5.

As the chemical transformations will mostly be carried out in aqueous solutions, the molar extinction coefficients of acetone at all three wavelengths of the excimer light sources (308, 282, 222 nm) were determined in water. As can be seen in Table 3-1, the extinction coefficient for acetone at 282 nm is the highest out of the three as this wavelength is closest to the maximum absorbance band at 270 nm. Therefore, more light will be absorbed by acetone at 282 nm compared to the other wavelengths at a fixed concentration.

Based on these molar extinction coefficients, the light penetration depth in the UV reactor can be calculated. This is important to maximise irradiation of acetone to avoid waste of photons. Using the Lambert-Beer equation (Equation 3-1), the acetone concentration at which 99 % of the incoming light is absorbed by acetone can be calculated. The path length in the UV reactor is 0.12 mm as discussed in Section 3.1

$$\log_{10} \frac{I_0}{I} = \epsilon\, c\, l \qquad 3\text{-}1$$

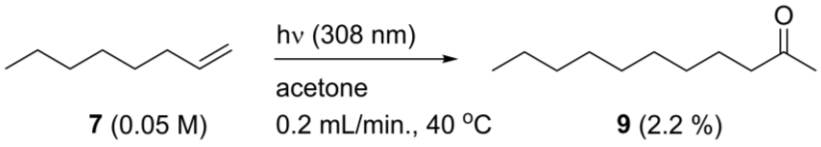
Table 3-1 Molar extinction coefficients of acetone in water at three different wavelengths.

Entry	Wavelength	ε (L/mol·cm)	Acetone concentration (M) for 99 % light absorption[a]
1	222 nm	4.89	34.1[b]
2	282 nm	12.1	13.8[b]
3	308 nm	0.937	177.9[b]

[a]Path length is 0.12 mm; [b]the concentration of pure acetone is 13.53 M, so all concentrations are theoretical values. Pumping pure acetone through the reactor ensures full irradiation of the solution when using all excimer lamps.

3.3 Initial Coupling 1-Octene and Acetone

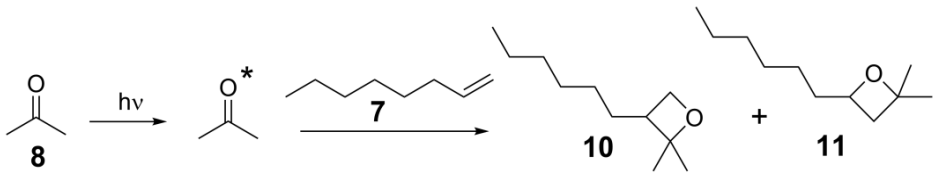
The first olefin and ketone coupling studied for this Thesis was the coupling of 1-octene (**7**) and acetone (**8**) to form 2-undecanone (**9**) (Scheme 3-5). Formation of this extended ketone under mild conditions can be difficult to achieve *via* conventional methods due to solubility issues in water.[19] Potential applications for **9** such as flavouring carrier in dairy products, a diesel fuel blending agent or natural insecticides in plants make this a worthwhile product.[1a]



*Scheme 3-5 Initial coupling of 1-octene (**7**) and acetone (**8**) to form 2-undecanone (**9**) in continuous flow.*

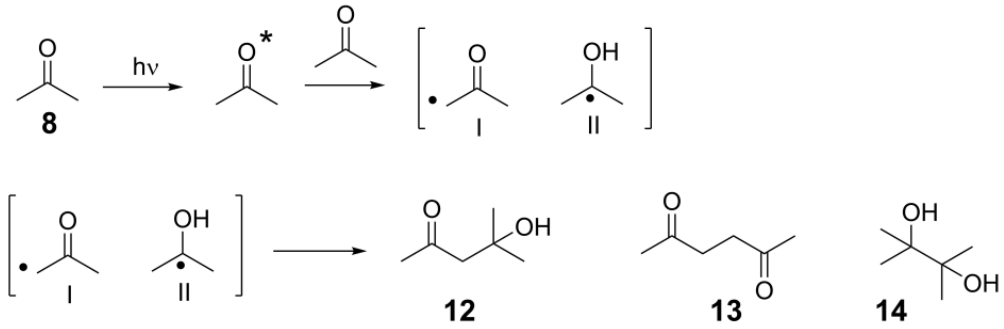
Shiraishi *et al.* proposed a mechanism to account for the products found in the reaction.[7] The first step in the reaction is the excitation of acetone (**8**). Subsequently, this excited state species can react with ground state 1-octene (**7**) to form oxetane products **10** and **11** (Scheme 3-6). The regioselectivity for oxetane formation is generally dictated by the Markovnikov rule, involving the

most stable biradical intermediate.[20] Therefore, the formation of **10** is more favourable than that of **11**.



*Scheme 3-6 Excitation of acetone (**8**) and subsequent coupling with 1-octene (**7**) to form oxetanes **10** and **11**.*

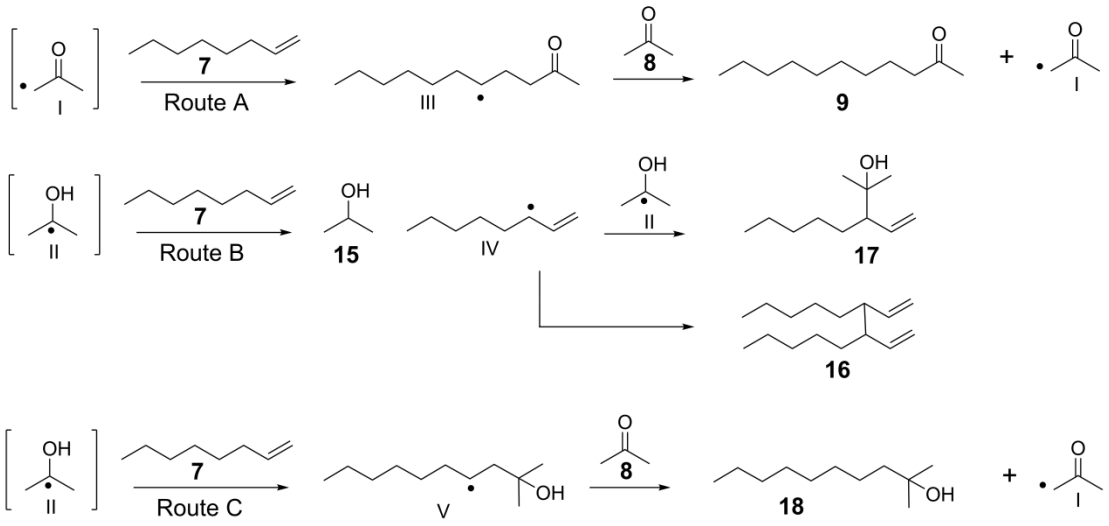
Excited state acetone can also abstract a hydrogen atom from a ground state acetone molecule, generating an α-keto and a ketyl radical, labelled compounds I and II respectively (Scheme 3-7).



*Scheme 3-7 Generation of radicals I and II and subsequent formation of products **12**-**14**.*

The coupling of these two radicals forms product **12**, while the combination of two α-keto radicals forms acetonylacetone (**13**). Dimerisation of the ketyl radical generates pinacol (**14**). Radicals I and II can also couple with **7** (Scheme 3-8). The coupling of 1-octene and the α-keto radical (Route A) generates the desired product, 2-undecanone (**9**) *via* radical intermediate III. In Route B, the ketyl radical abstracts a hydrogen atom from 1-octene after which the generated 1-octene radical IV can either dimerise to form product **16**, or can react with another ketyl radical II to form product **17**. Radical intermediate V is most likely

generated *via* the addition of radical II to **7** (Route C). Subsequent hydrogen atom abstraction leads to product **18**.



*Scheme 3-8 The coupling of radicals I and II with 1-octene (**7**) via Routes A-C.*

In the initial experiment, a mixture of 1-octene in acetone (0.05 M) was pumped through the continuous flow UV photoreactor at 0.2 mL/min while being irradiated by the 308 nm excimer lamp. This corresponds to a total irradiation time of 6.9 minutes. The reaction output was purified by column chromatography to isolate pure products and subsequent product characterisation was carried out with NMR spectroscopy. After elucidating the GC traces corresponding to most products, reaction monitoring was then carried out by GC analysis using a chiral column. The progress of the reaction was measured by the depletion of the 1-octene (**7**) signal in the gas chromatogram. Under the conditions described above, 13 % conversion of **7** was found. The selectivity for the desired product **9** was 17 %, which corresponds to a productivity of 0.013 mmol/h for the production of **9**. This is a 2-fold increase compared to the value reported by Shiraishi *et al.* for the formation of **9** in neat acetone.[7] This encouraging result indicates that the use of the in-house built UV excimer continuous flow photoreactor may provide advantages over a batch reaction set-up. In order to gain understanding of the relation between the different reaction pathways, the distribution of all the different products was analysed. As seen in Figure 3-2, products **9**, **10**, **17** and **18** were formed dominantly under these conditions.

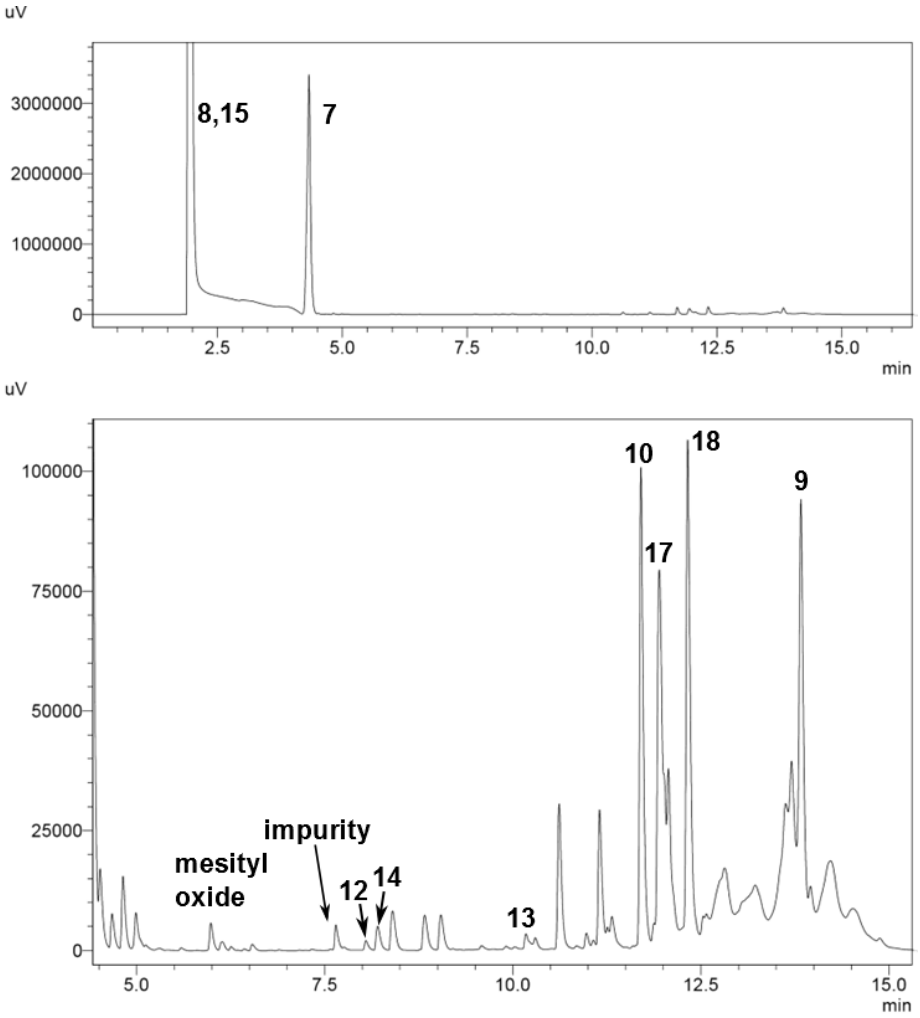


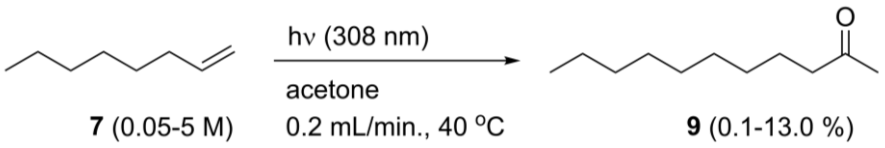
*Figure 3-2 Top: Full gas chromatogram of the reaction output in the coupling of 1-octene (**7**, 0.05 M in acetone) and acetone (**8**) to show the low conversion of **7**; Bottom: Expanded gas chromatogram showing the range of products. The reaction was carried out using the 308 nm excimer lamp, a flow rate of 0.2 mL/min and a temperature of 40 °C.*

Products **11** and **16** could not be isolated from the reaction mixture, but small unidentified peaks were present in the gas chromatogram corresponding to products which proved difficult to identify and characterise. Figure 3-2 shows the corresponding gas chromatogram in which acetone and isopropyl alcohol (2 min.) and 1-octene (4.3 min.) are the most prominent peaks. Unfortunately, it was not possible to separate the GC traces of acetone (**8**) from isopropyl alcohol (**15**) despite extensive experimenting. Moreover, some products were too volatile and could not be identified (for example products with GC traces at 10.6 and 11.2 min.).

GC analysis was successfully established as a method to study most reaction products. Multiple products were identified, but both the conversion of 1-octene and the selectivity for 2-undecanone were moderate. Therefore, reaction parameters were varied in order to obtain an insight into the mechanism of this complex reaction and to understand how the tested parameters influence both the conversion of 1-octene and the product selectivity. Ultimately, this would lead to the ability to run the reaction at the optimum reaction conditions in order to obtain the highest selectivity for the desired product 2-undecanone (**9**).

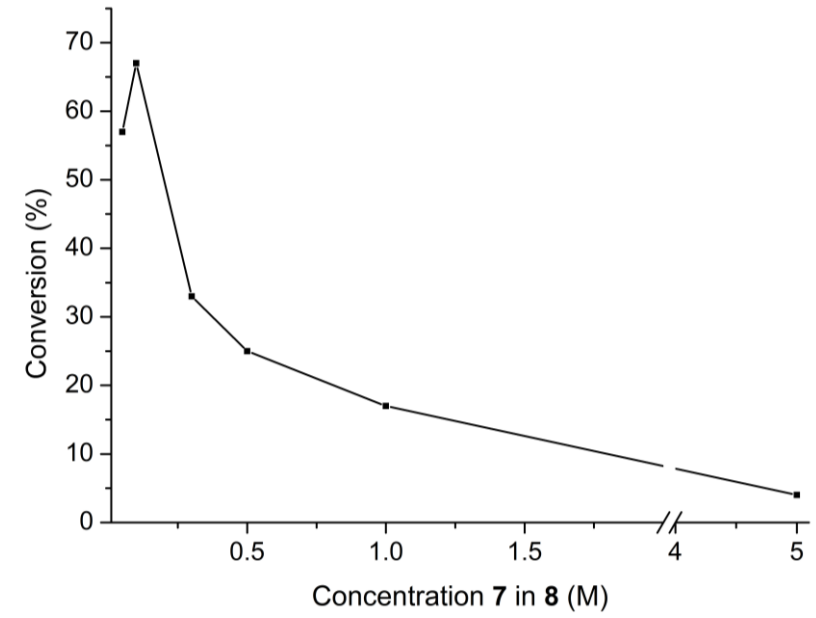
3.4 Optimising the Concentration of 1-Octene

The initial experiment carried out as part of this Thesis showed a 2-fold increase in productivity by using a concentration of 0.05 M of 1-octene (**7**) in acetone (**8**) instead of the optimum reported by Shiraishi *et al.* (0.02 M).[7] Therefore, the concentration of **7** in **8** was increased to a greater extent to investigate whether the productivity of the formation of **9** could be improved further and to determine the effect of reactant ratio on the product selectivity (Scheme 3-9).

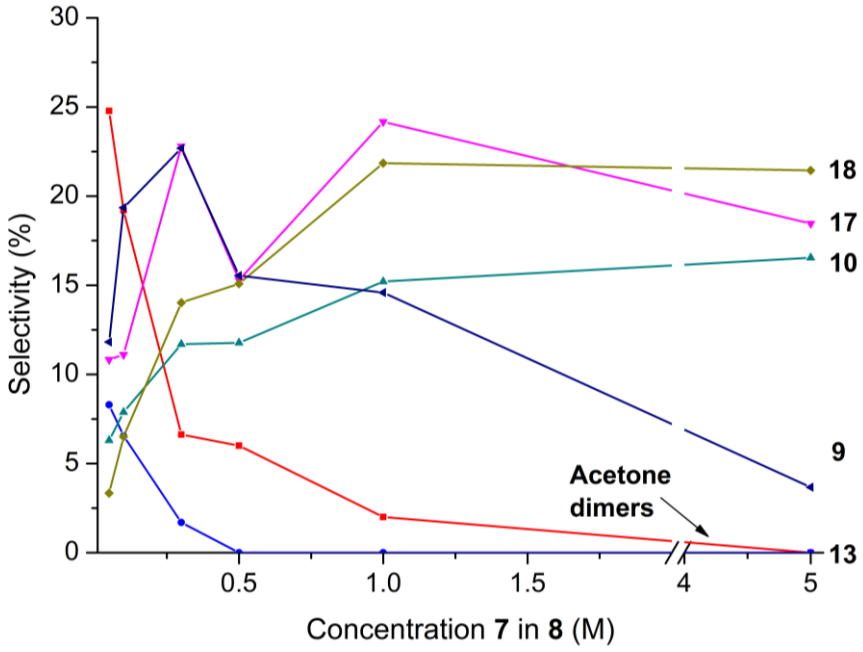


*Scheme 3-9 Reaction of 1-octene (**7**) and acetone (**8**) at different reactant ratios.*

The reactant mixture was pumped through the continuous flow UV photoreactor at 0.2 mL/min at a range of concentrations of **7** in acetone (0.05-5 M). Irradiation was carried out with the 308 nm excimer lamp. The conversion of **7** rapidly decreased at higher concentrations of **7** in **8** (Figure 3-3a). In order to compare the efficiency of the conversion of **7** at the range of concentrations, the amount of **7** reacted in each experiment was expressed in mmol per hour (Table 3-2).



(a)



(b)

*Figure 3-3 a) Conversion of **7** and b) the different product selectivities in the reaction of 1-octene (**7**) and acetone (**8**) at 0.2 mL/min and 40 °C with 308 nm light irradiation at different concentrations of **7** in **8**. Note the decrease in product selectivity for **9** at higher concentrations of **7** in acetone.*

In the tested concentrations of **7** in **8**, a maximum conversion of **7** was seen at a concentration of 1 M. This corresponds to a molar ratio of 1:14 of **7** to **8**. It is possible that based on the diffusion rate of the reactants, this was the optimum ratio for **7** to react with acetone or acetone derived radicals. Overcoming diffusion limitations as there is no active mixing in the reactor could also be an explanation for the initial increase in the conversion of **7** after doubling the concentration of **7** in **8** from 0.05 to 0.1 M. Under all the tested conditions, light penetrated the whole reactor volume. However, as the concentration of **7** in **8** increased, less acetone molecules were present to absorb the light and initiate the photochemical reaction. This could have led to a lower conversion of **7** at 5 M.

*Table 3-2 The amount of 1-octene (**7**) reacted (expressed in mmol/h) at a range of concentrations and the relation between concentration and molar ratio between 1-octene (**7**) and acetone (**8**).*

Concentration 7 (M in acetone)	0.05	0.1	0.3	0.5	1	5
Molar ratio **7** to **8**	1:274	1:135	1:46	1:27	1:14	1:2.7
mmol of **7** reacted per hour	0.33	0.80	1.13	1.38	1.74	1.28

The highest selectivity for the formation of acetone dimers over other products was observed at low concentrations of **7** in **8** (19-22 %) (Figure 3-3b). Although product **13** is an acetone dimer as well, this product was shown separately in Figure 3-3b. This is because in other experiments, product **13** was formed with different selectivity to the other acetone dimers. The increased concentration of **7** led to a sharp decrease in the selectivity for acetone dimers. This sharp decrease may be the explanation for the initial rise in selectivity for product **9** in the lower concentration region. After this initial increase in selectivity, selectivity for product **9** decreased at higher concentrations of **7** in **8**. Products that displayed an increase in selectivity at higher concentrations of **7** in **8** were products **10**, **17** and **18**. This selectivity remained close to constant for reaction mixtures higher in concentration than 1 M. The limitation of reactant diffusion might give a tentative explanation why product selectivity changed steeply only at lower concentrations of **7** in **8** but not at higher concentrations. Although product **16** could not be

identified from the reaction mixture, all other products derived from radical II displayed an increase in selectivity at higher concentrations of **7** in **8** while product **9**, derived from radical I showed a decrease in selectivity. More proof is needed to provide an explanation but the difference in stabilisation of radical I and II could be a contributing factor. The addition of **7** to **8** decreases the polarity of the reaction mixture and primary radical I is possibly less stable than radical II, and therefore radical II might be more reactive in this environment. Products involving radical II would therefore be formed more favourably.

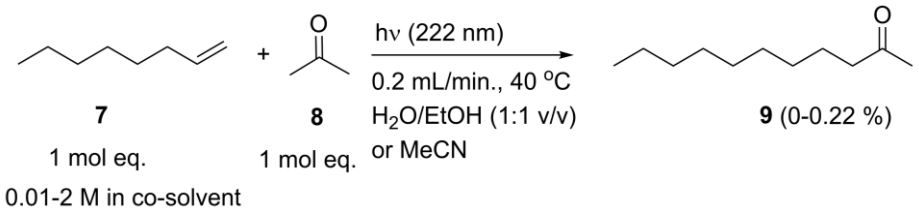
To conclude, reactant ratio was found to be crucial in obtaining a high selectivity for product **9** as great differences in product selectivity were observed when the concentration of **7** in **8** was varied from 0.05-1 M. At higher concentrations of **7** in **8**, product selectivity did not vary to a great extent. Moreover, the reaction rate seemed be to diffusion controlled at lower concentrations of **7** in **8** while being limited by the excitation of acetone at higher concentrations. The highest selectivity for **9** for the reaction parameters tested was obtained at 0.3 M 1-octene in acetone. However, this selectivity was only 23 % as by-products like acetone dimers were formed. A method to decrease the formation of acetone dimers is to lower the concentration of acetone molecules in solution.

3.5 Optimising the Concentration of Reactants

It is expected that a lower concentration of olefin **7** and ketone **8** could suppress the formation of acetone dimers as this reaction is concentration dependent. Such conditions could potentially increase the selectivity for product **9**. By adding either a water/ethanol mixture (1:1 v/v) or acetonitrile (MeCN), the concentration of **7** and **8** in the reaction mixture was reduced. MeCN was chosen as a non-hydrogen-bonding solvent in order to study the effect of reactant concentration. Having water/ethanol as a solvent mixture might offer hydrogen-bonding interactions with acetone which could affect the reaction outcome independent of the concentration difference.

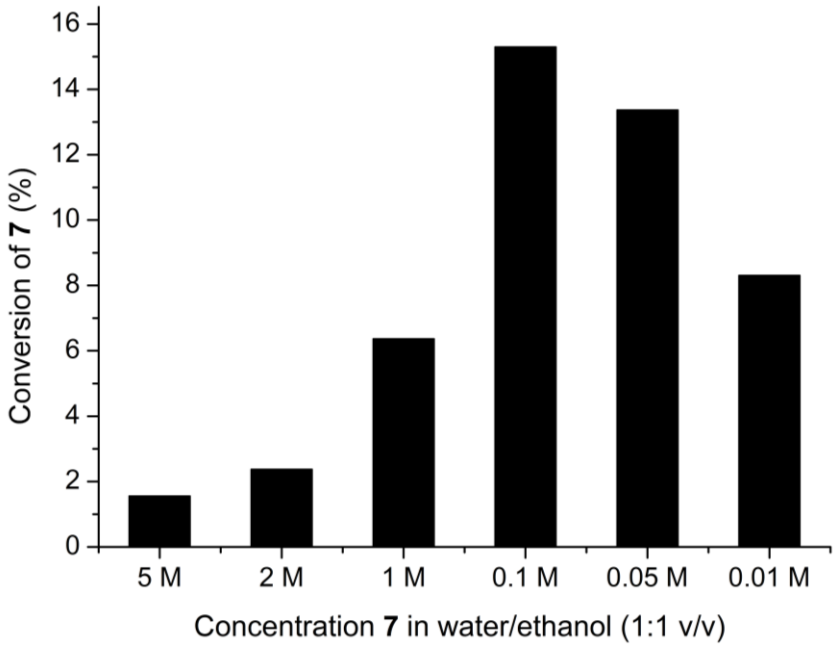
Reactant **7** was added to a co-solvent (0.01-2 M) while maintaining a 1:1 molar ratio to **8** (Scheme 3-10). The 222 nm excimer lamp was used to irradiate the

reaction mixture. At each of the concentrations used, light was able to penetrate through the whole reaction mixture.

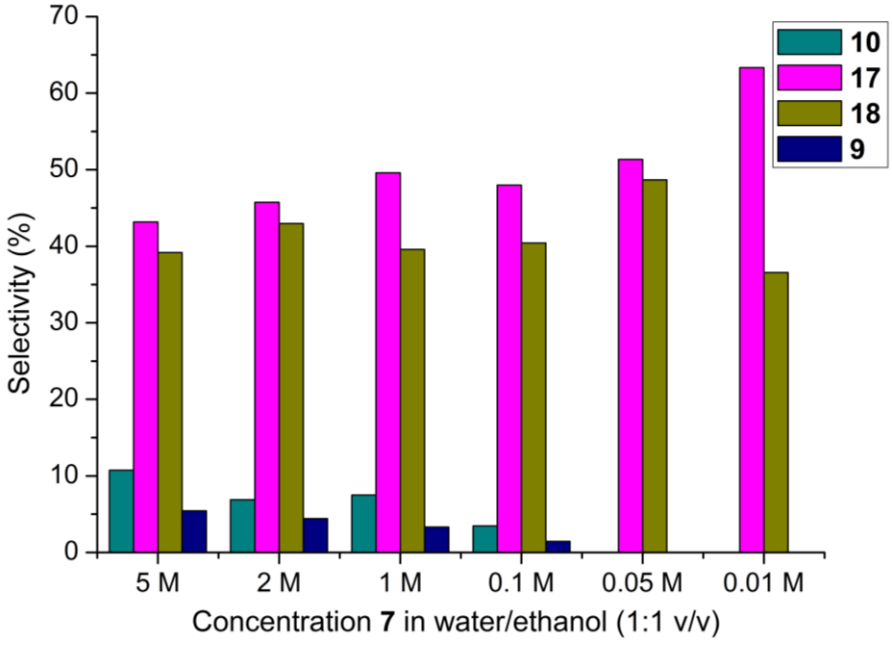


*Scheme 3-10 Reaction of 1-octene (**7**) and acetone (**8**) (1:1 mol eq.) at different concentrations in water/ethanol (1:1 v/v) or acetonitrile (MeCN).*

When this reaction was carried out in water/ethanol (1:1 v/v) as the co-solvent, no acetone dimers were formed. Products **17** and **18** were formed with high selectivity throughout the experiments (Figure 3-4b). It has been previously reported that the addition of ethanol to water disturbs the hydrogen-bonding network created by water.[21] At a 1:1 volume ratio of water and ethanol, the total hydrogen-bonding strength is lower than in pure water, as not all water molecules possess their maximum amount of hydrogen-bonds.[21] The expected result of the distorted hydrogen-bonded network is that the hydration of radicals I and II would have been lower in this water/ethanol mixture compared to pure water. This potentially could lead to an increased reactivity of both these radicals. This increased reactivity of radical II might explain the high selectivity for the coupling products of 1-octene and this radical, products **17** and **18**. It appeared that at higher concentrations of **7** in the solvent mixture, routes involving radical II (Scheme 3-8, Routes B, C) become less favourable and therefore, the selectivity for products **9** and **10** is increased. The polarity of the reactant mixture decreased upon increasing the concentration of **7** and **8**. It is possible that radical II is stabilised and therefore less reactive under these conditions, resulting in lower selectivity for products **17** and **18**. Next to polarity, the viscosity of the reaction mixture also changed under the different conditions. The higher viscosity of water/ethanol mixtures compared to pure water solutions may have resulted in lower diffusion rates of the reactants.[22] This could potentially explain why the conversion of **7** was found the highest (15 %) at 0.1 M of **7** in water/ethanol (Figure 3-4a). At lower concentrations, diffusion of the reactants could have been hindered by the increased viscosity of the solvent mixture.



(a)

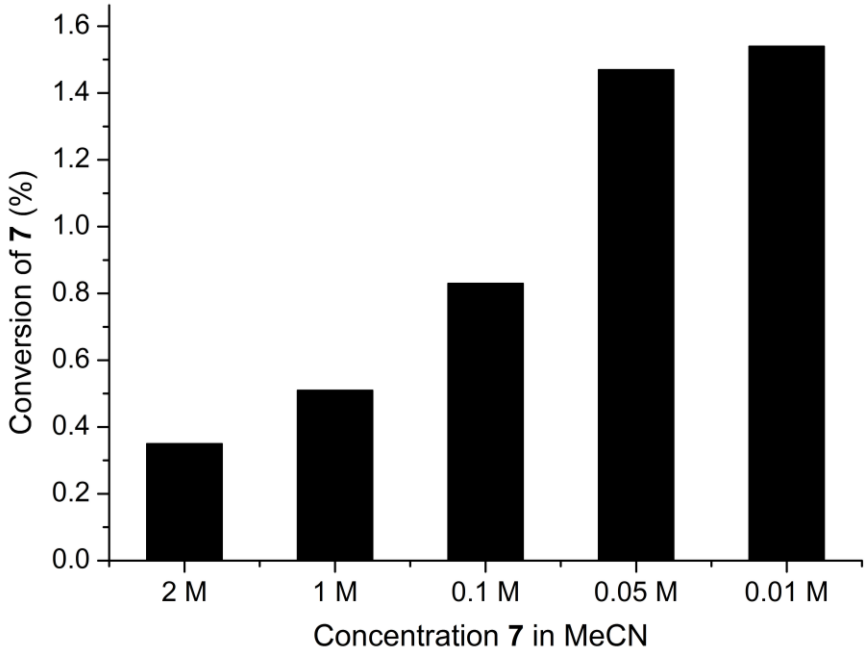


(b)

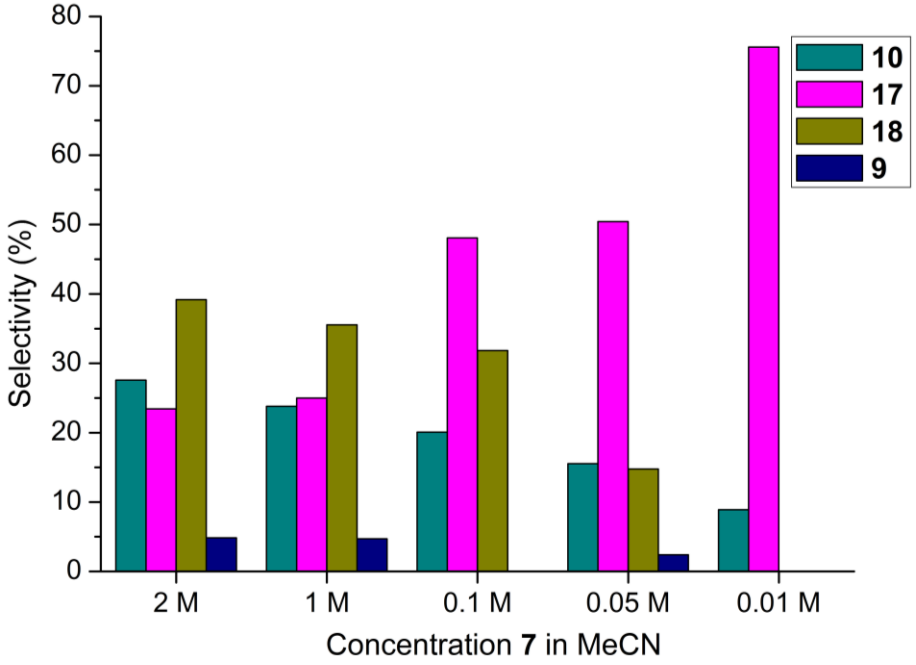
*Figure 3-4 Reaction of 1-octene (**7**) and acetone (**8**) at a molar ratio 1:1 at different concentrations in water/ethanol (1:1 v/v) at 40 °C employing the 222 nm excimer lamp. Flow rate was set at 0.2 mL/min. The graph shows a) the conversion of **7** and b) the products that changed selectivity at these different concentrations, showing a maximum conversion of **7** at 0.1 M in water/ethanol (1:1 v/v) and greater product selectivity at lower concentrations.*

Acetonitrile (MeCN) was used next as the co-solvent in order to eliminate any hydrogen-bonding interaction between the reactants and the co-solvent. The highest concentration of **7** in MeCN that could be tested was 2 M due to solubility limitations. The highest conversion of **7** was 1.5 % (Figure 3-5a) which is likely due to the lack of hydration of radicals I and II by the co-solvent. In diffusion controlled reactions, conversion is expected to be highest at higher reactant concentrations. This would suggest that the studied reaction was not diffusion controlled under these conditions as the highest conversion was at the lowest tested concentration. No acetone dimers were formed as was the case in the water/ethanol solvent mixture. It has been reported that undesired recombination of radicals I and II to ground state acetone could occur to a greater extent in less polar solutions which could provide an explanation for the lower conversion of **7** in when the reaction was carried out in MeCN compared to water/ethanol.[7, 23] The selectivity for product **17** was as high as 76 % at 0.01 M (Figure 3-5b). With the selectivity for product **17** decreasing at higher concentrations of **7** in MeCN, products **9**, **10** and **18** were formed more favourably. Interestingly, product **18** was formed to a greater extent in water/ethanol compared to the reaction in MeCN. Therefore, it is possible that intermediates to form product **18** benefitted from hydrogen-bonding interactions with the solvent.

No relevant information about the concentration dependence of acetone dimer formation could be extracted from the data as no acetone dimers were formed under any of the conditions tested. However, it appeared that solvents have a major effect on the reaction selectivity for other products. In water/ethanol, diffusion of the reactants seemed to play a significant role in reaction rate while in MeCN this seemed less significant. So far, no conditions were identified to increase the selectivity for product **9**. Product selectivity and the conversion of **7** were low in acetonitrile, especially at higher concentrations of **7** in MeCN. This underlines the need for hydrogen-bonding solvents for a selective conversion of **7**.



(a)



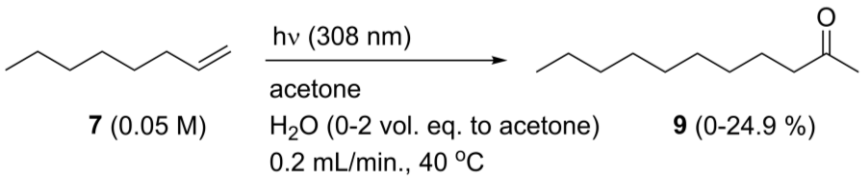
(b)

*Figure 3-5 Reaction of 1-octene (**7**) and acetone (**8**) at a 1:1 molar ratio at different concentrations in acetonitrile (MeCN) at 40 °C employing the 222 nm excimer lamp. Flow rate was set at 0.2 mL/min. The graph shows a) the conversion of **7** and b) the products that changed selectivity at these different concentrations, demonstrating the increase in product selectivity at lower concentration of **7** in MeCN.*

To exploit the influence of hydrogen-bonding solvents on the reaction and to enlarge the hydrogen-bonding ability of the solvent, water was employed next as the co-solvent for the reaction instead of a water/ethanol mixture. It was hypothesised that this could increase the selectivity for product **9** which is critical since the maximum selectivity for product **9** was only 5 % when using the water/ethanol mixture as the co-solvent. This is over 3-fold lower than the selectivity in the initial experiment carried out without any co-solvent.

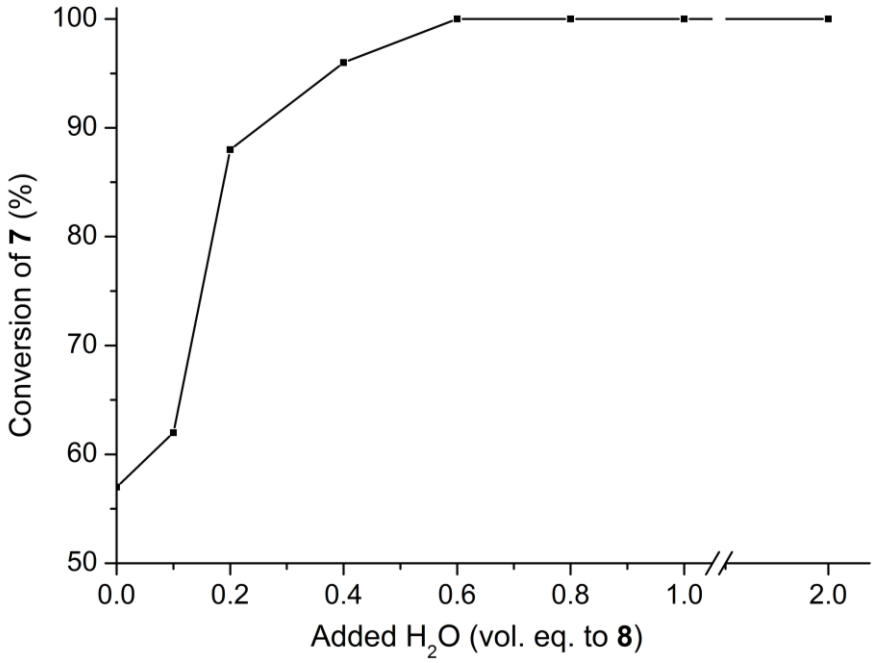
3.6 Adding Water as Co-solvent

Adding water as the co-solvent to the reaction mixture showed great enhancement for the selectivity for **9** as shown by Shiraishi *et al.* and Yamashita *et al.* due to solvation of radicals I and II.[7, 9] Under all tested conditions, a concentration of 0.05 M of olefin **7** in acetone was maintained independent of the water content. The amount of water added was chosen in volume equivalents to reactant **8** (Scheme 3-11).

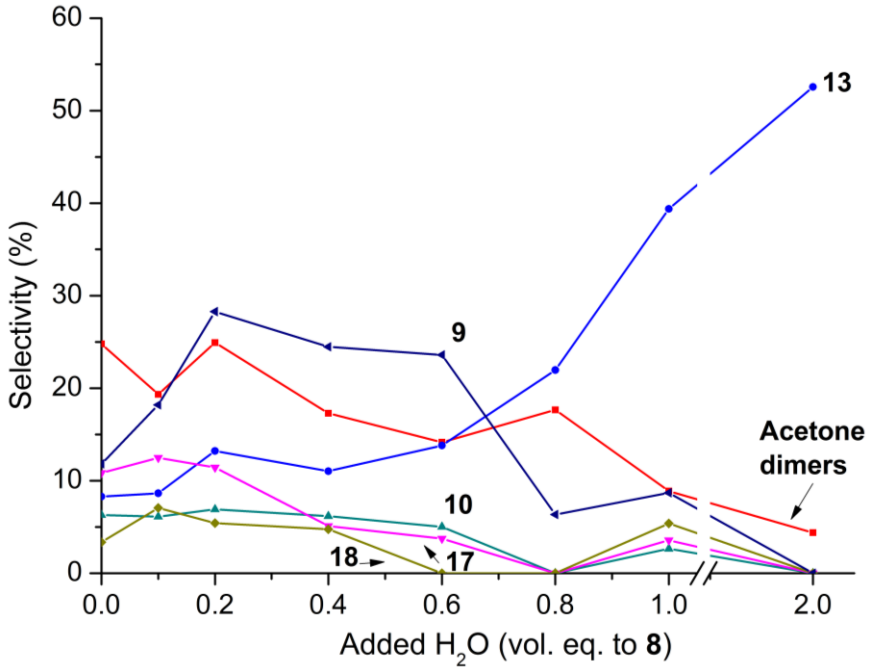


*Scheme 3-11 Reaction of 1-octene (**7**) and acetone (**8**) with the addition of deionised water (0-2 vol. eq. to **8**) as a co-solvent.*

The conversion of **7** increased significantly upon addition of water as a co-solvent (Figure 3-6a). It has been reported that solvation of the excited state of acetone by water increases the lifetime of this complex.[24] A longer excited state lifetime provides more time for the desired chemical reaction to occur before the excited state relaxes back to the ground state.



(a)



(b)

*Figure 3-6 a) Conversion of **7** and b) selectivity for different products when water is added as a co-solvent (0-2 vol. eq. to acetone) in the coupling of **7** and **8** at 0.2 mL/min and 40 °C employing the 308 nm excimer lamp. Note the increase in conversion of **7** and selectivity for diketone **13** with increased volumes of water.*

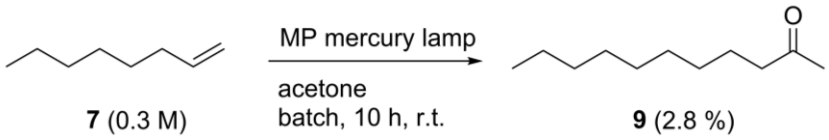
The initial increase in selectivity for extended ketone **9** could have resulted from a difference in the hydration of radicals I and II by water *via* hydrogen-bonding interactions. As radical II contains a highly polarised hydroxyl group, stronger hydration of this molecule will occur compared to radical I.[25] This hydration likely reduces the reactivity of radical II, enhancing the product formation with radical I (Scheme 3-8, route A). Therefore, products obtained *via* routes B and C in Scheme 3-8 are less likely to be formed when more water is present which was observed experimentally (Figure 3-6b). A hydrophobic effect could have played a role as well in the higher selectivity for product **9**. Upon the addition of water, molecules of **7** could have been driven into closer proximity to each other due to its non-polar character. This would minimise the need for diffusion. The addition of water to the reaction mixture increased the formation of acetonylacetone (**13**) in relation to acetone dimers **12** and **14** (Figure 3-6b). The hydration difference of radicals I and II by water could again explain this result as **13** is formed by the dimerisation of two of the more reactive radicals I. Chapter 4 will exploit this difference in reactivity by studying the selective formation of **13** over other acetone dimers.

The addition of water as the co-solvent in the photochemical coupling of **7** and **8** greatly enhanced both the conversion of **7** and the selectivity for **9**. Shiraishi *et al.* found that the addition of 0.4 vol. eq. of deionised water (vol. eq. to **8**) to their reaction mixture was optimum in terms of yield of product **9**.[7] Under the conditions studied in the work described in this Thesis, the optimum appeared to be 0.6 vol. eq. as full conversion of **7** was obtained while maintaining improved selectivity for product **9** (24 %). So far, reaction monitoring took place after the reaction was stopped. In order to study the reaction on a shorter time scale, the reaction was carried out in a batchwise fashion.

3.7 Monitoring the Coupling of 1-Octene and Acetone in Batch

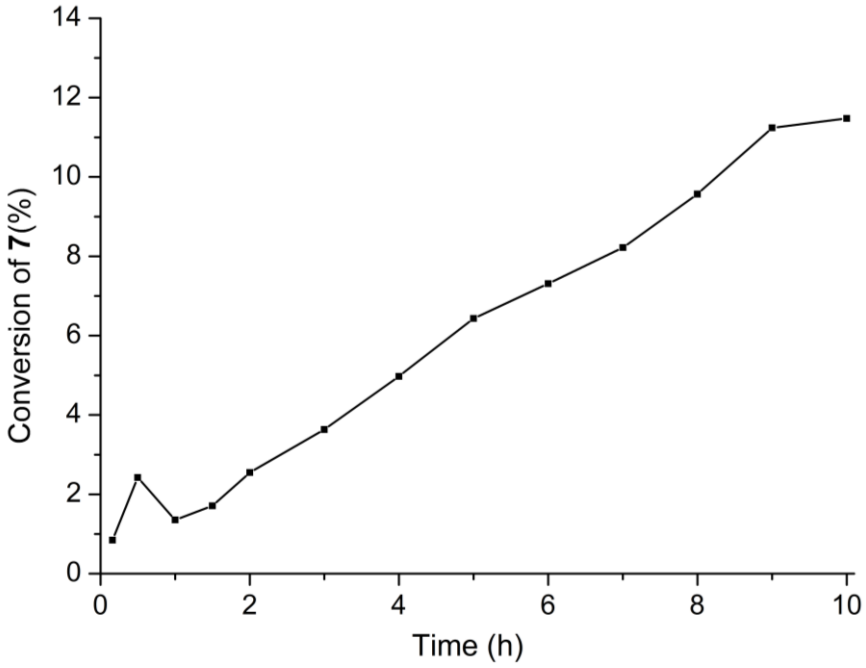
In order to investigate whether the selectivity for certain products changes during the reaction and to identify possible reaction intermediates, the coupling of

1-octene (**7**) and acetone (**8**) was performed in batch. Aliquots were taken over time and analysed with GC. The reaction mixture was placed in a 3 mL quartz cuvette and continuously stirred while being irradiated with a water cooled medium-pressure (MP) mercury arc lamp (emitting light between 220-620 nm). Details about the reaction set-up can be found in the Experimental Chapter. The first set of conditions was chosen so that product selectivity was low in order to study a broad range of reaction products (Scheme 3-12).

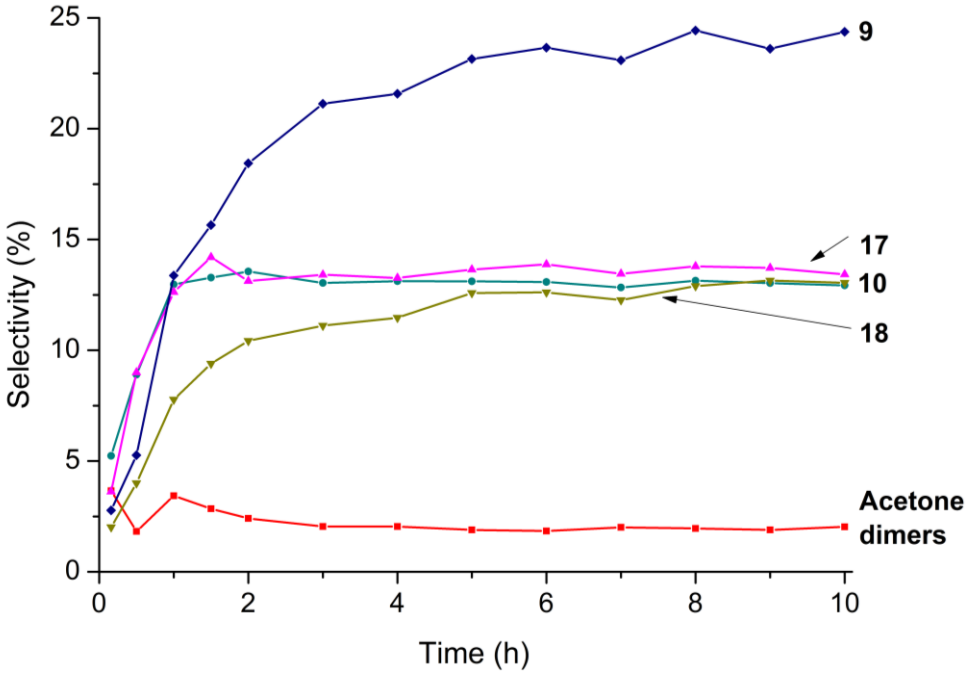


*Scheme 3-12 Reaction conditions in batch for the coupling of 1-octene (**7**, 0.3 M in acetone) and acetone (**8**) to form 2-undecanone (**9**).*

The conversion of **7** slowly increased over time, reaching 11 % after 10 hours of reaction time (Figure 3-7a). The long reaction time compared to the experiments in previous Sections in flow was most likely due to less efficient irradiation of the reaction mixture in batch. The mercury arc lamp employed in the batch experiments is a broad band emitter so only a part of the energy output of the lamp can be used to excite acetone. The overlap between the output spectrum of the mercury arc lamp and the absorption spectrum of acetone was small which can contribute to the need for the longer reaction time. GC traces of the aliquots taken over time did not reveal the presence of stable intermediates and the selectivity for the different products remained constant after 2 hours (Figure 3-7b). The initial rise in selectivity for all products in Figure 3-7b was likely due to inaccurate integration of the area of the corresponding GC signals as these were very small. Therefore, only selectivity differences after 2 hours will be taken into consideration. An initial increase in selectivity for products **9**, **10**, **17** and **18** was found but this could not be linked to a decrease in selectivity for any known products in the gas chromatogram. It is possible that the temperature of the reaction in batch was higher than in flow as no cooling of the reaction mixture was applied to the reaction conducted in batch. As explained by Shiraishi *et al.*, a higher reaction temperature results in a lower product selectivity for acetone dimers and products **10** and **17**.[7] This could explain why the selectivity for **9** was higher in the batch experiments compared to the flow experiments.



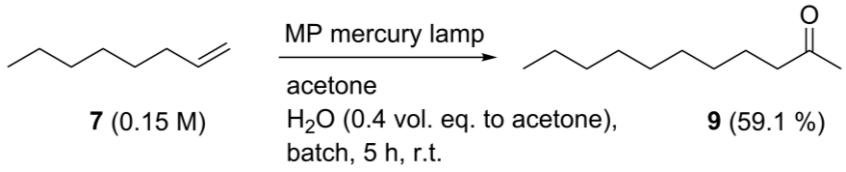
(a)



(b)

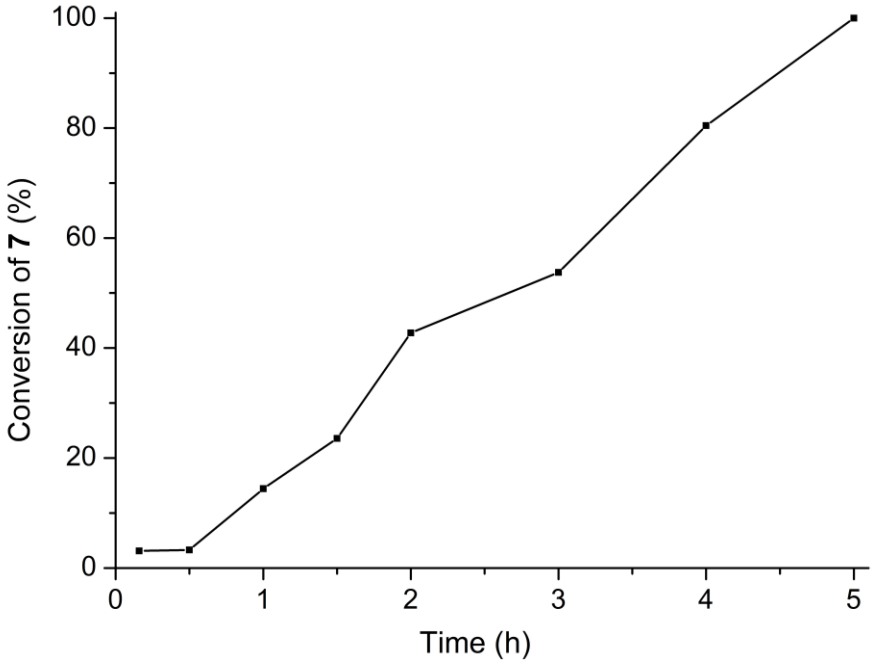
*Figure 3-7 a) Conversion of **7** and b) selectivity for different products over time in the coupling of **7** and **8** in batch employing a medium-pressure mercury arc lamp (125 W). No acetonylacetone (**13**) was formed while the conversion of **7** and the selectivity for product **9** increased over time.*

As shown in Section 3.6, the addition of water as a co-solvent to the reaction mixture can drastically increase reaction rates. Therefore, the reaction between **7** and **8** was repeated in batch, but with deionised water as the co-solvent (Scheme 3-13).

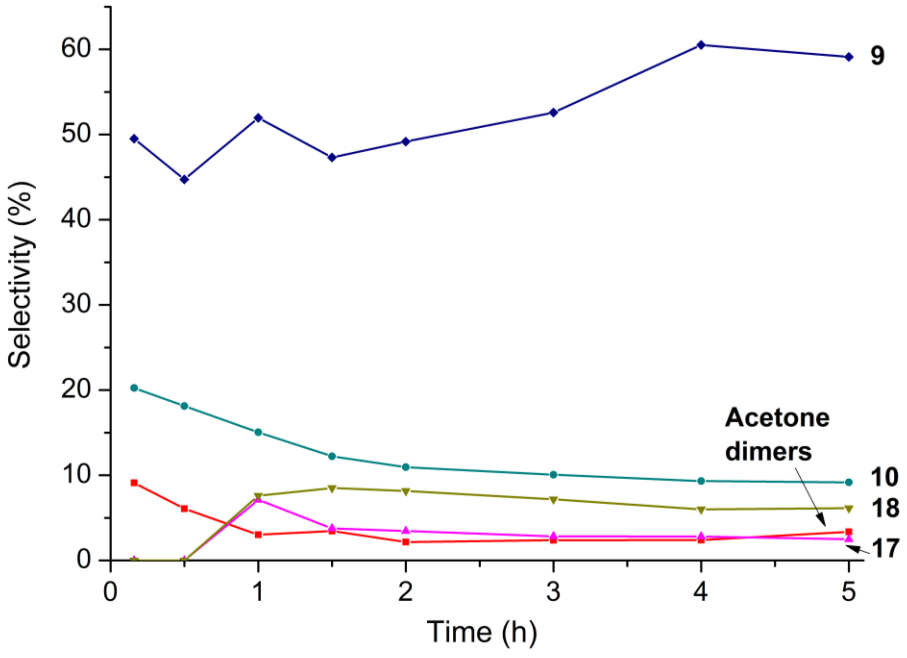


*Scheme 3-13 Reaction conditions in batch for the coupling of 1-octene (**7**, 0.15 M in **8**) and acetone (**8**) in water (0.4 vol. eq. to **8**) to form 2-undecanone (**9**).*

As expected, the addition of water increased both the reaction rate and the selectivity for product **9**. Full conversion of 1-octene (**7**) was reached between 4 and 5 hours (Figure 3-8a). The selectivity for the different products remained near constant throughout the reaction with no clear intermediates visible (Figure 3-8b). When comparing batch and flow experiments, the selectivity for **9** was around 2 times higher in batch compared to flow with the same ratio of reagents. This could be partly linked to the supressed formation of acetone dimers in the batch experiments. As a result of less efficient irradiation in batch, it is likely that less excited state acetone molecules were formed which limits the chance of dimerisation to form products **12**-**14**. The increased selectivity of **9** compared to products **10**, **17** and **18** in batch experiments compared to flow experiments could be a result of differences in the hydration of radicals I and II due to variations in mixing in the reaction mixtures. The influence of reaction temperature could also provide an explanation for the difference in product selectivity between batch and flow experiments as mentioned previously.



(a)



(b)

*Figure 3-8 a) Conversion of **7** and b) selectivity for different products over time in the coupling of **7** and **8** in batch employing a medium-pressure mercury arc lamp (125 W) without additional cooling. No acetonylacetone (**13**) was formed while full conversion of **7** was reached within 5 hours with high selectivity for product **9**.*

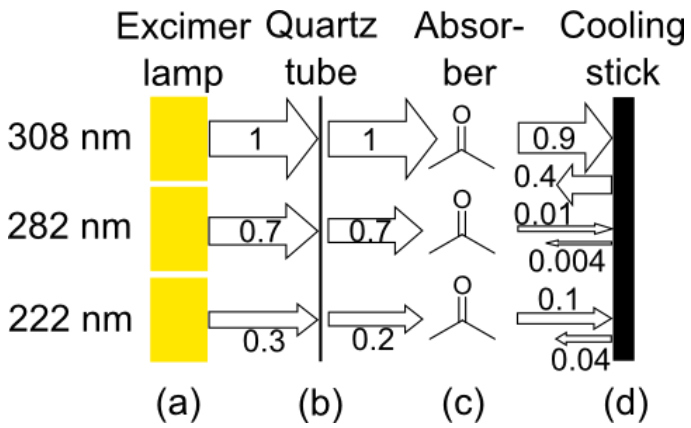
The experiments carried out in batch showed that no stable intermediates were formed in the reaction. Moreover, the addition of water showed a significant increase in reaction rate and enhanced the selectivity of product **9**. The use of a medium-pressure mercury lamp instead of the UV excimer lamp appeared to have a great negative influence on the rate of conversion of **7** as shown in this Section. To study the influence of irradiation wavelength further, acetone was irradiated using three different UV excimer lamps in the continuous flow photoreactor and the reaction productivity was compared.

3.8 Coupling of 1-Octene and Acetone with Different Irradiation Wavelengths

Irradiation of a starting material with different wavelength light has been shown previously to influence product selectivity.[26] Crespi *et al.* reported that the irradiation of aryl azosulfones with either visible light or UV light initiates a n-π* or π-π* transition respectively. Subsequent intermediates formed from both transitions afforded different reaction products. Ismael *et al.* demonstrated the different routes to transform methyl-substituted 5-aminotetrazoles after irradiation with different wavelengths of UV light.[26b] DeLaney *et al.* investigated the use of the three excimer light sources used in this project (222/282/308 nm) for the decarboxylative cyclisation of potassium *N*-phthalimidobutanoate.[10] The 222 nm excimer lamp facilitated a different transition in the molecule compared to the 282/308 nm excimer lamps. Despite this difference, a single reaction product was formed. Moreover, they found little difference in space time yield between the three irradiation wavelengths when normalised by the number of photons in the reactor.

In the work described in this Thesis, three different excimer lamps emitting at either 222/282/308 nm were used to investigate the coupling of 1-octene and acetone. It was aspired to elucidate whether the excitation of 1-octene could play a role in reaction efficiency. Moreover, reaction efficiencies and productivities under several conditions were investigated. However, comparing the results obtained from reactions using different irradiation wavelengths is not straight

forward. Although all photons emitted from all three light sources possess enough energy to facilitate a n-π* transition in ground state acetone, the efficiency of this process is different at the different excitation wavelengths. Scheme 3-14 illustrates the relative number of photons present at different stages of the chemical reaction. At stage 'a', the relative number of photons emitted per excimer lamp is demonstrated. Based on the different radiant exitance (the amount of radiant energy emitted from a source per unit of time and area) and photon energy of these different light sources, three times less photons are emitted by the lamp that emits photons at 222 nm compared to 308 nm. At the next stage (b), a portion of photons is absorbed by the quartz tube. No quantitative measurement was obtained to determine the exact amount of absorbance, and therefore only a relative number is given in Scheme 3-14.

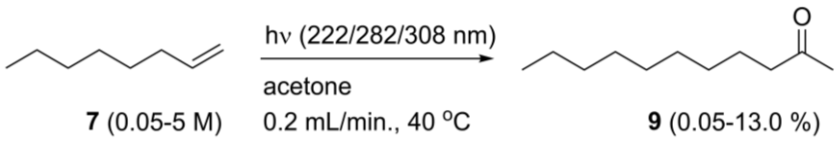


Scheme 3-14 Approximation of the relative photon count in the process of the photochemical experiment, a) number of photons emitted by excimer lamp, b) absorbance of photons by the quartz tube, c) absorbance of the photons by the absorber in the reaction mixture (in this case acetone), d) number of photons reaching the cooling stick and subsequent reflection of photons by the stainless steel.

As these are relative values, the number of photons absorbed by the quartz tube in relation to the 308 nm quartz tube is set negligible. The quartz tube in the reactor absorbs 25 % more of the light emitted at 222 nm compared to 308 nm, resulting in less photons reaching the reaction mixture when using the 222 nm excimer lamp. Subsequently, the photons reach the absorber in the reaction mixture, which is acetone. Scheme 3-14 displays the relative difference in the absorbance of photons between the three different excimer lamps, independent of concentration.

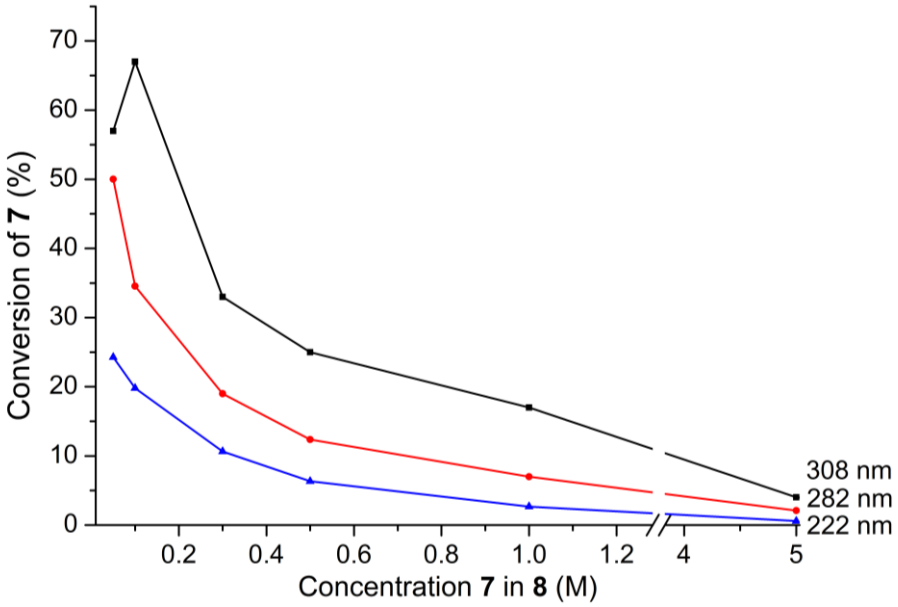
As the molar extinction coefficient of acetone at 282 nm is 12 times higher than at 308 nm, acetone molecules will absorb light more strongly at 282 nm. This has implications for how far the light can penetrate the reaction solution. 308 nm Light can travel 12 times further than 282 nm light at the same concentration, according to the Lambert-Beer law. When not all photons are absorbed by acetone, they reach the stainless steel cooling tube (stage d). About 40 % of the photons hitting the stainless steel get reflected back into the reaction mixture.[27] However, it is very hard to estimate how many of these reflected photons will excite an acetone molecule. Therefore, the reflected photons will not be considered in the analysis of reaction efficiency discussed later in this Section.

The influence of irradiation wavelength was tested experimentally employing several sets of conditions. Initially, conditions were chosen which have shown previously to result in limited reaction selectivity. At a concentration of 0.05-5 M of 1-octene in acetone, the reaction mixture was pumped through the reactor at 0.2 mL/min (Scheme 3-15). That way, a broad range of products was generated and could be studied.

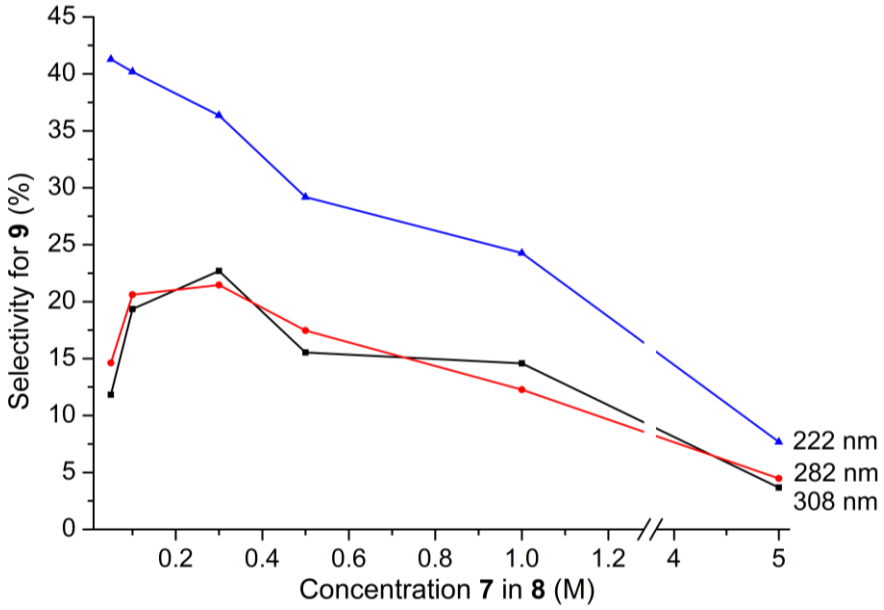


*Scheme 3-15 Reaction of 1-octene (**7**) and acetone (**8**) at different reactant ratios and different irradiation wavelengths.*

Section 3.4 described the trends of product selectivity over the range of concentrations, focussed on irradiation with the 308 nm excimer lamp. Therefore, only differences in product selectivity as apparent by the change in irradiation wavelength will be discussed in the Section below. The highest conversion of **7** was obtained when the reaction mixture was irradiated with the 308 nm excimer lamp at any given concentration of **7** in **8** (Figure 3-9a). The lowest conversion of **7** was found when the reaction mixture was irradiated with the 222 nm excimer lamp.



(a)



(b)

*Figure 3-9 a) Conversion of **7** and b) selectivity for product **9** at different concentrations of **7** in **8** at 40 °C and with three different irradiation wavelengths. Flow rate was set at 0.2 mL/min. **Black line** = 308 nm, **Red line** = 282 nm, **Blue line** = 222 nm excimer lamp. The highest selectivity for **9** was observed using the 222 nm excimer lamp while the lowest conversion of **7** was observed under these conditions.*

Acetone absorbs 282 nm light more strongly than 308 nm light due to the difference in molar extinction coefficient. However, the conversion of **7** was lower when the reaction mixture was irradiated with the 282 nm excimer lamp compared to irradiation with the 308 nm excimer lamp. This was despite the higher molar extinction coefficient of acetone at 282 nm. The main contribution to this difference in conversion is the photon output by the excimer lamp as will be discussed further later in this Section.

The highest selectivity for product **9** was obtained when irradiation was carried out with the 222 nm light source (Figure 3-9b). It is possible that at this wavelength light was absorbed by 1-octene as well as acetone, since 1-octene has an absorption maximum at 226 nm, corresponding to a π-π* transition (Figure 3-10).

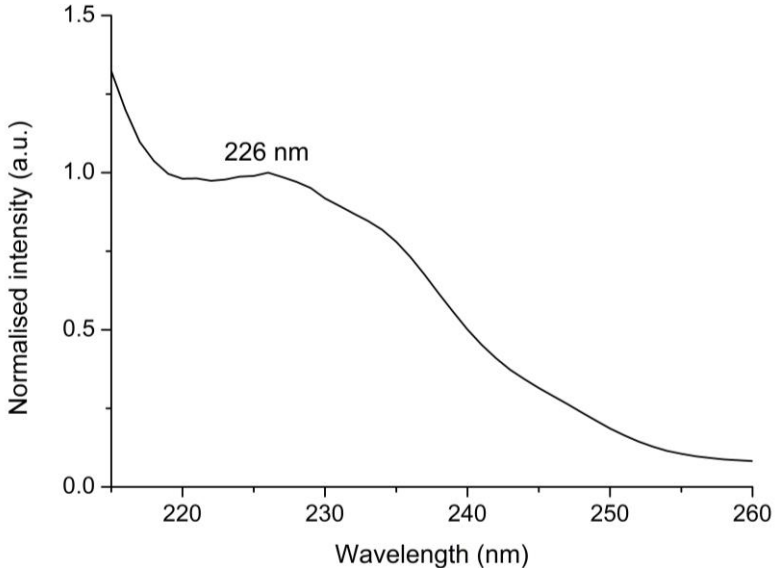
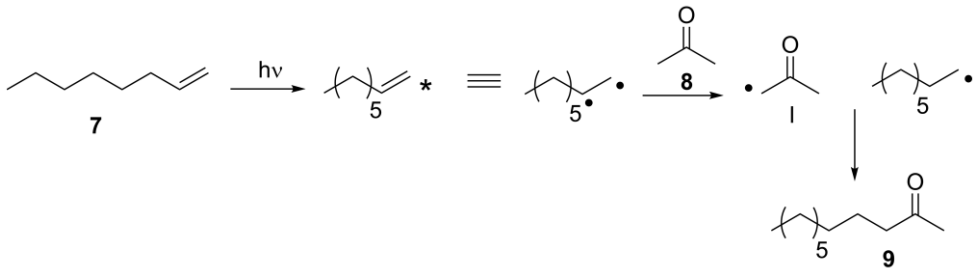


Figure 3-10 UV-Vis spectrum of 1-octene recorded in ethanol. Maximum intensity at 226 nm is normalised to 1.0.

The molar extinction coefficient of 1-octene at 222 nm is 2.6 times lower than that of acetone.[28] Therefore, the absorption of photons by 1-octene is most likely to play a more significant role at higher concentrations of olefin **7** in acetone. This absorption of light by 1-octene could possibly also account for the fact that the formation of acetone dimers was lower when irradiation was performed with the 222 nm excimer lamp. Interestingly, the selectivity for **9** was highly affected

by the change of irradiation wavelength while the other coupling products of **7** and **8** (products **10**, **17**, **18**) did not display such variation. A tentative explanation for this enhanced selectivity for extended ketone **9** might be the formation of radical I and a terminal alkyl radical after ground state acetone abstracted a hydrogen atom from excited state 1-octene. (Scheme 3-16). As these two radicals are formed in close proximity to each other, they can combine to form product **9**.



*Scheme 3-16 Possible route from excited state 1-octene to form product **9**.*

A control experiment was carried out to see whether 1-octene could participate in a photochemical reaction without acetone present. 1-Octene (**7**) was dissolved in MeCN and irradiated with 222 nm light. However, no reaction products were observed.

High selectivity for the formation of acetone dimers was observed at low concentrations of olefin **7** in acetone at all irradiation wavelengths (Figure 3-11). Irradiation of the reaction mixture with the 282 nm excimer lamp afforded the highest selectivity for acetone dimers. This could possibly be assigned to the greatest molar extinction coefficient of acetone at this wavelength. As more of the acetone molecules were excited, the probability for dimerisation increased. Acetone dimer formation was lowest when the 222 nm excimer lamp was used which might be because of the competitive light absorption by **7** at this wavelength.

Products **10** and **18** were both formed most selectively at each concentration when the reaction mixture was irradiated with the 282 nm excimer lamp compared to the other irradiation wavelengths. At 282 nm, most of the acetone molecules in solution will likely have absorbed the incoming light. Therefore, it

could be possible that this restricted reaction selectivity, allowing the production of by-products **10** and **18**.

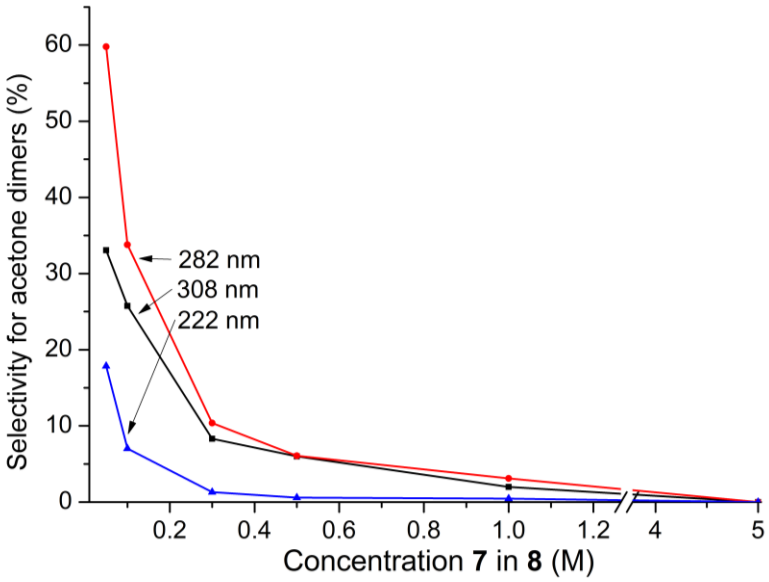


*Figure 3-11 Selectivity for all acetone dimers (products **12-14**) at different concentrations of olefin **7** in **8** at 40 °C and with three different irradiation wavelengths showing the highest selectivity when employing the 282 nm excimer lamp. Flow rate was set at 0.2 mL/min. **Black line** = 308 nm, **Red line** = 282 nm, **Blue line** = 222 nm excimer lamp.*

The productivity and reaction efficiencies of the reactions carried out with the different excimer lamps were calculated. The productivity of the conversion of **7** represents the amount of **7** consumed per hour while the productivity of the formation of **9** represents the amount of **9** formed per hour. Under all tested conditions, light penetrated the whole reaction solution. As explained previously, the number of photons emitted by the three different excimer lamps is different. Moreover, not all emitted photons will have been absorbed by acetone. Most of the 282 nm photons reaching the reaction solution will be absorbed by acetone due to the high molar extinction coefficient of acetone at this wavelength. Contrastingly, a relatively low molar extinction coefficient of acetone at 308 nm will result in absorption of only a small number of incoming photons and most photons will therefore reach the stainless steel cooling stick. The number of photons potentially absorbed by acetone was approximated based on the different molar extinction coefficients of acetone at each of these wavelengths. In calculating this number, it was assumed that the concentration of acetone

remains constant throughout the reaction but in reality, the concentration of acetone decreased as it participated in the photochemical reaction. Moreover, this approximation also assumes that no other molecules than acetone absorb the light. The reaction efficiency (RE) was formulated employing this number of photons that can initiate a photochemical reaction (Equation 3-2).

$$RE = \frac{productivity\ of\ reaction\ (\frac{mmol}{h})}{approximation\ of\ photons\ absorbed\ by\ acetone\ (\frac{mmol}{h})} \qquad 3\text{-}2$$

The RE was approximated for both the level of conversion of **7** and the formation of product **9** (Figures 3-12, 3-13 respectively). The reflectance of photons of the stainless steel surface back into the reaction solution was neglected in the estimation of the number of photons that are available for the photochemical reaction.

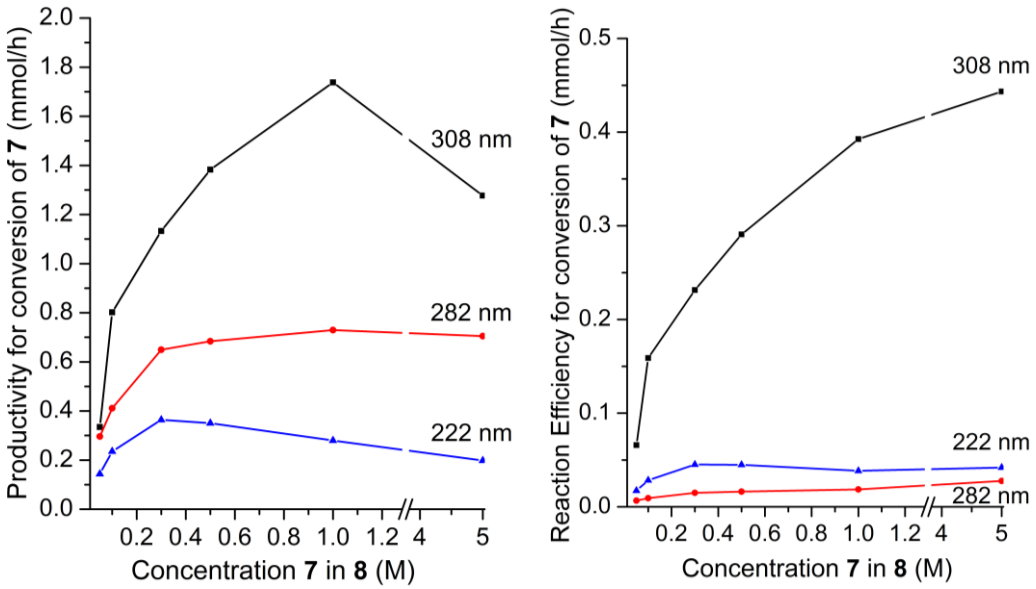
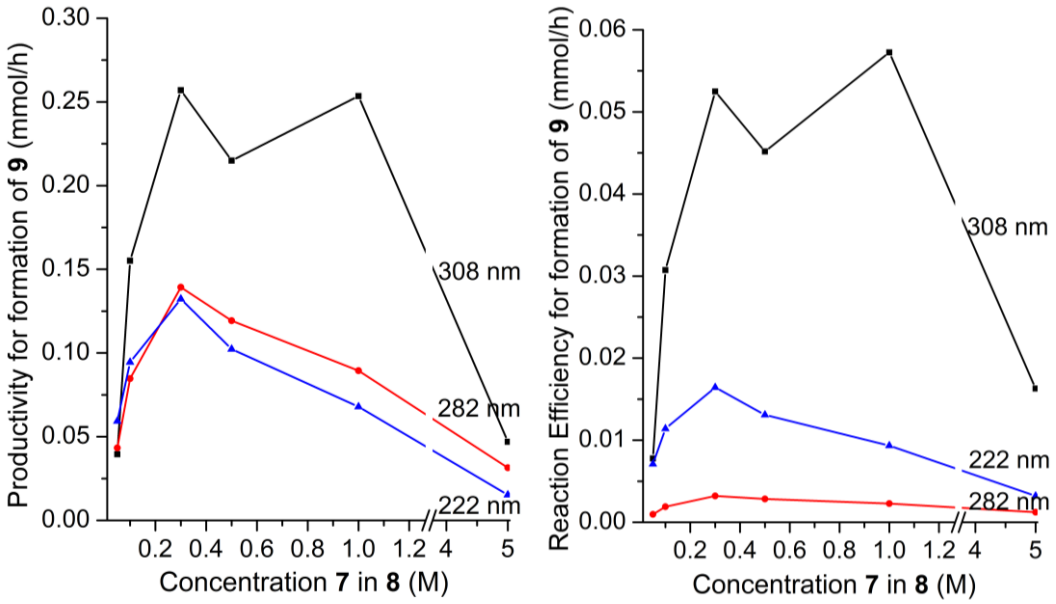


*Figure 3-12 a) Productivity and b) reaction efficiency for the conversion of **7** at different concentrations of **7** in **8** at 40 °C and with three different irradiation wavelengths which demonstrates that employing the 308 nm excimer lamp resulted in both the highest productivity and reaction efficiency under these conditions. Flow rate was set at 0.2 mL/min. **Black line** = 308 nm, **Red line** = 282 nm, **Blue line** = 222 nm excimer lamp.*

The productivity for the conversion of olefin **7** rose initially with increasing concentration of **7** in **8** for all three irradiation wavelengths (Figure 3-12a). This could suggest that diffusion is a limiting factor for conversion at the low concentrations of **7** in acetone. The maximum productivity for the conversion of **7** when the reaction mixture was irradiated with the 222 nm excimer lamp was at a lower concentration of **7** in acetone compared to the experiments carried out with the 282/308 nm excimer lamps. The productivity for the conversion of **7** did not keep increasing with higher concentrations of **7** in acetone when irradiated with the 222 nm excimer lamp. Therefore, it could be assumed that the excitation of acetone instead of alkene **7** remained the main pathway for the conversion of olefin **7**.

The RE of the conversion of **7** was higher with 222 nm compared to the 282 nm excimer lamp (Figure 3-12b). This could potentially be linked to the excitation of **7** at 222 nm if the quantum yield of the transformation of excited state 1-octene was higher than that of excited state acetone. The highest RE was obtained with the 308 nm excimer lamp. It could be possible that a large number of the photons reaching the stainless steel cooling stick got reflected back into the reaction mixture and contributed to a chemical transformation.

When considering the formation of extended ketone **9**, both the productivity and RE for the formation of **9** were highest when the reaction mixture was irradiated with 308 nm light (Figure 3-13). The maximum for both the productivity and RE in Figure 3-13 corresponded to the concentration at which the selectivity for **9** was highest at 282/308 nm. It was expected that the productivity for **9** would be higher using 222 nm light compared to 282 nm light at low concentrations of **7** in **8** due to the high selectivity for product **9** under these conditions. However, the productivity for the formation of **9** is comparable for both 282 and 222 nm excimer lamps at these concentrations. The low conversion of **7** with the 222 nm light could provide an explanation why the productivity for **9**, which is influenced by both the conversion of **7** and the selectivity for **9**, was similar for experiments using either 222 or 282 nm lamps.

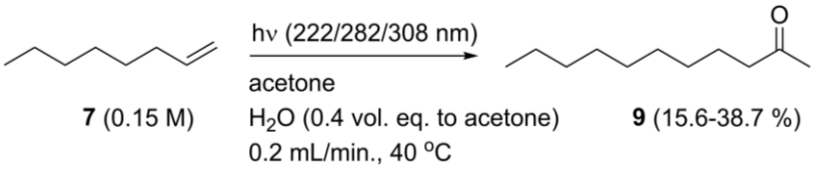


(a) (b)

*Figure 3-13 a) Productivity and b) reaction efficiency for the formation of **9** at different concentrations of **7** in **8** at 40 °C and with three different irradiation wavelengths, showing that employing the 308 nm excimer lamp resulted in both the highest productivity and reaction efficiency under these conditions. Flow rate was set at 0.2 mL/min. **Black line** = 308 nm, **Red line** = 282 nm, **Blue line** = 222 nm excimer lamp.*

To conclude, concentration differences of olefin **7** in acetone appeared to have the highest effect on product selectivity up to 1 M. The highest selectivity for extended ketone **9** was obtained at 0.3 M 1-octene in acetone when irradiating with both 282 and 308 nm light. However, this selectivity was only 23 %. Although a selectivity of 41 % was obtained with irradiation at 222 nm, this represents a very low productivity of 2-undecanone (**9**) formation due to low conversion of **7**. The excitation of 1-octene by the 222 nm excimer lamp could have been a contributing factor for reaction progression, but it was found that the excitation of acetone remained the most prominent route towards product formation.

Next, the influence of irradiation wavelength was tested when water was added as a co-solvent, as this has previously shown to result in higher selectivities for ketone **9** (Scheme 3-17).



*Scheme 3-17 Reaction of 1-octene (**7**) and acetone (**8**) with water (0.4 vol. eq. to **8**) as a co-solvent at different irradiation wavelengths.*

As found in the previous experiments shown in this Section, the highest conversion of **7** was reached with irradiation of the reaction mixture at 308 nm. Almost quantitative conversion of **7** occurred at this irradiation wavelength while the conversion was only around 50 % when using the other two wavelength excimer lamps (Figure 3-14). Acetone dimer formation was significantly reduced when the reaction mixture was irradiated with 222 nm light. The selectivity for **9** was again highest using 222 nm light. It might be possible that the hydration differences of radicals I and II by water play the most significant role in the selectivity for **9**. The additional excitation of **7** would therefore influence the selectivity for product **9** to a lesser extent.

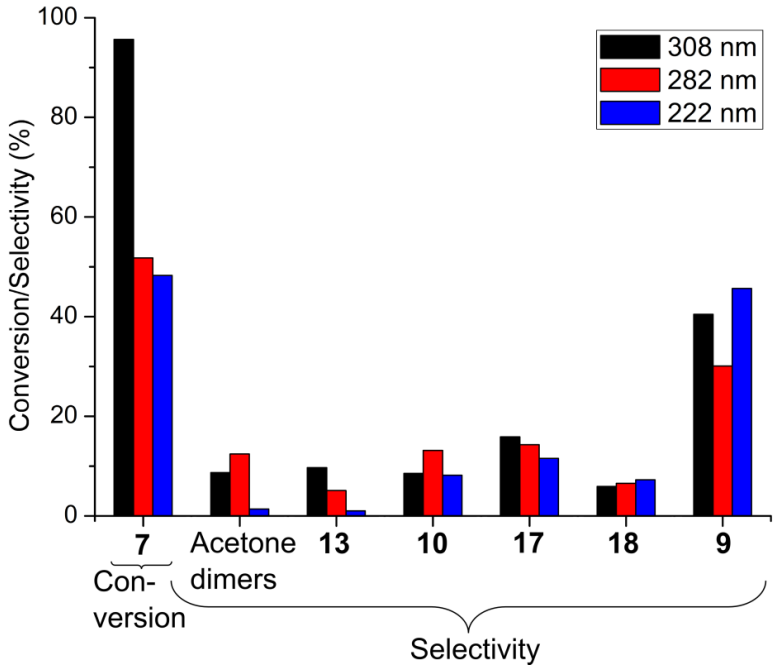


*Figure 3-14 Conversion of **7** at 0.15 M in acetone at 0.2 mL/min and 40 °C with water added (0.4 vol. eq. to **8**) and the selectivity of products at different irradiation wavelengths. **Black line** = 308 nm, **Red line** = 282 nm, **Blue line** = 222 nm excimer lamp.*

The productivity and reaction efficiencies were calculated for these experiments (Table 3-3). The maximum productivity for the formation of **9** was found to be 0.23 mmol/h (Table 3-3, entry 1). In terms of productivity for both the conversion of **7** and the formation of **9**, a higher concentration of **7** in **8** was found beneficial. However, product mixture purification plays a crucial role at these higher concentrations as the required product is not the major product and conversion of olefin **7** is low.

*Table 3-3 Productivity and reaction efficiency (RE) of both the conversion of **7** and the formation of **9**, given per excimer lamp.*

Entry	Excimer lamp	Productivity Conversion of 7 (mmol/h)	Productivity Formation of 9 (mmol/h)	RE[a] Conversion of 7	RE[a] Formation of 9
1	308 nm	0.57	0.23	$1.6x10^{-1}$	$6.5x10^{-2}$
2	282 nm	0.31	0.09	$9.7x10^{-3}$	$2.9x10^{-3}$
3	222 nm	0.29	0.13	$4.9x10^{-2}$	$2.2x10^{-2}$

*Reaction conditions: **7** (0.15 M in acetone), co-solvent: deionised water (0.4 vol. eq. to acetone), 0.2 mL/min, 40 °C; [a]Reaction Efficiency (RE) was estimated as productivity in mmol/h per mmol of photons absorbed by acetone per h*

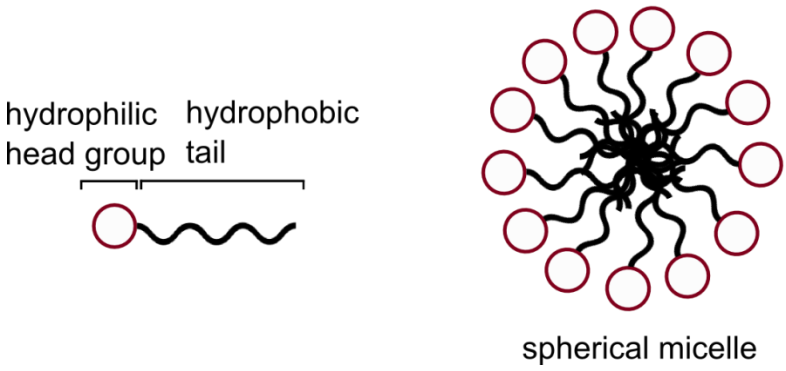
To conclude this Section, it appeared that the both the highest productivity for conversion of **7** and formation of product **9** can be obtained when the reaction mixture is irradiated with the 308 nm excimer lamp (0.57 and 0.23 mmol/h respectively). The excitation of 1-octene appeared to contribute to a higher conversion of **7** and a higher selectivity for product **9**, but the excitation of acetone remained the main route to product formation. Moreover, it was found that using light that is absorbed most efficiently by the absorber does not necessarily corresponds to the highest reaction efficiency.

With product selectivity being concentration dependent, the use of micro-heterogeneous environments created using ionic surfactants was investigated next to potentially increase the selectivity for product **9** even further.

3.9 Coupling of Olefins and Ketones in Micellar Media

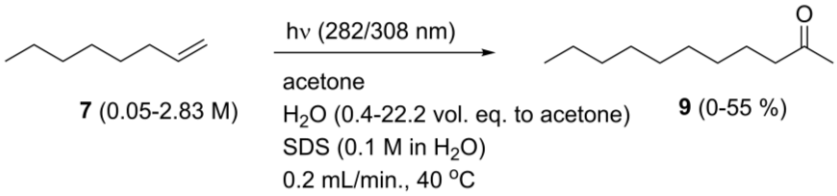
The use of ionic surfactants was investigated to potentially increase the selectivity for product **9**. The presence of micelles has been known to increase the reaction rate and/or selectivity of given chemical reactions as outlined in the examples below.[29] For example, enone dimerisation was reported more efficient in micelles and the regioselectivity was enhanced compared to non-micellar solutions.[30] Oehme *et al.* reported the asymmetric hydrogenation of amino acid precursors which showed increased enantioselectivity in micellar media compared to using methanol as the solvent.[31] This suggests that interactions between the surfactant and reactant can introduce orientational preferences. Photochemical reactions have been employed in micellar media as well as shown by Ivanov *et al.*[32] In the presence of micelles, a photodimerisation product of a naphthalene derivative was observed which was absent in aqueous media. Lee *et al.* observed a reversal in regioselectivity in the photodimerisation of an unsaturated ketone in a micellar solution compared to benzene.[30] Next to photodimerisation reactions, photorearrangements and photo-induced substitution reactions have been reported in which the reaction rate benefitted from the presence of micellar reaction media.[33]

Micelles are formed by amphiphilic molecules in water or media similar to water.[29] Amphiphiles are compounds with a hydrophilic head group and at least one hydrophobic chain (Scheme 3-18).[31] Non-polar solutes are likely to be located inside the micelle, close to the hydrophobic chains which often consist of hydrocarbons. The dehydration of these chains upon micelle formation gives rise to a hydrophobic effect. That in turn increases the entropy of the reaction system which is the driving force of micelle formation.[31] Micelles are thermodynamically stable though kinetically labile. Association and dissociation of micelles occurs on a millisecond time scale.[31]



Scheme 3-18 Simplified schematic showing a) amphiphile containing a hydrophilic head group and a hydrophobic tail, b) spherical micelle formed from amphiphiles.

For photochemical reactions, the transparency of the micellar solution to the light emitted by the light source is crucial. Sodium dodecyl sulfate (SDS) was chosen as the surfactant as it is transparent to the output of the excimer light sources as measured by UV-Vis spectroscopy. Moreover, SDS does not possess a halogen atom based counter ion as is the case in other commonly used surfactants. This is important as the UV photoreactor contains stainless steel tubing which is incompatible with halogen containing compounds. The first reaction studied in micellar reaction medium was the coupling of 1-octene (**7**) with acetone (**8**) (Scheme 3-19). The same continuous flow UV photoreactor as described previously was used in these experiments.



*Scheme 3-19 Reaction scheme for the coupling of 1-octene (**7**) and acetone (**8**) in micellar media.*

The lowest concentration at which spherical micelles form is called the critical micelle concentration (cmc) and for SDS,[29] this concentration is 8.1×10^{-3} M. To

ensure micelle formation, over 100 times the cmc was used in the experiments described in this Thesis.[33c] Reaction output was analysed by GC as in the experiments without micelles. The investigation into micellar media was started with the use of the 308 nm excimer light source as higher reaction efficiencies were obtained compared to experiments with either the 282 or 222 nm excimer lamps.

*Table 3-4 Screening of reaction conditions to optimise for conversion of **7** and selectivity for product **9** in the coupling of 1-octene (**7**) and acetone (**8**) in micellar solutions.*

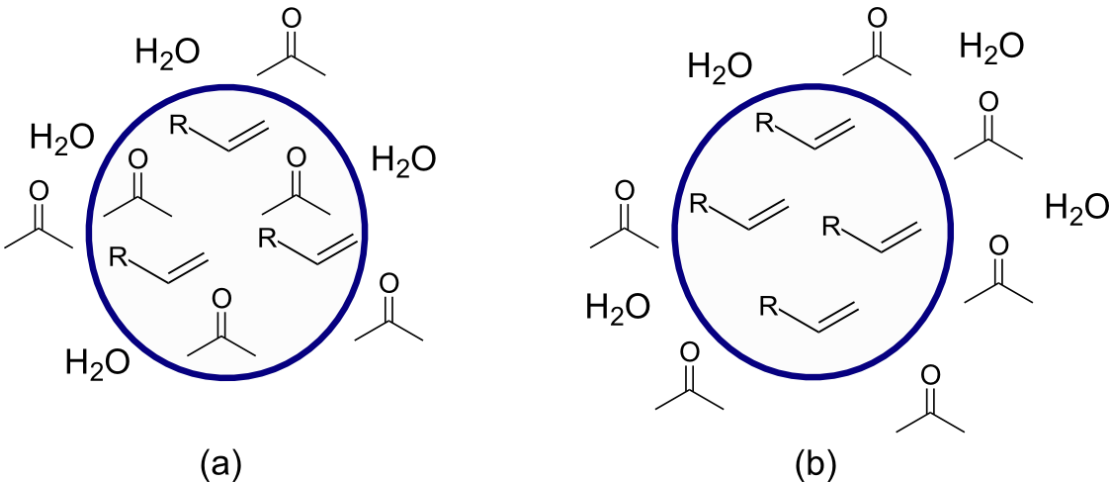
Entry	7 (M in acetone)	DI water[a]	Excimer lamp	Conversion of 7	Selectivity for 9	Selectivity for 13
1	0.05	0.4	308 nm	84 %	52 %	16 %
2[b]	0.05	0.4	308 nm	95 %	58 %	10 %
3	0.05	2	308 nm	> 99 %	14 %	60 %
4[b]	0.05	2	308 nm	> 99 %	0 %	53 %
5	0.1	0.6	308 nm	> 99 %	24 %	49 %
6[b]	0.1	0.6	308 nm	> 99 %	58 %	18 %
7	0.15	0.6	308 nm	> 99 %	53 %	16 %
8	2.83	22.2	282 nm	88 %	21 %	10 %
9	0.71	22.2	282 nm	98 %	19 %	20 %

*Reaction conditions: **7** (0.05-2.83 M in **8**), deionised (DI) water (0.4-22.2 vol. eq. to **8**), SDS (0.1 M in DI water), 0.2 mL/min, 40 °C; [a]in vol. eq. to acetone, [b]No SDS*

It was envisioned that the greater local concentration of **7** inside the micelles could potentially accelerate intermolecular coupling of **7** and **8**. However, the use of micellar reaction media resulted in diminished conversion of **7** and lower selectivity for the desired product **9** (Table 3-4, entries 1,2). It might be possible that the fast entrance and exit of acetone molecules from micelles[34] limited a possibly higher local concentration of substrates inside the micelle. The concentration of reactants in the micellar solution was high under the initial tested reaction conditions (Table 3-4, entry 1). It is possible that not all the reactants experienced an influence by the presence of micelles which would explain the small change in conversion and selectivity. To test this, the

concentrations of **7** and **8** in water was lowered a factor 5 (Table 3-4, entry 3). However, as found previously in non-surfactant based reaction media, increasing the water content as the co-solvent increased the selectivity for product **13** (Table 3-4, entries 1,3).

A higher selectivity for acetone dimerisation was observed in micellar reaction mixtures compared to aqueous solutions (Table 3-4, compare entries 1,2 and entries 3,4). Leigh *et al.* reported that in micellar media over 90 % of acetone molecules are in the aqueous phase instead of inside the micelles.[34] Therefore, the spatial separation of compounds **7** and **8** in solution might be larger when micelles are present which likely reduced the efficiency of intermolecular reactions due to diffusion limitations.[29] For efficient intermolecular reactions between **7** and **8**, the scenario depicted in Scheme 3-20a is favourable. However, based on the paper published by Leigh *et al.*,[34] the scenario depicted in Scheme 3-20b might be more accurate for the distribution of reaction substrates **7** and **8**.



*Scheme 3-20 Two different scenarios regarding the average distribution of reaction substrates 1-octene (**7**) and acetone (**8**) in micellar medium, a) both **7** and **8** are located inside the micelle (**blue ring**), b) only **7** is located inside the micelle while **8** and water are located outside the micelle.*

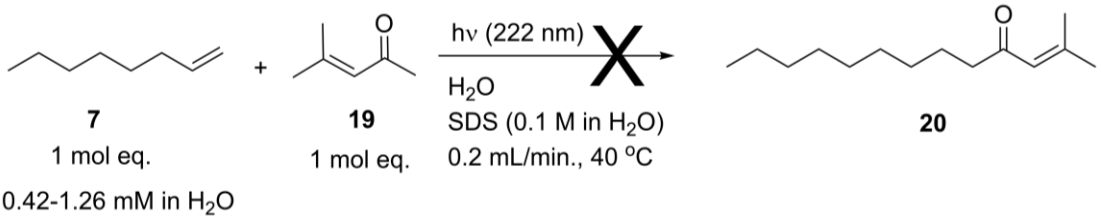
Another reason for the diminished selectivity for product **9** in the presence of micelles could be the lack of water when **7** and **8** react inside the micelle. As shown in previous sections, water is crucial for the solvation of radicals I and II. Without this interaction, radicals I and II are more likely to react at the same rate.

It has been reported that hydrogen atom abstraction from SDS by the triplet excited state of acetone is an important pathway when no other quenchers are present.[34-35] In the reaction of **7** and **8**, this would lead to an increased generation of radical II over radical I. Therefore, product formation with radical II would be favoured over product formation with radical I, which would decrease the selectivity for product **9**. An indication that this could potentially be the case in the studied reactions could come from the ratio in which the acetone dimers increase when SDS is present in the reaction medium. In the cases studied, product **14**, which is formed by the combination of two radical II molecules, increased a factor 2.2 and 6.0 more compared to the other two dimers when SDS was present. This corroborates the possible hydrogen atom abstraction from SDS. The highest factor corresponded to the highest concentration of acetone in water (Table 3-4, entries 5,6). As the conditions described in entry 5 in Table 3-4 provided full conversion of **7**, the concentration of **7** was increased (Table 3-4, entry 7) in order to increase the productivity of the reaction. Due to solubility limitations, these conditions could not be tested without the presence of surfactant. Moreover, it was envisioned that this higher concentration of **7** would decrease the high selectivity for product **13**. While maintaining quantitative conversion, the selectivity for product **13** decreased and the selectivity for desired product **9** increased which is an encouraging result.

Lower concentrations of reactants in the surfactant medium were tested to investigate different levels of encapsulation of the reactants in the micelles. To maintain efficient irradiation of the reaction mixture, the 282 nm excimer light source was used. As acetone absorbs more strongly at this wavelength, a lower concentration of acetone can still absorb a large portion of the light. Despite the high water content, the selectivity for product **13** was only 10 % (Table 3-4, entry 8). The selectivity for product **18** was found to be 29 %. As explained previously, possible hydrogen donation from SDS to excited state acetone generates a higher concentration of radical II molecules. The relatively high concentration of **7** in water, could lead to an increase in reactions between these two compounds. As these conditions afforded a conversion of **7** of 88 %, the concentration of **7** was decreased to obtain full conversion (Table 3-4, entry 9). Although conversion of **7** increased, the selectivity for product **13** doubled (Table 3-4, entries 8,9). The selectivity for product **9** remained around 20 %. It is encouraging to know that a high water content does not need to result in a high

selectivity for product **13**. However, the lower concentration of reactants in micellar media did not encourage the selectivity for product **9**.

With deionised water as the co-solvent in the coupling of olefins and ketones, substrate and product solubility can become an issue when varying the reactants. Shiraishi *et al.* who reported on the olefin and ketone coupling only described the coupling of acetone with a variety of olefins but did not test any ketones other than acetone.[7] This could be due to poor solubility of ketones other than acetone in water. Therefore, the use of SDS as the surfactant to overcome solubility issues was investigated as part of this Thesis. This way, a micro-heterogeneous solution was created for the coupling of 1-octene (**7**) with mesityl oxide (**19**) (Scheme 3-21). Mesityl oxide was chosen since conjugated ketones generally possess a π-π* transition at a longer wavelength compared to non-conjugated ketones. The excimer lamp can therefore activate the π-π* transition instead of the n-π* transitions. This transition exhibits a higher molar extinction coefficient compared to n-π* transitions so that more photons emitted by the excimer lamp can be absorbed by the ketone. Although **19** did not dissolve in pure deionised water, the addition of SDS (0.1 M in deionised water) afforded a visually clear micro-hetereogeneous solution. A concentration of 437 mM of **19** in the deionised water/SDS mixture was found to be the maximum concentration to fully solubilise **19**.



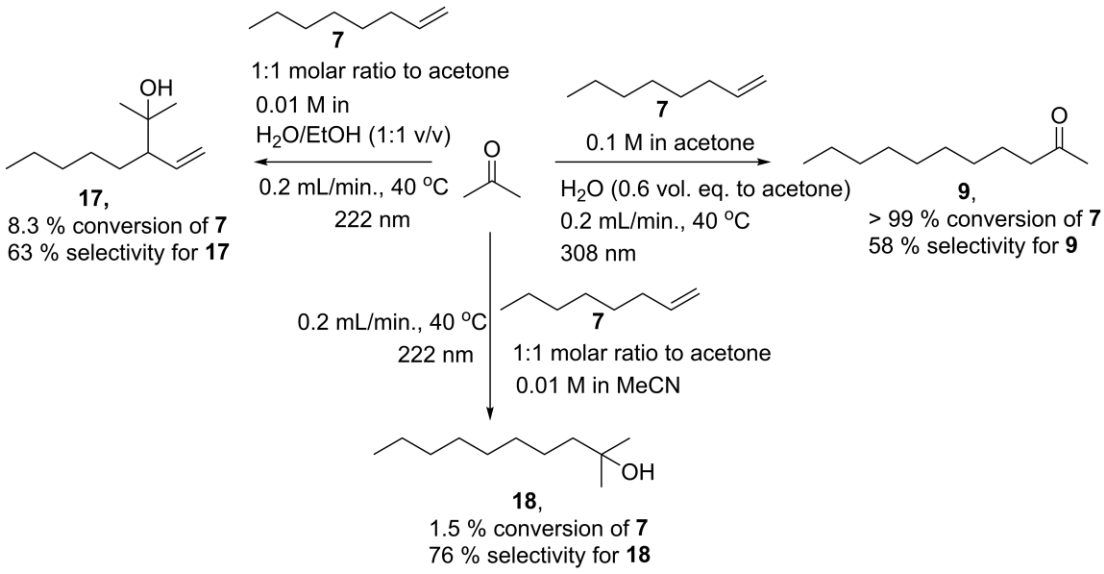
*Scheme 3-21 Reaction scheme in the photochemical coupling of 1-octene (**7**) and mesityl oxide (**19**) under different conditions.*

Mesityl oxide has an absorption maximum at 243 nm in water which corresponds to a π-π* transition of the conjugated C=O bond. Only the 222 nm excimer lamp overlaps with the absorption spectrum of **19**. Scheme 3-21 only shows coupling product **20**, but many other products could potentially be formed. Initially, a

concentration of **19** in deionised water was used so that 99 % of the incoming light would be absorbed (0.42 M). However, no reaction took place. Increasing the concentration of **19** three fold while keeping a 1:1 molar ratio between **7** and **19** did also not result in any product formation.

3.10 Conclusions and Future Work

The aim of this work was to produce a clean route for the formation of extended methyl ketones while maintaining a high productivity. By employing an in-house built UV continuous flow reactor, methyl ketone **9** was formed with a productivity of 0.69 mmol/h, which is a 23-fold increase compared to the value published by Shiraishi *et al.* for this transformation.[7] In the process of reaction optimisation, conditions were identified to obtain products **17** and **18** with good selectivities (Scheme 3-22, 63 and 76 % respectively). Potential recycling of the reaction mixtures could improve on the low conversion of **7**.



*Scheme 3-22 Different reaction conditions to achieve highest product selectivity for **9**, **17** and **18** starting from acetone and 1-octene. Conversions were based on the depletion of the signal for 1-octene in GC analysis.*

Further investigation could include performing the reaction at increased pressures. Product selectivity appeared to be concentration dependent and increasing the pressure might therefore change the product selectivity and favour the formation of products which benefit from higher reactant concentrations which could be achieved by using $scCO_2$ at elevated pressures. As liquids such as water and ethanol are hardly compressible, the use of $scCO_2$ could potentially be investigated as a co-solvent for the coupling of olefins and ketones. In order to carry out these reactions, a high-pressure UV photochemical reactor needs to be built.

It might also be interesting to examine the scope of this olefin and ketone coupling further. Shiraishi *et al.* demonstrated that varying the olefin has little influence on the reactivity.[7] Different ketones could be used for the coupling with olefins to investigate whether this reaction could be employed to generate more complex methyl ketones. Solubility issues for these ketones in water could be resolved by the use of micellar media. Examples of ketones could include pinacolone or acetophenone. Ketones bearing other functional groups for example a carboxylic acid moiety as in the case of acetoacetic acid could provide useful information about functional group tolerance.

3.11 References

1. (a) Beller, H. R.; Lee, T. S.; Katz, L., *Nat. Prod. Rep.* **2015,** *32* (10), 1508-1526, and references therein; (b) Forney, F. W.; Markovetz, A. J., *J. Lipid Res.* **1971,** *12* (4), 383-395; (c) Javidpour, P.; Pereira, J. H.; Goh, E.-B.; McAndrew, R. P.; Ma, S. M.; Friedland, G. D.; Keasling, J. D.; Chhabra, S. R.; Adams, P. D.; Beller, H. R., *Appl. Environ. Microb.* **2014,** *80* (2), 497-505; (d) Cseke, L. J.; Kirakosyan, A.; Kaufman, P. B.; Warber, S.; Duke, J. A.; Brielmann, H. L., *Natural products from plants*. CRC press: Boca Raton, Florida, 2006.
2. Ley, S. V.; Norman, J.; Griffith, W. P.; Marsden, S. P., *Synthesis* **1994,** *1994* (07), 639-666.
3. Tohma, H.; Kita, Y., *Adv. Synth. Catal.* **2004,** *346* (2-3), 111-124.
4. Caron, S.; Dugger, R. W.; Ruggeri, S. G.; Ragan, J. A.; Ripin, D. H. B., *Chem. Rev.* **2006,** *106* (7), 2943-2989.
5. (a) Liu, R.; Liang, X.; Dong, C.; Hu, X., *J. Am. Chem. Soc.* **2004,** *126* (13), 4112-4113; (b) Shibuya, M.; Osada, Y.; Sasano, Y.; Tomizawa, M.;

Iwabuchi, Y., *J. Am. Chem. Soc.* **2011,** *133* (17), 6497-6500; (c) Holan, M.; Jahn, U., *Org. Lett.* **2014,** *16* (1), 58-61.

6. He, X.; Shen, Z.; Mo, W.; Sun, N.; Hu, B.; Hu, X., *Adv. Synth. Catal.* **2009,** *351* (1-2), 89-92.
7. Shiraishi, Y.; Tsukamoto, D.; Hirai, T., *Org. Lett.* **2008,** *10* (14), 3117-3120.
8. Biella, S.; Rossi, M., *Chem. Commun.* **2003,** (3), 378-379.
9. Yamashita, T.; Matsushita, S.; Nagatomo, T.; Yamauchi, R.; Yasuda, M., *Res. Chem. Intermed.* **2013,** *39* (1), 111-126.
10. DeLaney, E. N.; Lee, D. S.; Elliott, L. D.; Jin, J.; Booker-Milburn, K. I.; Poliakoff, M.; George, M. W., *Green Chem.* **2017,** *19* (6), 1431-1438.
11. (a) Montalti, M.; Credi, A.; Prodi, L.; Gandolfi, M. T., *Handbook of photochemistry*. CRC press: Boca Raton, Florida, 2006; (b) Zhang, J. Y.; Boyd, I. W.; Esrom, H., *Appl. Surf. Sci.* **1997,** *109–110*, 482-486; (c) Kuhn, H. J.; Braslavsky, S. E.; Schmidt, R., *Pure Appl. Chem.* **2004,** *76* (12), 2105-2146.
12. Leighton, W. G.; Forbes, G. S., *J. Am. Chem. Soc.* **1930,** *52* (8), 3139-3152.
13. Kisch, H., *Semiconductor Photocatalysis: Principles and Applications*. Wiley-VCH: Weinheim, 2015.
14. (a) Dalton, J. C.; Turro, N. J., *Annu. Rev. Phys. Chem.* **1970,** *21* (1), 499-560; (b) Coyle, J. D., *Introduction to Organic Photochemistry*. Wiley-VCH: 1986.
15. Borkman, R. F.; Kearns, D. R., *J. Chem. Phys.* **1966,** *44* (3), 945-949.
16. (a) Goncharov, V.; Herath, N.; Suits, A. G., *J. Phys. Chem. A* **2008,** *112* (39), 9423-9428; (b) Haas, Y., *Photochem. Photobiol. Sci.* **2004,** *3* (1), 6-16; (c) Maeda, S.; Ohno, K.; Morokuma, K., *J. Phys. Chem. Lett.* **2010,** *1* (12), 1841-1845.
17. (a) El-Sayed, M. A., *J. Chem. Phys.* **1963,** *38* (12), 2834-2838; (b) El-Sayed, M. A., *Acc. Chem. Res.* **1968,** *1* (1), 8-16.
18. Kasha, M., *Disc. Faraday Soc.* **1950,** *9* (0), 14-19.
19. ten Brink, G.-J.; W. C. E. Arends, I.; Papadogianakis, G.; A. Sheldon, R., *Chem. Commun.* **1998,** (21), 2359-2360.
20. Wang, Z., Paterno-Büchi Reaction. In *Comprehensive Organic Name Reactions and Reagents*, John Wiley & Sons, Inc.: 2010.
21. Burikov, S.; Dolenko, T.; Patsaeva, S.; Starokurov, Y.; Yuzhakov, V., *Mol. Phys.* **2010,** *108* (18), 2427-2436.
22. Yoshida, K.; Kitajo, A.; Yamaguchi, T., *J. Mol. Liq.* **2006,** *125* (2–3), 158-163.
23. (a) Nakashima, M.; Hayon, E., *J. Phys. Chem.* **1971,** *75* (13), 1910-1914; (b) Shimizu, N.; Miyahara, T.; Mishima, M.; Tsuno, Y., *Bull. Chem. Soc. Jpn.* **1989,** *62* (6), 2032-2039.
24. Hurley, S. M.; Dermota, T. E.; Hydutsky, D. P.; Castleman Jr, A. W., *Int. J. Mass spectrom.* **2003,** *228* (2–3), 677-686.

25. Kamlet, M. J.; Abboud, J. L. M.; Abraham, M. H.; Taft, R. W., *J. Org. Chem.* **1983,** *48* (17), 2877-2887.

26. (a) Crespi, S.; Protti, S.; Fagnoni, M., *J. Org. Chem.* **2016,** *81* (20), 9612-9619; (b) Ismael, A.; Fausto, R.; Cristiano, M. L. S., *J. Org. Chem.* **2016,** *81* (23), 11656-11663.

27. Karlsson, B.; Ribbing, C. G., *J. Appl. Phys.* **1982,** *53* (9), 6340-6346.

28. *The molar extinction coefficient was determined in ethanol due to solubility issues in water.*

29. Dwars, T.; Paetzold, E.; Oehme, G., *Angew. Chem. Int. Ed.* **2005,** *44* (44), 7174-7199.

30. Lee, K.-H.; de Mayo, P., *J. Chem. Soc., Chem. Commun.* **1979,** (11), 493-495.

31. Oehme, G.; Grassert, I.; Paetzold, E.; Fuhrmann, H.; Dwars, T.; Schmidt, U.; Iovel, I., *Kinet. Catal.* **2003,** *44* (6), 766-777.

32. Ivanov, V. L.; Lyashkevich, S. Y., *High Energ. Chem.* **2016,** *50* (1), 32-36.

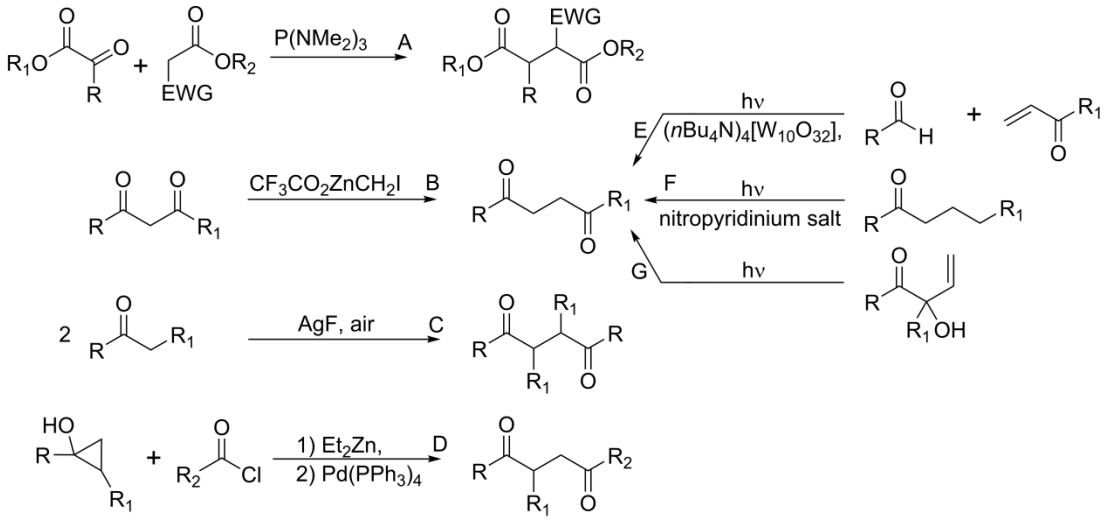
33. (a) Turro, N. J.; Grätzel, M.; Braun, A. M., *Angew. Chem. Int. Ed.* **1980,** *19* (9), 675-696; (b) Schütz, A.; Wolff, T., *J. Photoch. Photobio. A.* **1997,** *109* (3), 251-258; (c) Iguchi, D.; Erra-Balsells, R.; Bonesi, S. M., *Photochem. Photobiol. Sci.* **2016,** *15* (1), 105-116.

34. Leigh, W. J.; Scaiano, J. C., *J. Am. Chem. Soc.* **1983,** *105* (17), 5652-5657.

35. Scaiano, J. C.; Abuin, E. B.; Stewart, L. C., *J. Am. Chem. Soc.* **1982,** *104* (21), 5673-5679.

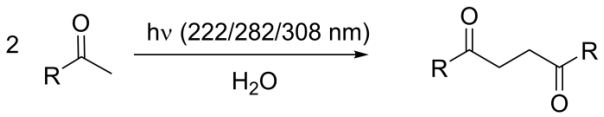
Chapter 4 Ketone Dimerisation

Chapter 3 focussed on the formation of extended methyl ketones by the coupling of olefins and ketones and it was found that changing reaction parameters influenced the product selectivity. In an attempt to utilise this result, reaction parameters were varied to optimise for different products and to that aid the formation of 1,4-diketones from ketones was investigated. 1,4-Diketones are important compounds as they appear as motifs in bioactive natural products.[1] Moreover, they can be used as precursors for the synthesis of heterocycles such as pyrroles and furans.[2] The formation of these compounds *via* a clean and mild method is therefore highly desirable to decrease the burden of commonly employed synthetic routes on the environment. Various methods for the formation of 1,4-diketones have been reported,[3] some of which are highlighted in Scheme 4-1.



Scheme 4-1 Overview of various reported routes to form 1,4-diketones, involving methods employing both metal based catalysts and photochemical transformations.

1,4-Diketones can be formed starting from either 1,2-diketones or 1,3-diketones, using a phosphorus compound[4] or a zinc based reactant[5] respectively (Scheme 4-1, Routes A, B). Phosphorus reagents were also employed by Huang *et al.* for the coupling of aryl hydrazines with ketones to generate enantio-enriched 1,4-diketones.[6] Radical based transformations that involve an enolate intermediate generated by a metal catalyst have been reported by Mao *et al.* (Scheme 4-1, Route C).[7] Acyl chlorides have been known to facilitate the formation of 1,4-diketones by coupling with cyclopropanol derivatives (Scheme 4-1, Route D).[3b] Photochemical methods to form 1,4-diketones include the tungsten catalysed aldehyde-ketone coupling (Scheme 4-1, route E)[8], the photo-oxidation of extended ketones by nitropyridinium salts (Scheme 4-1, route F)[9] and the irradiation of α-hydroxy-β,γ-unsaturated ketones (Scheme 4-1, route G).[10] Numerous routes to 1,4-diketones require metal catalysts,[3b, 5, 7] halogenated species,[3b, 11] or employ harsh reaction conditions for example the use of halogenated solvents.[4-5, 11d] The aim for the work presented in this Thesis was to synthesise 1,4-diketones photochemically while remaining an environmentally friendly transformation (Scheme 4-2). Utilising water as the co-solvent and UV light as the energy source, direct transformation of ketones to form 1,4-diketones was envisioned. This reaction could allow for a clean and atom economic synthesis of these compounds.

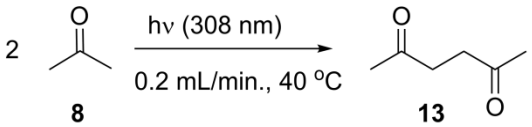


Scheme 4-2 The continuous flow photochemical dimerisation of ketones to form 1,4-diketones in aqueous solution, employing three different excimer lamps emitting at either 222, 282 or 308 nm.

The direct transformation of acetone to acetonylacetone creates an opportunity to increase both the chemical value and complexity in a single step. This has been achieved before employing a titanium based catalyst, albeit in low yield.[12] Singh *et al.* reported the photo-induced conversion of acetone to form acetonylacetone in maximum theoretical yield (25 %).[13] However, this reaction was carried out in benzene. The work presented in this Chapter will primarily focus on the photochemical dimerisation of acetone in water to form acetonylacetone. Preliminary studies on the photochemical dimerisation of other ketone substrates will be discussed later in this Chapter.

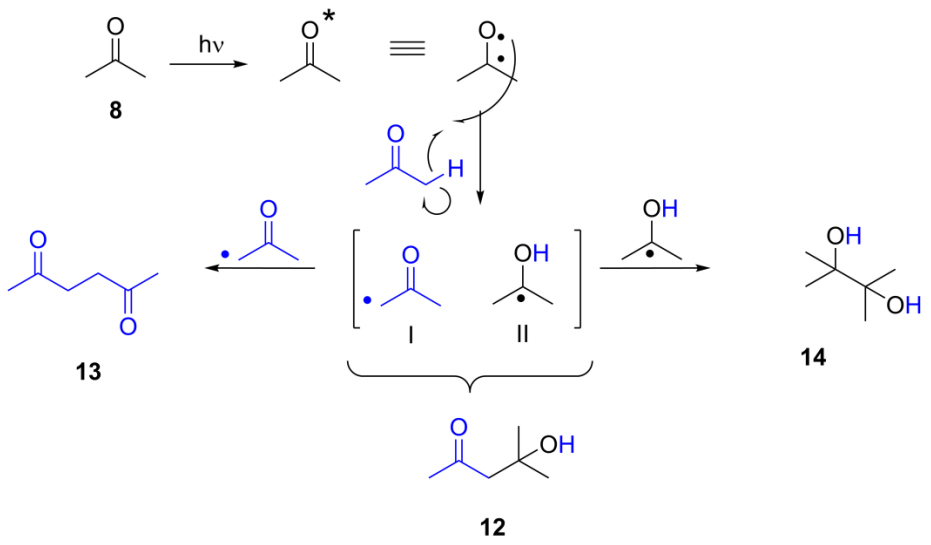
4.1 Initial Dimerisation of Acetone

The first reaction studied for this Thesis was the dimerisation of acetone (**8**) to form acetonylacetone (**13**) utilising 308 nm light (Scheme 4-3). The reaction was performed in the continuous flow UV photoreactor as described in Chapter 3.



*Scheme 4-3 Photo-induced dimerisation of acetone (**8**) to form acetonylacetone (**13**) in continuous flow.*

Product selectivity is key in this reaction as acetonylacetone (**13**) is only one of the possible products of acetone irradiation. Product **13** is formed when two α-keto radicals (radical I) combine (Scheme 4-4). Pinacol (**14**) is formed by the combination of two ketyl radicals (radical II) and **12** is the product of the combination of radical I and II.[14]



*Scheme 4-4 Reaction scheme for the generation of products **12**-**14** after the excitation of acetone (**8**).*

The theoretical maximum yield for products **13** and **14** is 25 %. Two acetone molecules are required to generate one set of radicals I and II. For the dimerisation of these radicals, a second set of these radicals is needed and therefore with 100 % conversion of acetone, only 25 % could have been converted to product **13** or **14**. The theoretical maximum yield for product **12** is 50 % as only one set of radicals I and II is needed which requires two acetone molecules.

The reaction mixture was analysed with gas chromatography (Figure 4-1). Signals with retention times between 10.5-17.0 minutes were present in the gas chromatogram of acetone before irradiation and do not correspond to reaction products formed. The yield of the reaction was determined by relating the area of the GC signals of all products compared to that of an external standard (2-undecanone). However, as the GC signal for 2-propanol (**15**) overlapped with

that of acetone (**8**), the calculated yield does not include the formation of by-product **15**. The conversion of **8** might therefore be significantly greater than the calculated total product yield.

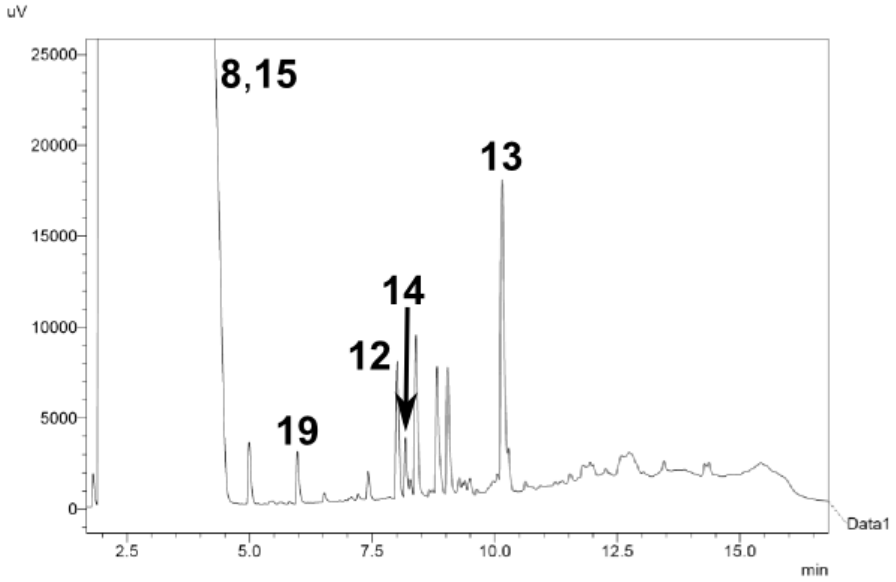
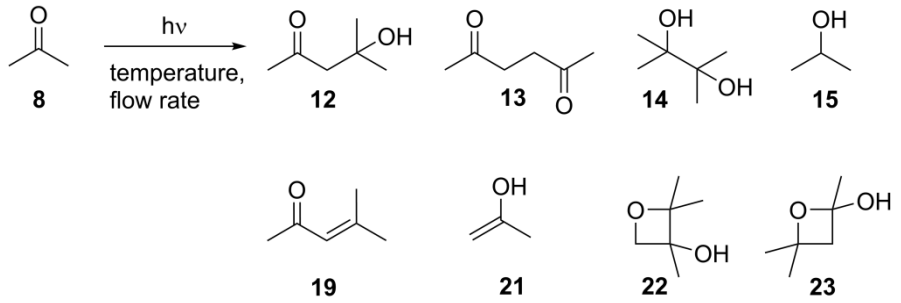


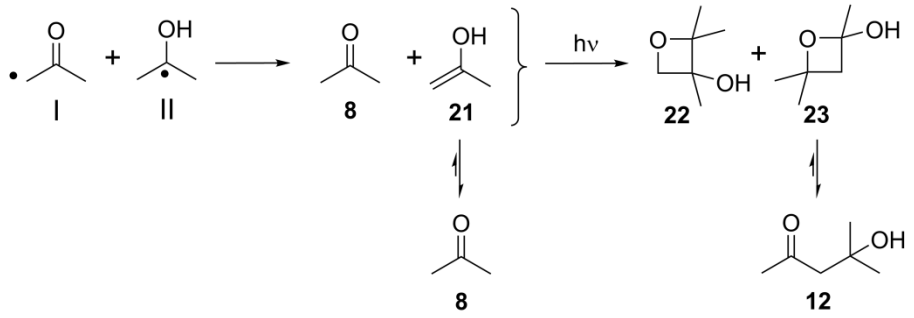
*Figure 4-1 Gas chromatogram of the reaction output in the dimerisation of acetone (**8**) carried out with a 308 nm excimer lamp, at a flow rate of 0.2 mL/min and at 40 °C.*

The selectivity for product **13** was 28 %. More product peaks were observed than can be explained by the formation of solely products **12**-**15**. These GC signals were also observed in the gas chromatogram of the coupling of 1-octene and acetone as described in Chapter 3. However, due to low yields of these products, isolation and identification of these compounds was problematic. The formation of more products has been reported and these compounds are depicted in Scheme 4-5. Mesityl oxide (**19**) can be formed *via* the dehydration of product **12**.[15]



Scheme 4-5 Reaction schematic showing different products possibly formed when acetone is irradiated.

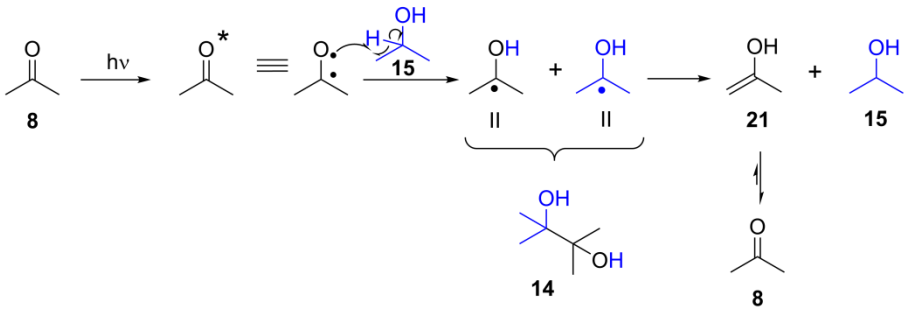
The enolic form of acetone (**21**) is generated *via* disproportionation of radicals I and II (Scheme 4-6).[16] However, the lifetime of **21** is only 14 seconds,[16] after which it tautomerises to acetone. Therefore, it is likely that this product cannot be measured with GC analysis of the product mixture.



*Scheme 4-6 Reaction schematic for the formation of mesityl oxide (**19**), the enolic form of acetone (**21**) and oxetanes **22** and **23**. Also shown is the isomerisation of **21** to **8** and the conversion of **23** to **12**.*

It has been reported that the excitation of acetone can lead to the formation of oxetanes **22** and **23** *via* the photocycloaddition between acetone (**8**) and its enol (**21**).[13] Oxetane **23** is a regioisomer of **22** and its formation has been reported as a reaction product of the irradiation of acetone.[17] Although product **12** is formed primarily by the coupling of radicals I and II, oxetane **23** can act as a precursor for **12** as well.[17] The photoreduction of **8** yields 2-propanol (**15**) as mentioned previously.[16] Once **15** is formed, excited state acetone can abstract a hydrogen

atom from hydrogen donor **15** generating two molecules of radical II (Scheme 4-7), providing another pathway to **14**.

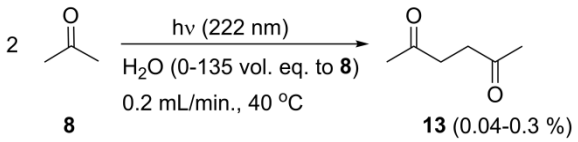


*Scheme 4-7 Reaction schematic for the reaction between acetone (**8**) and 2-propanol (**15**) forming pinacol (**14**), the enolic form of acetone (**21**) and regeneration of **8** and **15**.*[16]

This initial reaction to generate **13** *via* the irradiation of acetone has shown moderate selectivity. Therefore, reaction parameters were varied to improve this selectivity and to understand how these parameters influence the likelihood of the different reaction pathways occurring.

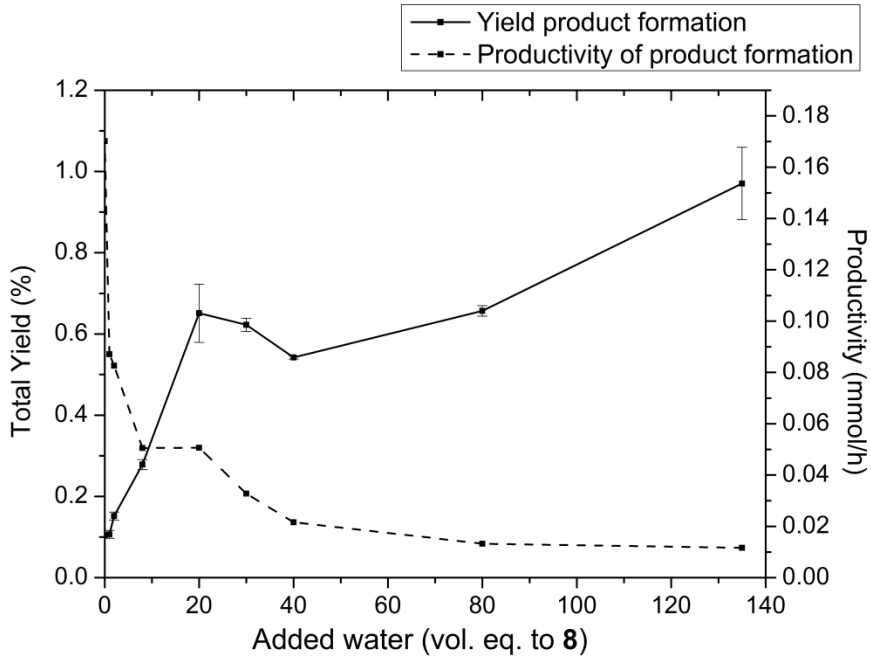
4.2 The Addition of Water as a Co-solvent

Dimerisation reactions have been reported to be concentration dependent.[18] Therefore, an extensive study was carried out to investigate the influence of acetone concentration and the use of water as a co-solvent on product formation. (Scheme 4-8).

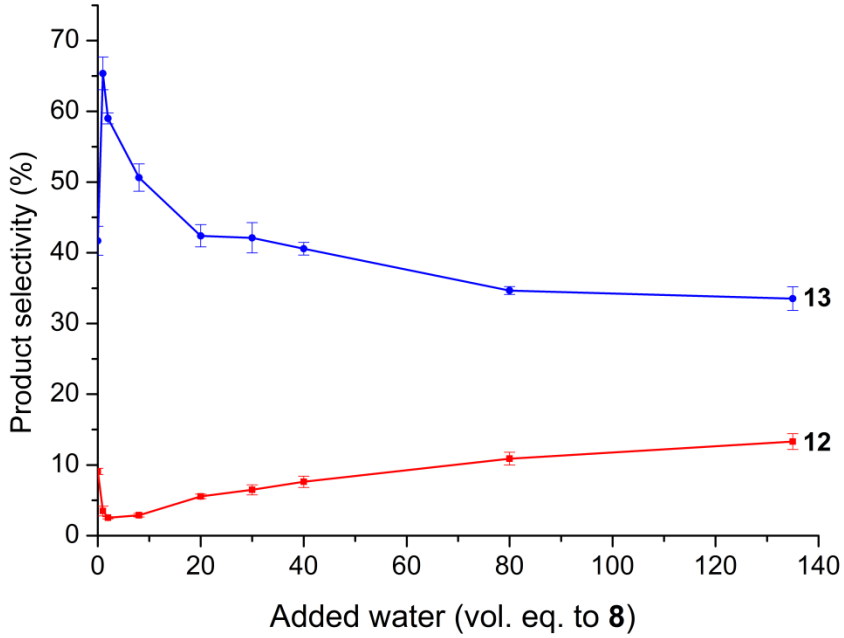


*Scheme 4-8 Investigation of the influence of the addition of water as a co-solvent (0-135 vol. eq. to **8**) on the dimerisation of acetone (**8**).*

Product formation increased upon the increased addition of water (Figure 4-2a, black line). The initial steep rise in product yield could have been the result of the hydration of both radicals I and II which inhibits radical recombination and therefore increases the overall product yield.[19] The concentration of acetone in the reaction mixture reduced when water was added, which means that a higher product yield in more dilute acetone solutions does not necessarily corresponds to a higher amount of products formed. Therefore, the productivity of product formation was calculated (Figure 4-2a, dashed black line). The productivity indicates how much mmol of product is formed over time. As for other dimerisation reactions,[18] the formation of products appeared to be concentration dependent as the productivity of product formation decreased in more dilute acetone solutions. Diffusion limitations could have played a role as well as the viscosity of the reaction solution which increased when more water was present. Howard *et al.* described the change in viscosity of acetone/water mixtures depending on the ratio.[20] The values published by Howard *et al.* were used as a guideline for the relative comparison of viscosity and reaction productivity. The highest viscosity of the reaction mixture was most likely when 2 vol. eq. of water was added to acetone (approximately 0.98 mPa·s at 37.8 °C). Neat acetone has a viscosity of 0.27 mPa·s, which is 3.6-fold lower. The productivity of product formation was 2.1-fold higher using neat acetone compared to aqueous acetone (2 vol. eq. of water to acetone). This indicates that the effect of viscosity on the productivity of product formation is either not first order or not the only contributing factor. Increased viscosity and decreased concentration of acetone both contribute to diffusion restrictions. Another feature that could have played a role is the fact that hydrogen-bonding between acetone and water is able to reduce efficient ISC in ketones.[21] This could inhibit efficient product formation.



(a)



(b)

*Figure 4-2 a) Total yield of product formation in % (**black line**) and in productivity (mmol/h) (**dashed black line**) in the irradiation of acetone (**8**) in water (0-135 vol. eq. to **8**) at 40 °C, using the 222 nm excimer lamp, b) the selectivity towards products **12** (**red line**) and **13** (**blue line**). Note that no pinacol (**14**) was formed during the reaction and the selectivity for **13** decreased when an increased amount of water was added.*

When focussing on product selectivity, no pinacol (**14**) was formed under any of the tested conditions (Figure 4-2b). As discussed in Chapter 3 of this Thesis and reported by Kamlet *et al.*,[22] the hydration of radical II is stronger than that of radical I in aqueous solutions of acetone. This suppresses the reactivity of radical II which could prevent the formation of pinacol (**14**). This difference in hydration levels most likely explains the initial increase in selectivity for diketone **13** when water is added at 1 vol. eq. to **8**. The optimum molar ratio of acetone to water appeared to be 1:4 as these conditions led to the highest selectivity for diketone **13** (66 %). The addition of more water decreased the selectivity for diketone **13** and increased the selectivity for **12**. As explained previously, diffusion appeared to play an important role in product formation in more dilute acetone solutions. When diffusion is limited, it is more likely that radical I and II, formed in the same photochemical process, combine to form **12** rather than for two radical I or II molecules, formed in two separate photochemical processes, to diffuse together to form diketone **13** or diol **14** respectively.[23] This could explain the increase in selectivity for **12** at lower acetone concentrations. Additionally, the enol tautomer of acetone (**21**) increased in concentration in aqueous solutions of acetone. The addition of **21** to radical I provides a direct route to product **12** which would explain the more selective formation of **12** when more water was added. The product that corresponds to a GC signal with a retention time of 8.33 min. was also seen to increase in selectivity in more dilute acetone solutions. In neat acetone, the selectivity for this product was 1.6 % while it reached 16 % in a solution of acetone and water (135 vol. eq. to **8**). Although this product could not be isolated, it is likely that this product was formed *via* a route involving radical II as opposed to radical I since products involving radical II increased in selectivity upon the addition of water to the reaction mixture.

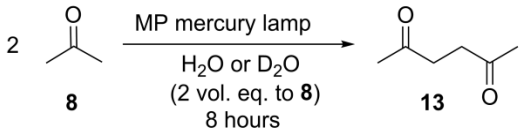
The experiment was repeated with the 308 nm excimer lamp to ensure the change in product selectivity as observed with the addition of 0-10 vol. eq. of water using the 222 nm lamp was reproducible. The highest selectivity for diketone **13** was observed with the addition of 1 vol. eq. of water and the selectivity for both **12** and diketone **13** changed in a similar pattern when using either the 308 or 222 nm lamp. Pinacol (**14**) was formed in neat acetone when irradiation was carried out with the 308 nm excimer lamp, but its formation was inhibited in the reactions where water was present as the co-solvent. Section 4.6 will evaluate the difference in product selectivity based on irradiation wavelength in further detail.

The above findings seem to reveal an optimum molar ratio of 1:4 between acetone and water, likely influenced by the diffusion of reactants and the hydration of radical II by water. These conditions resulted in the highest selectivity for diketone **13** (66 %). The highest yield for product formation (0.97 %) was found at the lowest tested concentration of acetone in water while the highest productivity for product formation (0.17 mmol/h) was found when the reaction was carried out in neat acetone.

Next, the effect of radical hydration was investigated further by comparing H_2O and D_2O as co-solvents in the reaction.

4.3 Formation of Acetonylacetone in Batch

To provide further evidence for the hypothesis that the solvation differences of radicals I and II by water caused the shift in product selectivity, the dimerisation of acetone was performed with D_2O as the co-solvent. It has been reported that D_2O provides greater solvation of solutes than H_2O due to stronger hydrogen-bonding interaction.[24] The hydration of radical II by D_2O as opposed to H_2O would therefore be stronger and the selectivity for diketone **13** should increase as a result. The lifetime of excited state acetone in D_2O is higher compared to H_2O (29 µs *versus* 20 µs)[25] which could also increase the yield of all reaction products when using D_2O as a co-solvent. This reaction was carried out in batch to limit the amount of waste of D_2O and the same reaction set-up was used as for the experiments carried out in batch described in Chapter 3. The reaction was repeated in H_2O for comparison (Scheme 4-9). Details on the reaction set-up can be found in the Experimental Chapter.



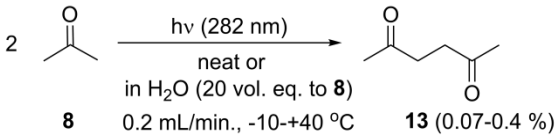
*Scheme 4-9 Photo-induced dimerisation of acetone (**8**) in batch using either H_2O or D_2O as a co-solvent (2 vol. eq. to **8**) to investigate the effect of hydration of radicals I and II on the product selectivity.*

Performing this reaction in batch could also help identify the formation of possible stable reaction intermediates. Reactions carried out in the continuous flow UV photoreactor had a 6.9 minute irradiation time thus far. However, due to the large total reactor volume, GC analysis of this reaction mixture performed in flow was 43.1 minutes after the irradiation ended, when the irradiated mixture reached the outlet of the reactor. GC analysis of the aliquots from the experiments in batch was performed immediately after the sample was taken (the first aliquot was taken after 30 minutes of irradiation time) which could provide an insight in product formation at the early stages of the reaction. Moreover, the reaction proceeded much slower in the batch set-up compared to the flow set-up which means that aliquots from the experiment carried out in batch were from an earlier point in the reaction. However, GC analysis of aliquots taken from the experiment in batch over time (every 30 minutes up to 2 hours, then every hour) revealed no new peaks compared to analysis of the reactions carried out in flow. This indicates that no stable intermediates were formed when **8** is irradiated in either D_2O or H_2O. The selectivity for products **12** and **13** remained constant over the reaction time. No pinacol (**14**) was formed under any of the tested conditions most likely due to the hydration of radical II by the co-solvent. Surprisingly, no significant difference in the selectivity for products **12** and **13** (2.3 and 54 % respectively) was observed when comparing H_2O and D_2O as co-solvent. This would indicate that there was no difference in the hydration of radicals I and II by H_2O *versus* D_2O.

No reaction intermediates could be identified from the irradiation of acetone in batch. Moreover, no significant difference in product selectivity was observed when the reaction was carried out in D_2O as opposed to H_2O but this could be due to an error in reaction set-up. Therefore, no information about the influence of radical hydration on product selectivity was obtained.

4.4 Formation of Acetonylacetone at Different Temperatures

Another way to vary the level of radical hydration is by changing the reaction temperature. Temperature differences alter the hydrogen-bonding strength between acetone and water[24] which has an effect on the hydration of the acetone based radicals. Therefore, the temperature of the reaction was varied to investigate its influence on product selectivity. Two sets of conditions were tested, using neat acetone as the reaction solution and using a mixture of acetone and water (Scheme 4-10). Performing the dimerisation of acetone in neat reaction conditions could provide information on diffusion rates of molecules and radicals involved in this reaction. The highest temperature tested was 40 °C as the maximum temperature was restricted by the boiling point of acetone when using neat acetone. The lowest temperature tested was -10 °C due to the risk of freezing of the reaction mixture at lower temperatures when water was present at such high concentrations.



*Scheme 4-10 Investigation of the influence of reaction temperature on the dimerisation of acetone (**8**).*

When neat acetone (**8**) was irradiated with 282 nm light, a temperature rise of 50 °C doubled the selectivity for diketone **13** (Figure 4-3). Under these conditions, the selectivity for product **12** increased by 3.5-fold whereas the selectivity for diol **14** halved. It may be suggested that radical II is less reactive than radical I at higher temperatures, resulting in a higher selectivity for products formed with radical I such as **12** and diketone **13**. It is difficult to pinpoint the exact cause of this trend without additional data, but a tentative explanation could be the difference in relative stability between radicals I and II. As a secondary radical, radical II is more stable[26] and therefore less reactive whereas radical I is a primary radical and therefore more reactive. Moreover,

hydrogen-bonding interactions between radical II and acetone can stabilise this radical, further diminishing its reactivity. At lower temperatures, diffusion rates are generally lower and the likelihood of two radical I molecules interacting decreases as a result, leading to a lower selectivity for product **13**. It might be possible that the increased stabilisation of radical II compared to radical I increased its lifetime. As a result, the combination of two radical II molecules rather than two radical I molecules would be more likely, which would lead to an increased selectivity for diol **14** at lower temperatures.

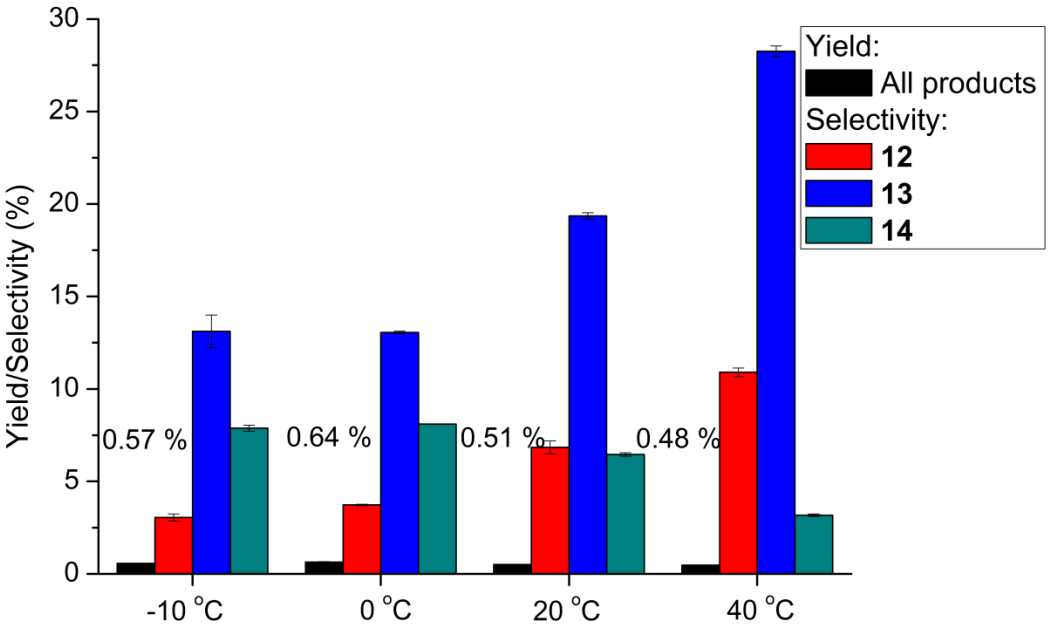


*Figure 4-3 Total yield of product formation (**black line**) and the selectivity towards products **12** (**red line**), **13** (**blue line**) and **14** (**dark cyan line**) in the irradiation of neat acetone (**8**) at different reaction temperatures using the 282 nm excimer lamp and a flow rate of 0.2 mL/min, showing increased selectivity for **13** but lower total product yield at higher temperatures.*

The highest total product yield was obtained at 0 °C (0.64 %). It might be suggested that diffusion is not the rate limiting process in the reaction carried out under these conditions as diffusion rates generally decrease at lower temperatures. This would result in lower reaction rate and product yield at lower temperatures. It is possible that the rise in temperature above 0 °C resulted in rapid deactivation of the excited state acetone *via* a radiationless transition while the quantum yield of intersystem crossing by excited state acetone remained constant for the reactions carried out below 25 °C.[19, 27] A contributing factor could

be the small decrease in the dielectric constant of acetone at higher temperatures (19.6 at 20 °C to 17.8 at 40 °C).[28] Since the reaction intermediates are stabilised by a polar environment, this could be a contributing factor in lower product formation at higher temperatures. The decrease in total product yield at elevated temperatures is according to the results reported by Shiraishi *et al.*[19]

When the dimerisation of acetone was carried out in aqueous solutions, no pinacol (**14**) was formed (Figure 4-4). Hydrogen-bonding is strengthened at higher temperatures,[24] further encouraging the hydration of radical II. As hydration of the radical reduces its reactivity, this could explain why the selectivity for product **12** decreased at higher temperatures as the route to **12** requires radical II to be reactive.

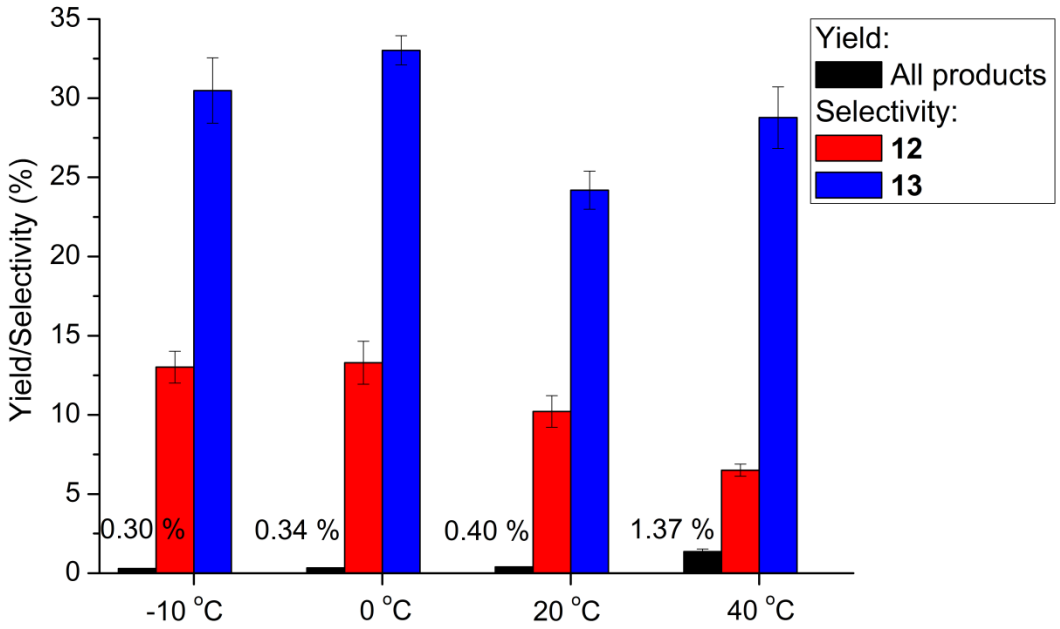


*Figure 4-4 Total yield of product formation (**black line**) and the selectivity towards products **12** (**red line**) and **13** (**blue line**) in the irradiation of acetone (**8**) in water (20 vol. eq. to **8**) at different reaction temperatures using the 282 nm excimer lamp and a flow rate of 0.2 mL/min. The results demonstrated that no pinacol (**14**) was formed during the reaction and that the highest product yield was achieved at the highest temperature.*

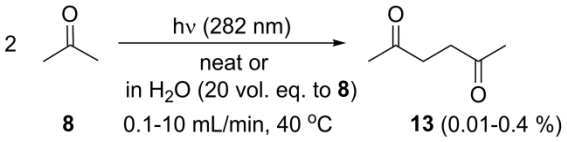
A clear increase in total yield was observed when the reaction was carried out at 40 °C compared to lower operating temperatures (0.30-1.4 %). This is the opposite trend to when the reaction was carried out in neat acetone. As the viscosity of aqueous acetone is higher than that of neat acetone,[20] it is possible

that the reaction of acetone becomes diffusion limited in aqueous acetone solutions. A higher temperature increases the rate of diffusion which could possibly explain the higher product yield at higher temperature. This limitation on diffusion would be present at all reaction temperatures. The further change in diffusion rates at the different temperatures did not appear to be a large contributing factor to product selectivity in aqueous solutions of acetone as less clear enhancement of selectivity was observed for diketone **13** at higher temperature compared to when the reaction carried out in neat acetone. It might be suggested that the hydration of radicals I and II was the main contributing factor to product selectivity in aqueous acetone solutions rather than the change in diffusion rates related to the difference in temperature.

To conclude, the use of aqueous solution for the formation of diketone **13** from **8** can suppress the formation of by-products. Under these conditions, the highest selectivity for product **13** was observed when the reaction was carried out at 0 °C. The highest total yield and the lowest by-product formation were observed when the reaction was carried out at 40 °C. The influence of co-solvent on reaction selectivity and yield will be further discussed *vide infra*. In neat acetone, the highest selectivity for diketone **13** was obtained at the highest tested temperature. The results suggest that the rate-determining step in aqueous solutions of acetone was the diffusion of reactants, but further research is required to corroborate this statement.

4.5 Formation of Acetonylacetone at Different Flow Rates

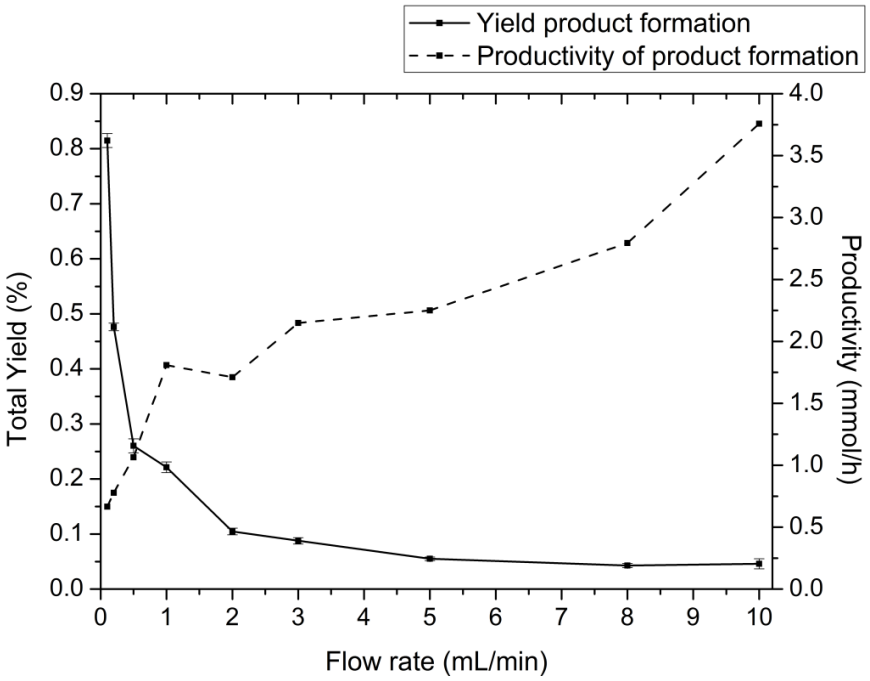
Improved mixing of the reactants in the reactor could potentially reduce diffusion limitations. As stirring was not possible in the continuous flow UV photoreactor, the effect of mixing was studied by changing the flow rate of the reactants. A higher flow rate generally leads to a more turbulent flow and therefore better mixing. Two reaction conditions were tested as both neat acetone and acetone in water (20 vol. eq. to **8**) were flowed through the reactor at varying flow rates (0.1-10 mL/min) (Scheme 4-11).



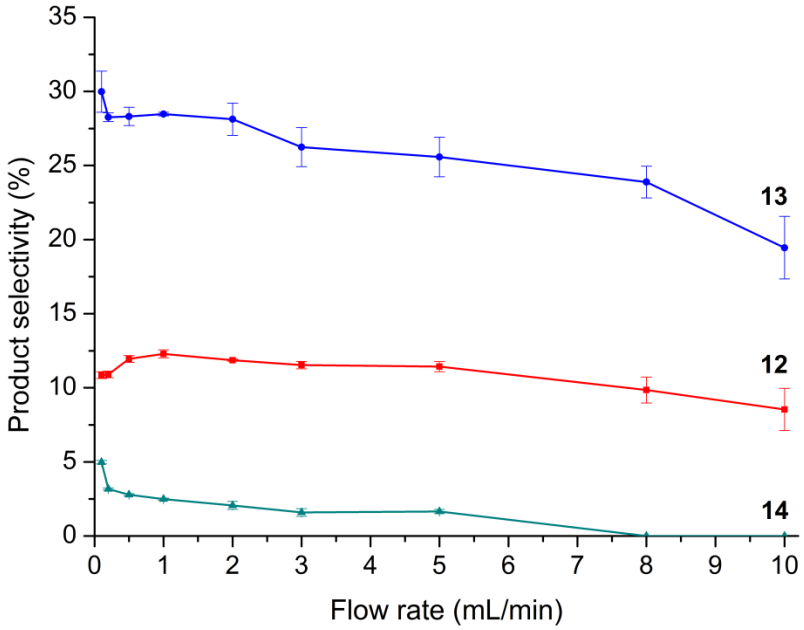
*Scheme 4-11 Irradiation of neat acetone (**8**) and in aqueous solution to form acetonylacetone (**13**) in a range of flow rates (0.1-10 mL/min).*

When the reaction was carried out in neat acetone, the total product yield increased with decreasing flow rate (Figure 4-5a). This was expected as a lower flow rate increases the irradiation time of acetone in the reactor. Interestingly, the difference in residence time alone could not account for the change in total yield as shown by the productivity values depicted in Figure 4-5a. If the change in residence time were to be the only contributing factor, the productivity of total product formation would be a constant value. However, the productivity clearly increased at increasing flow rates. It is probable that mixing is more efficient at higher flow rates. Moreover, the diffusion of reactants will be greater at higher flow rates, increasing the probability of intermolecular reactions and possibly limiting degradation reactions.

It was observed that a decrease in flow rate increased the formation of by-products as more signals were present in the gas chromatogram during these experiments. When evaluating the product selectivity at the different flow rates, the selectivity for acetonylacetone (**13**) and pinacol (**14**) decreased at higher flow rates (Figure 4-5b) while the selectivity for **12** did not differ much with the different flow rates. It was hypothesised that at higher flow rates, the removal of local areas of heat was more efficient compared to the heat removal at lower flow rates. These local areas of heat could be the result of vibrational relaxation processes. As photons excite electrons in ground state acetone into a higher vibrational state, rapid vibrational relaxation takes place to the lowest vibrational state. This process produces heat which can build up when this heat is not removed quickly.



(a)



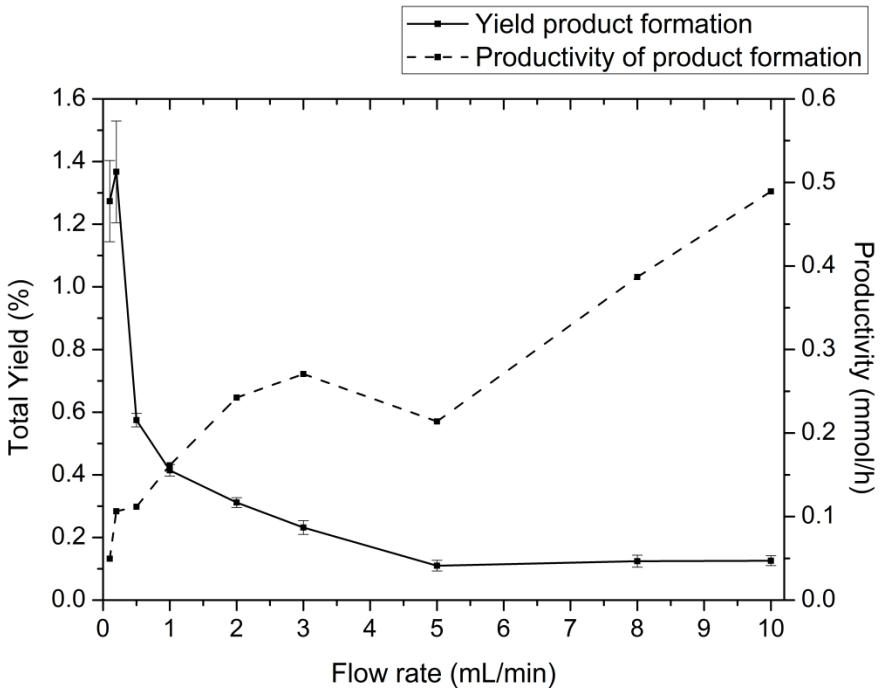
(b)

*Figure 4-5 a) Total yield of product formation in % (**black line**) and in productivity (mmol/h) (**dashed black line**) in the irradiation of neat acetone (**8**) at different flow rates (0.1-10 mL/min), at 40 °C using the 282 nm excimer lamp, b) the selectivity towards products **12** (**red line**), **13** (**blue line**) and **14** (**dark cyan line**) showing a decrease in selectivity for all products at higher flow rates.*

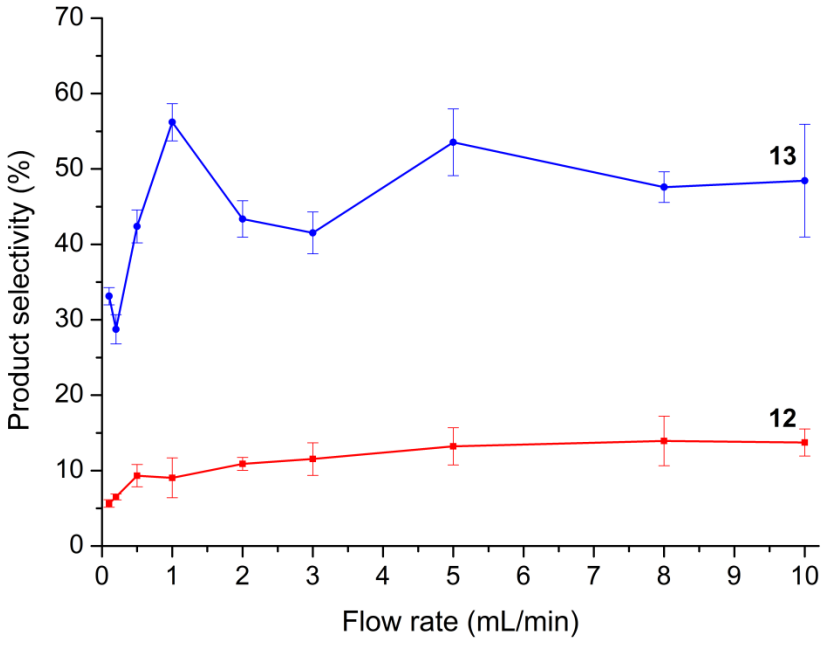
Results in Section 4.4 indicated that the selectivity for diketone **13** was higher at higher temperatures which would be the case at lower flow rates as the generated heat sports are removed less efficiently at lower flow rates. At lower flow rates where the formation of products is high, the formation of **15** will probably also be substantial. As a result, the formation of diol **14** will be more efficient according to Scheme 4-7. This could be a contributing factor to the higher selectivity for diol **14** at lower flow rates. The selectivity for products corresponding to GC signals at 8.91 and 9.11 min. increased by a factor 2.8 and 2.3 respectively between the lowest and highest flow rate. However, these products could not be identified.

In aqueous acetone solutions, as was in the case in the experiments carried out in neat acetone, a rise in productivity for product formation was observed when the reagent solution was flowed at higher flow rates (Figure 4-6a). A steep initial increase in this productivity at the lower flow rates might suggest that insufficient mixing indeed limited diffusion of the reactants. It is unclear whether the dip in productivity corresponding to a flow rate of 5 mL/min is an error in measurement or part of the trend. It might be possible that in this flow regime, the concentration of radicals I and II was lower due to a shorter irradiation time. This combined with a potentially little effect of improved mixing when comparing reactions performed at 2 and 3 mL/min could potentially account for lower product formation.

Pinacol (**14**) formation was supressed as already observed in previous experiments carried out with aqueous acetone. Under these conditions, the concentration of acetone in solution was 21 times lower compared to neat acetone. As a result, the concentration of acetone based radicals in solution at high flow rate was expected to be lower compared to irradiating neat acetone. Moreover, the higher viscosity of aqueous acetone could further hinder the diffusion of radicals. These parameters combined were thought to lead to a decrease in selectivity for diketone **13** at higher flow rates. However, no decrease in selectivity for diketone **13** was observed (Figure 4-6b) although the relatively large error in the GC analysis makes data evaluation more difficult. It is possible that the hydration of radicals I and II by water prevented recombination[19] and therefore extended their lifetimes. This would allow more time for radical I molecules to diffuse together, combine and form diketone **13**.



(a)



(b)

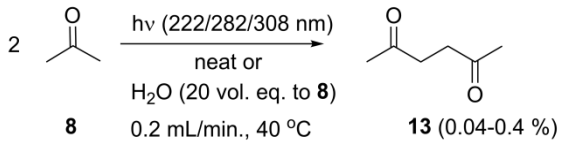
*Figure 4-6 a) Total yield of product formation in % (**black line**) and expressed in productivity (mmol/h) (**dashed black line**) in the irradiation of acetone (**8**) in water (20 vol. eq. to **8**) at different flow rates (0.1-10 mL/min), at 40 °C using the 282 nm excimer lamp, b) the selectivity towards products **12** (**red line**) and **13** (**blue line**). No pinacol (**14**) was formed during the reaction.*

The initial increase in selectivity for products **12** and **13** at lower flow rates might be explained by an initial rise in mixing efficiency when the flow rate is increased. The gradual increase in selectivity for **12** and diketone **13** at higher flow rates could possibly be attributed to the decrease in the formation of other products under these conditions.

However, a higher flow rate cannot provide the full solution to improving reaction performance as it lowers product yield due to shorter reaction times.

4.6 Formation of Acetonylacetone with Different Irradiation Wavelengths

To further investigate the reactivity of acetone, the dimerisation of acetone was performed using three different excimer lamps (Scheme 4-12). The same excimer lamps as described in Chapter 3 were employed, emitting light at either 222, 282 or 308 nm. Photons emitted from these light sources will have a different energy, which could potentially influence product yield and selectivity. As before, two sets of reaction conditions were tested; the irradiation of neat acetone and that of acetone in aqueous solution.



*Scheme 4-12 Investigation of the influence of irradiation wavelength on the dimerisation of acetone (**8**).*

In neat acetone, the product yield was low for the reactions carried out with the 282 and 222 nm excimer lamps (0.1 and 0.5 % respectively) (Figure 4-7). The product yield obtained with the 308 nm lamp was not determined. The highest product yield was obtained with the 282 nm lamp which could be attributed to a higher molar extinction coefficient of acetone at this wavelength and the higher

number of photons emitted by the light source compared to 222 nm light. Moreover, the quartz tube most likely absorbed more 222 nm photons than 282 nm photons as explained in Chapter 3 which would also result in a lower product yield when using 222 nm light.

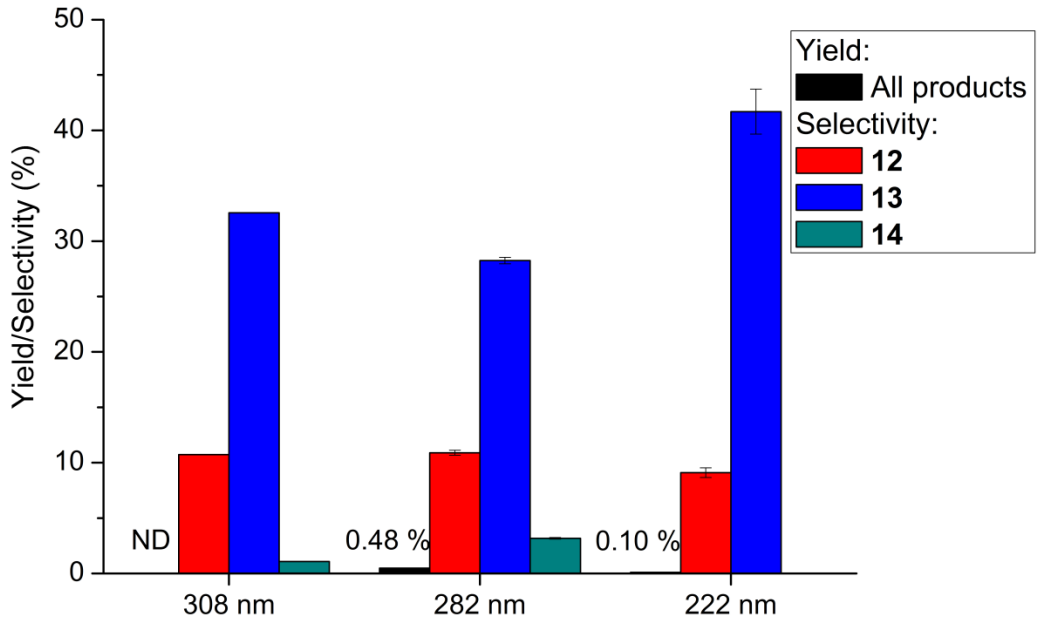


*Figure 4-7 Total yield of product formation (**black line**) and the selectivity towards products **12** (**red line**), **13** (**blue line**) and **14** (**dark cyan line**) in the irradiation of neat acetone (**8**) when irradiated at 40 °C by lamps with different emitting wavelengths (308, 282, 222 nm). The flow rate was set at 0.2 mL/min. The product yield when **8** was irradiated with the 308 nm lamp was not determined (ND). The highest selectivity for **13** was obtained using the 222 nm excimer lamp although the lowest total product yield was obtained under these conditions.*

The lowest selectivity for diketone **13** was obtained when the 282 nm excimer lamp was used. It is possible that more side reactions occurred because of the generation of the largest number of radicals compared to the other two wavelength excimer lamps. No pinacol (**14**) was observed as a reaction product with 222 nm light irradiation. The highest selectivity for diketone **13** was observed when acetone was irradiated with 222 nm light. Initially, it was hypothesised that this could be related to the number of photons emitted by the different excimer lamps and the difference in the molar extinction coefficient of acetone at these wavelengths. To compare the results more fairly, the productivity and reaction efficiency of both the total yield and the selectivity for diketone **13** were estimated (Table 4-1). The reaction efficiency of a process is

depicted relative to the number of photons absorbed theoretically by acetone, which takes into account both the number of photons emitted by the excimer lamp and the molar extinction coefficient of acetone at the different wavelengths. The reflection of photons of the stainless steel cooling stick back into the reaction solution was neglected. The highest reaction efficiency was found when acetone was irradiated with 222 nm light (Table 4-1, entry 3). This indicates that the molar extinction coefficient of acetone and the number of photons emitted by the excimer lamps alone cannot account for the differences in product selectivity as observed. A tentative explanation for the product selectivity at the different irradiation wavelengths could be the local temperature rise during the reaction with the 222 nm light. As 222 nm photons have more energy than both 282 and 308 nm photons, electrons in ground state acetone are excited into a higher vibrational state. As for now it is unclear how this influences reaction selectivity. Despite the low yield of reaction products, the productivity for product yield was as high as 0.78 mmol/h (Table 4-1, entry 2). The productivity for the formation of product **13** was highest when acetone was irradiated with 282 nm light (0.22 mmol/h).

*Table 4-1 Productivity and reaction efficiency (RE) of both the product yield and the formation of **13**, given per excimer lamp for the dimerisation of acetone in neat solution.*

Entry	Excimer lamp	Productivity Product yield (mmol/h)	Productivity Formation of 13 (mmol/h)	RE[a] Product yield	RE[a] Formation of 13
1	308 nm	ND	ND	ND	ND
2	282 nm	0.78	2.2×10^{-1}	3.6×10^{-1}	1.0×10^{-1}
3	222 nm	0.17	7.1×10^{-2}	4.2×10^{-1}	1.8×10^{-1}

*Reaction conditions: **8**, 0.2 mL/min, 40 ^{o}C; [a]Reaction efficiency (RE) was estimated as productivity in mmol/h per mmol of photons absorbed by acetone per h*

With the use of aqueous solutions of acetone, total product yield increased significantly compared to the experiments carried out in neat acetone (Figure 4-8). It could be possible that the hydration of the reactants by the hydrogen-bonding interaction with water reduced the recombination of radicals as explained previously. The highest selectivity for diketone **13** was obtained with 222 nm light as it was in neat acetone. The formation of diol **14** was suppressed

at each irradiation wavelength. This could be assigned to the hydration of radical II by water as explained previously. Interestingly, the product corresponding to the GC signal at 5.76 min. was formed 71 % selective when acetone was irradiated with 308 nm light in aqueous solution while the selectivity was only 5.8 and 14 % for irradiation with the 222 and 282 nm lamps respectively. However, this product could not be identified. A tentative explanation might be that one of the photochemical products was able to absorb 308 nm light and was involved in another photochemical transformation. However, no further proof was obtained for this hypothesis.

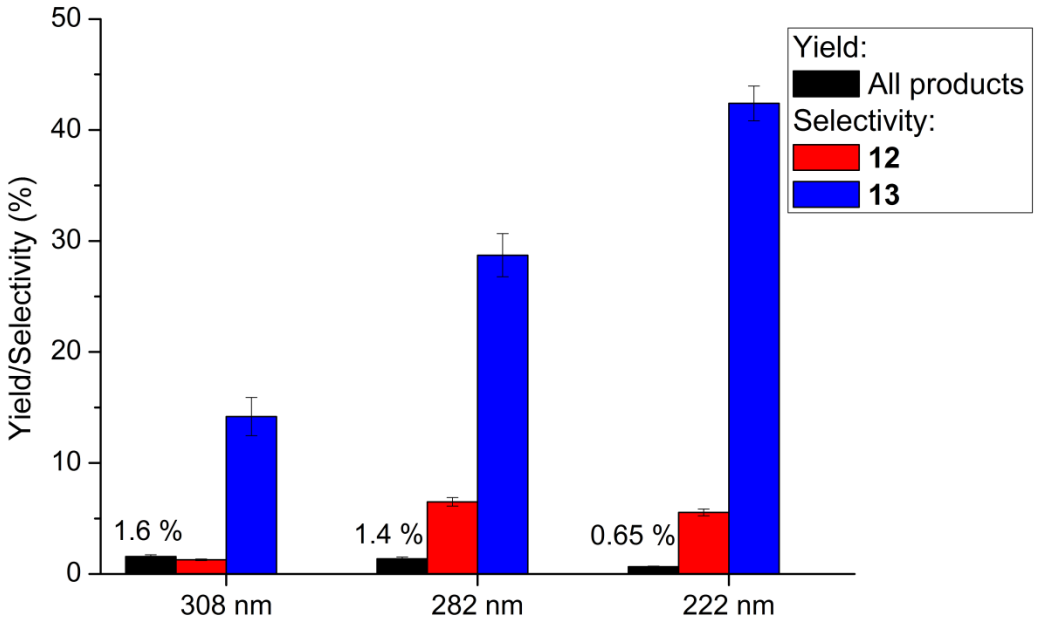


*Figure 4-8 Total yield of product formation (**black line**) and the selectivity towards products **12** (**red line**) and **13** (**blue line**) in the irradiation of acetone (**8**) in water (20 vol. eq. to **8**) when irradiated at 40 °C by lamps with different emitting wavelengths (308, 282, 222 nm). The flow rate was set at 0.2 mL/min. No pinacol (**14**) was formed during the reaction and again the highest selectivity for **13** was obtained using the 222 nm excimer lamp.*

The highest yield was obtained using the 308 nm excimer lamp (1.6 %) whereas the lowest yield was obtained when aqueous acetone was irradiated with the 222 nm excimer lamp (0.65 %). Compared to the experiments carried out in neat acetone, the total product yield was higher in aqueous acetone. However, the productivity for product formation was lower in aqueous acetone solutions, most likely due to the lower concentration of acetone in these experiments. The

reaction efficiency (RE) of the product yield for both the 282 and 222 nm lamps was found higher in aqueous acetone compared to neat acetone (Tables 4-1,4-2, entries 2,3). The highest RE for the formation of diketone **13** was with irradiation at 282 nm (Table 4-2, entry 3) despite the lowest RE for product yield at this wavelength.

*Table 4-2 Productivity and reaction efficiency (RE) of both the product yield and the formation of **13**, given per excimer lamp for the dimerisation of acetone in aqueous solution.*

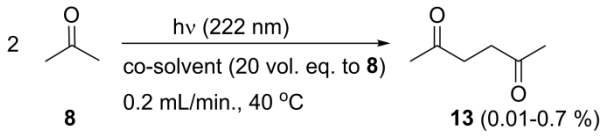
Entry	Excimer lamp	Productivity Product yield (mmol/h)	Productivity Formation of 13 (mmol/h)	RE[a] Product yield	RE[a] Formation of 13
1	308 nm	0.12	$1.7x10^{-2}$	$5.0x10^{-1}$	$7.1x10^{-2}$
2	282 nm	0.11	$3.0x10^{-2}$	$4.9x10^{-2}$	$1.4x10^{-2}$
3	222 nm	0.05	$2.2x10^{-2}$	$1.3x10^{-1}$	$5.4x10^{-2}$

*Reaction conditions: **8**, deionised water (20 vol. eq. to **8**), 0.2 mL/min, 40 °C; [a]Reaction Efficiency (RE) was estimated as productivity in mmol/h per mmol of photons absorbed by acetone per h*

When performing the dimerisation of **8** to form diketone **13**, the highest productivity was obtained in neat acetone using 282 nm light (Table 4-1, entry 2). However, product yields were exceptionally low (0.10-1.6 %) and need to improve in order to limit the waste of reactants. The highest selectivity for product **13** (42 %) was obtained using the 222 nm excimer lamp in both neat acetone and acetone in aqueous solution.

4.7 Formation of Acetonylacetone in Different Co-solvents

The effect of water as a co-solvent in the formation of diketone **13** from **8** has been discussed in previous Sections. Therefore, other co-solvents were tested to investigate the hydrogen donor ability of these solvents and the influence they have on the product yield and selectivity in the photo-induced dimerisation of acetone (Scheme 4-13). 2-Propanol (IPA), methanol (MeOH) and ethanol (EtOH) were tested as potential hydrogen donors. Acetonitrile (MeCN) was tested as a non-hydrogen-bonding co-solvent.



*Scheme 4-13 Irradiation of acetone (**8**) to form acetonylacetone (**13**) in a range of co-solvents (H_2O, MeOH, EtOH, MeCN or IPA).*

When IPA was used as a co-solvent, pinacol (**14**) was formed with 93 % selectivity (Figure 4-9). With 2-propanol being a good hydrogen donor, it can donate a hydrogen atom to excited state acetone forming two radical II molecules.[29] Those two radicals can combine to produce **14**. However, the total yield of product formation was only 0.56 %. The total yield was 0.65 % when the reaction was carried out in water. The addition of water to IPA as the co-solvent increased the yield 4-fold compared to neat IPA. A reasonable explanation is that hydration of radicals I and II prevented undesired radical recombination which resulted in a higher product yield.[19] The stabilisation of ketyl radical II when water was added as the co-solvent decreased the selectivity for diol **14** while increasing the selectivity for products **12** and **13**. Although hydrogen-bonding between IPA and H_2O is possible, it is likely that hydrogen-bonding existed predominantly between identical species.[30] Irradiation of **8** in neat MeOH afforded several MeOH-acetone adducts and low selectivity for diketone **13** (1 %). The addition of water as the co-solvent did not increase the total yield of the reaction, despite the increase in hydrogen-bonding in MeOH/H_2O mixtures compared to

neat MeOH.[31] Formation of diol **14** was suppressed and diketone **13** was formed with 39 % selectivity. The results obtained in pure EtOH were almost identical to those obtained in pure MeOH. However, reactions carried out in a EtOH/H_2O mixture (1:1 v/v) provided interesting results. A total yield of 43 % for product formation was observed when acetone was reacted in a mixture of ethanol and water. This reasonably high yield was due to by-product formation corresponding to GC signals with retention times of 8.63 and 9.26 min. which were formed with 32 and 18 % selectivity respectively. These signals were not observed in previous experiments which makes it a reasonable assumption that these are ethanol-acetone adducts. These adducts were formed in only small quantities in pure EtOH. It might be possible that the presence of H_2O as a better hydrogen-donor than EtOH facilitated these adduct formations. Another contributing factor to the increased formation of adducts in ethanol/water mixtures could be the increase in solvent polarity compared to neat ethanol.[32] This could potentially stabilise excited state acetone and allow for more efficient coupling reactions with ethanol.

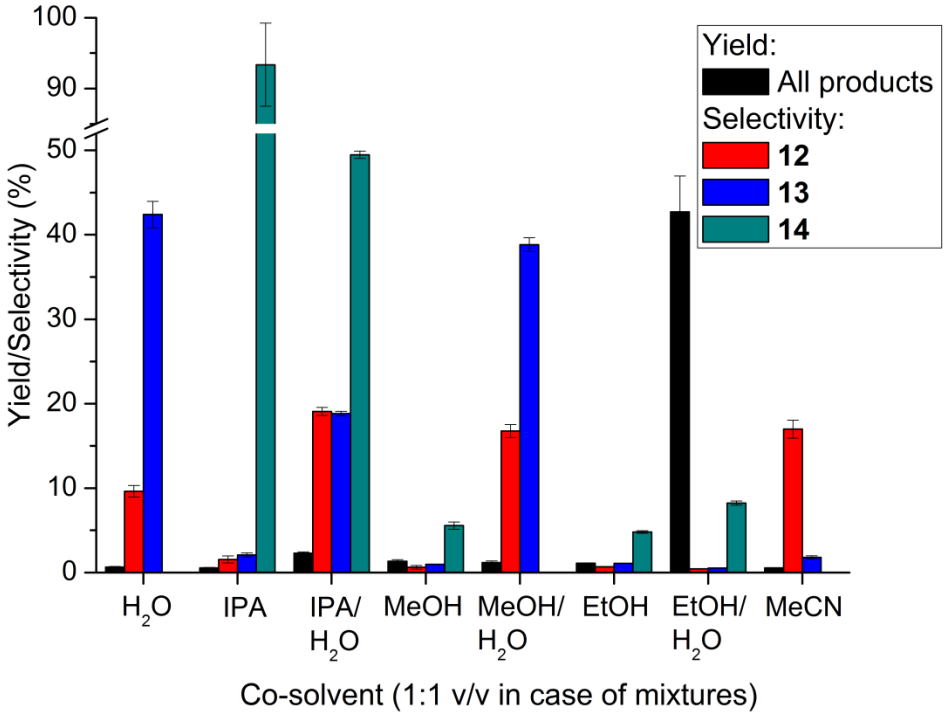


*Figure 4-9 Total yield of product formation (**black line**) and the selectivity towards products **12** (**red line**), **13** (**blue line**) and **14** (**dark cyan line**) in the irradiation of acetone (**8**) in different co-solvents (20 vol. eq. to **8**, co-solvent mixtures were 1:1 v/v) when irradiated at 40 °C by 222 nm light. The flow rate was set at 0.2 mL/min.*

The total product yield obtained using MeCN as the co-solvent was identical to using IPA. Interestingly, **12** was formed most selective out of products **12**-**14** under these conditions. It appeared that the coupling of either two radical I or radical II species was not favourable in MeCN. Instead, the coupling of radical I and II took place leading to the formation of **12** as the major reaction product.

Different ratios of ethanol and water were tested next as the co-solvent mixture in the irradiation of acetone. It was envisioned that it might be possible to increase the total product yield of the reaction while maintaining a high selectivity for diketone **13** if the co-solvent of the reaction would be mostly water with a small quantity of ethanol. It appeared that EtOH disrupted the strong hydrogen-bonding of radicals I and II by water as the selectivity for diol **14** only started to decrease at a 100:1 volume ratio of H_2O to EtOH (Figure 4-10). The total product yield decreased with an increasing ratio of water to ethanol, due to the lower production of ethanol-acetone adducts. This reduction of ethanol in the solvent mixture resulted in the steep increase selectivity for diketone **13**. However, the selectivity was found only to be 24 % at a 1000:1 volume ratio of H_2O to EtOH. Moreover, less differentiation between the selectivity for **12** and **13** was observed compared to when the reaction was carried out in H_2O.

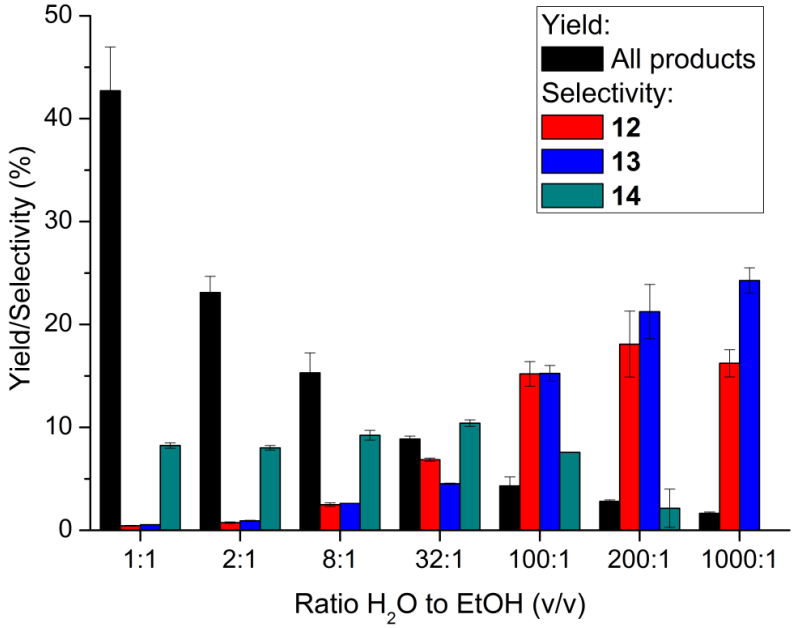


*Figure 4-10 Total yield of product formation (**black line**) and the selectivity towards products **12** (**red line**), **13** (**blue line**) and **14** (**dark cyan line**) in the irradiation of acetone (**8**) in different H_2O/EtOH co-solvents mixtures (v/v, maintaining 20 vol. eq. to **8**) when irradiated at 40 °C by 222 nm light. The flow rate was set at 0.2 mL/min.*

The variation of co-solvent showed that diol **14** can be formed highly selectively when IPA is employed as the solvent. Other hydrogen donors such as MeOH and EtOH showed to generate solvent-acetone adducts which reduced the selectivity for the desired diketone **13** even further. Hydration of radicals I and II was found to be most efficient with water as the reaction solvent as the highest selectivity for diketone **13** was obtained under these conditions. The addition of ethanol as the co-solvent for the reaction decreases the selectivity for **13**, even at small quantities.

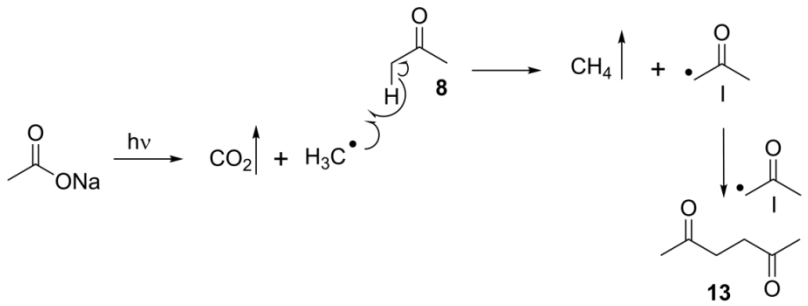
4.8 Improving the Yield of Acetonylacetone Formation

The total yield of the photo-induced dimerisation of acetone to form acetonylacetone is low and needs to improve in order to make this reaction industrially relevant. Three different strategies were explored in this work to potentially increase the total yield of the reaction.

4.8.1 Variation of Photo Absorbers

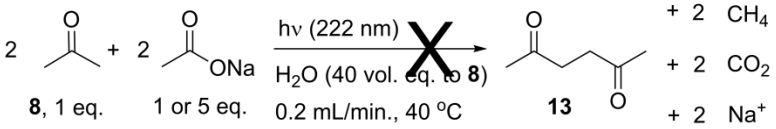
The formation of diketone **13** is based on the formation and coupling of two radical I molecules (Scheme 4-4). A way to increase the selectivity for diketone **13** from acetone (**8**) would be to generate radical I without radical II. This would also increase the theoretical maximum yield for diketone **13** of 25 % to 50 % when all acetone is converted. If a hydrogen acceptor other than excited state acetone participates in the reaction, radical II would not be formed. As an initial test, sodium acetate was utilised as the potential hydrogen acceptor. It was envisioned that sodium acetate would be able to absorb 222 nm light, leading to a decarboxylation reaction to generate CO_2 and a methyl radical (Scheme 4-14). This unstable methyl radical could abstract a hydrogen atom from ground state acetone which would form methane and radical I. Another radical I molecule can be produced by repeating this process after which the combination of these two

radical species leads to acetonylacetone (**13**). The theoretical maximum yield for **13** would be 50 % and only gaseous by-products would be generated.



*Scheme 4-14 Envisioned irradiation of sodium acetate generating a methyl radical which can abstract a hydrogen atom from ground state acetone (**8**) leading to the clean production of acetonylacetone (**13**).*

Initially, a 1:1 molar ratio of **8** to sodium acetate in water (40 vol. eq. to **8**) was irradiated with 222 nm light. Additionally, a reaction containing a 1:5 molar ratio of **8** to sodium acetate was carried out (Scheme 4-15). The system pressure was closely monitored as both methane and carbon dioxide could be formed as gaseous reaction products. No increase in pressure or generation of bubbles in the collection flask were observed.



*Scheme 4-15 Reaction scheme for the photochemical generation of acetonylacetone (**13**) from acetone (**8**) and sodium acetate (NaOAc).*

Unfortunately, the total product yield decreased considerably upon the addition of sodium acetate to the reaction mixture (Figure 4-11). It has been reported previously that acetate ions can quench excited state species[33] which could potentially lead to the observed decrease in product yield. As seen previously when using aqueous mixtures of acetone, no pinacol (**14**) was formed. Interestingly, the selectivity for **12** and diketone **13** increased when NaOAc was added to the reaction mixture. The addition of 5 mol eq. of NaOAc even provided

a product mixture of solely products **12** and **13** as visible in the gas chromatogram. It is probable that product **15** was formed but this could not be confirmed with GC analysis. The presence of sodium acetate in water could have generated hydroxyl anions, which could form hydrogen-bonds with the compounds in the reaction mixture. As for now, it is unclear how this different type of hydrogen-bonding influenced product distribution. Another explanation might be that sodium acetate acted as a basic scavenger to prevent the formation of by-products.[34] Again, details on the mechanism of this are unclear. The excitation of acetone was not prevented by the addition of NaOAc to the reaction mixture as radical II must have been present to participate in the formation of product **12**.

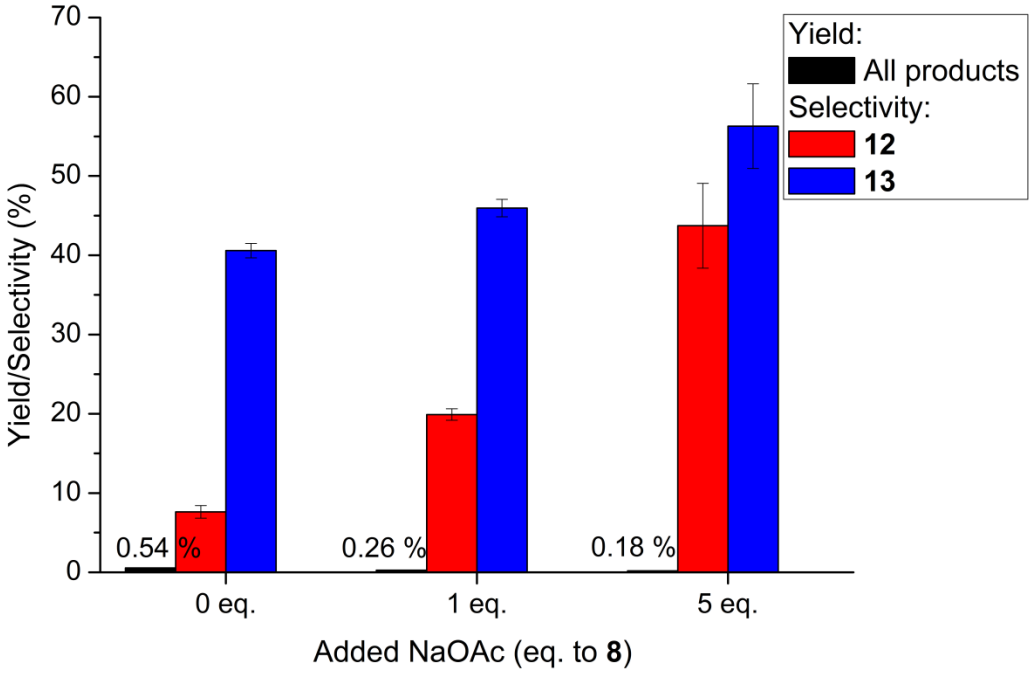
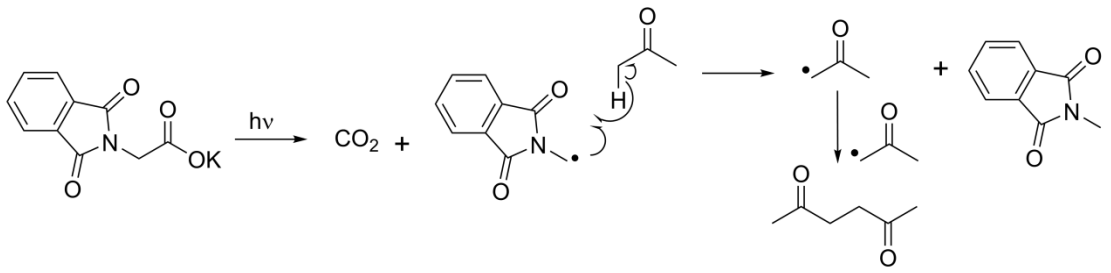


*Figure 4-11 Total yield of product formation (**black line**) and the selectivity towards products **12** (**red line**) and **13** (**blue line**) in the irradiation of acetone (**8**) in the presence of sodium acetate (0-5 mol eq. to **8**) in water (40 vol. eq. to **8**) when irradiated at 40 °C by 222 nm light. The flow rate was set at 0.2 mL/min. Note that no pinacol (**14**) was formed during the reaction and that the addition of 5 eq. of NaOAc resulted in low product yield but little formation of products other than **12** and **13**.*

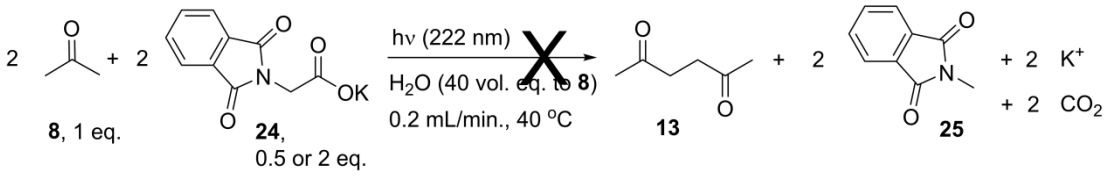
As sodium acetate did not absorb strongly at 222 nm, phthalimido acetate (**24**) was used as another photo absorber in the reaction of **8** to form **13** (Scheme 4-16). With a molar extinction coefficient of 40×10^3 L/mol·cm, **24**

exhibits an absorption maximum at 222 nm. This extinction coefficient is $8x10^3$-fold higher than that of acetone at 222 nm which would theoretically ensure the excitation of **24** over that of **8**.



*Scheme 4-16 Irradiation of phthalimido acetate (**24**) leading to decarboxylation, generating a radical which can abstract a hydrogen atom from ground state acetone (**8**) leading to the production of acetonylacetone (**13**).*

It was hypothesised that the irradiation of **24** with 222 nm light would lead to efficient generation of diketone **13** while avoiding the formation of **12** and diol **14**. Two different ratios of **8** to **24** were tested, 2:1 and 1:2 (mol eq.) (Scheme 4-17). Even if diketone **13** can be generated selectively under the proposed reaction conditions, this method is not atom economic as two molecules of **25** are formed during each reaction.



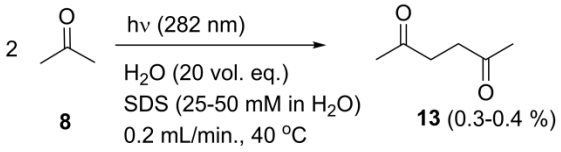
*Scheme 4-17 Reaction scheme for the photochemical generation of acetonylacetone (**13**) from acetone (**8**) and phthalimido acetate (**24**).*

GC analysis of the reaction product mixture revealed no formation of acetone dimers under any of the tested reaction conditions. This result indicates that the excitation of **8** was inhibited by the addition of **24**. Additional signals in the gas chromatogram of the product mixture were observed compared to that of the starting mixture but the products corresponding to these GC signals were not identified. The presence of new GC signals could indicate that the excitation of **24**

was successful but did not lead to the desired reaction with ground state acetone. As no progress was made in the use of photosensitisers other than acetone for the formation of diketone **13**, this project was discontinued.

4.8.2 The Use of Micellar Media

The use of confined micro-environments introduced by the use of for example micellar media, zeolites and dendrimers has shown to effect product distribution in photochemical reactions.[35] Already shown in Chapter 3 of this Thesis, the selectivity for diketone **13** in the coupling of 1-octene and acetone increased in micellar media compared to aqueous reaction solutions. Therefore, the irradiation of acetone in micellar media was investigated further to increase selectivity for product **13**. Additionally, it was envisioned that the introduction of confined reaction space would increase the local concentration of radicals which would hopefully result in a higher product yield compared to the irradiation of acetone in solely deionised water. Sodium dodecyl sulfate (SDS) was chosen as the surfactant to generate micelles for reasons explained in the previous Chapter. To investigate the influence of the micellar media on the reaction yield and selectivity of photoproducts from the irradiation of acetone, two different concentrations of surfactant in water were used, namely 25 and 50 times the critical micelle concentration of SDS in water (Scheme 4-18).



*Scheme 4-18 Irradiation of acetone (**8**) in micellar media to form acetonylacetone (**13**).*

The product yield was not greatly influenced by the addition of SDS to the reaction mixture (Figure 4-12), although the formation of **15** was not monitored. This is an encouraging result as it has been reported that the lifetime of excited state acetone decreases in apolar environments, such as the core of a micelle.[35h]

A shorter excited state lifetime of acetone was thought to result in lower product yield as the excited state species will have less time to perform the desired photochemical reaction before it reaches the unreactive ground state.

In contrast, the product selectivity decreased significantly in the presence of surfactant. The dominant formation of diketone **13** in aqueous solution with surfactant was diminished and products **12**-**14** were formed in almost equal amounts when 50 mM of SDS was used. The increased formation of diol **14** under these conditions might be attributed to the process of hydrogen atom abstraction from SDS by triplet excited state acetone.[36] This would lead to the formation of radical II without the formation of α-keto radical I. Therefore, it is more likely that two radical II molecules combine to generate diol **14** than that radical I is involved in a chemical transformation.

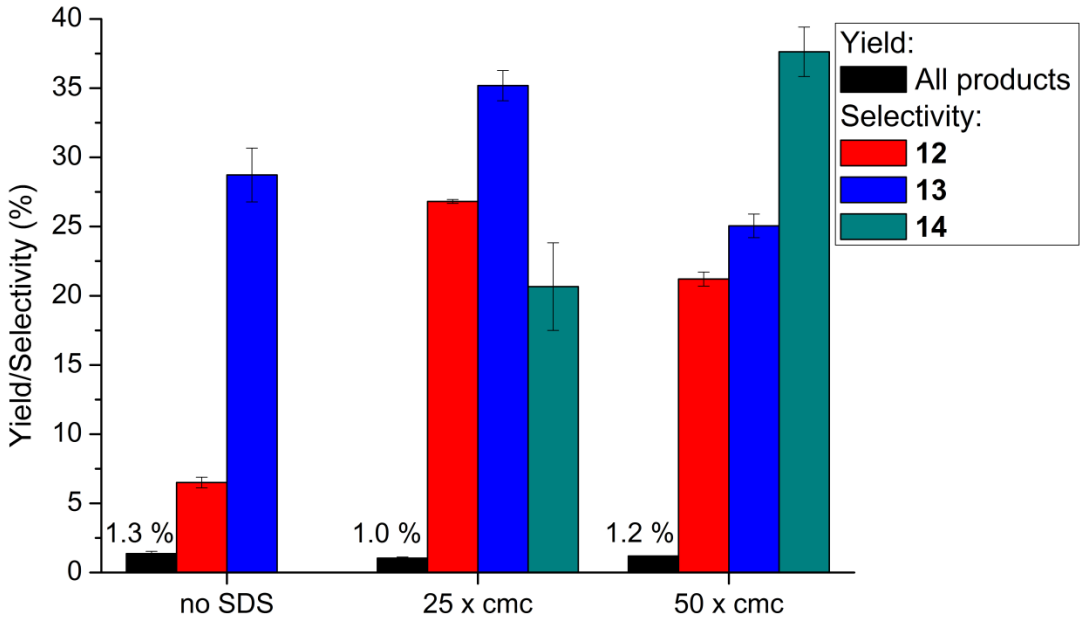


*Figure 4-12 Total yield of product formation (**black line**) and the selectivity towards products **12** (**red line**), **13** (**blue line**) and **14** (**dark cyan line**) in the irradiation of acetone (**8**) in water (20 vol. eq. to **8**) by 282 nm light in the presence of ionic surfactant SDS (0.1 M in water). The flow rate was set at 0.2 mL/min and the reaction temperature was 40 °C. The addition of SDS resulted in lower product selectivity while the total product yield did not change significantly.*

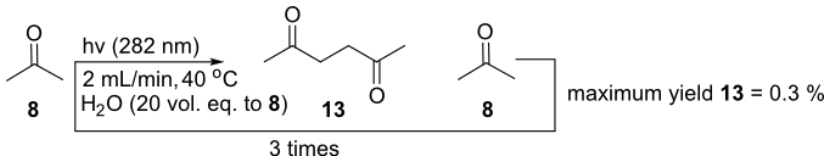
The isolation of SDS from the reaction mixture was accomplished by extraction from EtOAc. Reaction products dissolved in the EtOAc layer while SDS remained

in the water phase. This could provide a method to recycle and reuse the SDS in several experiments, reducing the waste produced in the chemical reaction.

With no improved product yield observed after the addition of ionic surfactant SDS to the aqueous reaction medium, other strategies were investigated to facilitate the increased formation of products in the irradiation of acetone.

4.8.3 Recirculation of the Reaction Mixture

A different approach to increasing the total yield of a reaction is to recycle the reaction mixture.[37] Therefore, recirculation of the reaction mixture after irradiation of ketone **8** in water with 282 nm light while flowing at 2 mL/min through the continuous flow UV photoreactor was performed to increase the yield of the reaction. The reaction mixture after the irradiation of **8** contains predominantly **8**, a combination of acetone derived products including diketone **13** and most likely **15**. This mixture was recycled three times, increasing the irradiation time by 41 seconds each pass (Scheme 4-19).



*Scheme 4-19 Three time recirculation of the reaction mixture containing acetone (**8**) and acetone irradiation products to increase product yield.*

One of the concerns with recycling this reaction mixture was the build-up of **15** over time. As **15** is a better hydrogen donor than **8**,[17] this higher concentration can result in increased hydrogen atom abstraction of excited state acetone from **15** instead of **8**. This in turn would increase the formation of diol **14** in later runs of the same reaction and decrease the selectivity for diketone **13** (Scheme 4-7). However, under the tested conditions, no **14** was formed and product selectivity remained unchanged at any of the runs (Figure 4-13). It is possible that the presence of water as the co-solvent prevented the efficient reaction of radical II.

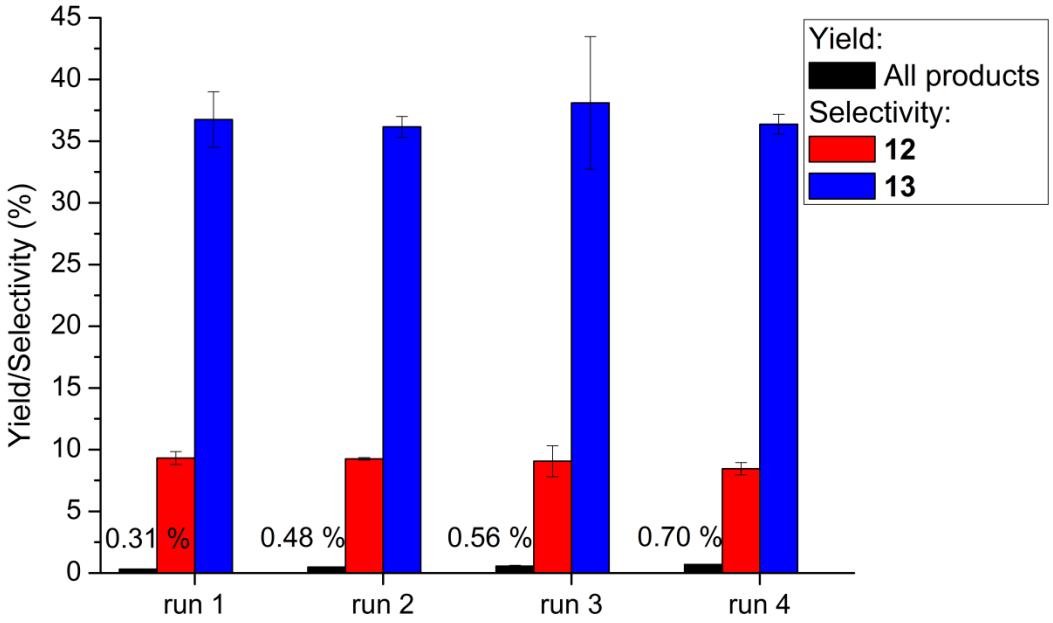


*Figure 4-13 Total yield of product formation (**black line**) and the selectivity towards products **12** (**red line**) and **13** (**blue line**) in the irradiation of acetone (**8**) in water (20 vol. eq. to **8**) at 2 mL/min and 40 °C. The reaction mixture was recirculated three times while being irradiated with 282 nm light. No pinacol (**14**) was formed during the reaction and the selectivity for **13** remained stable over 4 runs while the total product yield increased.*

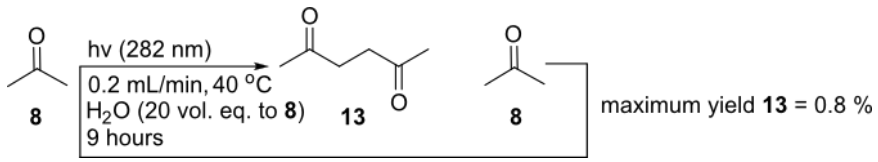
This is an encouraging result as it indicates that recycling the reaction mixture can increase the total yield of the reaction without compromising on the selectivity for product **13**. The increase in total yield after each pass was 1.5-fold between runs 1 and 2 and 1.2-fold between runs 2,3 and 4. The productivity for total product formation was as high as 0.54 mmol/h after 4 runs which is a 2.3-fold increase compared to run 1 (Table 4-3, entries 1,4). With the selectivity for diketone **13** constant over the 4 runs, the productivity for the formation of this product increased at the same rate as total product formation and was 0.20 mmol/h after 4 runs (Table 4-3, entry 4).

*Table 4-3 Productivity and reaction efficiency (RE) of both the product yield and the formation of **13**, given per pass through the UV photoreactor for the dimerisation of acetone in aqueous solution.*

Entry	Pass through reactor	Productivity Product yield (mmol/h)	Productivity Formation of 13 (mmol/h)	RE[a] Product yield	RE[a] Formation of 13
1	Pass 1	0.24	$8.9x10^{-2}$	$1.1x10^{-1}$	$4.1x10^{-2}$
2	Pass 2	0.37	$1.4x10^{-1}$	$1.7x10^{-1}$	$6.3x10^{-2}$
3	Pass 3	0.44	$1.7x10^{-1}$	$2.0x10^{-1}$	$7.7x10^{-2}$
4	Pass 4	0.54	$2.0x10^{-1}$	$2.5x10^{-1}$	$9.0x10^{-2}$

*Reaction conditions: **8**, deionised water (20 vol. eq. to **8**), 2 mL/min, 40 °C, 282 nm excimer lamp; [a]Reaction Efficiency (RE) was estimated as productivity in mmol/h per mmol of photons absorbed by acetone per h*

After this proof of concept, the reaction mixture was circulated continuously for 9 hours at 0.2 mL/min and aliquots were taken every hour to monitor the total product yield and selectivity (Scheme 4-20). The total irradiation volume of the continuous flow UV reactor is 1.37 mL whereas the total reactor volume is 10 mL. At 0.2 mL/min, a single pass of reagents through the reactor represents 6.9 min. irradiation time and a total of 50 minutes in the reactor.



*Scheme 4-20 Continuous recirculation of the reaction mixture containing acetone (**8**) and acetone irradiation products for 9 hours to increase product yield.*

In contrast to the results shown in Figure 4-13, the continuous recirculation of reagents at 0.2 mL/min did decrease the selectivity for diketone **13** significantly over time (Figure 4-14). The selectivity for product **12** remained constant within analytical error and again no pinacol (**14**) was formed. It is possible that product **13** was more sensitive to over-irradiation and degraded or reacted further more rapidly than product **12**. The total product yield was found at a maximum after 5

hours of recirculation (2.6 %) which is a 2.2-fold increase in total yield compared to one hour of reaction time. A reaction time of 5 hours represents an average of 6 passes through the reactor and a reaction time of 41.4 minutes. This 2.2-fold increase in yield is significantly less than the theoretical 6-fold increase which was expected when reaction times were 6 times longer. This optimum of a total yield of 2.6 % relates to a productivity of 0.20 mmol/h of total product formation and 0.059 mmol/h of product **13** formation (Figure 4-15).

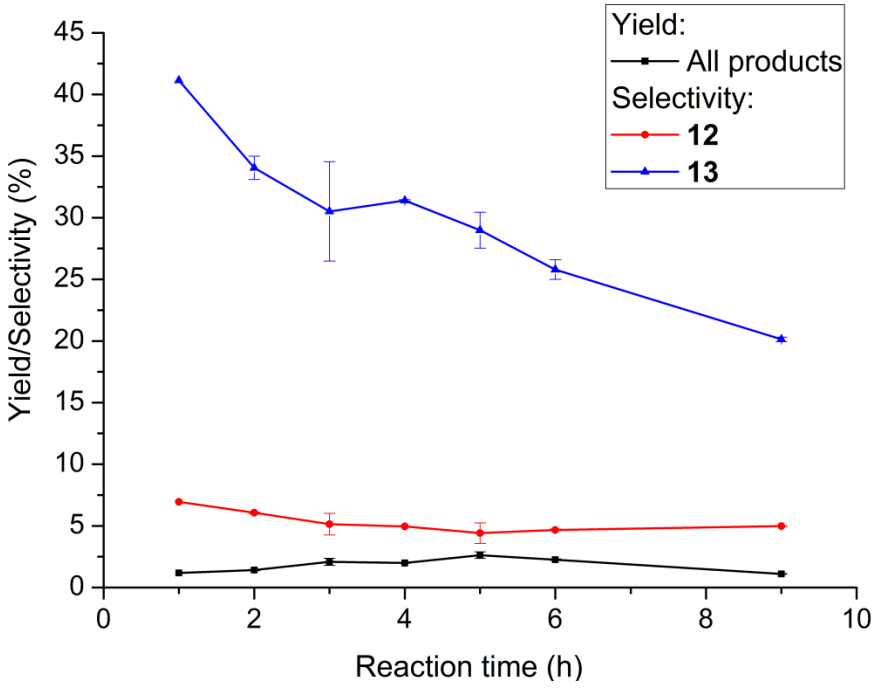


*Figure 4-14 Total yield of product formation (**black line**) and the selectivity towards products **12** (**red line**) and **13** (**blue line**) in the irradiation of acetone (**8**) in water (20 vol. eq. to **8**) when the reaction mixture is recirculated continuously for 9 hours at 0.2 mL/min and 40 °C while being irradiated with 282 nm light. The experiment demonstrated that no pinacol (**14**) was formed during the reaction and that product degradation occurred after 5 hours of irradiation time resulting in a lower total product yield after 5 hours.*

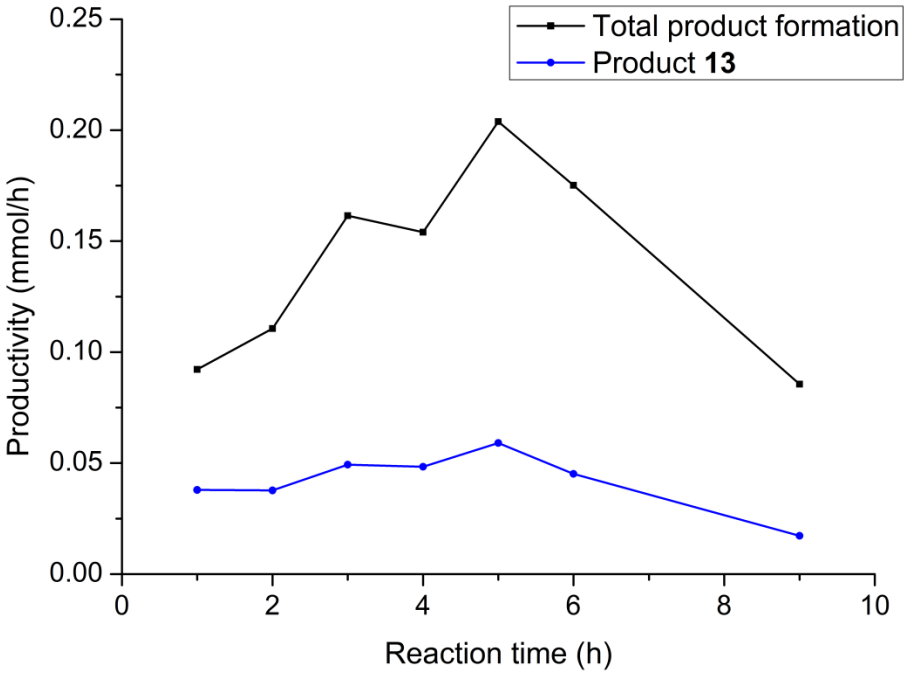
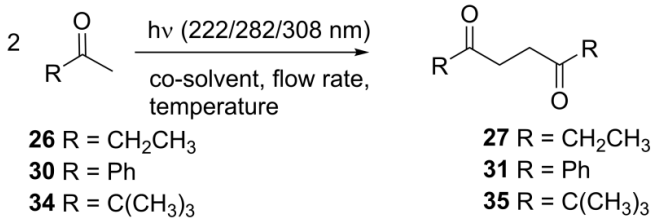


*Figure 4-15 Productivity of total product formation (**black line**) and the formation of **13** (**blue line**) expressed in mmol/h in the reaction of acetone (**8**) in water (20 vol. eq. to **8**) at 0.2 mL/min and 40 °C when the reaction mixture is recirculated continuously for 9 hours while being irradiated with 282 nm light, showing product degradation after 5 hours.*

The recirculation of reaction mixture was proven to increase the total product yield. It was observed that not every extra pass through the reactor increased the yield by a 2-fold. It could be possible that the reaction products were able to absorb photons which would lead to less efficient irradiation of acetone. The highest total product yield (2.6 %) was obtained when the reaction mixture was recirculated continuously for 5 hours at 0.2 mL/min. However, during these 5 hours, the selectivity for product **13** decreased significantly. Operating at a faster flow rate (2 mL/min) prevented this decrease in selectivity for product **13** and the so far highest total product productivity was obtained in this reaction set-up (0.54 mmol/h).

4.9 Scope of Ketone Dimerisation

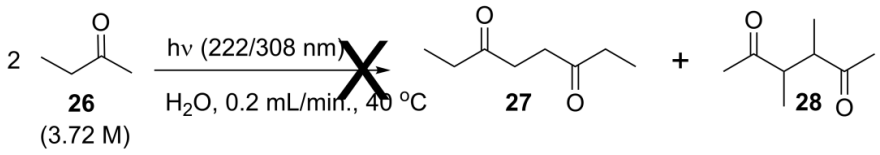
Preliminary studies were undertaken to examine if the scope of ketone dimerisation can be extended beyond the use of acetone. The other substrates tested were 2-butanone (**26**), acetophenone (**30**) and pinacolone (**34**) (Scheme 4-21). The aim was to synthesise substituted and relatively bulky 1,4-diketones which can be valuable substrates for the formation of substituted furans and pyrroles as will be discussed in Section 4.10. The Sections below will discuss the experiments that were carried out for this Thesis.



*Scheme 4-21 Photochemical dimerisation of 2-butanone (**26**), acetophenone (**30**) and pinacolone (**34**) under various conditions.*

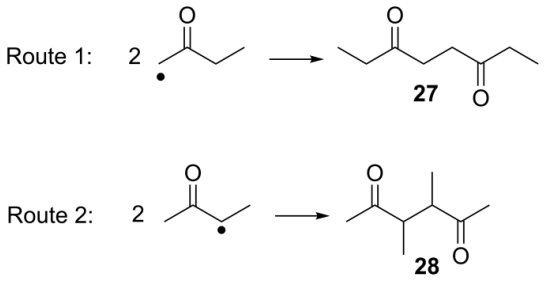
4.9.1 Dimerisation of 2-Butanone

The dimerisation of 2-butanone (**26**) in water was investigated employing either the 222 or 308 nm excimer lamp (Scheme 4-22). Crude reaction mixtures were analysed by GC followed by purification with column chromatography and characterisation with NMR and MS analysis.



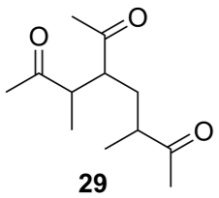
*Scheme 4-22 Photochemical dimerisation of 2-butanone (**26**) to form octane-3,6-dione (**27**) and 3,4-dimethylhexane-2,5-dione (**28**).*

2-Butanone (**26**) has two positions to form an α-keto radical. Product **27** is the result of the formation of a primary α-keto radical (Scheme 4-23, Route 1) whereas 3,4-dimethylhexane-2,5-dione (**28**) can be formed when a secondary α-keto radical is formed (Scheme 4-23, Route 2). Alternatively, a methyl and a methylene radical could cross-couple to give another 1,4-diketone product.



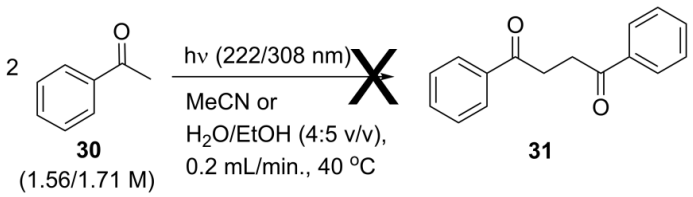
*Scheme 4-23 Formation of **27** via the coupling of two primary α-keto radicals (Route 1) and the formation of **28** via the coupling of two secondary α-keto radicals (Route 2).*

NMR analysis showed that under all the tested conditions, low conversion of **26** was achieved. The product distribution obtained when the reaction was carried out with 222 nm light was identical to when the reaction was carried out with the 308 nm lamp. Purification and characterisation of products in the reaction mixture revealed the formation of **29**, a trimer of **26**. No conclusive evidence was obtained for the formation of either **27** or **28**. Mass spectroscopy (MS) showed the presence of dimer but dimer formation during MS is a known phenomenon. Screening reaction conditions followed by a large scale reaction could possibly provide enough material to determine after purification whether dimer **26** can be formed in this photochemical transformation.



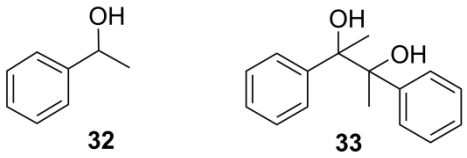
4.9.2 Dimerisation of Acetophenone

The dimerisation of acetophenone (**30**) to form **31** was tested next. Solubility issues can arise when ketones other than acetone are employed as substrates in aqueous solvent mixtures. As **30** is not water soluble to a large extent, other solvents than water were tested to ensure a homogeneous reaction solution (Scheme 4-24). The absorbance maximum of **30** is at 241 nm but a second absorbance band is present with a maximum at 279 nm. Therefore, the dimerisation of **30** was studied with both the 222 and 308 nm excimer lamps.



*Scheme 4-24 Photochemical dimerisation of acetophenone (**30**) to form 1,4-diphenyl-butane-1,4-dione (**31**).*

While no conversion of **30** was observed when the reaction was carried out in acetonitrile, two products (**32** and **33**) could be identified when the reaction was performed in aqueous ethanol mixtures (Scheme 4-25).



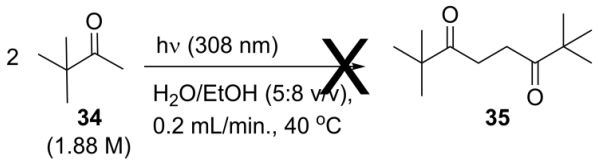
*Scheme 4-25 Products 1-phenylethan-1-ol (**32**) and 2,3-diphenylbutane-2,3-diol (**33**) in the irradiation of acetophenone (**30**) in aqueous ethanol.*

The different irradiation wavelengths did not influence product formation. The formation of **32** and **33** indicates that the excitation of **30** was successful and that the ketyl radical was reactive. The coupling of two ketyl radicals led to the

formation of **33** whereas **32** is the photoreduction product of **30**. However, no **31** was formed.

4.9.3 Dimerisation of Pinacolone

The dimerisation of pinacolone (**34**) was tested using the 308 nm excimer lamp (Scheme 4-26). As **34** does not dissolve in water, a mixture of water/ethanol (5:8 v/v) was employed as the co-solvent in the reaction.



*Scheme 4-26 Photochemical dimerisation of pinacolone (**34**) to form 2,2,7,7-tetramethyl-octane-3,6-dione (**35**) in water/ethanol (5:8 v/v).*

Under the tested conditions, approximately 27 product peaks were visible in the gas chromatogram of the crude reaction mixture (Figure 4-16). It is encouraging that **34** was found to be reactive, but no clear product selectivity was achieved. The concentration of the various products was very low and identification of these products was not successful.

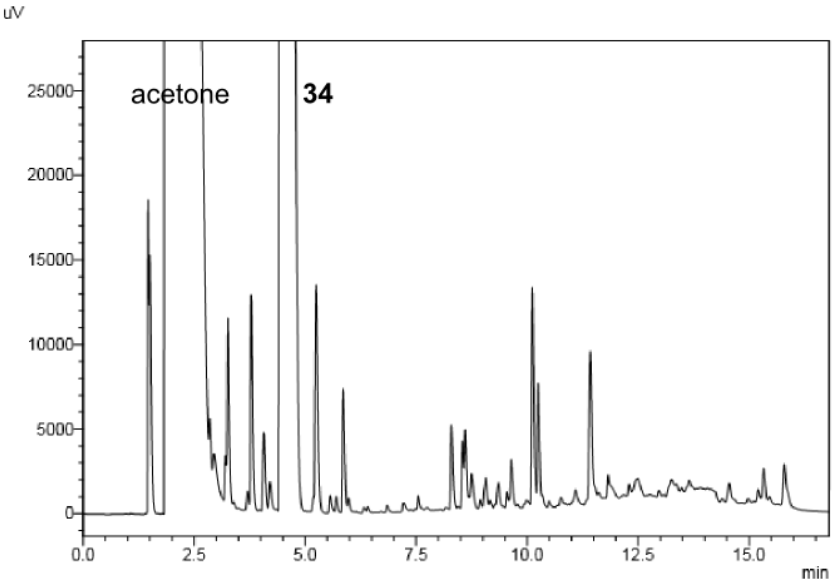
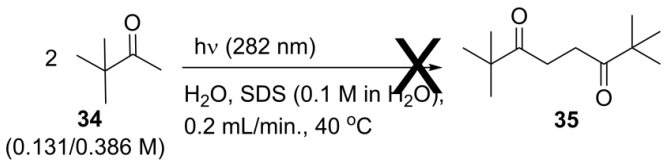


*Figure 4-16 Gas chromatogram of the reaction output in the photochemical dimerisation of **34** in H_2O/EtOH (5:8 v/v) at 0.2 mL/min and 40 °C employing the 308 nm excimer lamp. The syringe for injections into the GC was rinsed with acetone which is why there is a GC signal of acetone.*

It was thought that the use of water as the only co-solvent could potentially increase the yield of the reaction and aid product selectivity as it did in the dimerisation of acetone. Micellar media were employed to overcome the issue of substrate solubility in water. Sodium dodecyl sulfate (SDS) was chosen as the surfactant for reasons explained in Chapter 3. Acetone exhibits high exit rates from the micellar core as discussed previously, leading to most reactions being carried out outside the micelle. It was envisioned that the influence of micellar media is potentially greater when ketones other than acetone are utilised since these other ketones will hopefully exhibit lower exit rates from the micelles. The 282 nm excimer lamp was used in these experiments because of the greatest overlap with the absorption spectrum of **34** (Scheme 4-27). An external standard (2-undecanone) was employed to estimate the product yield. The response factor of **34** in relation to 2-undecanone was determined prior to GC analysis, but the response factor of the other products in relation to the external standard was not determined.



*Scheme 4-27 Photochemical dimerisation of pinacolone (**34**) to form 2,2,7,7- tetramethyloctane-3,6-dione (**35**) in micellar media.*

GC analysis of the crude reaction mixture showed no formation of new reaction products compared to when the reaction was carried out in H_2O/EtOH as the solvent. The total product yield was estimated to be 8.4 % using the external standard as a reference. The selectivity for a number of products did change when micellar media were employed instead of an aqueous ethanol mixture. Comparison of the peak area of the signals in the gas chromatograms (Figures 4-16,4-17) revealed a 3.6-fold increase in selectivity for the product corresponding to a GC retention time of 3.3 min. when pinacolone was irradiated in micellar solution instead of in a water/ethanol mixture. Products corresponding to GC signals with retention times of 8.3 and 8.6 min. decreased in selectivity by 1.7- to 1.9-fold respectively when irradiation took place in micellar media. The selectivity for the products corresponding to GC signals with retention times of 5.3, 10.1 and 10.2 min. remained unchanged. Although no product identification took place, it is encouraging to see an effect of micellar media on product distribution. Moreover, 8.4 % conversion of **34** is a promising result as the dimerisation of acetone did not take place in such yields.

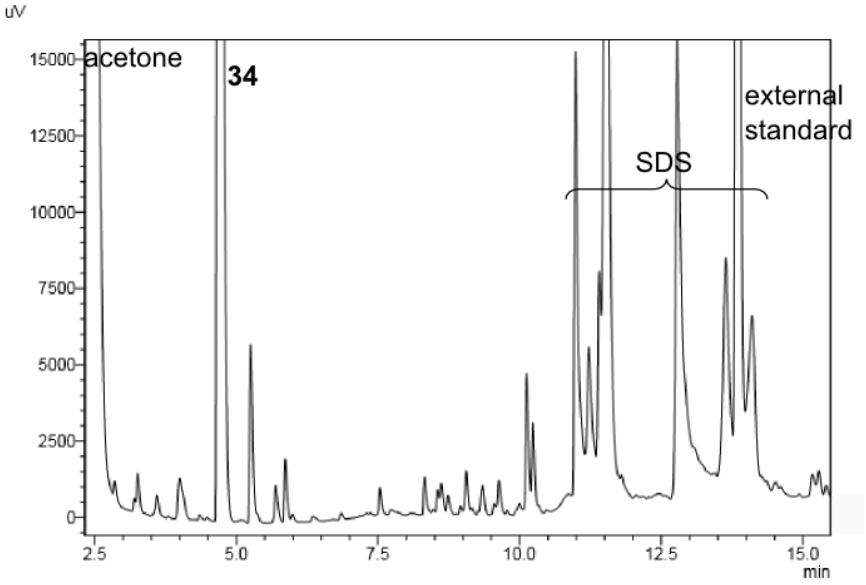


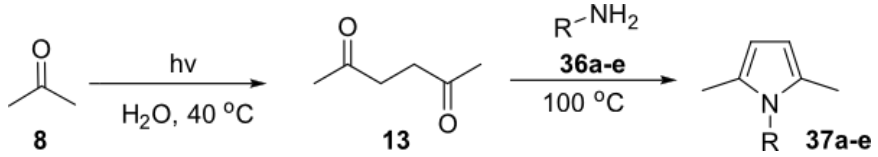
*Figure 4-17 Gas chromatogram of the reaction output in the photochemical dimerisation of **34** in H_2O, in the presence of a surfactant (SDS) at 0.2 mL/min and 40 °C, employing the 282 nm excimer lamp and using 2-undecanone as the external standard. The syringe for injections into the GC was rinsed with acetone which is why there is a GC signal of acetone.*

Despite the promising results in the dimerisation of **34** in micellar media, it was chosen to continue the investigation of ketone dimerisation in micelles once a method would have been developed to increase the selectivity of the reaction. That way the purification of the reaction mixture and identification of product **35** would be more feasible.

4.10 Cyclisation of 1,4-Diketones

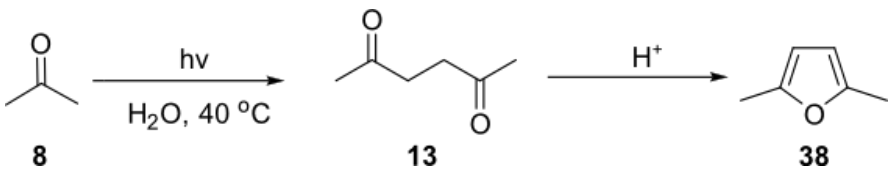
A useful pathway to utilise 1,4-diketones such as **13** is to form pyrrole and furan derivatives *via* the Paal-Knorr synthesis. These heterocyclic five-membered rings are important moieties in many natural products and medicinal compounds as they exhibit antibacterial, antitumor and antioxidant properties.[7b, 38] However, long reaction times and/or additional catalysts are often required for efficient Paal-Knorr syntheses.[39] Although the formation of 1,4-diketones followed by

Paal-Knorr cyclisation has been reported, the initial synthesis of 1,4-diketones often required harsh reaction conditions and toxic reagents.[7b, 40] The work presented in this Thesis will describe preliminary results on an overall sustainable route from a ketone to pyrroles and a furan derivative *via* the photochemical generation of a 1,4-diketone. The Paal-Knorr pyrrole synthesis has been carried out in water and aqueous mixtures[39a-c, 41] which offers the opportunity to perform the photochemical synthesis of **13** and the subsequent pyrrole synthesis in the same reaction solvent. It was envisioned that two reactors could be coupled in which **13** is synthesised photochemically from acetone (**8**) after which a second pump introduces a flow of primary amines to allow for formation of pyrrole derivatives (Scheme 4-28).



*Scheme 4-28 Photodimerisation of acetone (**8**) to form acetonylacetone (**13**) and subsequent reaction with a range of amines (**36a-e**) for pyrrole formation (**37a-e**).*

The formation of furan analogues *via* the Paal-Knorr synthesis is based on acid mediated dehydrative cyclisation of 1,4-diketones. The continuous synthesis of 2,5-dimethylfuran (**38**) could potentially be achieved by the photochemical dimerisation of **8** to form **13** after which this solution flows through a solid acid catalyst reactor to form **38** (Scheme 4-29). Ideally the whole reaction would be carried out in water, but the furan Paal-Knorr synthesis has not yet been reported in water. The use of a solid acid allows for easy separation from the reaction products resulting in a clean reaction process.

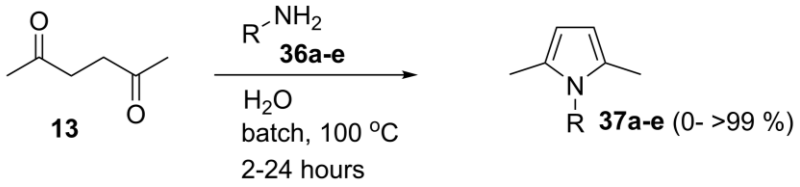


*Scheme 4-29 Photodimerisation of acetone (**8**) to form acetonylacetone (**13**) and subsequent acid mediated formation of 2,5-dimethylfuran (**38**).*

To test the viability of this approach, the formation of 2,5-dimethylfuran and pyrroles was attempted in batch with pure acetonylacetone. In a round bottom flask, **13** and either an amine or a solid acid were heated under reflux in either water or toluene until completion. Details on the reaction set-up can be found in the Experimental Chapter.

4.10.1 Synthesis of Pyrrole Derivatives

The synthesis of pyrrole derivatives was carried out with five different primary amines (**36a-e**) in a 1:1 molar ratio to **13** (Scheme 4-30).

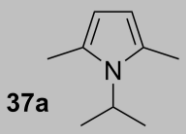
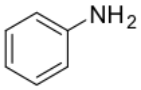
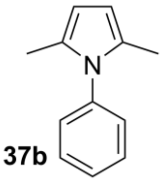
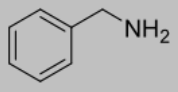
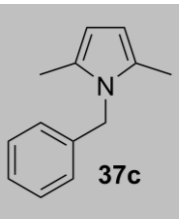
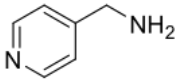
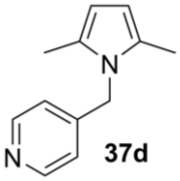
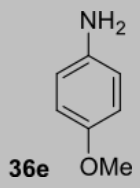
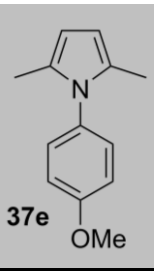


*Scheme 4-30 The Paal-Knorr reaction between pure acetonylacetone (**13**) and primary amines **36a-e** to form pyrrole derivatives **37a-e**.*

No conversion to 1-isopropyl-2,5-dimethyl-1*H*-pyrrole (**37a**) was observed when 2-aminopropane (**36a**) was reacted with acetonylacetone (**13**) (Table 4-4, entry 1). Amine **36a** has been shown previously to inhibit efficient pyrrole formation due to steric hindrance of the methyl moieties.[42] ^{1}H NMR analysis of the reaction mixture showed the presence of **36a** in the mixture, indicating that the low boiling point of **36a** (34 °C) did not cause evaporation of **36a** before it could react with **13**. The reaction between **13** and aniline (**36b**) successfully generated 2,5-dimethyl-1-phenyl-1*H*-pyrrole (**37b**) in > 95 % yield after 24 hours (Table 4-4, entry 2). Elevated temperatures were required to obtain this result. The reaction time to form 1-benzyl-2,5-dimethyl-1*H*-pyrrole (**37c**) was considerably shorter compared to the previously tested substrates (Table 4-4, entry 3). The extra carbon spacer between the phenyl moiety and the amino substituent releases the steric hindrance effect caused by the aromatic ring. Moreover, the phenyl ring reduces the electron density on the nitrogen of the

amino group due to its electron withdrawing properties. The extra carbon spacer reduces the effect of this phenomenon, leading to faster reaction times.[2b] Pyrrole derivative 4-((2,5-dimethyl-1*H*-pyrrol-1-yl)methyl)pyridine (**37d**) was formed at the fastest rate (Table 4-4, entry 4).

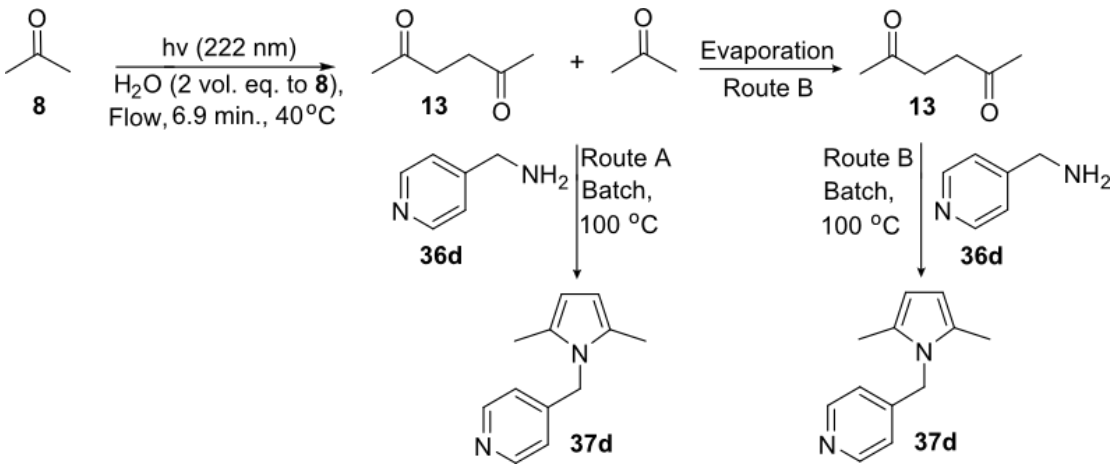
*Table 4-4 Reaction of acetonylacetone (**13**) with primary amines **36a-e** to form pyrrole derivatives **37a-e**.*

Entry	Amine	Time (h)	Product	^{1}H NMR yield (%)
1	 **36a**	19	 **37a**	n.o.[a]
2	 **36b**	24	 **37b**	> 95 %
3	 **36c**	2	 **37c**	95 %
4	 **36d**	< 2	 **37d**	> 99 %
5	 **36e**	3.5	 **37e**	82 %

*Reaction conditions: Acetonylacetone (**13**) (0.293 mL, 2.5 mmol, 1 eq.), amine (**36a-e**) (2.5 mmol, 1 eq.), deionised water (5 mL), reflux. Primary amines: 2-aminopropane (**36a**), aniline (**36b**), benzylamine (**36c**), 4-(aminomethyl)pyridine (**36d**), 4-methoxyaniline (**36e**); [a]n.o. not observed.*

It was observed that the formation of 1-(4-methoxyphenyl)-2,5-dimethyl-1*H*-pyrrole (**37e**) from **13** and 4-methoxyaniline (**36e**) proceeded smoothly despite the possible effect of steric hindrance by the phenyl moiety in **36e** (Table 4-4, entry 5). Due to electron resonance effects, the methoxy moiety in the *para*-position to the amino substituent increased the nucleophilicity of the amino moiety compared to substrate **36b**.

Interestingly, no additional catalyst was required to form the pyrrole derivatives which is contrast to some literature precedents.[39a-c] After these encouraging results, preliminary studies were performed using the reaction mixture from the photochemical acetone dimerisation for the synthesis of pyrroles despite the low concentration of acetonylacetone **13** in this mixture. Primary amine **36d** was chosen for the pyrrole synthesis as this allowed for the fastest reaction to pyrrole **37d**. Two different reaction set-ups were tested; one reaction was carried out with the crude reaction mixture from the photodimerisation of acetone (Scheme 4-31, Route A). In the second reaction set-up, the reaction mixture from the photochemical reaction was concentrated *in vacuo* to allow for a higher concentration of **13** in the mixture (Scheme 4-31, Route B). It was envisioned that this would increase the rate of pyrrole synthesis.

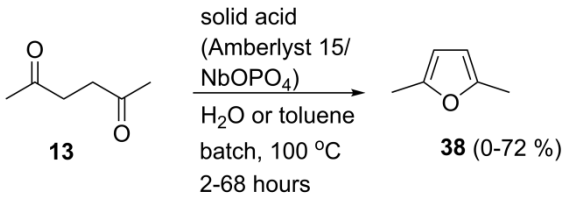


*Scheme 4-31 Formation of acetonylacetone (**13**) after the irradiation of acetone (**8**) in flow, and subsequent reaction of this mixture with 4-(aminomethyl)pyridine (**36d**) to form pyrrole **37d** in batch via route A; or via route B: first concentration of the photochemical reaction mixture followed by the reaction with **36d** to form **37d** in batch.*

Aliquots for qualitative analysis were taken after 5 hours and the formation of **37d** was observed in the ^{1}H NMR spectra of the crude reaction mixtures obtained *via* both routes. All acetonylacetone was consumed indicating the full conversion of diketone **13** to **37d**. The reaction proceeded smoothly even with a mixture of photoproducts, which is an encouraging result. As pointed out previously, efficient formation of diketone **13** requires further optimisation to increase the yield of the reaction. After successful optimisation, the conversion of acetone to several pyrrole derivatives can be repeated with quantitative analysis to establish reaction productivities in this tandem reaction.

4.10.2 Synthesis of Furan Derivative

The synthesis of 2,5-dimethylfuran (**38**) was carried out using two different solid acid catalysts, Amberlyst 15 and niobium phosphate ($NbOPO_4$) (Scheme 4-32). Both catalysts have been employed successfully for heterogeneous acid catalysed reactions.[43] For initial studies, pure acetonylacetone (**13**) was used and the transformation of **13** to **38** was carried out in batch with the same set-up as for the pyrrole derivative synthesis.



*Scheme 4-32 The Paal-Knorr reaction between pure acetonylacetone (**13**) to form 2,5-dimethylfuran (**38**) over a solid acid catalyst (either Amberlyst 15 or $NbOPO_4$).*

With deionised water being the co-solvent for the photochemical formation of **13** from **8**, the first attempt to synthesise **38** was carried out in this solvent. However, no formation of **38** was observed after 20 hours (Table 4-5, entry 1). Conducting the reaction in toluene provided full conversion of **13** after 92 hours, but unidentified side products were observed. The highest yield of furan **38**

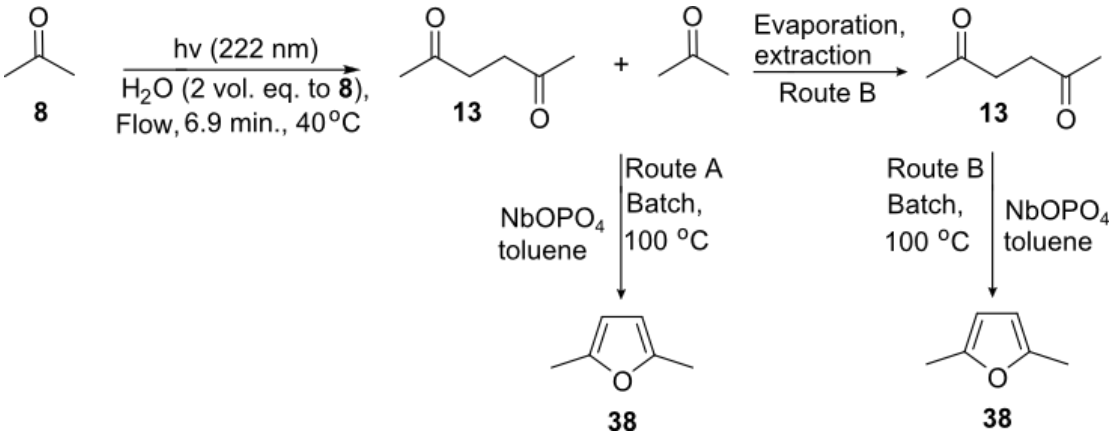
(50 %) was reached after 68 h (Table 4-5, entry 2). Next, $NbOPO_4$ was tested as the solid acid catalyst. No conversion of **13** was observed when the reaction was carried out in either water or THF (Table 4-5, entries 3,4). In contrast, fast formation of **38** was obtained in toluene (Table 4-5, entry 5). After 2 hours, 91 % conversion of diketone **13** and 72 % yield for furan **38** were obtained.

*Table 4-5 Reaction of acetonylacetone (**13**) to form 2,5-dimethylfuran (**38**) over solid acid.*

Entry	Solid acid catalyst	Solvent	Time (h)	^{1}H NMR yield 38 (%)[c]
1[a]	Amberlyst 15	H_2O	20	n.o.[d]
2[a]	Amberlyst 15	toluene	68	50 %
3[b]	$NbOPO_4$	H_2O	19	n.o.[d]
4[b]	$NbOPO_4$	THF	4	n.o.[d]
5[b]	$NbOPO_4$	toluene	2	72 %

*[a]Reaction conditions: Acetonylacetone (**13**) (1.0 mL, 8.5 mmol, 1 eq.), Amberlyst 15* (2.7 g, 13 mmol, 1.5 eq.)*, solvent (20 mL), reflux; [b]Reaction conditions: Acetonylacetone (**13**) (100 µL, 0.85 mmol, 1 eq.), $NbOPO_4$ (2.0 g, 0.71 mmol, 0.89 eq.), solvent (5 mL), reflux; [c]Yield determined from crude mixture, [d]n.o. not observed.*

For preliminary testing, the reaction mixture of the photochemical transformation of **8** to **13** instead of pure **13** was used for the formation of furan **38**. Niobium phosphate was employed as the solid acid and toluene was chosen as the reaction solvent as these conditions provided the highest and quickest conversion to **38** when pure diketone **13** was used as shown in Table 4-5. Two routes were explored using both the crude photochemical product mixture and a concentrated solution (Scheme 4-33). However, no **38** was formed under any of the tested conditions as analysed by GC over time for 3 days. Although **13** was observed in the gas chromatogram of the sample obtained *via* route A, no GC signal for **13** was observed in the mixture obtained *via* route B. New peaks in the gas chromatograms of the reaction mixtures obtained *via* both route A and B indicate that the acid catalyst was active, but reacted with compounds other than **13**. It is worth repeating this experiment when compounds other than **13** are less abundant in the reaction mixture of the photochemical reaction. That way, by-product formation could be suppressed in the Paal-Knorr synthesis of **38**.



*Scheme 4-33 Formation of acetonylacetone (**13**) after the irradiation of acetone (**8**) in flow, and subsequent reaction of this mixture with $NbOPO_4$ to form 2,5-dimethylfuran (**38**) in batch via route A; or via route B: first concentration of the photochemical reaction mixture and extraction to remove water followed by the reaction with $NbOPO_4$ in toluene to form (**38**) in batch.*

The formation of **38** from **13** was unsuccessful in water thus far. The formation of water as a by-product during the Paal-Knorr transformation could possibly inhibit the efficient formation of **13** from **38**. This provides a challenge for combining the UV photochemical dimerisation of **8** into **13** and the subsequent cyclisation into **38** into one continuous reactor. It could be possible to introduce a flow of a suitable solvent such as toluene into the reactor in between the photochemical and the Paal-Knorr reaction. It would be beneficial to investigate the use of solvents for the Paal-Knorr transformation that are miscible with water to ensure a homogeneous solution during the reaction.

Both furan and pyrrole synthesis from **13** has been proven to be successful. By performing the Paal-Knorr synthesis in continuous flow, reaction times could be shortened significantly due to homogeneous heating and efficient mixing. In the synthesis of **38**, as the reaction mixture flows through the reactor, an excess of solid acid catalyst is present to convert **13** into **38** which can increase the efficiency of this reaction in flow compared to batch.

4.11 Conclusions and Future Work

The efficient synthesis of acetonylacetone by performing photodimerisation of acetone was the main goal of the work presented in this Chapter. Despite obtaining satisfactory selectivity for acetonylacetone in this reaction (up to 65 %), the conversion of acetone remained problematic, even after optimisation (0.10-0.70 %). Recirculation of the reaction mixture appeared to be the most efficient way to increase the yield of the reaction. Despite the low conversion of acetone, productivities up to 0.22 mmol/h were obtained for acetonylacetone formation which are on the same order of magnitude as other productivities reported in literature for UV based photochemical reactions.[44] However, in order to employ the developed method for its potential applications, both the conversion of acetone and the productivity for product **13** need to be improved. An interesting route to achieve this could be the investigation into the effect of pressure on the conversion of **8** and the selectivity for **13** as the formation of **13** is concentration dependent. Although solvents such as water are hardly compressible, $scCO_2$ is and could potentially be investigated as a co-solvent for the reaction. It is hypothesised that the selectivity for **13** would go up with increased pressure as molecules are located closer together and diffusion could become less of a limiting factor.

The use of other photosensitisers could potentially benefit from further study as well. For example, water-soluble xanthone derivatives have been reported to undergo photo-mediated decarboxylation to generate alkyl radicals which could act as a substitute for the sodium and phthalimido acetate photosensitisers.[45] Another interesting route for increased conversion of acetone to form acetonylacetone could be the use of thiourea derivatives. This compound can form a non-covalent complex with a ketone and it was shown by Telmesani *et al.* and Vallavoju *et al.* that the yield of intersystem crossing was enhanced and the excited state lifetime of the complex was extended.[46] This could potentially help to increase the likelihood of a chemical transformation happening leading to the formation of **13** as opposed to non-radiative quenching of the excited state acetone.

4.12 References

1. (a) Fang, W.; Liu, S.; Nie, Y., *Molecules* **2011,** *16* (8), 6243; (b) Li, S.-H.; Wang, J.; Niu, X.-M.; Shen, Y.-H.; Zhang, H.-J.; Sun, H.-D.; Li, M.-L.; Tian, Q.-E.; Lu, Y.; Cao, P.; Zheng, Q.-T., *Org. Lett.* **2004,** *6* (23), 4327-4330; (c) Furusaki, A.; Matsumoto, T.; Ogura, H.; Takayanagi, H.; Hirano, A.; Omura, S., *J. Chem. Soc., Chem. Commun.* **1980,** (15), 698; (d) He, H.; Ding, W.-D.; Bernan, V. S.; Richardson, A. D.; Ireland, C. M.; Greenstein, M.; Ellestad, G. A.; Carter, G. T., *J. Am. Chem. Soc.* **2001,** *123* (22), 5362-5363.
2. (a) Bharadwaj, A. R.; Scheidt, K. A., *Org. Lett.* **2004,** *6* (14), 2465-2468; (b) Cho, H.; Madden, R.; Nisanci, B.; Torok, B., *Green Chem.* **2015,** *17* (2), 1088-1099; (c) Amarnath, V.; Amarnath, K., *J. Org. Chem.* **1995,** *60* (2), 301-307; (d) Amarnath, V.; Anthony, D. C.; Amarnath, K.; Valentine, W. M.; Wetterau, L. A.; Graham, D. G., *J. Org. Chem.* **1991,** *56* (24), 6924-6931.
3. (a) Stepherson, J. R.; Fronczek, F. R.; Kartika, R., *Chem. Commun.* **2016,** *52* (11), 2300-2303; (b) Parida, B. B.; Das, P. P.; Niocel, M.; Cha, J. K., *Org. Lett.* **2013,** *15* (7), 1780-1783, and references therein.
4. Zhao, W.; Fink, D. M.; Labutta, C. A.; Radosevich, A. T., *Org. Lett.* **2013,** *15* (12), 3090-3093.
5. Xue, S.; Li, L.-Z.; Liu, Y.-K.; Guo, Q.-X., *J. Org. Chem.* **2006,** *71* (1), 215-218.
6. Huang, S.; Kötzner, L.; De, C. K.; List, B., *J. Am. Chem. Soc.* **2015,** *137* (10), 3446-3449.
7. (a) Mao, S.; Gao, Y.-R.; Zhang, S.-L.; Guo, D.-D.; Wang, Y.-Q., *Eur. J. Org. Chem.* **2015,** *2015* (4), 876-885; (b) Mao, S.; Zhu, X.-Q.; Gao, Y.-R.; Guo, D.-D.; Wang, Y.-Q., *Chem. Eur. J.* **2015,** *21* (32), 11335-11339.
8. Esposti, S.; Dondi, D.; Fagnoni, M.; Albini, A., *Angew. Chem.* **2007,** *119* (14), 2583-2586.
9. Negele, S.; Wieser, K.; Severin, T., *J. Org. Chem.* **1998,** *63* (4), 1138-1143.
10. Hancock, K. G.; Wylie, P. L.; Lau, J. T., *J. Am. Chem. Soc.* **1977,** *99* (4), 1149-1156.
11. (a) Setzer, P.; Beauseigneur, A.; Pearson-Long, M. S. M.; Bertus, P., *Angew. Chem.* **2010,** *122* (46), 8873-8876; (b) Setzer, P.; Forcher, G.; Boeda, F.; Pearson-Long, M. S. M.; Bertus, P., *Eur. J. Org. Chem.* **2014,** *2014* (1), 171-180; (c) Chan, C.-K.; Chan, Y.-L.; Tsai, Y.-L.; Chang, M.-Y., *J. Org. Chem.* **2016,** *81* (17), 8112-8120; (d) Luo, J.; Jiang, Q.; Chen, H.; Tang, Q., *RSC Adv.* **2015,** *5* (83), 67901-67908; (e) Rössle, M.; Werner, T.; Frey, W.; Christoffers, J., *Eur. J. Org. Chem.* **2005,** *2005* (23), 5031-5038.
12. Nishimoto, S.-i.; Ohtani, B.; Kagiya, T., *J. Chem. Soc., Faraday Trans.1* **1985,** *81* (10), 2467-2474.

13. Przybytek, J. T.; Singh, S. P.; Kagan, J., *J. Chem. Soc. D* **1969**, 1224a.

14. Dalton, J. C.; Turro, N. J., *Annu. Rev. Phys. Chem.* **1970,** *21* (1), 499-560.

15. (a) Reichle, W. T., *J. Catal.* **1980,** *63* (2), 295-306; (b) Salvapati, G. S.; Ramanamurty, K. V.; Janardanarao, M., *J. Mol. Catal.* **1989,** *54* (1), 9-30; (c) Thotla, S.; Agarwal, V.; Mahajani, S. M., *Ind. Eng. Chem. Res.* **2007,** *46* (25), 8371-8379.

16. Laroff, G. P.; Fischer, H., *Helv. Chim. Acta* **1973,** *56* (6), 2011-2020.

17. Shimizu, N.; Miyahara, T.; Mishima, M.; Tsuno, Y., *Bull. Chem. Soc. Jpn.* **1989,** *62* (6), 2032-2039.

18. (a) Izquierdo, J. F.; Vila, M.; Tejero, J.; Cunill, F.; Iborra, M., *App. Catal. A-Gen.* **1993,** *106* (1), 155-165; (b) Matsushima, R.; Terada, K., *J. Chem. Soc. Perk. T. 2* **1985**, 1445-1448; (c) Yu, X.; Scheller, D.; Rademacher, O.; Wolff, T., *J. Org. Chem.* **2003,** *68* (19), 7386-7399; (d) CRC Handbook of Organic Photochemistry and Photobiology, Volumes 1 & 2. Second ed.; Horspool, W. M.; Lenci, F., Eds. CRC Press: 2003.

19. Shiraishi, Y.; Tsukamoto, D.; Hirai, T., *Org. Lett.* **2008,** *10* (14), 3117-3120.

20. Howard, K. S.; McAllister, R. A., *AIChE Journal* **1958,** *4* (3), 362-366.

21. Pelliccioli, A. P.; Klán, P.; Zabadal, M.; Wirz, J., *J. Am. Chem. Soc.* **2001,** *123* (32), 7931-7932.

22. Kamlet, M. J.; Abboud, J. L. M.; Abraham, M. H.; Taft, R. W., *J. Org. Chem.* **1983,** *48* (17), 2877-2887.

23. Kaji, E.; Komori, T.; Yokoyama, M.; Kato, T.; Nishino, T.; Shirahata, T., *Tetrahedron* **2010,** *66* (23), 4089-4100.

24. Takebayashi, Y.; Yoda, S.; Sugeta, T.; Otake, K.; Nakahara, M., *J. Phys. Chem. B* **2003,** *107* (36), 9847-9852.

25. Porter, G.; Dogra, S. K.; Loutfy, R. O.; Sugamori, S. E.; Yip, R. W., *J. Chem. Soc., Faraday Trans.1* **1973,** *69*, 1462-1474.

26. Haidasz, E. A.; Li, B.; Pratt, D. A., *Annu. Rep. Prog. Chem., Sect. B: Org. Chem.* **2013**.

27. Borkman, R. F.; Kearns, D. R., *J. Chem. Phys.* **1966,** *44* (3), 945-949.

28. Äkerlöf, G., *J. Am. Chem. Soc.* **1932,** *54* (11), 4125-4139.

29. Nakashima, M.; Hayon, E., *J. Phys. Chem.* **1971,** *75* (13), 1910-1914.

30. Fileti, E. E.; Chaudhuri, P.; Canuto, S., *Chem. Phys. Lett.* **2004,** *400* (4-6), 494-499.

31. Lam, R. K.; Smith, J. W.; Saykally, R. J., *J. Chem. Phys.* **2016,** *144* (191103).

32. Hemwimon, S.; Pavasant, P.; Shotipruk, A., *Sep. Purif. Technol.* **2007,** *54* (1), 44-50.

33. Ahmad, I.; Anwar, Z.; Iqbal, K.; Ali, S. A.; Mirza, T.; Khurshid, A.; Khurshid, A.; Arsalan, A., *AAPS PharmSci Tech.* **2014,** *15* (3), 550-559.

34. Panferova, L. I.; Smirnov, V. O.; Levin, V. V.; Kokorekin, V. A.; Struchkova, M. I.; Dilman, A. D., *J. Org. Chem.* **2017,** *82* (1), 745-753.

35. (a) Kulasekharan, R.; Choudhury, R.; Prabhakar, R.; Ramamurthy, V., *Chem. Commun.* **2011,** *47* (10), 2841-2843; (b) Pattabiraman, M.; Kaanumalle, L. S.; Ramamurthy, V., *Langmuir* **2006,** *22* (5), 2185-2192; (c) Kaanumalle, L. S.; Nithyanandhan, J.; Pattabiraman, M.; Jayaraman, N.; Ramamurthy, V., *J. Am. Chem. Soc.* **2004,** *126* (29), 8999-9006; (d) Turro, N. J., *Acc. Chem. Res.* **2000,** *33* (9), 637-646; (e) Arumugam, S.; Kaanumalle, L. S.; Ramamurthy, V., *J. Photoch. Photobio. A.* **2007,** *185* (2–3), 364-370; (f) Yuan, Z.; Chen, J.; Zeng, Y.; Li, Y.-Y.; Han, Y.; Li, Y., *Org. Biomol. Chem.* **2011,** *9* (18), 6256-6264; (g) Yuan, Z.; Zheng, S.; Zeng, Y.; Chen, J.; Han, Y.; Li, Y.; Li, Y., *New J. Chem.* **2010,** *34* (4), 718-722; (h) Bhattacharyya, K., *Acc. Chem. Res.* **2003,** *36* (2), 95-101; (i) Tung, C.-H.; Wu, L.-Z.; Zhang, L.-P.; Chen, B., *Acc. Chem. Res.* **2003,** *36* (1), 39-47; (j) Weiss, R. G.; Ramamurthy, V.; Hammond, G. S., *Acc. Chem. Res.* **1993,** *26* (10), 530-536.

36. (a) Scaiano, J. C.; Abuin, E. B.; Stewart, L. C., *J. Am. Chem. Soc.* **1982,** *104* (21), 5673-5679; (b) Leigh, W. J.; Scaiano, J. C., *J. Am. Chem. Soc.* **1983,** *105* (17), 5652-5657.

37. (a) Meyer, S.; Tietze, D.; Rau, S.; Schäfer, B.; Kreisel, G., *J. Photoch. Photobio. A.* **2007,** *186* (2–3), 248-253; (b) Vaske, Y. S. M.; Mahoney, M. E.; Konopelski, J. P.; Rogow, D. L.; McDonald, W. J., *J. Am. Chem. Soc.* **2010,** *132* (32), 11379-11385; (c) Hernandez-Perez, A. C.; Vlassova, A.; Collins, S. K., *Org. Lett.* **2012,** *14* (12), 2988-2991.

38. (a) Tang, J.; Yang, M.; Yang, M.; Wang, J.; Dong, W.; Wang, G., *New J. Chem.* **2015,** *39* (6), 4919-4923; (b) Bellina, F.; Rossi, R., *Tetrahedron* **2006,** *62* (31), 7213-7256; (c) Alizadeh, A.; Rezvanian, A.; Bijanzadeh, H. R., *Synthesis* **2008,** *2008* (05), 725-728.

39. (a) Banik, M.; Ramirez, B.; Reddy, A.; Bandyopadhyay, D.; Banik, B. K., *Org. Med. Chem. Lett.* **2012,** *2* (1), 1-4; (b) He, Y.-H.; Wang, G.-Q.; Guan, Z., *J. Heterocycl. Chem.* **2010,** *47* (2), 486-489; (c) Jafari, A. A.; Amini, S.; Tamaddon, F., *J. Appl. Polym. Sci.* **2012,** *125* (2), 1339-1345; (d) Banik, B. K.; Banik, I.; Renteria, M.; Dasgupta, S. K., *Tetrahedron Lett.* **2005,** *46* (15), 2643-2645; (e) Curini, M.; Montanari, F.; Rosati, O.; Lioy, E.; Margarita, R., *Tetrahedron Lett.* **2003,** *44* (20), 3923-3925; (f) Chen, J.; Wu, H.; Zheng, Z.; Jin, C.; Zhang, X.; Su, W., *Tetrahedron Lett.* **2006,** *47* (30), 5383-5387.

40. (a) Minetto, G.; Raveglia, L. F.; Taddei, M., *Org. Lett.* **2004,** *6* (3), 389-392; (b) Alnabulsi, S.; Santina, E.; Russo, I.; Hussein, B.; Kadirvel, M.; Chadwick, A.; Bichenkova, E. V.; Bryce, R. A.; Nolan, K.; Demonacos, C.; Stratford, I. J.; Freeman, S., *Eur. J. Med. Chem.* **2016,** *111*, 33-45.

41. Akbaşlar, D.; Demirkol, O.; Giray, S., *Synth. Commun.* **2014,** *44* (9), 1323-1332.

42. de C. da Silva, F.; Fonseca, M. G.; de S. Rianelli, R.; Cunha, A. C.; de Souza, M. C. B. V.; Ferreira, V. F., *Beilstein J. Org. Chem.* **2008,** *4* (45).

43. (a) Galletti, A. M. R.; Antonetti, C.; De Luise, V.; Martinelli, M., *Green Chem.* **2012,** *14* (3), 688-694; (b) Carniti, P.; Gervasini, A.; Biella, S.; Auroux, A., *Catal. Today* **2006,** *118* (3–4), 373-378; (c) DeLaney, E. N.; Lee, D. S.; Elliott, L. D.; Jin, J.; Booker-Milburn, K. I.; Poliakoff, M.; George, M. W., *Green Chem.* **2017,** *19* (6), 1431-1438; (d) Stevens, J. G.; Bourne, R. A.; Poliakoff, M., *Green Chem.* **2009,** *11* (3), 409-416.

44. Knowles, J. P.; Elliott, L. D.; Booker-Milburn, K. I., *Beilstein J. Org. Chem.* **2012,** *8*, 2025–2052.

45. Balta, D. K.; Temel, G.; Aydin, M.; Arsu, N., *Eur. Polym. J.* **2010,** *46* (6), 1374-1379.

46. (a) Telmesani, R.; Park, S. H.; Lynch-Colameta, T.; Beeler, A. B., *Angew. Chem. Int. Ed.* **2015,** *54* (39), 11521-11525; (b) Vallavoju, N.; Selvakumar, S.; Jockusch, S.; Sibi, M. P.; Sivaguru, J., *Angew. Chem. Int. Ed.* **2014,** *53* (22), 5604-5608; (c) Vallavoju, N.; Selvakumar, S.; Pemberton, B. C.; Jockusch, S.; Sibi, M. P.; Sivaguru, J., *Angew. Chem.* **2016,** *128* (18), 5536-5541.

Chapter 5 General Conclusions and Future Directions

This Thesis aimed to present new approaches to combine continuous photochemistry, reactor design and the development of new methods to produce compounds for potentially widespread applications. Chapter 1 described a series of specific aims for the work presented in this Thesis and these were:

1. To demonstrate that visible light photochemistry can contribute to sustainable chemical production while maintaining high productivity and product selectivity.

2. To deepen the understanding of the mechanism of the hydroxylation of aryl boronic acids by performing quantum chemical calculations in order to investigate which reaction parameters would influence reaction productivity and selectivity most.

3. To achieve a mild and clean synthetic route to extended methyl ketones by employing a recently developed excimer lamp UV continuous flow reactor.

4. To optimise reaction parameters for the formation of 1,4-diketones by the photochemical dimerisation of several ketones.

5. To employ 1,4-diketones in the Paal-Knorr synthesis to form 2,5-dimethylfuran and several pyrrole derivatives.

The following Sections will describe the underlying rationale of these aims, what results have been obtained towards the aims and the future work that could be undertaken.

Aim 1 To demonstrate that visible light photochemistry can contribute to sustainable chemical production while maintaining high productivity and product selectivity.

Rationale

There is a drive to improve the sustainable character of chemical reactions[1] and photo-induced processes have been named to potentially facilitate mild transformations, avoiding harsh activation sources.[2] Although light used in photochemistry provides a clean source of activation energy, visible light often cannot initiate a chemical transformation directly. Therefore, a photocatalyst is usually required to absorb the visible light and perform electron transfer with the desired substrate which can initiate the chemical reaction. Catalysis has been recognised as one of the areas in Green Chemistry as stoichiometric amounts of activation reagents can be avoided.[1b, 2] To minimise catalyst waste, the photocatalyst could be immobilised to recycle and reuse it in several chemical reactions. These strategies of using immobilised photoredox catalysis and performing reactions in aqueous solvent mixtures were applied to the formation of aryl alcohols. Aryl alcohols are present in many pharmaceuticals as they exhibit antibacterial, antiviral, cardioprotective and antimutagenicity activities.[3] Mild transformations to these aryl alcohols are desirable and therefore, the hydroxylation of aryl boronic acids to aryl alcohols was investigated for this Thesis. Previous publications on this reaction revealed the need for long reaction times and/or metal based photocatalysts.[4] The aim of the research presented in this Thesis was to demonstrate the potential of using mild conditions to achieve high productivity for aryl alcohol formation.

Progress

An important factor in performing photoredox catalysis successfully is the efficiency of light penetration into the reaction solution. Therefore, a continuous flow photoreactor built in-house was employed in this research to facilitate efficient light irradiation of the reaction solution. To increase the sustainable character of this reaction, a non-metal based photocatalyst (Rose Bengal) was

employed in the hydroxylation of phenylboronic acid and provided faster conversion of phenylboronic acid to phenol than the metal based photocatalyst $[Ru(bpy)_3]Cl_2$. After parameter optimisation, the hydroxylation of phenylboronic acid to phenol was conducted successfully in the continuous flow reactor leading to a 90-fold increase in productivity compared to the reaction carried out under similar reaction conditions in batch. Amine based compounds are often used to quench the excited state photocatalyst. Although proven efficient quenchers, their toxicity is undesirable. Therefore, ascorbic acid was tested as an alternative reductive quencher. Despite its excellent use in combination with $[Ru(bpy)_3]Cl_2$, the acidity of this reductive quencher deactivated Rose Bengal.

Reaction selectivity is important in a chemical transformation and flow chemistry can potentially contribute to control over selectivity. Therefore, desymmetrisation of benzene diboronic acid compounds was studied in the above mentioned continuous flow reactor. Using Rose Bengal as the non-metal photocatalyst, moderate to high selectivities for the mono-hydroxylated compounds was achieved in continuous flow.

Another route that was investigated to enhance the sustainable character of the reaction was the immobilisation of metal based photocatalyst $[Ru(bpy)_3]Cl_2$ on Amberlyst 15. After successful immobilisation, the heterogeneous catalyst could be recycled and reused three times without loss of conversion. However, catalyst leaching out of the support was observed. Poly(ethylene oxide) (PEO) was tested as another support for the immobilisation of $[Ru(bpy)_3]Cl_2$ and this catalyst complex was tested in the continuous flow reactor. Preliminary results suggest a promising start for this immobilised catalyst complex as the hydroxylation of phenylboronic acid proceeded reaching 7 % conversion in 7 minutes.

To summarise, visible light photoredox catalysis has been applied in combination with different techniques such as catalyst immobilisation and continuous flow reactors. This led to an increase in productivity of phenol formation by employing continuous flow photochemistry. Moreover, different strategies including changing toxic reagents and reusing the photocatalyst were developed to increase the sustainable character of this transformation.

Future Directions

Further studies could be directed towards the improved reactor set-up for the use of immobilised catalysts. In the immobilisation of $[Ru(bpy)_3]Cl_2$ on PEO, thin

circular sheets of PEO containing the immobilised catalyst were employed. A method to enlarge the surface area of this immobilised catalyst would be to coat glass beads in the photoreactor with this immobilised catalyst complex. Enlarging the surface area of the photocatalyst enables more contact with the substrate which would hopefully speed up the reaction. Immobilisation of Rose Bengal photocatalyst on Amberlite IRA 900 or Seralite SRA 400 could be an interesting research area as well in order to improve the sustainable character of this reaction even further as the use of more expensive metals is avoided.[5]

To use immobilised catalysts for a broad range of reactions, other catalyst supports could be investigated to ensure catalyst activity without leaching of the catalyst from the support. A catalyst support that could provide strong interaction between the catalyst and the support, which is a contributing factor to potentially inhibit catalyst leaching, is phosphotungstic acid.[6] The acidity of this support must be considered as this could potentially facilitate undesired acid mediated reactions.

Another immobilisation approach for photocatalysts could be supported ionic liquid catalysis (SILC). By employing ionic liquids, a strong interaction between the photocatalyst and the support can be present in the case of charged photocatalysts and no solvent is required in the chemical reaction as the ionic liquid can act as solvent. Therefore, a homogeneous reaction mixture is created and easy separation can be accomplished by filtering the reaction mixture through a membrane.[7]

Aim 2 To deepen the understanding of the mechanism of the hydroxylation of aryl boronic acids by performing quantum chemical calculations in order to investigate which reaction parameters would influence reaction productivity and selectivity most.

Rationale

Two different mechanisms for the hydroxylation of aryl boronic acids to aryl alcohols have been published.[4] The mechanism proposed by Zou *et al.* describes the addition of superoxide, which is generated by the oxidation of the photocatalyst, to the boron atom of the aryl boronic acid, followed by hydrolysis.[4b] Jiang *et al.* describes a non-photocatalyst mediated route in which

an aryl radical and a hydroxyl radical combine to form the aryl alcohol.[4a] In order to investigate which of the two mechanisms is more thermodynamically favourable, quantum chemical density functional theory (DFT) calculations were carried out for this Thesis to investigate the mechanistic aspects of this reaction further. Moreover, obtaining information on the rate-determining step could prove helpful in the process of reaction optimisation.

Progress

As shown in Chapter 2, the value of DFT calculations in this context has been demonstrated. DFT calculations on the mechanisms proposed by Zou *et al.* indicated that the insertion of superoxide into phenylboronic acid could be the rate-determining step in the hydroxylation of phenylboronic acid with an energy barrier of 14.7 kcal/mol to the corresponding transition state. Performing calculations on this mechanism using different solvent field parameters showed to have little effect on the energy levels, which would indicate that the choice of reaction solvent does not influence the reaction efficiency based on its dielectric constant.

Computing the different steps in the mechanism proposed by Jiang *et al.* proved to be difficult. No stable phenylboronic acid-DIPEA exciplex could be found and therefore, only later steps in this mechanism were calculated. In these steps, the insertion of a hydroxyl radical into phenylboronic acid appeared to be the rate-determining step with an energy barrier of 17.1 kcal/mol to the corresponding transition state. This would indicate that the mechanism as proposed by Zou *et al.* is more thermodynamically favourable and would be the dominant pathway. However, without having full detail on the energy levels of all the steps in both proposed mechanisms, more proof is needed to derive relevant information on the rate of the different pathways. Building on the results obtained from the calculations, the oxygen concentration is important for efficient transformation if the rate-determining step indeed requires the presence of an oxygen based molecule. This was collaborated by experiments which showed that the levels of oxygen in the reaction played a dominant role in determining reaction efficiency.

Future Directions

Unfortunately, the DFT calculations could not provide an explanation for the difference in experimentally found reactivity between the *ortho*-, *meta*- and *para*-substituted benzene diboronic acids. In order to obtain theoretical support

for this observation, the Hammett parameters of the different substituted benzene diboronic acids could be determined. These parameters provide information on how the different substituents on the benzene ring influence the reaction rate. Both substituent constants and reaction constant (hydroxylation reaction) need to be acquired.

Another method for acquiring information on the mechanism in radical based reactions is electron paramagnetic resonance (EPR) spectroscopy. This technique is used to study reactive species with unpaired electrons, which includes radical based compounds. EPR spectra can potentially reveal the different radical species present in the reaction mixture by comparing the signal pattern obtained experimentally with a simulated pattern. Radicals can also be trapped with a trapping agent like TEMPO after which NMR and Mass spectroscopy can provide evidence for identification of the radical species originally present in solution.

Aim 3 To achieve a mild and clean synthetic route to extended methyl ketones by employing a recently developed excimer lamp UV continuous flow reactor.

Rationale

Within the search for more environmentally friendly synthesis routes, the formation of ketones, in particular extended methyl ketones, is an important transformation to investigate as most natural products utilise this moiety either as a building block during synthesis or contain it in the end product.[8] Introducing ketone functionality is employed frequently in synthesis as explained in Chapter 3, but synthesis routes to ketone formation often raise environmental concerns. Therefore a mild and clean route to the formation of extended ketones was developed in the work described in this Thesis. UV light was employed to couple 1-octene with ketones in aqueous solutions to form extended ketones. This way, the use of any additional reagents and toxic solvents can be avoided. Excimer lamps have been recognised as suitable UV light sources in synthetic chemistry,[9] providing narrow irradiation wavelengths and low operation temperatures. Employing these lamps, a continuous flow reactor was built to facilitate the ketone formation.

Progress

Most emphasis was placed on the coupling of acetone and 1-octene to form 2-undecanone. Hydrogen-bonding solvents were proven essential to form 2-undecanone selectively. The highest selectivity obtained for 2-undecanone was 58 % with full conversion of 1-octene. This corresponds to a productivity of 0.69 mmol/h which is a 23-fold increase compared to the value published by Shiraishi *et al.* for this transformation.[10] This higher productivity contributes to a more environmentally benign procedure as it reduces the solvent waste. Tuning reaction conditions led to the selective formation of two other reaction products in the coupling of acetone and 1-octene. However, recycling of the reaction mixture would be required to improve the productivity of these reactions as the conversion of 1-octene was low in these cases.

In summary, a mild and efficient route towards 2-undecanone was demonstrated with an additional advantage of the ability to tune reaction conditions to facilitate the formation of other olefin-ketone coupling products.

Future Directions

Encouraged by the increase in productivity when using the UV excimer continuous flow photoreactor, the scope of the reaction could be extended. Preliminary studies into the coupling of 1-octene and mesityl oxide revealed no reaction products, but optimisation of reaction parameters might be needed to achieve efficient coupling of these substrates. To proof the versatility of this coupling, a range of ketones could be tested for the coupling with olefins. As illustrated by Shiraishi *et al.*, substrate solubility can become an issue since aqueous solutions are employed for this transformation.[10] To overcome this challenge, surfactants (such as sodium dodecyl sulfate (SDS)) could be employed. The surfactant could potentially be recycled *via* extraction and subsequently reused to limit the amount of waste generated. Using these surfactants, micelles are created in solution and non-water soluble ketones and olefins could be located in the hydrophobic cores of these micelles. This would also increase the local concentration of reactants which could potentially increase the rate of intermolecular reactions. For initial studies, ketones such as pinacolone or acetophenone could be employed in the coupling with olefins. Moreover, it would be interesting to test the functional group tolerance of the developed method by employing ketones with for example carboxylic acid moieties.

Aim 4 To optimise reaction parameters for the formation of 1,4-diketones by the photochemical dimerisation of several ketones.

Rationale

Other compounds that are commonly synthesised are 1,4-diketones as they are present in several bioactive natural products[11] and are also employed as precursors for the synthesis of heterocycles such as pyrroles, thiophenes and furans.[12] The formation of these compounds *via* a clean and mild method is therefore highly desirable as common routes to 1,4-diketones often employ metal catalysts,[13] halogenated species,[13a, 14] or harsh reaction conditions.[13b, 14d, 15] This Thesis described the initial results of a clean and atom economic synthesis of 1,4-diketones *via* the UV photodimerisation of simple ketones employing the previously described UV excimer continuous flow photoreactor.

Progress

The formation of acetonylacetone from the photodimerisation of acetone was accomplished in satisfactory selectivity (65 %). However, the conversion of acetone into products other than isopropanol was below 1 %. Optimising reaction conditions revealed that the presence of a hydrogen-bonding solvent was essential for the selective formation of acetonylacetone and that 40 °C was the optimum system temperature for selective acetonylacetone formation. Employing different irradiation wavelengths resulted in a change in product distribution, with the highest selectivity for acetonylacetone found when the 222 nm excimer lamp was used. Unfortunately, this excimer lamp emits the lowest number of photons which resulted in the lowest conversion of acetone under these conditions.

As highlighted, one of the major challenges in this reaction is the low conversion of acetone. Three different methods were investigated to potentially increase this yield. The first method involved the use of an alternative photo absorber to absorb the light as opposed to acetone. When acetone is excited, both a ketyl and an α-keto radical are formed. However, only the α-keto radical is required to form acetonylacetone. It was hypothesised that the formation of the ketyl radical could be avoided by employing an alternative photo absorber and solely generate the α-keto radical. Two α-keto radicals subsequently combine to form acetonylacetone. As for now, no suitable alternative photo absorber was found. The second method to potentially increase the conversion of acetone was to use

micellar reaction media. It was hypothesised that the introduction of confined areas in the core of the micelle would increase the local concentration of acetone and therefore increase its conversion. However, no increase in conversion of acetone was observed and product selectivity was decreased in the presence of surfactant. It was assumed that SDS performed hydrogen donation to an excited state acetone molecule, leading to the increased formation of pinacol. A third method employed to increase the conversion of acetone was the recirculation of the reaction mixture. This method proved the most successful with a 2.3-fold increase in total conversion of acetone after recycling the mixture three times. A productivity of 0.54 mmol/h was afforded for the conversion of acetone while the formation of acetonylacetone was achieved with a productivity of 0.20 mmol/h.

Preliminary studies were undertaken to perform photo-induced ketone dimerisation of 2-butanone, acetophenone and pinacolone. Product formation was observed in all cases, but no selective synthesis of the desired 1,4-diketone was achieved.

In summary, the formation of acetonylacetone *via* the photodimerisation of acetone was achieved with satisfactory productivity. The potential of this method has been demonstrated by the significant increase in product selectivity and reaction yield during initial optimisation studies. However, more research is required to optimise the method in order to increase the conversion of acetone and make it viable for its potential applications. Preliminary studies already revealed the potential use of surfactants in UV photochemical transformation for the successful reaction of less polar substrates in water.

Future Directions

Diffusion limitations of the radicals involved in this reaction may have had a large contribution to the low desired product formation. To overcome the diffusion restrictions, it could be interesting to perform the photo-induced dimerisation of ketones at elevated pressures. Water is hardly compressible and performing the ketone dimerisation in water at elevated pressures would most likely show little difference in terms of local ketone concentration. Therefore, the use of $scCO_2$ as a co-solvent could potentially be investigated. This supercritical fluid is compressible and could therefore potentially induce higher local concentration of ketones and that way limit diffusion restrictions.

Once routes are discovered to perform efficient ketone dimerisation, it would be interesting to enlarge the scope of ketones to test whether the developed method is applicable to a wide range of ketones. To maintain the environmental benign character of the reaction, surfactants could be used to solubilise the ketone in aqueous solutions as opposed to using organic solvents such as THF, MeCN or toluene to create homogenous reaction solutions. It has been reported that molecules can diffuse out of the SDS micelle relatively quickly (on the scale of 100 ps) due to a thin Stern layer, which is the shell around the micelle containing the hydrophilic head groups and the counter-ions of the surfactants.[16] Therefore, different surfactants could be utilised to inhibit this fast diffusion out of the micelle. This would allow for the possible observation of an effect on substrate conversion and product selectivity caused by this micro-heterogeneous environment. Non-ionic surfactants generally exhibit a thicker Stern layer to shield the material inside the micelle from the bulk water.[16a] As a result, diffusion of compounds in and out of the micelle is on the order of nanoseconds.[16a] Neutral surfactant such as polyoxyethylenealkyl ethers could therefore be interesting surfactants to investigate.[17] These ethers have a lower critical micelle concentration (cmc) than SDS due to their long alkyl tail. This allows for a lower concentration of surfactants in water to form micelles; reducing the amount of waste generated when the surfactant is disposed of. The use of dendrimers for solubilising apolar compounds in aqueous solutions has been reported to increase product selectivity and might be a viable route to investigate as well.[18]

Aim 5 To employ 1,4-diketones in the Paal-Knorr synthesis to form 2,5-dimethylfuran and several pyrrole derivatives.

Rationale

Pyrrole and furan derivatives have been acknowledged as examples of useful compounds and important building blocks in many functional materials and pharmaceuticals.[13d, 19] Some of the complex materials containing pyrrole moieties exhibit cytotoxic, antibacterial, antiviral and antioxidant activity.[13c, 13d, 19-20] Therefore, the direct synthesis of pyrrole and furan derivatives from simple ketones has been the topic of research for this Thesis. UV photochemistry can facilitate an atom economic route to transform ketones into 1,4-diketones, and especially clean when carried out in aqueous solutions. Subsequent reaction of

these 1,4-diketones into pyrrole and furan derivatives *via* Paal-Knorr synthesis would maintain the atom economic character of the reaction while introducing synthetic complexity.

Progress

Studies into the Paal-Knorr synthesis of 2,5-dimethylfuran and a variety of pyrrole derivatives showed the efficient formation of products in 2-24 h starting from acetonylacetone in batch. Five different primary amines were employed for the formation of pyrrole derivatives of which four resulted in high yielding products when the reaction was performed in water at elevated temperatures. With this reaction proceeding smoothly in water, there is no need to change reaction solvent after the photochemical generation of acetonylacetone in the UV reactor mentioned in Chapter 4. The formation of 2,5-dimethylfuran was accomplished using niobium phosphate as the solid acid catalyst. However, the reaction proceeded only in toluene. These encouraging results led to the use of the UV light based reaction mixture containing acetonylacetone to perform the Paal-Knorr synthesis in batch. Preliminary results reveal that the formation of the corresponding pyrrole occurred within 5 hours. However, no 2,5-dimethylfuran formation was observed.

In conclusion, acetonylacetone was successfully converted into a pyrrole derivative *via* the Paal-Knorr synthesis when using a UV reaction mixture containing acetonylacetone. This is a very encouraging result as the yield of acetonylacetone in the UV reaction mixture was low. Moreover, a variety of pyrrole derivatives were synthesised in batch using pure acetonylacetone. The synthesis of 2,5-dimethylfuran from acetonylacetone requires further study in order to use the output solution of the UV reaction containing acetonylacetone as the starting mixture for the Paal-Knorr synthesis.

Future directions

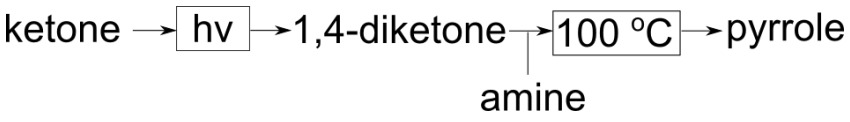
Highly functionalised pyrroles, furans and thiophenes are considered valuable chemical moieties as they occur in natural products, agrochemicals, functional materials and pharmaceuticals.[19a, 19b, 21] The Paal-Knorr synthesis has been performed on asymmetric and highly substituted 1,4-diketones before which demonstrates the potential of this method,[19c, 21b, 22] and it would be interesting to investigate the applicability of the designed route in this Thesis to the formation of asymmetric and highly substituted pyrroles, furans and thiophenes. To start,

the formation of functionalised heterocycles from 1,4-diketones derived from the photodimerisation reaction of acetophenone and 2-butanone could be investigated.

Further research could be directed into building a continuous flow reactor set-up containing multiple reactors. The first reactor would be the UV excimer reactor as described in Chapter 3 in this Thesis, coupled to a second reactor to form furan and pyrrole derivatives *via* the Paal-Knorr synthesis (Scheme 5-1). This could potentially provide an efficient and clean transformation from ketones directly to (highly substituted) furans and pyrroles *via* a single reaction set-up without any need for purification or solvent change at the intermediate stage. This method provides a route towards process intensification and could potentially minimise solvent waste due to this removal of a purification step after the 1,4-diketone formation.



(a)



(b)

Scheme 5-1 Daisy-chained process for the continuous synthesis of furans and pyrroles from ketones. 1,4-Diketones are formed via the UV light based photodimerisation of ketones in aqueous solution followed by a) the 1,4-diketone passing through a stainless steel reactor containing solid acid to undergo the Paal-Knorr transformation to the furan derivative; or b) the addition of a flow of primary amine to react with the 1,4-diketone at elevated temperatures in a stainless steel reactor to form the pyrrole derivative.

Final Word

The work in this Thesis has demonstrated that product selectivity can be achieved in a variety of synthetic transformation by employing various continuous flow photoreactors, using either UV or visible light. Moreover, more environmentally benign routes for the synthesis of compounds for widespread applications have been shown to proceed without compromising on efficiency. Synthetic photochemistry in general is showing enormous potential for selective transformations and the introduction of structural complexity in only a few steps.[2, 23] Based on the versatility of visible light photoredox catalysis, Staveness *et al*. predicted a rise of visible light-mediated methods in the pharmaceutical and commodity chemical sectors.[24] Therefore, I think it is important to continue to investigate the use of photochemistry in synthetic methods and apply these techniques on a larger scale.

Als je alles van tevoren wist,

dan kwam je met een

dubbeltje de wereld rond.

-Nederlands spreekwoord

Inès Penders, 24th of August 2017

References

1. (a) Sheldon, R. A., *Green Chem.* **2014,** *16*, 950-963; (b) Sheldon, R. A., *Chem. Soc. Rev.* **2012,** *41* (4), 1437-1451; (c) Sheldon, R. A., *J. Environ. Monit.* **2008,** *10* (4), 406-407; (d) Prat, D.; Pardigon, O.; Flemming, H.-W.; Letestu, S.; Ducandas, V.; Isnard, P.; Guntrum, E.; Senac, T.; Ruisseau, S.; Cruciani, P.; Hosek, P., *Org. Process Res. Dev.* **2013,** *17* (12), 1517-1525; (e) Henderson, R. K.; Jimenez-Gonzalez, C.; Constable, D. J. C.; Alston, S. R.; Inglis, G. G. A.; Fisher, G.; Sherwood, J.; Binks, S. P.; Curzons, A. D., *Green Chem.* **2011,** *13* (4), 854-862; (f) Hoffmann, N., *ChemSusChem* **2012,** *5* (2), 352-371.

2. Yoon, T. P.; Ischay, M. A.; Du, J., *Nat. Chem.* **2010,** *2* (7), 527-532.

3. (a) Gogoi, P.; Bezboruah, P.; Gogoi, J.; Boruah, R. C., *Eur. J. Org. Chem.* **2013,** *2013* (32), 7291-7294; (b) He, Z.; Jamison, T. F., *Angew. Chem.* **2014,** *126* (13), 3421-3425; (c) Tyman, J., *Synthetic and Natural Phenols*. Elsevier: New York: 1996; (d) Quideau, S.; Deffieux, D.; Douat-Casassus, C.; Pouységu, L., *Angew. Chem. Int. Ed.* **2011,** *50* (3), 586-621.

4. (a) Jiang, M.; Li, Y.; Yang, H.; Zong, R.; Jin, Y.; Fu, H., *RSC Adv.* **2014,** *4* (25), 12977-12980; (b) Zou, Y.-Q.; Chen, J.-R.; Liu, X.-P.; Lu, L.-Q.; Davis, R. L.; Jørgensen, K. A.; Xiao, W.-J., *Angew. Chem.* **2012,** *124* (3), 808-812.

5. Gazi, S.; Ananthakrishnan, R., *Appl. Catal., B.* **2011,** *105* (3–4), 317-325.

6. Augustine, R. L.; Tanielyan, S. K.; Mahata, N.; Gao, Y.; Zsigmond, A.; Yang, H., *Appl. Catal. A-Gen.* **2003,** *256* (1–2), 69-76.

7. Mehnert, C. P., *Chem. Eur. J.* **2005,** *11* (1), 50-56.

8. (a) Beller, H. R.; Lee, T. S.; Katz, L., *Nat. Prod. Rep.* **2015,** *32* (10), 1508-1526, and references therein; (b) Forney, F. W.; Markovetz, A. J., *J. Lipid Res.* **1971,** *12* (4), 383-395; (c) Javidpour, P.; Pereira, J. H.; Goh, E.-B.; McAndrew, R. P.; Ma, S. M.; Friedland, G. D.; Keasling, J. D.; Chhabra, S. R.; Adams, P. D.; Beller, H. R., *Appl. Environ. Microb.* **2014,** *80* (2), 497-505; (d) Cseke, L. J.; Kirakosyan, A.; Kaufman, P. B.; Warber, S.; Duke, J. A.; Brielmann, H. L., *Natural products from plants*. CRC press: Boca Raton, Florida, 2006.

9. (a) Boyd, I. W.; Zhang, J. Y., *Nucl. Instrum. Methods Phys. Res. B* **1997,** *121* (1–4), 349-356; (b) Griesbeck, A. G.; Maptue, N.; Bondock, S.; Oelgemöller, M., *Photochem. Photobiol. Sci.* **2003,** *2* (4), 450-451; (c) Sosnin, E. A.; Oppenländer, T.; Tarasenko, V. F., *J. Photochem. Photobiol. C Photochem. Rev.* **2006,** *7* (4), 145-163; (d) Lomaev, M. I.; Sosnin, E. A.; Tarasenko, V. F., *Chem. Eng. Technol.* **2016,** *39* (1), 39-50; (e) DeLaney, E. N.; Lee, D. S.; Elliott, L. D.; Jin, J.; Booker-Milburn, K. I.; Poliakoff, M.; George, M. W., *Green Chem.* **2017,** *19* (6), 1431-1438.

10. Shiraishi, Y.; Tsukamoto, D.; Hirai, T., *Org. Lett.* **2008,** *10* (14), 3117-3120.

11. (a) Fang, W.; Liu, S.; Nie, Y., *Molecules* **2011,** *16* (8), 6243; (b) Li, S.-H.; Wang, J.; Niu, X.-M.; Shen, Y.-H.; Zhang, H.-J.; Sun, H.-D.; Li, M.-L.; Tian, Q.-E.; Lu, Y.; Cao, P.; Zheng, Q.-T., *Org. Lett.* **2004,** *6* (23), 4327-4330; (c) Furusaki, A.; Matsumoto, T.; Ogura, H.; Takayanagi, H.; Hirano, A.; Omura, S., *J. Chem. Soc., Chem. Commun.* **1980,** (15), 698; (d) He, H.; Ding, W.-D.; Bernan, V. S.; Richardson, A. D.; Ireland, C. M.; Greenstein, M.; Ellestad, G. A.; Carter, G. T., *J. Am. Chem. Soc.* **2001,** *123* (22), 5362-5363.

12. (a) Bharadwaj, A. R.; Scheidt, K. A., *Org. Lett.* **2004,** *6* (14), 2465-2468; (b) Cho, H.; Madden, R.; Nisanci, B.; Torok, B., *Green Chem.* **2015,** *17* (2), 1088-1099; (c) Amarnath, V.; Amarnath, K., *J. Org. Chem.* **1995,** *60* (2), 301-307; (d) Amarnath, V.; Anthony, D. C.; Amarnath, K.; Valentine, W. M.; Wetterau, L. A.; Graham, D. G., *J. Org. Chem.* **1991,** *56* (24), 6924-6931.

13. (a) Parida, B. B.; Das, P. P.; Niocel, M.; Cha, J. K., *Org. Lett.* **2013,** *15* (7), 1780-1783, and references therein; (b) Xue, S.; Li, L.-Z.; Liu, Y.-K.; Guo, Q.-X., *J. Org. Chem.* **2006,** *71* (1), 215-218; (c) Mao, S.; Gao, Y.-R.; Zhang, S.-L.; Guo, D.-D.; Wang, Y.-Q., *Eur. J. Org. Chem.* **2015,** *2015* (4), 876-885; (d) Mao, S.; Zhu, X.-Q.; Gao, Y.-R.; Guo, D.-D.; Wang, Y.-Q., *Chem. Eur. J.* **2015,** *21* (32), 11335-11339.

14. (a) Setzer, P.; Beauseigneur, A.; Pearson-Long, M. S. M.; Bertus, P., *Angew. Chem.* **2010,** *122* (46), 8873-8876; (b) Setzer, P.; Forcher, G.; Boeda, F.; Pearson-Long, M. S. M.; Bertus, P., *Eur. J. Org. Chem.* **2014,** *2014* (1), 171-180; (c) Chan, C.-K.; Chan, Y.-L.; Tsai, Y.-L.; Chang, M.-Y., *J. Org. Chem.* **2016,** *81* (17), 8112-8120; (d) Luo, J.; Jiang, Q.; Chen, H.; Tang, Q., *RSC Adv.* **2015,** *5* (83), 67901-67908; (e) Rössle, M.; Werner, T.; Frey, W.; Christoffers, J., *Eur. J. Org. Chem.* **2005,** *2005* (23), 5031-5038.

15. Zhao, W.; Fink, D. M.; Labutta, C. A.; Radosevich, A. T., *Org. Lett.* **2013,** *15* (12), 3090-3093.

16. (a) Bhattacharyya, K., *Acc. Chem. Res.* **2003,** *36* (2), 95-101; (b) Stigter, D., *J. Phys. Chem.* **1975,** *79* (10), 1008-1014.

17. Dwars, T.; Paetzold, E.; Oehme, G., *Angew. Chem. Int. Ed.* **2005,** *44* (44), 7174-7199.

18. Kaanumalle, L. S.; Nithyanandhan, J.; Pattabiraman, M.; Jayaraman, N.; Ramamurthy, V., *J. Am. Chem. Soc.* **2004,** *126* (29), 8999-9006.

19. (a) Alizadeh, A.; Rezvanian, A.; Bijanzadeh, H. R., *Synthesis* **2008,** *2008* (05), 725-728; (b) Bellina, F.; Rossi, R., *Tetrahedron* **2006,** *62* (31), 7213-7256; (c) Tang, J.; Yang, M.; Yang, M.; Wang, J.; Dong, W.; Wang, G., *New J. Chem.* **2015,** *39* (6), 4919-4923.

20. (a) Binder, J. T.; Kirsch, S. F., *Org. Lett.* **2006,** *8* (10), 2151-2153, and references therein; (b) Boger, D. L.; Boyce, C. W.; Labroli, M. A.; Sehon, C. A.; Jin, Q., *J. Am. Chem. Soc.* **1999,** *121* (1), 54-62; (c) Wang, C.; Dong, H.; Hu, W.; Liu, Y.; Zhu, D., *Chem. Rev.* **2012,** *112* (4), 2208-2267; (d) Khalili, B.; Jajarmi, P.; Eftekhari-Sis, B.; Hashemi, M. M., *J. Org. Chem.* **2008,** *73* (6), 2090-2095.

21. (a) Minetto, G.; Raveglia, L. F.; Taddei, M., *Org. Lett.* **2004,** *6* (3), 389-392; (b) Alnabulsi, S.; Santina, E.; Russo, I.; Hussein, B.; Kadirvel, M.; Chadwick, A.; Bichenkova, E. V.; Bryce, R. A.; Nolan, K.; Demonacos, C.; Stratford, I. J.; Freeman, S., *Eur. J. Med. Chem.* **2016,** *111*, 33-45.

22. Almeida, Q. A. R., *Green Chem. Lett. Rev.* **2013,** *6* (2), 129-133.

23. (a) Ghosh, I.; Ghosh, T.; Bardagi, J. I.; König, B., *Science* **2014,** *346* (6210), 725-728; (b) Rossi, R. A.; Pierini, A. B.; Peñéñory, A. B., *Chem. Rev.* **2003,** *103* (1), 71-168; (c) Hernández-Linares, M. G.; Guerrero-Luna, G.; Pérez-Estrada, S.; Ellison, M.; Ortin, M.-M.; Garcia-Garibay, M. A., *J. Am. Chem. Soc.* **2015,** *137* (4), 1679-1684.

24. Staveness, D.; Bosque, I.; Stephenson, C. R. J., *Acc. Chem. Res.* **2016,** *49* (10), 2295-2306.

Chapter 6 Experimental

This Chapter describes the experimental procedures, equipment and materials used in the work outlined in this Thesis. Detailed standard operating procedures and shutdown procedures for the photoreactors can be found in the Appendix.

6.1 Materials and General Procedures

^{1}H NMR spectra were recorded in $CDCl_3$ on either a Bruker AV 400 MHz, a Bruker AV III 400 MHz or a Bruker DPX 400 MHz. Chemical shifts are given in ppm. Coupling constants (*J*) are given in Hertz (Hz) and the following abbreviations are used to designate the multiplicity of each signal: s = singlet; d = doublet; t = triplet; q = quartet; qu = quintuplet; m = multiplet; br = broad. UV-Vis experiments were carried out on a Perkin Elmer Lambda 25 spectrometer. Diffuse reflectance UV-Vis spectra were taken using a DT-MINI-2-GS UV-Vis-NIR light source consisting of both a deuterium and halogen lamp, fibre optics (model P200-2-Vis-NIR, OOS-001311-04) and a USB-2000+UV-Vis-ES detector, all from Ocean Optics. A zero background PXRD silica plate was used as the ideal reflecting surface.

High-resolution mass spectra were recorded on a Bruker MicroTOF spectrometer using a positive electrospray ionisation (ESI) method. Excitation, emission and lifetime data was collected using Edinburgh Instruments with either a Xe900 lamp or a picosecond pulsed diode laser (model EPL-405) from the same make. Solid

samples were mounted on adhesive in the sample compartment of the fluorometer and were aligned carefully in the focus of either the lamp or the laser. Gas Chromatography analysis was carried out on a GC-2014 Shimadzu chromatograph, fitted with a chiral BetaDex 225 column (column ID 19708-03A). The oven temperature program was set to ensure optimal compound separation (see below).

Chemicals were purchased from commercial suppliers and were used without further purification unless stated otherwise.

6.1.1 Quantum Chemical Calculations

The Gaussian 03 package together with the B3LYP functional[1] and the 6-311G+(d,p) basis set were used to carry out density functional theory (DFT) calculations. IR and Raman frequency calculations were performed on optimised ground state structures. Employing GaussSum, the output frequencies were scaled by a factor of 0.975.[2] The vibrational modes were visualised with Avogadro application version 1.1.1. For open-shell complexes which exhibit doublet or triplet multiplicity, an unrestricted B3LYP method was used. Solvent fields were added with the integral equation formalism, polarisable continuum model (IEF PCM). As *N*,*N*-dimethylformamide (DMF) was not a default solvent option in Gaussian 03, the values stated in Table 6-1 were written in the Gaussian input file.[3]

Table 6-1 Solvent field parameters for DMF for the use of DFT calculations with Gaussian.

Parameter	**Gaussian abbreviation**	**Values at 298 K**
Dielectric constant (unitless)	eps	36.71
Dielectric constant at infinite frequency (unitless)	epsinf	1.75
Molecular radius (Å)	rsolv	2.647
Density ($Å^{-3}$)	density	0.00778

Thermodynamic information was obtained from a frequency calculation of the molecule in the ground state. The Gibbs free energy was taken as the sum of the total electronic energy (ε_0) and the thermal free energy (G_{corr}). The zero-point correction was added to this value. Berry transition states were calculated using

the same basis set, function and solvent model, calculating one force constant. Excited state energies were calculated using time-dependent DFT (TD DFT), with again the same basis set, function and solvent model. The optimised ground state structure was employed as the input geometry for the calculation of both singlet and triplet excited states and the lowest 10 excited states were obtained. The transitions were visualised using GaussSum, stating the wavelength of the transition and the oscillator strength. The nature of the transition was elucidated with Avogadro application version 1.1.1.

6.2 Visible Light Photochemistry

Visible light LEDs were employed as the light source in the visible light photochemistry reactions. Batch experiments were carried out at both ambient and elevated pressures. The experimental set-up at ambient pressure consisted of a round bottom flask containing all reagents, equipped with a condenser, positioned in a water bath. Batch experiments were also carried out in specialised high-pressure equipment using $scCO_2$ as a solvent. Continuous flow experiments were carried out in specialised high-pressure equipment, using both conventional organic solvents and $scCO_2$. The Sections below describe the equipment and experimental procedures used.

6.2.1 Visible Light Sources

For batch experiments at ambient pressures, visible light irradiation was carried out using a fan cooled bank of Citizen Electronics Co. Ltd 1000 lumen white light LEDs (arranged in set of 5 diode arrays, part code CL-L233-C13N1-C, Figure 6-1a). The continuous photochemistry set-up contained the same Citizen white light LEDs, but mounted on a water cooled bank (arranged in 3 sets of 5 diode arrays, part code CL-L233-C13N1-C, Figure 6-1b).



(a) (b)

Figure 6-1 Pictures of a) fan cooled white light LED bank, b) water cooled white light LED bank.

Batch experiments at high-pressure were carried out using a single white light LED (1000 lumen, OSRAM, part code: LEUWE3B-PZQZ-4C8F). This LED was mounted on an aluminium heat sink, fitted with a cooling fan (Figure 6-2). The LED was placed in front of the window of the batch cell (see Section 6.2.3.1) which matches the LED in diameter so that all light can enter the photochemical batch cell.

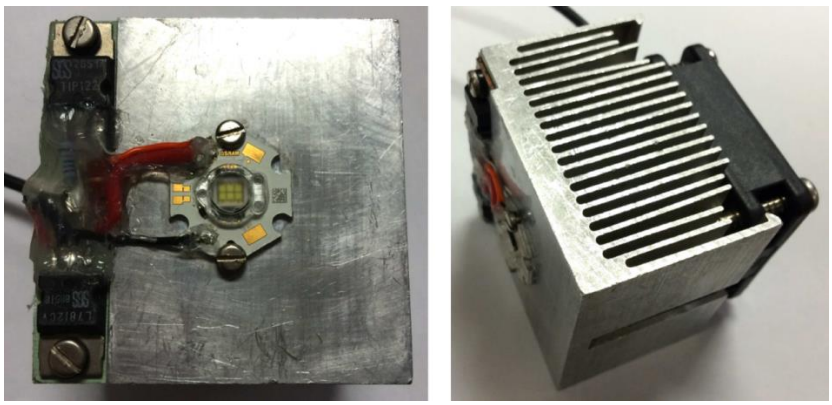
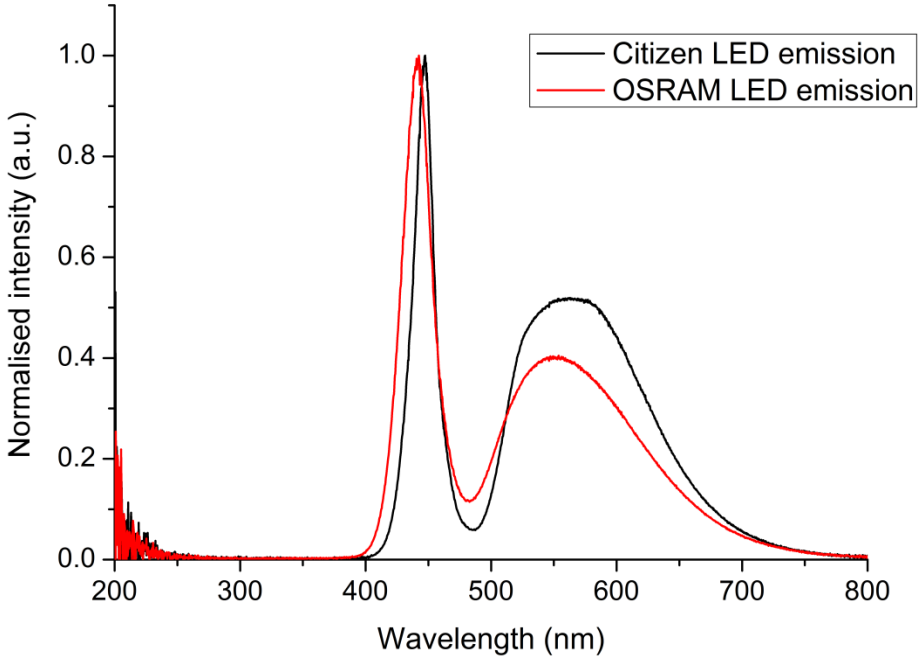
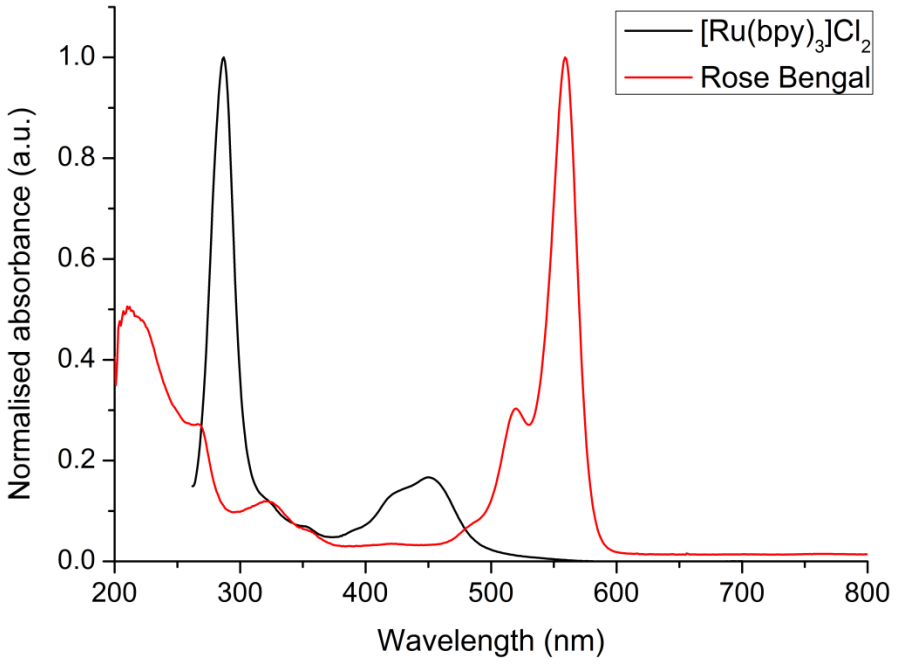


Figure 6-2 Pictures of the single white light LED used in high-pressure batch experiments.[4]

To ensure efficient excitation of the photocatalyst by the incoming light, the emission of the LED light source must match the absorption of the photocatalyst. Figure 6-3 shows the output of both the OSRAM and Citizen white light LEDs and the absorbance spectra of the photocatalysts used in this project.



(a)

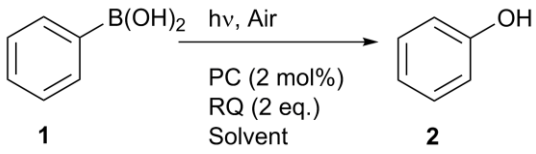


(b)

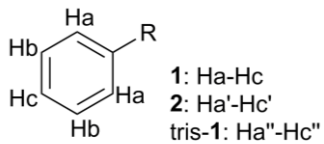
Figure 6-3 a) The spectral output of both the Citizen and OSRAM type white LED lights and b) the absorbance spectra of both $[Ru(bpy)_3]Cl_2$ and Rose Bengal (recorded in EtOH).

6.2.2 Batch Experiments at Ambient Pressure

6.2.2.1 Hydroxylation of Phenylboronic Acid to Phenol



The aerobic hydroxylation of phenylboronic acid was carried out according to the method described by Zou *et al*.[5] Phenylboronic acid (**1**) (50 mg, 0.41 mmol, 1 eq.), reductive quencher (RQ, 0.82 mmol, 2 eq.) and photocatalyst (PC, 8.2 µmol, 2 mol%) were added to 4 mL of solvent. The solution was stirred at room temperature under LED light irradiation in a round bottom flask equipped with a condenser open to air until full conversion to phenol (**2**) was reached. The reaction was monitored using ^{1}H NMR. Aliquots used for analysis were extracted with diethyl ether (3 x 5 mL) followed by washing with brine and drying with Na_2SO_4. ^{1}H NMR (400 MHz, $CDCl_3$) δ (ppm) 8.26 (d, *J* = 7.2 Hz, 2H, **1** Ha), 7.77 (d, *J* = 7.2 Hz, 2H, tris-**1** Ha''), 7.62 (t, *J* = 7.4 Hz, 1H, **1** Hc), 7.52 (t, *J* = 7.4 Hz, 2H, **1** Hb), 7.49 (t, *J* = 7.4 Hz, 1H, tris-**1** Hc''), 7.41 (t, *J* = 7.2 Hz, 2H, tris-**1** Hb**''**), 7.25 (t, *J* = 8.0 Hz, 2H, **2** Hb'), 6.92 (t, *J* = 7.4 Hz, 1H, **2** Hc'), 6.84 (d, *J* = 8.0 Hz, 2H, **2** Ha').

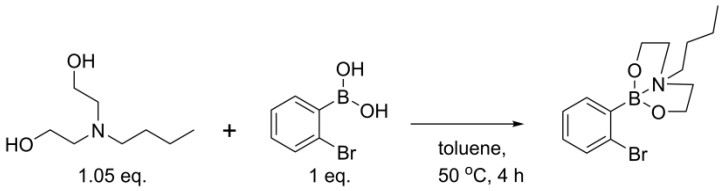


Solvents: *N*,*N*-dimethylformamide (DMF), methanol (MeOH)

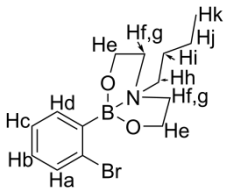
Reductive quenchers: *N*,*N*-diisopropylethylamine (DIPEA), triethylamine (TEA), ascorbic acid (H_2A)

Photocatalysts: Rose Bengal (RB), $[Ru(bpy)_3]Cl_2.6H_2O$

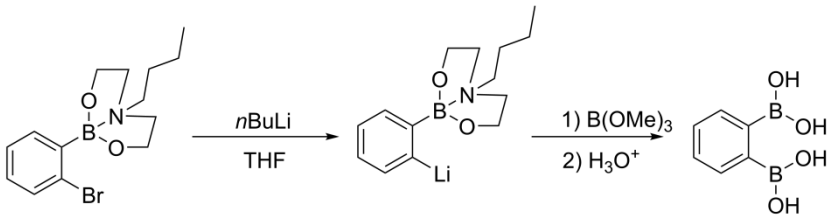
6.2.2.2 Synthesis of 1,2-Benzenediboronic Acid



The synthesis of 2-(2'-bromophenyl)-butyl[1,3,6,2]dioxazaborocane, a precursor in the synthesis of 1,2-benzenediboronic acid, was carried out according to a patent by Anacor Pharmaceuticals Inc.[6] *N*-butyldiethanolamine (8.55 mL, 52.3 mmol, 1.05 eq.) was added dropwise to a suspension of 2-bromophenylboronic acid (10.0 g, 49.8 mmol, 1 eq.) in toluene (105 mL). This mixture was stirred continuously and heated at 50 °C for 4 hours, after which the reaction mixture was allowed to cool. Subsequently, toluene was removed under reduced pressure and heptane (100 mL) was added to the flask. After sonication for 10 minutes, the mixture was left overnight at room temperature. The white precipitate formed was filtered off, washed with heptane and dried in a vacuum for 6 hours to yield the product in 95.8 % (15.28 g). ^{1}H NMR (400 MHz, $CDCl_3$)



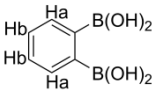
δ (ppm) 7.83 (dd, *J* = 7.5, 1.9 Hz, 1H, Hd), 7.53 (dd, *J* = 7.9, 1.2 Hz, 1H, Ha), 7.26 (td, *J* = 7.5, 1.2 Hz, 1H, Hb), 7.12 (td, *J* = 7.2, 1.9 Hz, 1H, Hc), 4.26-4.14 (m, 4H, He), 3.37-3.31 (m, 2H, Hf), 3.10-3.05 (m, 2H, Hg), 2.70-2.66 (m, 2H, Hh), 1.63-1.55 (m, 2H, Hi), 1.22 (sextet, *J* = 7.5, 2H, Hj), 0.88 (t, *J* = 7.5, 3H, Hk). ^{13}C NMR (400 MHz, $CDCl_3$) δ (ppm) 136.9 (**C**H), 133.4 (**C**H), 129.4 (**C**H), 126.3 (**C**H), 63.0 (**C**H_2), 58.3 (2x **C**H_2), 58.3 (2x **C**H_2), 27.1 (**C**H_2), 20.2 (**C**H_2), 13.8 (**C**H_3). Quaternary carbons could not be allocated.



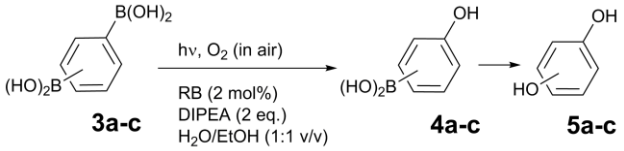
The synthesis of 1,2-benzenediboronic acid from 2-(2'-bromophenyl)-butyl[1,3,6,2]dioxazaborocane was carried out according to the procedure reported by Durka *et al.*[7]

n-BuLi (2.5 M in hexane) was titrated against menthol and 4,4'-dimethyl-2,2'-dipyridyl prior to use to confirm its activity. A flame-dried two-necked round bottom flask was charged with dry THF (120 mL) at -90 °C, followed by *n*-BuLi (15.6 mL, 2.5 M in hexane, 39 mmol, 1.05 eq.) under oxygen-free conditions. A solution of 2-(2'-bromophenyl)-butyl[1,3,6,2]dioxazaborocane (12.2 g, 37.5 mmol, 1 eq.) in THF (37.5 mL) was added dropwise to the solution in the round bottom flask at -90 °C. The reaction mixture was allowed to reach -75 °C,

and was left to react for 1.5 hours while being continuously stirred. The resulting white slurry was cooled to -90 °C after which trimethyl borate (4.8 mL, 39 mmol, 1.05 eq.) was added extremely slowly while maintaining the reaction temperature below -85 °C. After a further reaction time of 20 minutes, the mixture was allowed to reach -30 °C after which it was hydrolysed with aqueous HCl (10 %, 45 mL). The layers were separated and the water phase was washed with diethyl ether (3 x 30 mL). Subsequently, all organic layers were combined and concentrated under reduced pressure. A white precipitate was formed when hexane was added and this was dried under vacuum overnight to yield 1,2-benzenediboronic acid (37.6 mg, 0.6 %). ^{1}H NMR (400 MHz, D_2O) δ (ppm) 8.16 (*br* s, 4H, B(O**H**)$_2$), 7.60 (dd, *J* = 5.5, 3.3 Hz , 2H, Hb), 7.31 (dd, *J* = 5.4, 3.3 Hz, 2H, Ha). ^{13}C NMR (400 MHz, D_2O) δ (ppm) 133.6 (2x **C**H), 128.02 (2x **C**H) ^{11}B NMR (400 MHz, D_2O) δ (ppm) 19.4. Minor signals other than the signals for 1,2-benzenediboronic acid were present in the ^{1}H (7.50 (m), 7.40 (m)), ^{11}B (29.10 ppm (s)) and ^{13}C (133.3, 132.3, 131.7, 131.1, 129.0, 126.7 ppm) spectra and could potentially correspond to benzoxadiborole and other small impurities.

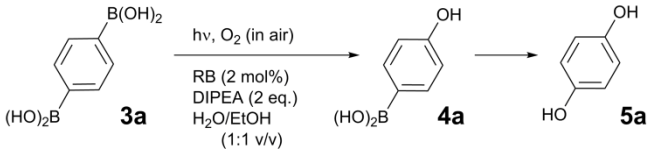


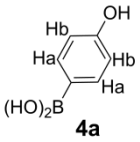
6.2.2.3 Desymmetrisation of Aryl Diboronic Acids



Rose Bengal (RB, 10.4 mg, 10 µmol, 2 mol%) and DIPEA (179 µL, 1.0 mmol, 2 eq.) were added to a solution of **3a-c** (83 mg, 0.50 mmol, 1 eq.) in H_2O/EtOH (1:1 v/v, 10 mL). The solution was stirred at room temperature under LED light irradiation in a round bottom flask equipped with a condenser open to air until completion. Aliquots were quenched with 10 % HCl before the solvent was evaporated under reduced pressure and ^{1}H NMR spectra were recorded. The reaction with substrate **3c** was carried out on a 2.2-fold lower scale than the conditions described above.

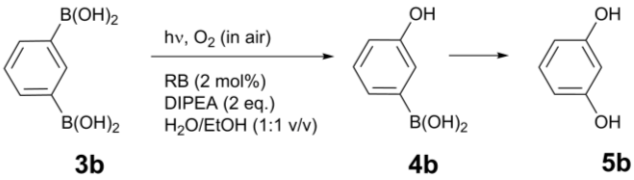
Desymmetrisation of 1,4-benzenediboronic acid (3a)

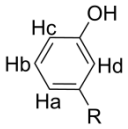




^{1}H NMR of **4a** (400 MHz, DMSO-d_6): δ (ppm) 9.45 (*br* s, 1H, Ar-O**H**), 7.60 (d, J = 8.5 Hz, 2H, Ha), 6.70 (d, J = 8.5 Hz, 2H, Hb). ^{1}H NMR of **5a** (400 MHz, DMSO-d_6): δ (ppm) 8.79 (*br* s, 2H, Ar-O**H**), 6.55 (s, 4H, Ar-**H**).

Desymmetrisation of 1,3-benzenediboronic acid (3b)

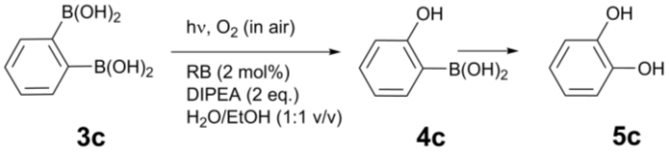


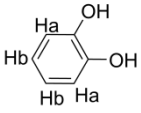


4b: Ha-Hd
5b: Ha'-Hd'

^{1}H NMR of **4b** (400 MHz, DMSO-d_6): δ (ppm) 9.12 (*br* s, 1H, Ar-O**H**), 7.89 (*br* s, 2H, B(O**H**)$_2$), 7.19 (m, 2H, Hc, Hd), 7.11 (t, J = 7.4 Hz, 1H, Hb), 6.79 (m, 1H, Ha). ^{1}H NMR of **5b** (400 MHz, DMSO-d_6): δ (ppm) 9.15 (*br* s, 2H, Ar-O**H**), 6.88 (t, J = 7.8 Hz, 1H, Hb'), 6.22 (m, 3H, Ha', Hc', Hd'). The spectral data of **5b** matches that of the literature.[8]

Desymmetrisation of 1,2-benzenediboronic acid (3c)





^{1}H NMR of **5c** (400 MHz, D_2O): δ (ppm) 6.84 (m, 2H, Hb), 6.78 (m, 2H, Ha).

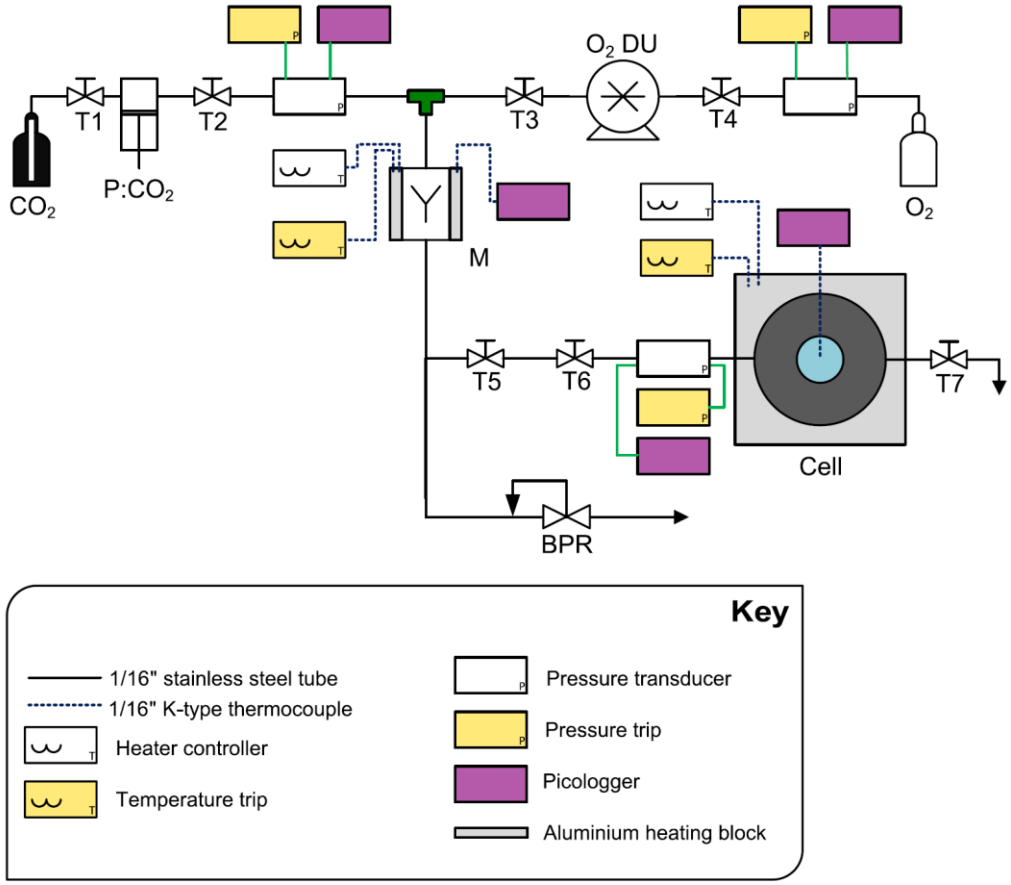
6.2.3 High-pressure Equipment

High-pressure experiments were carried out in both batch and continuous flow fashion. Descriptions of these reactor set-ups and general reaction procedures are presented in the Sections below. Full standard operating procedures (SOPs) can be found in the Appendix.

6.2.3.1 Batch Reactions at High-pressure

For the work described in this Thesis, the hydroxylation of phenylboronic acid to phenol was carried out in batch at elevated pressure using a reactor built in-house, developed previously in the research group.[4, 9] Many elements in the apparatus for this reactor were identical to the continuous flow reactors described in later Sections. The different parts of the rig are connected by 1/16'' outer diameter stainless steel tubing using primarily Swagelok™ fittings (Scheme 6-1, adapted from the Thesis by J. Bellamy).[4] The only exception is the connections of the 1/16'' tubing with the pressure transducer; these are Scientific Systems, Inc. (SSI) fittings. High Pressure Equipment Company (HiP) provided the manual valves. CO_2 is delivered into the reactor system *via* a Jasco™ PU-1580-CO_2 pump. A modified six port HPLC Rheodyne® 7000L was used to dose oxygen into the reactor. Two sample loops, which can be varied in size, are connected to two of these ports to regulate the amount of oxygen administered to the reactor system. A rotor driven valve switches between those two sample loops to simultaneously deliver oxygen to the system out of one sample loop and fill the other sample loop with oxygen from the cylinder. The oxygen dosage is dictated by both the size of the sample loops and the rotor switching speed. Further details on this dosage unit can be found in the Thesis by J. Bellamy.[4] The CO_2 and O_2 streams are connected *via* a stainless steel T-piece and mix further in a mixing chamber (M). Initially, manual valve T5 is closed and the gas stream exits the reactor *via* the back pressure regulator (BPR) which is set to the desired pressure (typically 190 bar). Reagents other than CO_2 and O_2 are added to the view cell, which was developed in-house to monitor reactions at high-pressure *in situ*.[10] This cell contains two CaF_2 windows (0.6" diameter, 0.4" thickness) which are glued into a stainless steel body and a removable holder. By removing the holder, reagents can be placed into the stainless steel body of the view cell and after

screwing the holder back in, the cell is sealed leaving an internal volume of 1.47 mL. The temperature of the view cell is maintained by the positioning of an external heating block (controlled *via* a Tempatron TC4800 temperature controller) around the stainless steel cell. A thermocouple placed inside the view cell monitors the reaction temperature.



Scheme 6-1 Representation of the high-pressure batch photochemical reactor, adapted from the Thesis by J. Bellamy.[4] The labelling is as follows: CO_2 - delivered from a chilled Jasco™ PU-1580-CO_2 pump; O_2 - added via a Rheodyne® dosage unit (DU); BPR - Jasco™ BP-1580-81 back pressure regulator; M - mixing chamber 15 cm 1/4'' SS316 tubes at 50 °C, surrounded by an aluminium heating block; PT - pressure transducer (RDP Electronics); Cell - view cell with 5 mm path length (1.47 mL) and a LED block with 1 LED light placed in front of the window; T1-7 - manual valve.

Once the gas mixture is equilibrated, valves T5 and T6 are opened extremely slowly to introduce the CO_2 and O_2 into the view cell. When the cell reaches the set pressure, manual valves T5 and T6 are closed to isolate the cell and a LED block positioned in front of the CaF_2 window in the view cell is turned on to start irradiation of the reaction mixture. Meanwhile, the rest of the system is depressurised and both the CO_2 and O_2 flow are stopped while the area between

manual valves T5 and T7 maintains the desired pressure. After irradiation, manual valve T7 is opened very slowly to release pressure from the high-pressure cell, followed by the product collection from the view cell.

General reaction procedure for the hydroxylation of phenylboronic acid to phenol in batch at high-pressure

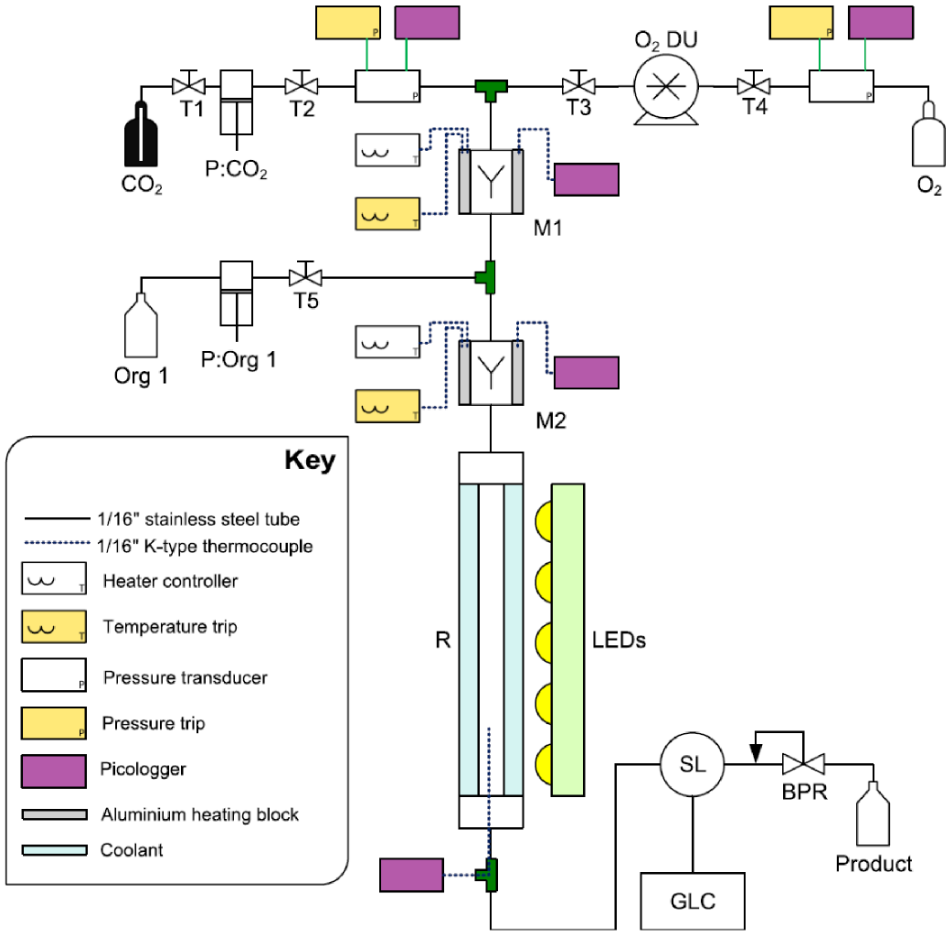
The batch cell was filled with phenylboronic acid (5.4 mg, 0.1 M in ethyl acetate), $[Ru(bpy)_3]Cl_2.6H_2O$ (0.6 mg, 0.88 µmol, 2 mol%) and reductive quencher (88.6 µmol, 2 eq.) after which the cell was closed. Ethyl acetate (440 µL, which resulted in 30 % in $scCO_2$ during the reaction) was added *via* the top of the cell. After heating the cell to 40 °C, a mixture of 3.7 % O_2 in $scCO_2$ at 190 bar was slowly added to the batch cell until the pressure in the cell read 190 bar. The batch cell was isolated and a LED block with one LED (1000 lumen) was placed in front of the batch cell. After irradiation for 4 h, the batch cell was slowly depressurised and product was collected. An aliquot was taken for ^1H NMR analysis to measure the conversion.

Reductive quenchers: DIPEA, TEA

The continuous hydroxylation of phenylboronic acid to phenol was carried out in both conventional solvents and $scCO_2$. The following Sections will describe the reactor set-ups used in both types of experiments.

6.2.3.2 Flow Reactions at High-pressure with $scCO_2$

High-pressure experiments were carried out using a sapphire tube continuous flow reactor set-up. First generations of this flow rig were designed by R. Bourne, X. Han and further developed by J. Bellamy.[4, 9b, 11] Originally, this reactor was built for photochemical reactions involving $^1O_2$ in $scCO_2$. Both CO_2 and O_2 are dosed into the reactor *via* the same set-up as described for the high-pressure batch reactor (Scheme 6-2).



Scheme 6-2 Representation of the high-pressure continuous flow reactor, adapted from the Thesis by J. Bellamy.[4] The labelling is as follows: CO_2 - delivered from a chilled Jasco™ PU-1580-CO_2 pump; O_2 – added via a Rheodyne® dosage unit (DU); T1-5 - manual valve; BPR - Jasco™ BP-1580-81 back pressure regulator; M1/M2 - mixing chamber 15 cm 1/4" SS316 tubes at 50 °C, surrounded by an aluminium heating block; Org 1 - reaction mixture containing the photocatalyst, reductive quencher and substrate, dissolved in the required solvent system, which is pumped by P:Org 1 (Jasco™ PU-980 HPLC pump); R - sapphire tube reactor, which is temperature controlled via a recirculating water/ethylene glycol bath (1:1 v/v); LEDs - light source (3 × 5 × Citizen Electronics Co. Ltd CL-L233-C13N1-C mounted on water cooled stainless steel blocks); SL - high-pressure sample loop to allow for in-line GC sampling of the reaction mixture; GLC - Shimadzu GC-17A gas chromatograph

After mixing in static mixer M1, CO_2 and O_2 are combined with a flow of reaction mixture (Org 1) pumped into the reactor *via* a Jasco™ PU-980 HPLC pump. By altering the flow rates of both gases and the reaction mixture, the concentration of reactants in the reactor can be controlled. After further mixing in M2, the gas-liquid mixture enters the sapphire tube reactor (R). Reactor R is primarily constructed from stainless steel and contains a sapphire tube (Saint-Gobain crystals, 10 mm OD, 120 mm long, 1 mm wall thickness) in its centre (Figure

6-4). The sapphire tube is held in place by EPDM O-rings at both the top and bottom of the tube and is connected to the flow of reagents *via* 1/8" Autoclave Engineer fittings. A thermocouple is placed in the middle of the sapphire tube to monitor the reaction temperature. Surrounding the sapphire tube is a cylindrical sheet of Lexan™ (18 mm OD, 2 mm wall thickness, 95 mm in length) which is transparent to visible LED light. Cooling liquid is recirculated in the area between the sapphire tube and the Lexan™ casing (*ca* 2 mm) to ensure efficient temperature control. Three water cooled LED blocks are positioned in the stainless steel construction and provide irradiation of the reaction mixture. Glass beads (6 mm diameter) were loaded into the sapphire tube. The irradiated volume was 4.3 mL without the glass beads and 2.8 mL with the glass beads. The total volume of the sapphire tube reactor was 6.2 mL without the glass beads and 4.0 mL with the glass beads. After irradiation, the reaction mixture passes through a GC sample loop, in order to take aliquots when desired, and a back pressure regulator (BPR).



(a) (b)

Figure 6-4 a) Photo of the visible light photoreactor containing the sapphire tube, b) photo of the visible light photoreactor with the sapphire tube filled with glass beads and surrounded by 2 of the 3 LED blocks.

General reaction procedure for the hydroxylation of phenylboronic acid in continuous flow with $scCO_2$

Before starting a reaction, the rig was flushed with CO_2 for 30 minutes at 1.0 mL/min, 180 bar and 40 °C. Afterwards, the CO_2 flow rate was set to the appropriate flow rate for the reaction and O_2 was added to this flow so that the oxygen concentration was 3.7 % of the total reactants flow. Subsequently, the flow of organics was started from a HPLC pump. The content of this organic substrate mixture is described in the Sections below. The flow of substrate, $scCO_2$ and O_2 was pumped through the reactor where it was irradiated by 1000 lumen white light LEDS, mounted on 3 stainless steel banks (each bank equipped with 5 LEDs). The reactor temperature and the temperature of the LED blocks were maintained at 40 and 25 °C respectively. A switching valve between a sample loop and the outlet of the sapphire tube reactor allowed for the in-line analysis of the reaction mixture by GC. The GC method consisted of a 2 min. hold at 50 °C before increasing the temperature to 85 °C at a speed of 10 °C/min. After a 5 min. hold, the temperature was increased further to 300 °C at 20 °C/min. The conversion of the reaction was calculated by the ratio of the internal standard mesitylene (RT=5.50 and 5.96 min.) to phenol (RT=5.83 min.). After the reaction was terminated, pure CO_2 was pumped through the reactor for 30 min. to remove oxygen. Then, the whole system was depressurised and pure co-solvent was flushed through the rig for 45 min. at 5 mL/min after which a $scCO_2$ flow at 1 mL/min, 180 bar and 40 °C was used to remove any solvent residues.

Method 1

Procedure as described above with the organic reaction mixture containing MeOH (40 mL), phenylboronic acid (500 mg, 4.0 mmol, 1 eq., 0.1 M in MeOH), DIPEA (1.43 mL, 8.2 mmol, 2 eq.), mesitylene (570 µL, 1 eq.) and $[Ru(bpy)_3]Cl_2.6H_2O$ (60 mg, 0.8 mmol, 2 mol%). Using a flow rate of 0.5 mL/min for $scCO_2$ and 0.05 mL/min for the organics mixture, 10 vol% of MeOH was achieved in $scCO_2$. The molar ratio of O_2 to substrate was a 40:1 molar excess.

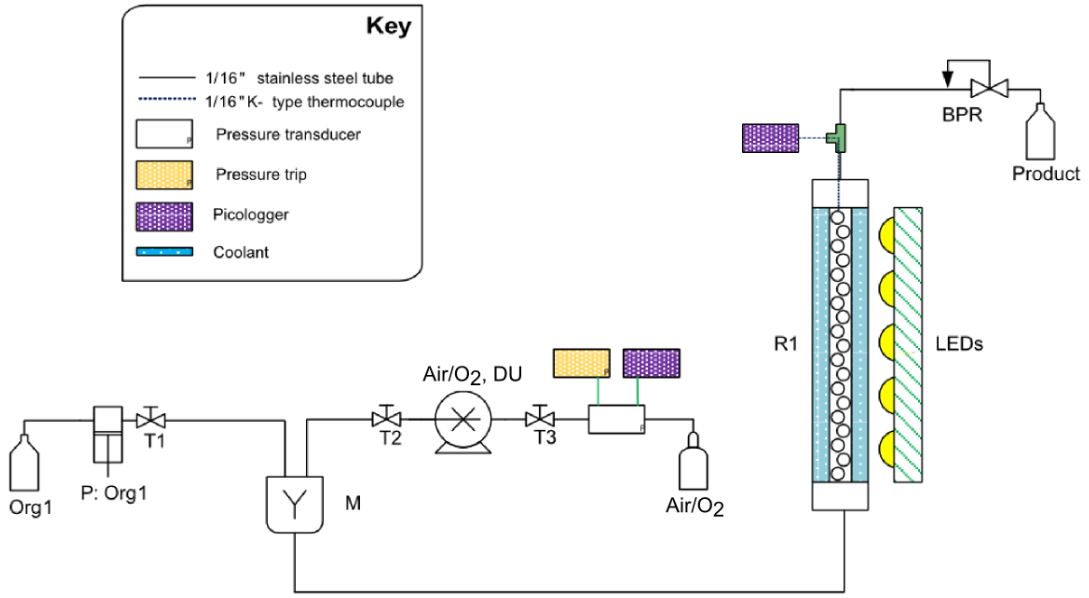
Method 2

Procedure as described above with the organics mixture containing EtOAc (40 mL), phenylboronic acid (500 mg, 4.0 mmol, 1 eq., 0.1 M in EtOAc), DIPEA (1.43 mL, 8.2 mmol, 2 eq.), mesitylene (570 µL, 1 eq.) and $[Ru(bpy)_3]Cl_2.6H_2O$ (60 mg, 0.8 mmol, 2 mol%). This mixture was sonicated for 30 minutes to

dissolve the photocatalyst in EtOAc. Using a flow rate of 0.3 mL/min for $scCO_2$ and 0.1 mL/min for the organics mixture, 10 vol% of EtOAc was achieved in $scCO_2$. The molar ratio of O_2 to substrate was a 40:1 molar excess.

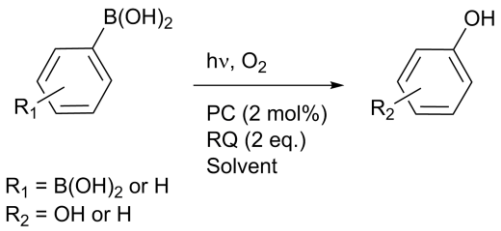
6.2.3.3 Flow Reactions at High-pressure without $scCO_2$

For high-pressure experiments without $scCO_2$, the reactor described in Section 6.2.3.2 was rebuilt to limit the dead volume in the reactor where flammable compounds can accumulate and cause a potential explosion risk. Both the tubing connecting the CO_2 line to the O_2 line and the heated mixer were removed (Scheme 6-3). In this adapted design, the air or oxygen was mixed with the reagent solution in a micromixer (M) before flowing into the photoreactor (R1). The other elements in this reaction set-up are identical to the apparatus described above.



Scheme 6-3 Reactor schematic for the aerobic hydroxylation of aryl boronic acids in flow. The labelling is as follows: Org 1 - reaction mixture containing the photocatalyst, reductive quencher and substrate, dissolved in the required solvent system, which is pumped by P:Org 1 (Jasco™ PU-980 HPLC pump); Air/O_2 DU - modified Rheodyne® unit to dose air or oxygen into the reactor system; M - micromixer (IMM, Mainz); R1 - sapphire tube reactor, which is temperature controlled via a recirculating water/ethylene glycol bath (1:1 v/v) and filled with glass beads (6 mm diameter); LEDs - light source (3 × 5 × Citizen Electronics Co. Ltd CL-L233-C13N1-C mounted on water cooled stainless steel blocks); BPR - Jasco™ BP 1580-81 back pressure regulator; T1-3 - manual valve.

General reaction procedure for the hydroxylation of phenylboronic acid in continuous flow without $scCO_2$



Arylboronic acid (0.26 mmol, 1 eq., 0.05 M), reductive quencher (0.52 mmol, 2 eq.) and photocatalyst (5.2 µmol, 2 mol%) were dissolved in the solvent (V_{org}/V_{H2O} ratios were calculated in the case of aqueous solvent mixtures to meet the required concentration). This solution was pumped into the flow system, mixed with air in a micromixer and irradiated in the photoreactor at 25 °C. The molar ratio of air to substrate was maintained during the reaction by a Rheodyne® dosage unit. The product solution collected from the photoreactor was quenched with 10 % HCl and a ^{1}H NMR spectrum was recorded in DMSO-d_6 after evaporating the solvents under vacuum.

Solvents: DMF, MeOH, ethanol (EtOH), H_2O/EtOH 1:1 v/v

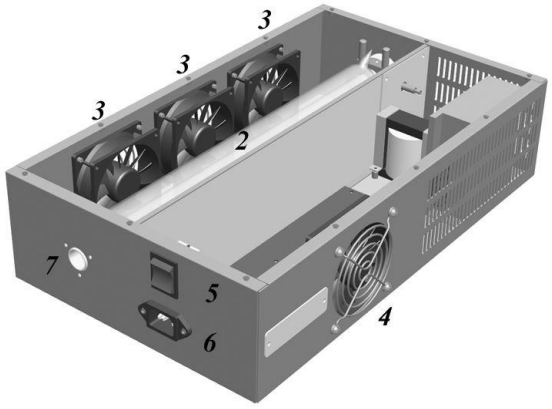
Reductive quenchers: DIPEA, ascorbic acid (H_2A)

Photocatalysts: Rose Bengal (RB), $[Ru(bpy)_3]Cl_2.6H_2O$

6.3 UV light Photochemistry

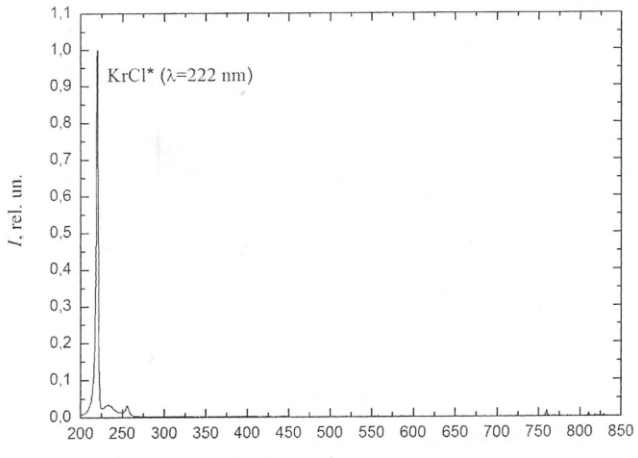
6.3.1 UV Light Sources

Three different excimer lamps were used in the UV light photochemistry work described in this Thesis. These were custom made by the Institute of High Current Electronics in Tomsk, Russia. Scheme 6-4 shows the box in which the excimer lamps were encased.



Scheme 6-4 Schematic of the UV excimer lamps used in this work; 2) lamp bulb, 3) fans for lamp cooling, 4) fan for power supply cooling, 5) on/off switch, 6) power supply, 7) hole for quartz tube.

Each lamp contained a different gas mixture, resulting in three light sources emitting at different wavelengths. The gas mixtures were KrCl*, XeBr* and XeCl*, resulting in output spectra with narrow emission bands at 222, 282 and 308 nm respectively (Figure 6-5). The power supplied to each lamp was 113 W and these lamps operated *via* a barrier discharge mechanism.



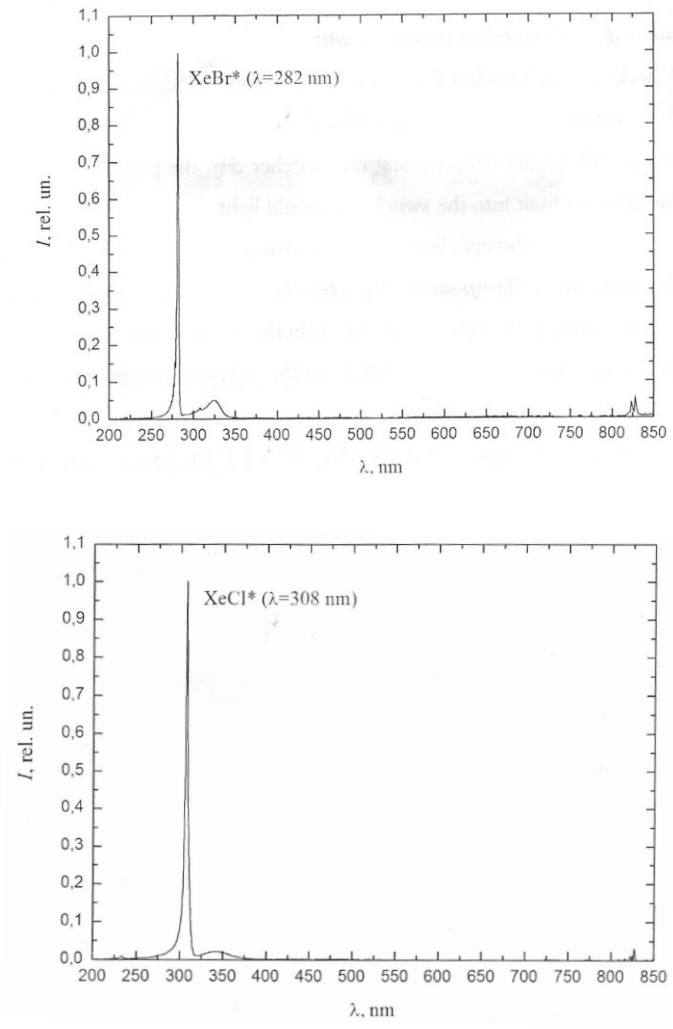


Figure 6-5 Output spectra of three different excimer lamps containing KrCl, XeBr* and XeCl*, emitting at 222, 282, 308 nm respectively.*

The supplier of the excimer lamps has provided radiant exitance values for the three different excimer light sources which are listed in Table 6-2.

Table 6-2 Radiant exitance of the excimer lamps.

	222 nm	**282 nm**	**308 nm**
Radiant exitance (mW/cm^2)[a]	21	36	49

[a]*Radiant exitance at an inner wall of the quartz tube (specification by supplier)*

UV experiments in batch were carried out using a medium-pressure 125 W lamp, emitting at a range of wavelengths of which the most prominent emission bands were at 435, 404, 365, 313 and 254 nm (Figure 6-6).

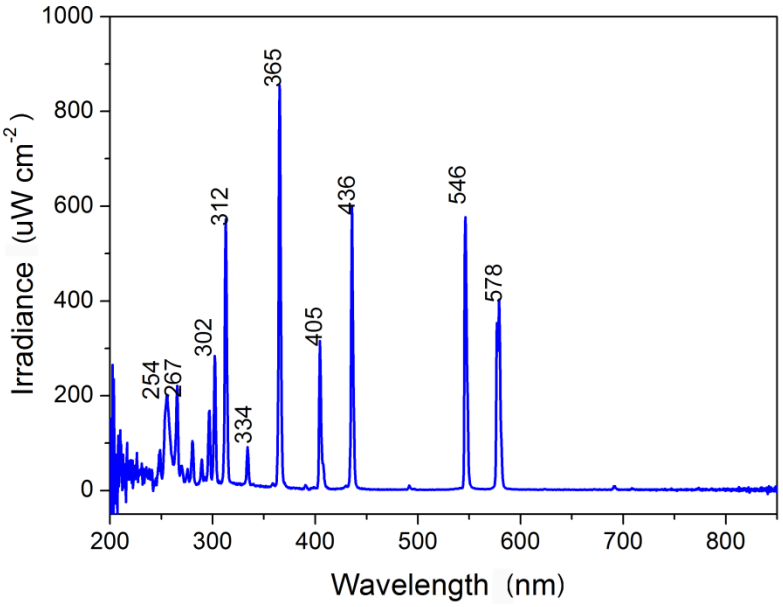
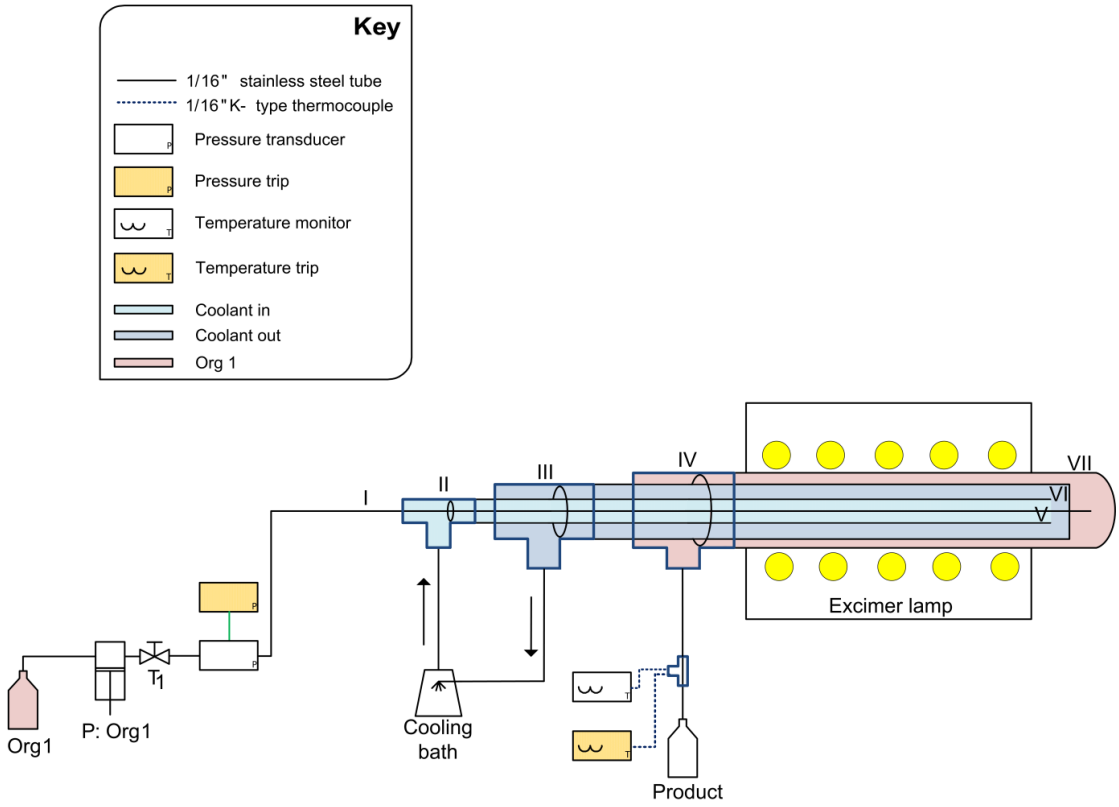


Figure 6-6 Emission spectrum of a 125 W Heraeus Noblelight medium-pressure mercury arc lamp (at 6 cm).

6.3.2 UV Photochemical Reactor Design

The continuous flow UV photochemistry reactor was designed and built in-house.[12] In order to run reactions at different wavelengths at the same time, a second, identical reactor was built following the same specifications. This reactor is outlined in Scheme 6-5. The reactants (Org1) are pumped into the reactor with a Jasco™ PU-986 self-priming HPLC Pump. The 1/16'' stainless steel tubing (I) containing the reactants runs inside the 1/4'' stainless steel tubing (V). The bottom of the 12 mm tube (VI) is welded closed using a drilled through NPT fitting, and the 1/16'' tube is passed through this fitting. Encasing all stainless steel tubing is a grade 214 quartz tube (12.24 mm ID, 15.54 mm OD) that has been sealed in-house on one end (VII). A Bola GL 32 PTFE T-Piece holds the quartz tube in place and connects it to the reactant outlet. The temperature of the reactants is measured at this reactant outlet and the temperature monitor is connected to a trip box. A pressure monitor is connected to a trip box as well. Therefore, the reactor will automatically shut down should the temperature or pressure exceed pre-set values. An earthing cable is positioned at the Swagelok™ T-piece near the product collection.



Scheme 6-5 Schematic of UV photochemistry rig; I) 1/16'' stainless steel tubing; II) Swagelok™ T-piece, drilled through in house on left side opening; III) Swagelok™ T-piece, drilled through in-house on left side opening; IV) Bola GL 32 PTFE T-Piece; V) 1/4'' stainless steel tubing; VI) 12 mm stainless steel tubing, welded closed at the bottom; VII) Quartz tube, sealed in-house; P: Org1 - Jasco™ PU-986 HPLC Pump; Cooling Bath - recirculating batch model Julabo® F32-HE, T1 - manual valve.

The cooling liquid (1:1 v/v ethylene glycol and water) flows into the reactor *via* a 1/4'' stainless steel tube (V) *via* the side arm of a 1/4'' stainless steel T-piece (II) and is forced through its open end into a 12 mm stainless steel tube (VI) where it is pumped out of the reactor *via* the side arm of a 12 mm stainless steel T-piece (III) and recirculated.

To reduce the system volume, the Bola T-Piece was filled with solid PTFE inserts (manufactured in-house), leaving enough space for liquid to flow through but limiting the dead volume and therefore total system volume in the reactor (Figure 6-7c,d).



(a)



(b)



(c)



(d)

Figure 6-7 a) UV reactor stick with A: inlet of the cooling liquid, B: outlet of the cooling liquid, C: inlet of the reactant solution, D: outlet of the reactant solution; b) UV reactor stick including cooling and lamp, inset: magnification of the tip of the reactor stick; c) Bola T-Piece with inserts; d) Bola T-piece with 2 inserts inside showing the gap for liquid.

Based on this design, Table 6-3 lists the dimension specifications as calculated or estimated.

Table 6-3 Specifications of the UV photochemistry rig.

	UV photochemistry rig
Total system volume (mL)[a]	~10
Irradiation volume (mL)[b]	1.37
Path length (mm)[b]	0.12
Distance from lamp (mm)[c]	~1.63

[a]The total system volume was estimated by flowing liquid at a known speed through an empty rig. [b]The irradiation volume and path length were calculated using the dimensions of the metal tubing and quartz tube. [c]The distance from the lamp is an estimate of the distance from the edge of the mesh inside the lamp to the position were the liquid flows through the rig.

6.3.2.1 UV-Light Absorption by the Quartz Tube

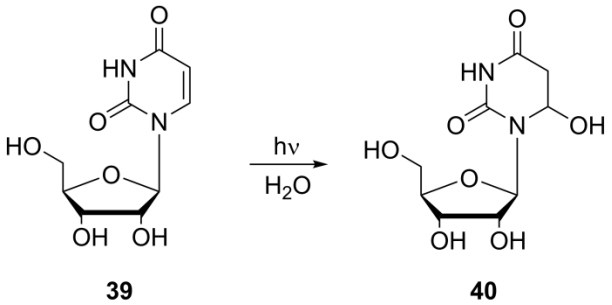
Although quartz does not strongly absorb UV light, a difference in the degree of transparency is present when comparing the different available light sources. Therefore, transmission spectra were recorded using the quartz tube to identify this differentiation. Due to the tubular shape of the quartz tube, only a relative difference in light absorption was measured. When comparing the transparency of the quartz tube for light at 222 and 282 nm, the quartz tube will absorb approximately 22 % more light at 222 nm compared to 282 nm. As a result, less of the photons emitted at 222 nm by the excimer lamp will reach the reactant solution compared to photons emitted at 282 nm. This difference is significant and needs to be taken into account when comparing reaction yields. The same is true when comparing reactions at 222 and 308 nm. However, the difference in light absorption by the quartz tube at 282 and 308 nm is only 5 %. This makes the comparison of results obtained from reactions carried out at these different wavelengths more accurate.

6.3.3 Chemical Actinometry Experiments

The Russian supplier of the excimer lamps reported the radiant exitance (which is the photon flux per centimetre squared) for all excimer lamps at the time of manufacturing. Their method involved measuring the photon flux of the reflected light on a small area of foil inside the lamp with a HAMAMATSU H8025-222 photodetector. Further extrapolation estimated the total radiant exitance of the excimer lamp. However, the quality of the lamp can deteriorate over time and therefore, it is important to determine the photon flux of each excimer lamp on a biannual basis. The Sections below will describe the chemical actinometry experiments carried out for the work in this Thesis to measure the photon flux emitted by each excimer lamp.

6.3.3.1 Chemical Actinometry of the 222 and 282 nm Excimer Lamps

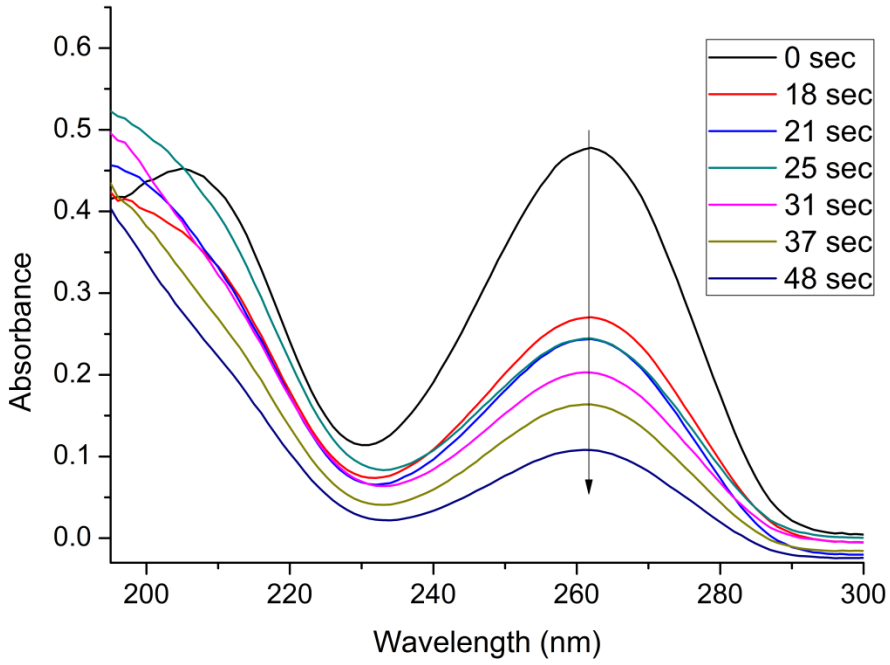
Uridine (1-β-D-ribofuranosyluracil) (**39**) was chosen as the photochemical actinometer for photon flux measurements with the 222 and 282 nm excimer lamps. The maximum of the absorbance band of uridine is at 262 nm in water and corresponds to a S_0-S_1 electronic transition, relating to a π-π* transition of the α,β-unsaturated carbonyl group of uracil.[13] The peak with a maximum at 205 nm can be assigned to a π-Rydberg transition.[14] Upon irradiation, photohydration of uridine (**39**) generates product **40** (Scheme 6-6), resulting in a depletion of the absorbance band at 262 nm.



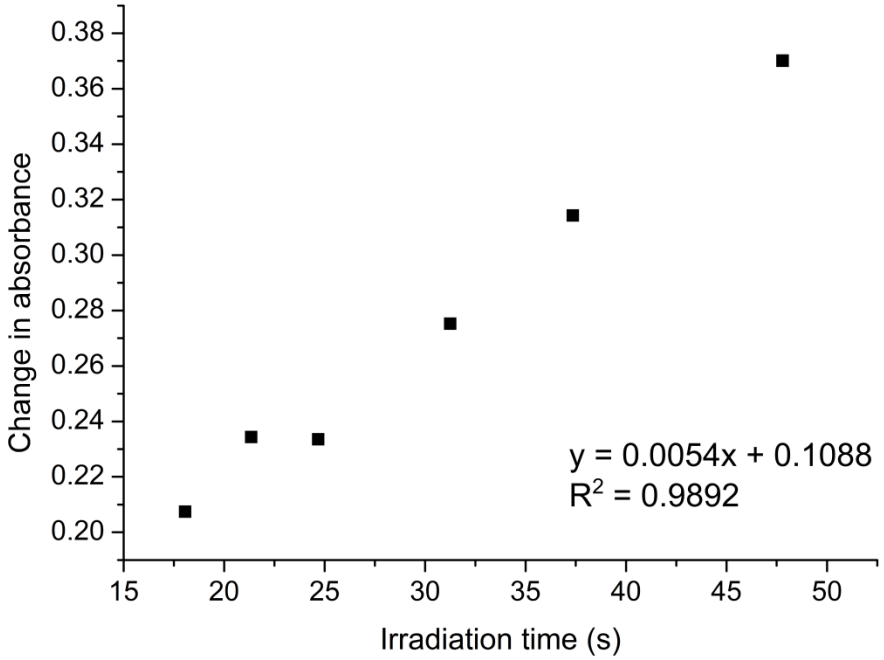
39 **40**

*Scheme 6-6 Photohydration reaction of uridine (**39**) to its photohydrate (**40**).*

The protocol for the chemical actinometry experiment was based on the method described by Zhang *et al.*[13c] and all measurements were conducted in triplicate. The concentration of **39** in deionised water was low (0.012 mM) to prevent photodimerisation which would interfere with the desired photohydration process.[15] Changes in the absorbance of uridine at different irradiation times were followed by UV-Vis measurements. Irradiation times were varied by pumping the uridine solution through the photoreactor at different flow rates. The rate of depletion of the absorbance band of uridine at 262 nm corresponds directly to the photon flux emitted by the light source. Upon irradiation of **39**, depletion of the absorbance bands at 205 and 262 nm was observed (Figure 6-8a). Therefore, it is likely that the 205 nm absorbance band corresponds at least partly to a π-Rydberg transition of the α,β-unsaturated carbonyl group of uracil. As the rate of depletion at 205 nm was less compared to the rate of depletion at 262 nm, it may be assumed that the absorbance band at 205 nm corresponds to a mixture of transitions in both **39** and **40**. When the change of absorbance of uridine at 262 nm was plotted against irradiation time, two regimes were observed (Figure 6-8b). It appeared that at shorter irradiation times (18-21 seconds), the change of absorbance is greater compared to longer irradiation times (> 21 seconds). A possible explanation is that at the shorter irradiation times, more of the π-π* transition in **39** was enabled and less of the π-Rydberg transition. However, when **39** was consumed to a higher degree, more 222 nm photons emitted by the light source would have been absorbed by **40** instead of **39**. Therefore, the change of absorbance of the π-π* transition in uridine is less at higher conversion of **39** corresponding to longer irradiation times. However, shorter irradiation could not be achieved due to restrictions on the pumps caused by the relatively high viscosity of water. The slope of the graph in Figure 6-8b was determined using a linear fit of all the data points.



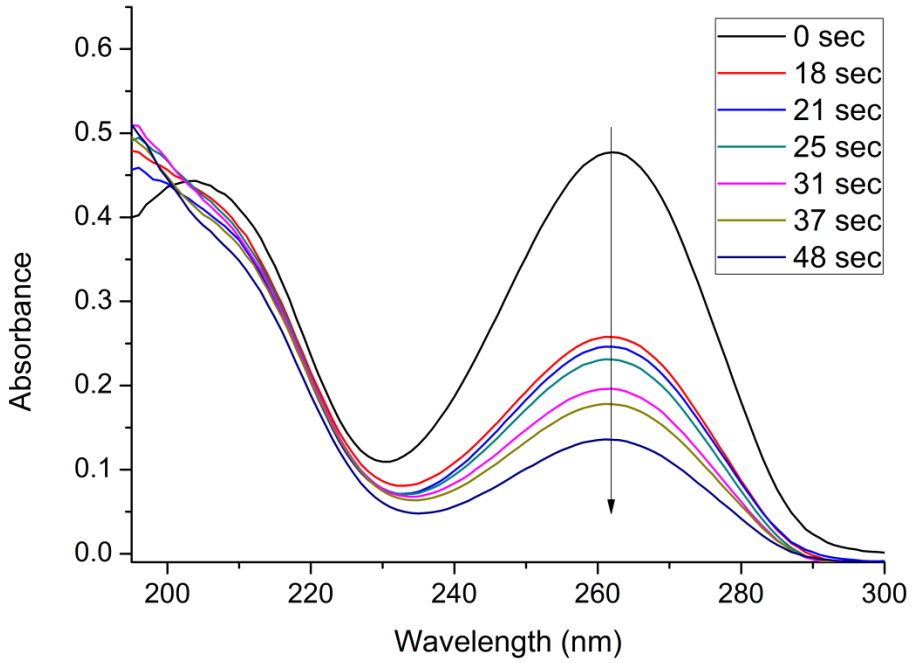
(a)



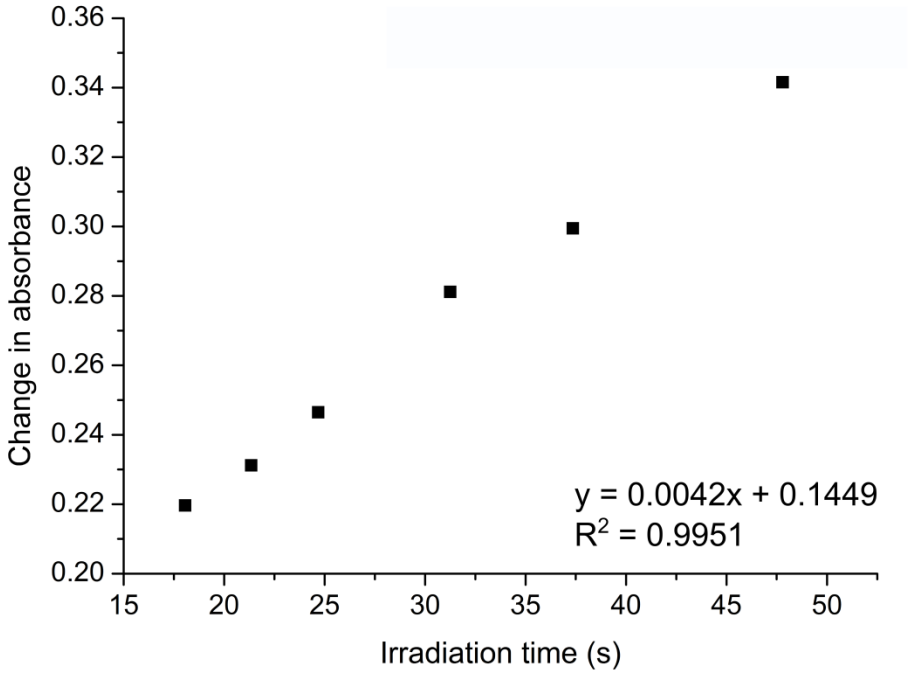
(b)

Figure 6-8 a) UV-Vis spectrum showing the absorbance of uridine at different irradiation intervals with the 222 nm excimer lamp, b) change in uridine absorbance at 262 nm at different irradiation intervals.

Irradiation of the uridine solution with the 282 nm excimer lamp showed again the depletion of the 205 and 262 nm absorbance bands (Figure 6-9a).



(a)



(b)

Figure 6-9 a) UV-Vis spectrum showing the absorbance of uridine at different irradiation times in seconds with the 282 nm excimer lamp, b) change in uridine absorbance at 262 nm at different irradiation intervals.

As 282 nm light only facilitates the π-π* transition, no product formation interfered with the light absorption by uridine. Therefore, the change in absorbance over time (Figure 6-9b) could be accurately fitted by a single linear line (R^2 = 0.9951). Using the obtained value for dA/dt from this linear fit, the number of photons absorbed by the actinometer (q_p) can be calculated using Equation 6-1 in which dA/dt is the change of absorbance over time, N_A Avogadro's number, V the irradiation volume, Φ the quantum yield of the actinometer at the wavelength of the light source, ε the molar extinction coefficient of the actinometer at the wavelength that the change in absorbance is measured, and l the path length of the UV-Vis cuvette.[16] Section 6.3.3.3 provides a detailed protocol on how to solve Equation 6-1.

$$q_p = \left(\frac{dA}{dt}\right) \frac{N_A V}{\Phi \varepsilon l} \qquad 6\text{-}1$$

A correction factor was applied to q_p in order to obtain the total photon flux emitted by the excimer lamp ($q_{p,tot}$). This is needed when the actinometer only absorbed a fraction of the incoming photons, which was the case for the experiments using uridine as the chemical actinometer due to the low concentration of the actinometer. The radiant exitance is obtained by dividing the total photon flux ($q_{p,tot}$) by the surface area of the excimer lamp (Table 6-4).

Table 6-4 Radiant exitance values for 222 and 282 nm excimer light sources.

Entry	Light source	Method	Radiant exitance (s^{-1} cm^{-2})	Relative efficiency to manual
1	222 nm	Supplier's manual	2.34×10^{16}	-
2[a]	222 nm	Chemical actinometry	2.76×10^{16}	118 %
3	282 nm	Supplier's manual	5.11×10^{16}	-
4[a]	282 nm	Chemical actinometry	5.69×10^{16}	111 %

[a]*Radiant exitance value obtained via chemical actinometry is an average over 3 datasets*

At both 222 and 282 nm, the radiant exitance measured by chemical actinometry is higher than the value given by the supplier's manual (18, 11 % respectively). A possible explanation for this error is the reflection of the incoming light by the stainless steel cooling stick in the centre of the reactor. It has been reported that stainless steel can reflect UV light and is estimated to reflect around 40 % at 222 and 282 nm.[17] This could result in a higher photon flux measurement than the true value as reflected photons can still participate in the chemical reaction.

Since several estimations and assumptions were made in the process of the chemical actinometry experiment, a discrepancy between the measured and given value was expected. For instance, the supplier of the excimer lamps did not mention the temperature at which their radiant exitance was measured. In our photochemical actinometry measurements, the quantum yield of the actinometer, the density of the fluid and possibly competing chemical processes could be temperature dependent.[15]

It was assumed that the fraction of the light absorbed by the actinometer was constant. This was needed to apply a single correction factor to the amount of light absorbed by uridine *versus* the total light emitted by the lamp. However, the fraction of the light absorbed by uridine decreased as the conversion of uridine progressed, especially at the low concentration of uridine that the experiment was conducted at. This could explain why the radiant exitance obtained *via* chemical actinometry is only 111-118 % of the value found in the manual rather than the expected 140 % based on the 40 % reflection of the light. Moreover, it was assumed that the photoproduct of uridine did not absorb any of the incoming photons in order to use Equation 6-1.

Furthermore, both the irradiation volume and the path length of the reactor were estimated using the dimensions given by the supplier and our own measurements. Possible defects on the inner surface of the quartz tube and outer surface of the cooling stick might also influence our measured surface area and volume and have not been taken into account. Therefore, an uncertainty arises from these values. Moreover, defects in the surface of the quartz tube will lead to a change in the refractive properties of the surface and could lead to further uncertainty in the measured photon flux.

Protocol for 222 and 282 nm excimer lamps

The protocol was based on the method described by Zhang *et al.*[13c] Uridine (30 mg) was dissolved in deionised water (100 mL) and after a 1000-fold dilution, this actinometer solution was pumped through the reactor with the recirculating bath set to 25 °C (Table 6-5). UV-Vis spectra were obtained through a 4.0 cm path length quartz cuvette using deionised water as the background.

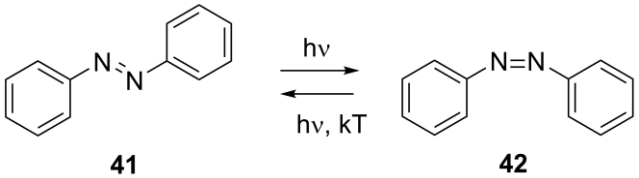
The output solution of the reactor was measured using UV-Vis spectroscopy after equilibration time was reached at each flow rate.

Table 6-5 Chemical actinometry specifications for the 222/282 nm excimer lamps.

Parameter	
Actinometer	uridine
Solvent	deionised water
Temperature	25 °C
Quantum Yield (222 nm)[13c]	0.034
Quantum Yield (280 nm)[15]	0.016
Molar extinction coefficient (222 nm)[13c]	3150 L/mol·cm
Molar extinction coefficient (262 nm)[18]	9900 L/mol·cm
Molar extinction coefficient (282 nm)	2650 L/mol·cm
Concentration actinometer	0.012 mmol/L
Quartz cuvette path length	4 cm
Flow rates	0, 2.00, 2.74, 3.29, 4.6, 5.48, 6.90 mL/min

6.3.3.2 Chemical Actinometry of the 308 nm Excimer Lamp

For chemical actinometry experiments conducted using the 308 nm excimer light source, uridine could not be utilised as the actinometer as it does not absorb the incoming light at this wavelength. Azobenzene was chosen as the chemical actinometer for evaluation of the 308 nm excimer lamp (Scheme 6-7). The *trans-cis* photoisomerisation can easily be followed by UV-Vis spectroscopy and the actinometer material is readily available and reusable.[19]

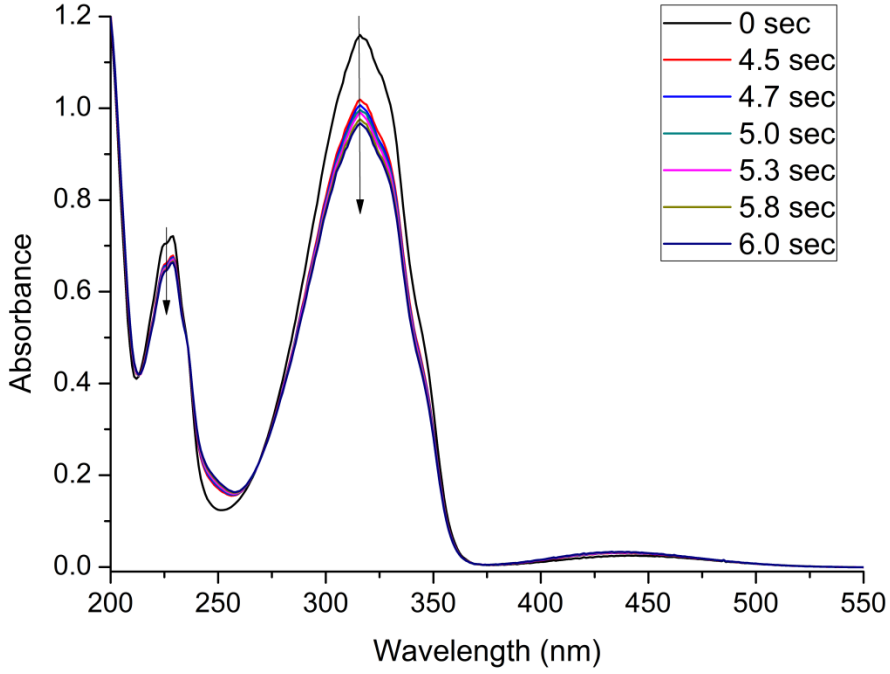


*Scheme 6-7 Photoisomerisation of trans-azobenzene (**41**) to cis-azobenzene (**42**).*

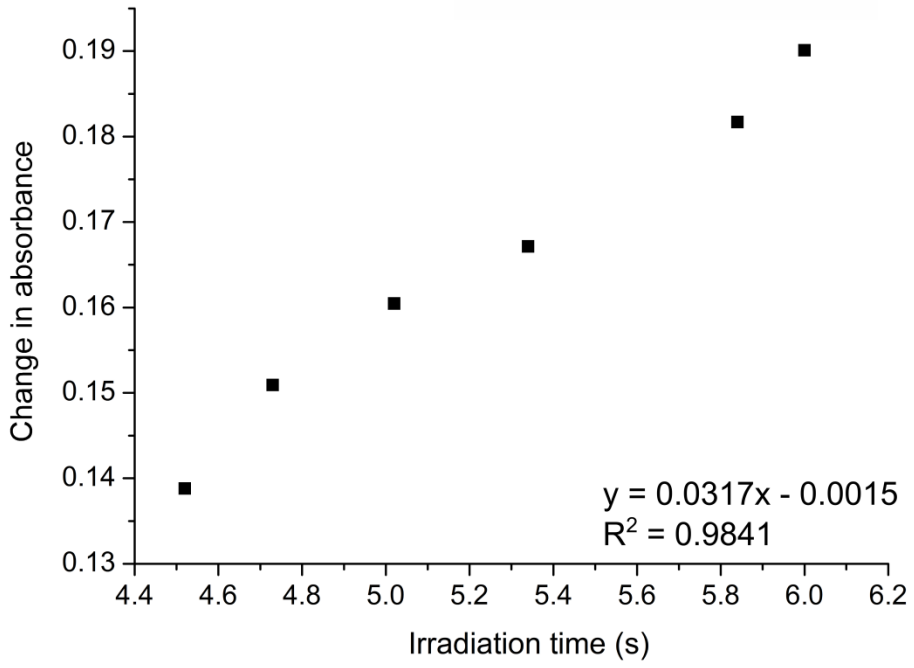
Irradiation of a solution of *trans*-azobenzene (**41**) in methanol with 308 nm light will initiate a π-π* transition in **41** to form *cis*-azobenzene (**42**).[20] The rate of depletion of the absorbance band of **41** at 317 nm was used to calculate the photon flux emitted by the light source. To limit the absorption of the light by **42**, the conversion of **41** was kept below 15 %. The temperature of the reactor was set at 15 °C to limit thermal isomerisation of **42** back to **41**. The concentration of **41** in methanol was high (0.1 M) so that 99.9 % of the light was absorbed. This way, almost all photons emitted by the excimer lamp were involved in the photoisomerisation of **41** and therefore, the reflection of photons of the stainless steel cooling stick was limited. As a result, the error in our calculated radiant exitance was thought to be lower compared to the chemical actinometry experiments carried out with the 222/282 nm excimer lamps. The protocol for the chemical actinometry experiment with the 308 nm excimer lamp was adapted from the method described by Kuhn *et al.*[15] which in turn was based on initial experiments carried out by Gauglitz *et al.*[19, 21] All measurements were conducted in triplicate.

When a solution of **41** in methanol was irradiated with 308 nm light, both the absorbance bands at 229 and 317 nm depleted (Figure 6-10a). The shortest residence time that could be used was 4.5 seconds due to the generation of back pressure in the reactor at the flow rates required to allow for these short irradiation times. The peak growing in at 438 nm corresponds to a n-π* transition in *cis*-azobenzene.

A satisfactory linear fit was found for the change in absorbance of **41** at 317 nm over time (Figure 6-10b). The radiant exitance was calculated *via* the method described previously. By working at a high concentration of **41** in methanol and a maximum conversion of **41** of 15 %, it could be assumed that the fraction of the light absorbed by the actinometer was constant. However, the obtained value for the radiant exitance was only 12.2 % of the value given by the supplier of the excimer lamp (Table 6-6). It is possible that the reaction solution exiting the reactor warmed up to room temperature and underwent partial back isomerisation from **42** to **41**.



(a)



(b)

*Figure 6-10 a) UV-Vis spectrum showing the absorbance of trans-azobenzene (**41**) at different irradiation intervals with the 308 nm excimer lamp, b) change in trans-azobenzene (**41**) absorbance at 317 nm at different irradiation intervals.*

To test whether the obtained value for the radiant exitance could signal a significant loss in photon count since the first use of the 308 nm excimer lamp, a chemical reaction performed 22 months before the chemical actinometer experiments was repeated and the yields of these reactions were compared. Identical product yield in this reaction suggest that the excimer lamp did not degrade over time and that the chemical actinometry experiment as described in this Section was not accurate.

Table 6-6 Radiant exitance values for the 308 nm excimer light source.

Entry	Light source	Method	Radiant exitance (s^{-1} cm^{-2})	Relative efficiency to manual
1	308 nm	Supplier's manual	7.60×10^{16}	-
2[a]	308 nm	Chemical actinometry	9.30×10^{15}	12.2 %

[a]*Radiant exitance value obtained via chemical actinometry is an average over 3 datasets*

Due to the presence of these estimations and assumptions, the obtained radiant exitance value by chemical actinometry can be used as a relative value for comparison to future chemical actinometry experiments using the same set-up. For the calculations regarding photon output reported in this Thesis, the radiant exitance as reported by the supplier will be used.

Protocol for 308 nm excimer lamp

The protocol was based on the method described by Kuhn *et al.*[15] To allow for faster flow rates, the Jasco™ PU-986 pump in the UV photoreactor was replaced by a Gilson 305 HPLC pump, equipped with a 50 SC pump head. Azobenzene (1.833 g) was dissolved in methanol (1 L) and this actinometer solution was pumped through the reactor with the recirculating bath set to 15 °C. UV-Vis spectra were obtained using methanol as the background. All measurements were taken through a Harrick cell containing CaF_2 windows, and lined with 50 µm spacers. The Harrick cell was placed in-line with the UV photoreactor, connected to the outlet of the reactor by 1/8" FEP tubing. The output solution of the reactor was measured using UV-Vis spectroscopy after equilibration time was reached at each flow rate.

Table 6-7 Chemical actinometry specifications for the 308 nm excimer lamp.

Parameter	
Actinometer	azobenzene
Solvent	methanol
Temperature	15 °C
Quantum Yield (308 nm)[15]	0.14
Molar extinction coefficient (317 nm)	21180 L/mol·cm
Molar extinction coefficient (308 nm)	19220 L/mol·cm
Concentration actinometer	10.1 mmol/L
Harrick cell path length	50 µm
Flow rates	15, 16, 17, 18, 19, 20 mL/min

6.3.3.3 Calculation of the Photon Flux

The photon flux of the incident light beam absorbed by the actinometer was calculated using Equation 6-1, as published by Lehóczki *et al.*[16] and provides the amount of photons absorbed by the actinometer per second (q_p).

$$q_p = \left(\frac{dA}{dt}\right) \frac{N_A V}{\Phi \varepsilon l} \qquad 6\text{-}1$$

All parameters and their units required for solving Equation 6-1 are depicted in Table 6-8.

Table 6-8 Parameters in Equation 6-1.

Parameter	**Full name**	**Value**	**Unit**
dA/dt	Slope of absorbance change over time	variable	s^{-1}
N_A	Avogadro's number	6.02214×10^{23}	mol^{-1}
V	Irradiation volume of the reactor	0.00137	dm^3
Φ	Quantum yield of the actinometer at the wavelength of the light source	variable	unitless
ε	Molar extinction coefficient of the actinometer at the measured absorbance	variable	L/mol·cm
l	Path length of the UV-Vis cuvette	variable	cm

The change in absorbance of the actinometer over time can be measured at any wavelength, but measuring it at the absorbance maximum is preferable. Plotting this change in absorbance (dA) against irradiation time in seconds should provide a linear relationship of which the value of the slope is required for solving Equation 6-1. The irradiation time in seconds (t) is calculated by Equation 6-2 in which V is the irradiation volume of the actinometer solution in the reactor (1.37 mL), FR_{set} the set flow rate in mL/min and PE the pump efficiency in %.

$$t = \left(\frac{V}{FR_{set} \ (\frac{PE}{100})} \right) x \ 60 \qquad 6\text{-}2$$

The value for q_p only represents the amount of photons absorbed by the actinometer. To attain the total photon flux emitted by the light source ($q_{p,tot}$), q_p was divided by F, the fraction of the light that was absorbed by the actinometer (Equation 6-3). The first step to obtain a value for 'F' is calculating the absorbance of the light by the actinometer according to the Lambert-Beer law (Equation 6-4) in which ε is the molar extinction coefficient of the actinometer at the wavelength of the light source, c_0 is the initial concentration of the actinometer in solution and l is the path length of the reactor (0.012 cm).

$$q_{p,tot} = \frac{q_p}{F} \qquad 6\text{-}3$$

$$A = \varepsilon \, c_0 \, l \qquad 6\text{-}4$$

According to Equations 6-5 to 6-7, the amount of light transmitted in the reactor can be calculated.

$$A = log_{10} \left(\frac{I}{I_0}\right) \qquad 6\text{-}5$$

$$T = \frac{I}{I_0} \qquad 6\text{-}6$$

$$T = 10^{-A} \qquad 6\text{-}7$$

$$F = 1 - T \qquad 6\text{-}8$$

The fraction of light absorbed by the actinometer (F) is obtained from Equation 6-8.

The radiant exitance in photons/s·cm^2 of the excimer light source can be calculated by dividing the total photon flux by the surface area (SA) of the lamp which is 115.4 cm^2 (Equation 6-9).

$$Radiant\ exitance = \frac{q_{p,tot}}{SA} \qquad 6\text{-}9$$

Estimations and assumptions

- It was assumed that the fraction of the light absorbed by the actinometer was constant throughout the reaction. However, the fraction of the light absorbed by the actinometer decreased as the conversion progressed and hence the concentration of actinometer decreased. This was especially the case at the low concentration of uridine that the experiment was conducted at. Moreover, it was assumed that the photoproduct of uridine did not absorb any of the incoming photons. However, in reality it is likely that this did occur, which further reduced the amount of photons absorbed by the actinometer. Therefore, the calculated photon flux is likely an underestimation of the real value.

- Both the irradiation volume and the path length of the reactor were estimated using the dimensions of the quartz and stainless steel tubing given by the supplier and our own measurements. Moreover, possible defects on the inner surface of the quartz tube and outer surface of the cooling stick might influence the actual surface area and volume of the reactor but have not been taken into account. Therefore, an uncertainty arises from the values used in the calculations. Furthermore, defects in the surface of the quartz will lead to a change in the refractive properties of the surface and could lead to further uncertainty in the measured photon flux.

6.3.4 Procedure for UV Photochemistry in Continuous Flow

This Section will describe the general reaction procedure as used during the work carried out for this Thesis. The full standard operating procedure (SOP) for the use of the continuous flow UV photoreactor can be found in the Appendix.

Deoxygenated solvent (250 mL) was flushed through the rig at a flow rate of 5.0 mL/min to clean the rig while at the same time the joints and fittings in the rig were tested for leaks by pressing paper towel onto each element. Subsequently, the recirculating bath was set to the desired temperature (between -20 °C and 40 °C) and the desired flow rate was set on the HPLC pump. The reagent solution was prepared and then deoxygenated by bubbling argon through the round bottom flask. The reaction mixture was kept under argon by placing a septum on top of the round bottom flask, pierced through with a balloon containing argon. To start the reaction, the UV lamp was turned on while wearing nitrile gloves and eye protection (laboratory safety glasses, Lexan™). When two system volumes had flowed through the reactor, product collection was started. In order to stop the reaction, the emergency stop button on the trip box was pushed which disconnects power to both the HPLC pump and the UV lamp. The UV lamp power switch was then turned to the off position and the whole rig was reset using the trip box. Cleaning of the rig was accomplished by pumping 200 mL of clean solvent through the rig at a flow rate of 5.0 mL/min after which the HPLC pump and the recirculating bath were switched off.

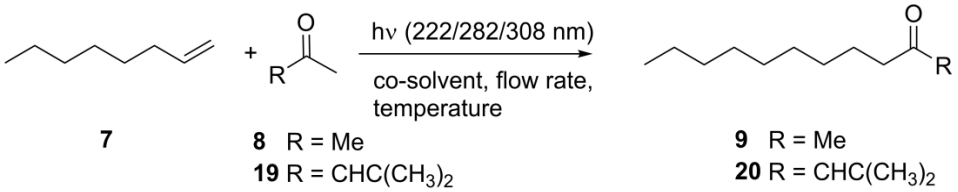
Reactor samples for GC analysis were prepared either with or without an external standard. When no external standard was used, GC analysis of the sample was done by directly injecting 1 µL of the sample into the GC. When using an external standard, a known amount of external standard was added to 1 mL of the reactor sample, plus 1 mL of a co-solvent (typically EtOH) to homogenise the mixture if necessary. The yield of the desired product was calculated using the ratio between the desired product and the external standard, with the response factor taken into account.

The GC method consisted of a 2 min. hold at 35 °C before increasing the temperature to 70 °C at a rate of 30 °C/min. After a 2 min. hold, the temperature was increased further to 110 °C at 15 °C/min. The temperature was kept at 110 °C for 1 min. after which the final temperature increase to 140 °C was started at a rate of 10 °C/min, followed by a 4 min. hold.

The following Sections describe the different experiments carried out in the continuous flow UV photoreactor.

6.3.4.1 Ketone and Olefin Coupling

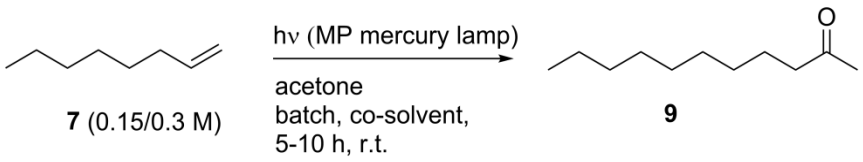
Continuous flow



7 **8** R = Me; **19** R = $CHC(CH_3)_2$ **9** R = Me; **20** R = $CHC(CH_3)_2$

Following the procedure outlined in Section 6.3.4, the reagent solution was prepared by dissolving the ketone (**8** or **19**) and 1-octene (**7**) in a co-solvent if required (either H_2O, MeCN or 1:1 v/v H_2O and EtOH) in a round bottom flask. The reactor was cooled to the set temperature (-10 °C to 40 °C) before the reagent solution was pumped through the reactor at the desired flow rate (0.05-2 mL/min) under irradiation by the desired excimer lamp (emitting at either 222, 282 or 308 nm). Throughout the reaction, a balloon filled with argon was attached to the top of the round bottom flask. Aliquots were taken after an equilibration period and analysed in triplicate by GC. An external standard (2-nonanone) was used in GC analysis and a response factor was calculated for 2-undecanone (**9**) *vs* 2-nonanone.

Batch



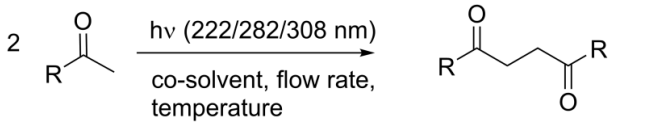
7 (0.15/0.3 M) **9**

The following reaction mixtures were prepared and 3 mL of these solutions was added to a quartz cuvette (1 cm path length): A mixture of 1-octene (**7**, 230 µL, 0.3 M in **8**) and acetone (**8**, 5 mL). A mixture of 1-octene (**7**, 115 µL, 0.15 M in **8**) and acetone (**8**, 5 mL) in deionised water (2 mL, 0.4 vol. eq. to **8**). The cuvette containing the reaction mixture was sealed with a septum and an argon balloon was applied. The cuvette was placed at a distance of approximately 2 cm

from a water cooled medium-pressure (MP) mercury arc lamp and irradiated while being continuously stirred. Aliquots were taken over time and analysed with GC.

6.3.4.2 Ketone Dimerisation

Continuous flow



8 R = Me
26 R = CH_2CH_3
30 R = Ph
34 R = $C(CH_3)_3$

13 R = Me
27 R = CH_2CH_3
31 R = Ph
35 R = $C(CH_3)_3$

Following the procedure outlined in Section 6.3.4, the reagent solution consisted of either neat ketone or ketone dissolved in a co-solvent (either H_2O, MeCN or H_2O and EtOH mixtures) in a round bottom flask. The reactor was cooled to the set temperature (-10 °C to 40 °C) before the reagent mixture was pumped through the reactor at the desired flow rate (0.05-2 mL/min) under irradiation by the desired excimer lamp (emitting at either 222, 282 or 308 nm). Throughout the reaction, a balloon filled with argon was attached to the top of the round bottom flask. Aliquots were taken after an equilibration period and analysed in triplicate with GC. An external standard (2-undecanone) was used in GC analysis and a response factor was calculated for acetonylacetone (**13**) *versus* 2-undecanone. This response factor was used for all ketone dimerisation products.

For ketones other than acetone as substrates, several conditions were tested, following the same procedure (Table 6-9).

Table 6-9 Overview of tested conditions for the dimerisation of ketones other than acetone as the substrate.

Entry	Ketone	Concentration ketone	Co-solvent	Excimer lamp
1[a]	2-butanone (**26**)	3.72 M	H_2O	222 nm
2	2-butanone (**26**)	3.72 M	H_2O	308 nm
3	acetophenone (**30**)	1.56 M	MeCN	222 nm
4	acetophenone (**30**)	1.56 M	H_2O/EtOH (4:5 v/v)	222 nm
5[b]	acetophenone (**30**)	1.71 M	H_2O/EtOH (4:5 v/v)	308 nm
6	pinacolone (**34**)	1.88 M	H_2O/EtOH (5:8 v/v)	308 nm
7[c]	pinacolone (**34**)	0.131 M	H_2O	282 nm
8[c]	pinacolone (**34**)	0.381 M	H_2O	282 nm

*Reaction conditions: Ketones **26**, **30** and **34**, co-solvent, 0.2 mL/min, 40 °C; [a]run at 0.2 and 0.1 mL/min; [b]run at both 0.2 and 0.05 mL/min; [c]Performed in micellar media (SDS in water (0.1 M)).*

For the reactions with ketones other than acetone as substrates, the appropriate excimer lamps were chosen based on the absorbance spectra of the various substrates (Figure 6-11).

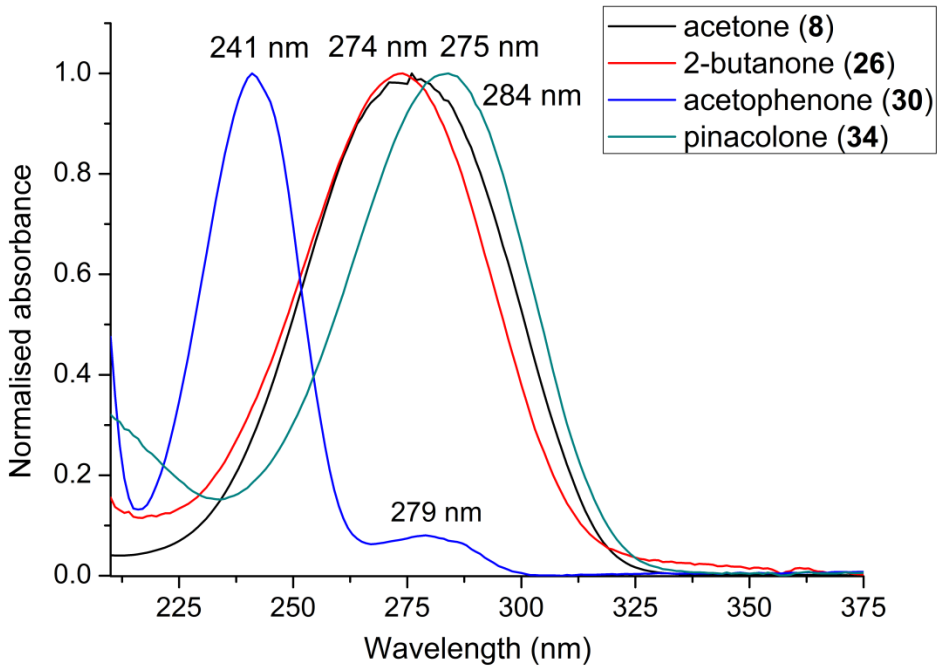
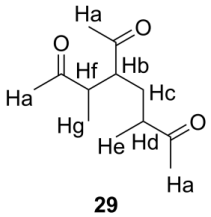


*Figure 6-11 Normalised UV-Vis spectra of acetone (**8**), 2-butanone (**26**), acetophenone (**30**) and pinacolone (**34**), all recorded in EtOH.*

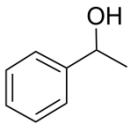
Characterisation of 4-acetyl-3,6-dimethyloctane-2,7-dione (**29**)



29

^{1}H NMR (400 MHz, $CDCl_3$) δ (ppm) 3.34-3.30 (m, 1H, Hb), 2.96-2.87 (m, 2H, Hd, Hf), 2.57-2.51 (m, 2H, Hc), 2.32 (s, 3H, Ha), 2.24 (s, 3H, Ha), 2.20 (s, 3H, Ha), 1.14 (d, *J* = 7.1, 3H, Hg), 1.02 (d, *J* = 7.3 Hz, 3H, He). ^{13}C NMR (400 MHz, $CDCl_3$) δ (ppm) 210.9 (**C**=O), 210.2 (**C**=O), 209.7 (**C**=O), 48.1 (**C**H), 48.0 (**C**H), 47.7 (**C**H), 30.3 (**C**H_3), 30.0 (**C**H_3), 29.7 (**C**H_3), 21.1 (**C**H_2), 14.7 (**C**H_3), 12.2 (**C**H_3). HRMS (ESI) m/z: 235.1310 calculated for $C_{12}H_{20}O_3Na$, found $[M+Na]^+$ = 235.1305 (100 %)

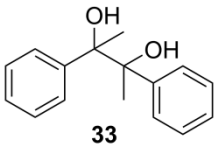
Characterisation of 1-phenylethan-1-ol (**32**)



32

^{1}H NMR (400 MHz, $CDCl_3$) δ (ppm) 7.51-7.28 (m, 5H, Ar-**H**), 3.93 (q, *J* = 6.4 Hz, 1H, C**H**(OH)), 0.99 (d, *J* = 6.4 Hz, 3H, Me-**H**). ^{13}C NMR (400 MHz, $CDCl_3$) δ (ppm) 145.8 (**C**H), 128.7 (2x **C**H), 127.2 (**C**H), 125.5 (**C**H), 74.3 (**C**OH), 26.9 (**C**H_3). The spectral data matches that of the literature.[22] Quaternary carbon signal could not be allocated.

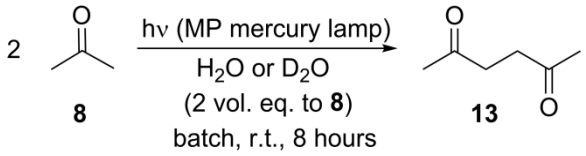
Characterisation of 2,3-diphenylbutane-2,3-diol (**33**)



33

The *syn*/*anti* isomers were formed in a 44:56 ratio as determined by ^{1}H NMR. *anti* Isomer: ^{1}H NMR (400 MHz, $CDCl_3$) δ (ppm) 7.29-7.19 (m, 10H, Ar-**H**), 1.53 (s, 6H, Me-**H**). ^{13}C NMR (400 MHz, $CDCl_3$) δ (ppm) 127.3 (2x **C**H), 127.3 (2x **C**H), 127.1 (2x **C**H), 127.1 (2x **C**H), 126.9 (2x **C**H), 25.1 (**C**H_3), 25.0 (**C**H_3). *syn* Isomer: ^{1}H NMR (400 MHz, $CDCl_3$) δ (ppm) 7.29-7.19 (m, 10H, Ar-**H**), 1.61 (s, 6H, Me-**H**). ^{13}C NMR (400 MHz, $CDCl_3$) δ (ppm) 127.3 (2x **C**H), 127.3 (2x **C**H), 127.1 (2x **C**H), 127.1 (2x **C**H), 126.9 (2x **C**H), 25.1 (**C**H_3), 25.0 (**C**H_3). The spectral data matches that of the literature.[23] Quaternary carbon signals could not be allocated.

Batch

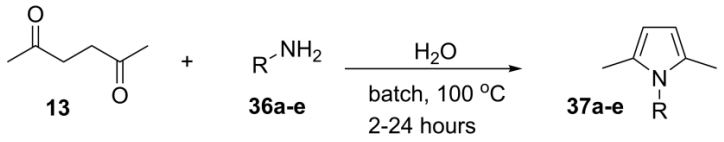


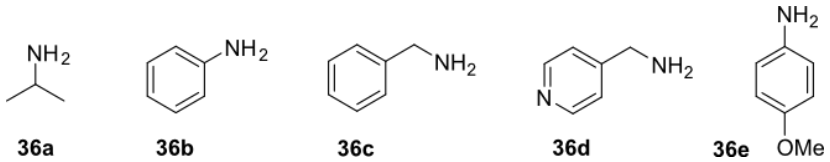
8 **13**

Acetone (**8**, 1 mL) was mixed with either H_2O or D_2O (2 mL, 2 vol. eq. to **8**) and was placed in a 3 mL quartz cuvette. The cuvette containing the reaction mixture was sealed with a septum and an argon balloon was applied. Placed at a distance of approximately 2 cm from a water cooled medium-pressure (MP) mercury arc lamp, the cuvette was irradiated while being continuously stirred. Aliquots were taken over time and analysed with GC.

6.4 Cyclisation of 1,4-Diketones

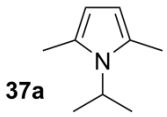
6.4.1 Formation of Pyrrole Derivatives





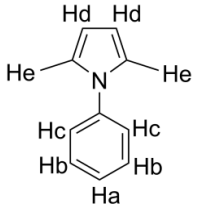
2,5-Hexadione (**13**) (0.293 mL, 2.5 mmol, 1 eq.) and primary amine (**36a-e**) (2.5 mmol, 1 eq.) were added to 5 mL of water in a round bottom flask. The solution was heated under reflux with continuous stirring until completion. The reaction was monitored using either ^{1}H NMR or GC analysis.

1-isopropyl-2,5-dimethyl-1*H*-pyrrole (37a)



^{1}H NMR analysis of both the crude reaction mixture and the mixture after extraction by diethyl ether did not show any signals corresponding to product **37a**.

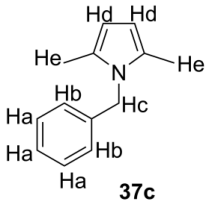
2,5-dimethyl-1-phenyl-1*H*-pyrrole (37b)



37b

^{1}H NMR (400 MHz, $CDCl_3$) δ (ppm) 7.51-7.46 (m, 2H, Hb), 7.44-7.40 (m, 1H, Ha), 7.25-7.22 (m, 2H, Hc), 5.93 (s, 2H, Hd), 2.06 (s, 6H, He). ^{13}C NMR (400 MHz, $CDCl_3$) δ (ppm) 139.0 (**C**H), 129.0 (**C**H), 128.8 (**C**H), 128.3 (**C**H), 127.6 (**C**H), 105.6 (2x **C**H), 13.01 (2x **C**H_3). The spectral data matches that of the literature.[24] Quaternary carbon signals could not be allocated. HRMS (ESI) m/z: 170.0975 calculated for $C_{12}H_{12}N$, found $[M-H]^+$ = 170.0965 (100 %)

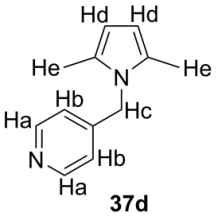
1-benzyl-2,5-dimethyl-1*H*-pyrrole (37c)



37c

^{1}H NMR (400 MHz, $CDCl_3$) δ (ppm) 7.34-7.23 (m, 3H, Ha), 6.90 (d, *J* = 9.1 Hz, 2H, Hb), 5.88 (s, 2H, Hc), 5.03 (s, 2H, Hd), 2.16 (s, 6H, He). The spectral data matches that of the literature.[25] HRMS (ESI) m/z: 186.1283 calculated for $C_{13}H_{16}N$, found $[M+H]^+$ = 186.1278

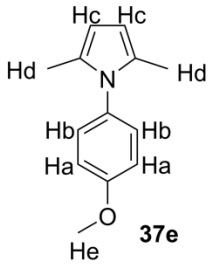
4-((2,5-dimethyl-1*H*-pyrrol-1-yl)methyl)pyridine (37d)



37d

^{1}H NMR (400 MHz, $CDCl_3$) δ (ppm) 8.55 (d, *J* = 6.3 Hz, 2H, Ha), 6.81 (d, *J* = 6.3 Hz, 2H, Hb), 5.91 (s, 2H, Hc), 5.02 (s, 2H, Hd), 2.21 (s, 6H, He). The spectral data matches that of the literature.[26] HRMS (ESI) m/z: 187.1235 calculated for $C_{12}H_{15}N_2$, found $[M+H]^+$ = 187.1232 (100 %)

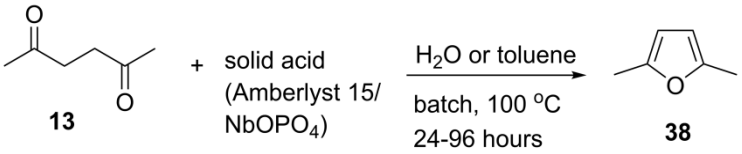
1-(4-methoxyphenyl)-2,5-dimethyl-1*H*-pyrrole (37e)



37e

^{1}H NMR (400 MHz, $CDCl_3$) δ (ppm) 7.14 (d, *J* = 8.9 Hz, 2H, Hb), 6.98 (d, *J* = 8.9 Hz, 2H, Ha), 5.90 (s, 2H, Hc), 3.88 (s, 3H, He), 2.03 (s, 6H, Hd). The spectral data matches that of the literature.[24] HRMS (ESI) m/z: 200.1080 calculated for $C_{13}H_{14}NO$, found $[M\text{-}H]^+$ = 200.1081 (100 %)

6.4.2 Procedure for the Formation of 2,5-Dimethylfuran

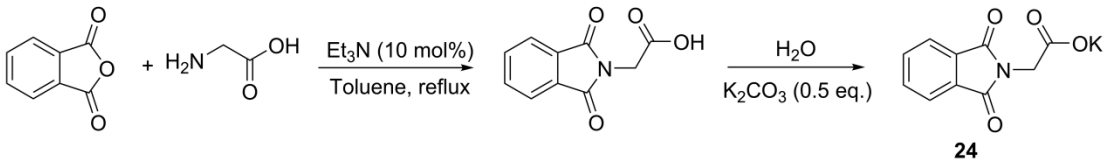


2,5-Hexadione (**13**) and solid acid were added to solvent in a round bottom flask (Table 6-10). The solution was heated under reflux until completion while being continuously stirred. The reaction was monitored using GC analysis. GC (FID) RT=3.78 min.

*Table 6-10 Reaction parameters for the formation of 2,5-dimethylfuran (**38**) from 2,5-hexadione (**13**).*

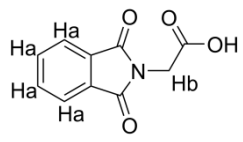
Entry	2,5-Hexadione (13)	Solid acid	Solvent
1	1.0 mL, 8.5 mmol, 1 eq.	Amberlyst 15 (2.7 g, 13 mmol, 1.5 eq.)	H_2O (20 mL)
2	1.0 mL, 8.5 mmol, 1 eq.	Amberlyst 15 (2.7 g, 13 mmol, 1.5 eq.)	toluene (20 mL)
3	100 µL, 0.85 mmol, 1 eq.	$NbOPO_4$ (2.0 g, 0.71 mmol, 0.89 eq.)	H_2O (5 mL)
4	100 µL, 0.85 mmol, 1 eq.	$NbOPO_4$ (2.0 g, 0.71 mmol, 0.89 eq.)	toluene (5 mL)
5	100 µL, 0.85 mmol, 1 eq.	$NbOPO_4$ (2.0 g, 0.71 mmol, 0.89 eq.)	THF (5 mL)

6.5 Synthesis of Phthalimido Acetate



The experimental procedure was adopted from Pintér *et al*.[27]

A mixture of phthalic anhydride (22.22 g, 150 mmol, 1 eq.), glycine (11.26 g, 150 mmol, 1 eq.) and trimethylamine (1.518 g, 15 mmol, 10 mol%) was stirred while being heated under reflux in toluene (90 mL). After completion, toluene was removed under reduced pressure. Subsequently, deionised water (100 mL) and concentrated hydrochloric acid (3 mL) were added to the mixture. The resulting white powder was filtered off and washed with copious amounts of water. After drying the product for 48 h at 80 °C, phthalimido acetic acid was obtained as a white solid in 89 % yield (27.42 g) and analysed by NMR (DMSO-d_6) and Mass (ESI) spectroscopy. ^{1}H NMR (400 MHz, DMSO-d_6): δ (ppm)



13.3 (*br* s, 1H, CO_2**H**), 7.97-7.87 (m, 4H, Ha), 4.32 (s, 2H, Hb). ^{13}C NMR (400 MHz, DMSO-d_6): δ (ppm) 168.9 (t, **C**O_2H), 167.2 (d, 2x PhtN **C**O), 134.8 (t, PhtN **C**H-3,4),

131.5 (t, PhtN **C**-1,6), 123.5 (t, PhtN **C**H-2,5), 38.7 (s, **C**H_2CO_2H). HRMS (ESI) m/z: 204.0302 calculated for $C_{10}H_6NO_4$, 160.0404 calculated for $C_9H_6NO_2$, found $[M-H]^+$ = 204.0300, $[M-CO_2OH-H]^+$ = 160.0401 (100 %).

Phthalimido acetic acid was reacted with 0.5 eq. of K_2CO_3 in water to form **24** prior to use as a photo absorber in UV photochemical reactions.

6.6 References

1. (a) Lee, C.; Yang, W.; Parr, R. G., *Phys. Rev. B.* **1988,** *37* (2), 785-789; (b) Becke, A. D., *J. Chem. Phys.* **1993,** *98* (7), 5648-5652; (c) Becke, A. D., *J. Chem. Phys.* **1993,** *98* (2), 1372-1377.
2. Walsh, P. J.; Gordon, K. C.; Officer, D. L.; Campbell, W. M., *J. Mol. Struc.-Theochem.* **2006,** *759* (1–3), 17-24.
3. Böes, E. S.; Livotto, P. R.; Stassen, H., *Chem. Phys.* **2006,** *331* (1), 142-158.
4. Bellamy, J. PhD Thesis. University of Nottingham, Nottingham, 2014.
5. Zou, Y.-Q.; Chen, J.-R.; Liu, X.-P.; Lu, L.-Q.; Davis, R. L.; Jørgensen, K. A.; Xiao, W.-J., *Angew. Chem.* **2012,** *124* (3), 808-812.
6. Anacor Pharmaceuticals, I.; Chen, D.; Orr, M.; Sligar, J.; Jacobs, R.; Plattner, J. J. WO2011/19618, 2011.
7. Durka, K.; Jarzembska, K. N.; Kamiński, R.; Luliński, S.; Serwatowski, J.; Woźniak, K., *Cryst. Growth Des.* **2013,** *13* (10), 4181-4185.
8. Chan, C.-C.; Chen, Y.-W.; Su, C.-S.; Lin, H.-P.; Lee, C.-F., *Eur. J. Org. Chem.* **2011,** *2011* (36), 7288-7293.
9. (a) Bourne, R. A.; Han, X.; Chapman, A. O.; Arrowsmith, N. J.; Kawanami, H.; Poliakoff, M.; George, M. W., *Chem. Commun.* **2008**, 4457-4459; (b) Han, X.; Bourne, R. A.; Poliakoff, M.; George, M. W., *Chem. Sci.* **2011,** *2* (6), 1059-1067; (c) Han, X. PhD Thesis, University of Nottingham, Nottingham, 2010.
10. Poliakoff, M.; Howdle, S. M.; Kazarian, S. G., *Angew. Chem. Int. Ed.* **1995,** *34* (12), 1275-1295.
11. Bourne, R. A.; Han, X.; Poliakoff, M.; George, M. W., *Angew. Chem. Int. Ed.* **2009,** *48* (29), 5322-5325.
12. DeLaney, E. N.; Lee, D. S.; Elliott, L. D.; Jin, J.; Booker-Milburn, K. I.; Poliakoff, M.; George, M. W., *Green Chem.* **2017,** *19* (6), 1431-1438.
13. (a) Nohr, R. S.; MacDonald, J. G.; Kogelschatz, U.; Mark, G.; Schuchmann, H. P.; von Sonntag, C., *J. Photoch. Photobio. A.* **1994,** *79* (1), 141-149; (b) Gustavsson, T.; Bányász, Á.; Lazzarotto, E.; Markovitsi, D.; Scalmani, G.; Frisch, M. J.; Barone, V.; Improta, R., *J. Am. Chem. Soc.* **2006,** *128* (2), 607-619; (c) Zhang, J. Y.; Boyd, I. W.; Esrom, H., *Appl. Surf. Sci.* **1997,** *109–110*, 482-486.

14. Bureekaew, S.; Hasegawa, J.-y.; Nakatsuji, H., *Chem. Phys. Lett.* **2006,** *425* (4–6), 367-371.

15. Kuhn, H. J.; Braslavsky, S. E.; Schmidt, R., *Pure Appl. Chem.* **2004,** *76* (12), 2105-2146.

16. Lehóczki, T.; Józsa, É.; Ősz, K., *J. Photoch. Photobio. A.* **2013,** *251*, 63-68.

17. Karlsson, B.; Ribbing, C. G., *J. Appl. Phys.* **1982,** *53* (9), 6340-6346.

18. Knies, C.; Hammerbacher, K.; Bonaterra, G. A.; Kinscherf, R.; Rosemeyer, H., *Chem. Biodivers.* **2016,** *13* (2), 160-180.

19. Gauglitz, G.; Hubig, S., *J. Photochem.* **1985,** *30* (2), 121-125.

20. Bandara, H. M. D.; Burdette, S. C., *Chem. Soc. Rev.* **2012,** *41* (5), 1809-1825.

21. (a) Gauglitz, G., *J. Photochem.* **1976,** *5* (1), 41-47; (b) Gauglitz, G.; Hubig, S., *J. Photochem.* **1981,** *15* (3), 255-257.

22. Roy, S. R.; Sau, S. C.; Mandal, S. K., *J. Org. Chem.* **2014,** *79* (19), 9150-9160.

23. Lemiègre, L. c.; Lesetre, F.; Combret, J.-C.; Maddaluno, J., *Tetrahedron* **2004,** *60* (2), 415-427.

24. Lee, H.; Kim, B. H., *Tetrahedron* **2013,** *69* (32), 6698-6708.

25. Cho, H.; Madden, R.; Nisanci, B.; Torok, B., *Green Chem.* **2015,** *17* (2), 1088-1099.

26. Xu, G.; Singh, M. P.; Gopal, D.; Sayre, L. M., *Chem. Res. Toxicol.* **2001,** *14* (3), 264-274.

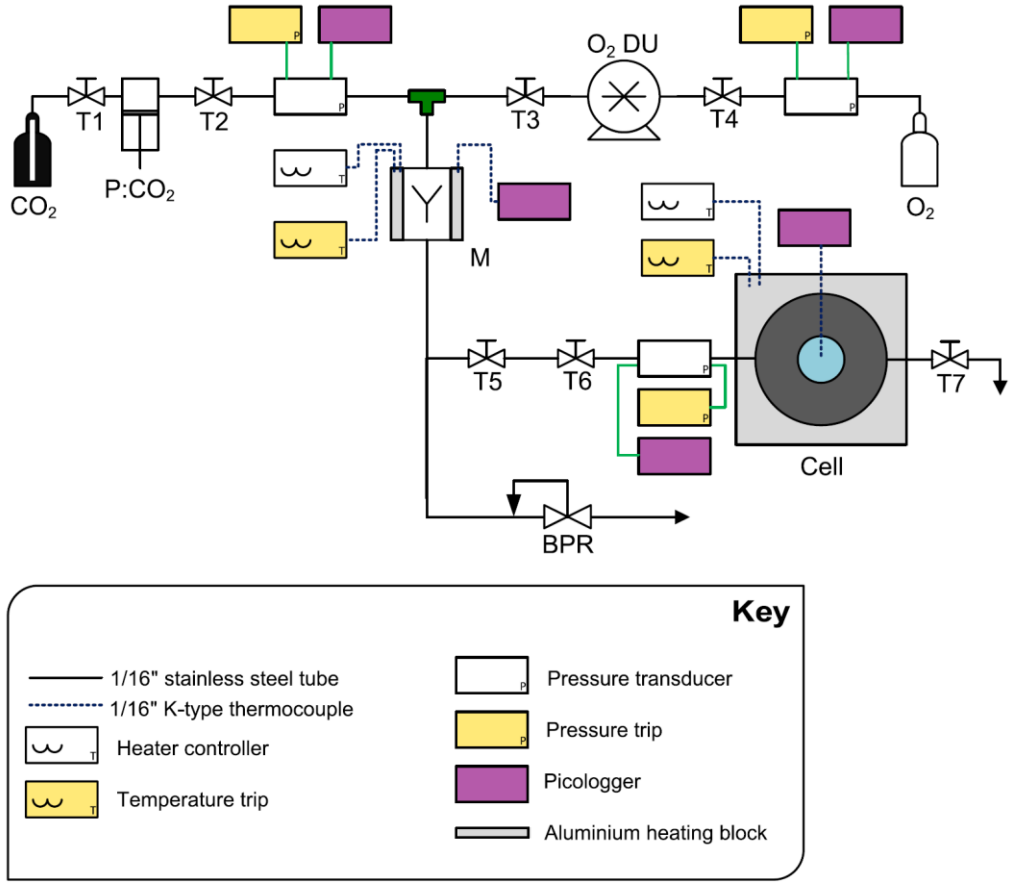
27. Pintér, Á.; Haberhauer, G.; Hyla-Kryspin, I.; Grimme, S., *Chem. Commun.* **2007,** (36), 3711-3713.

Chapter 7 Appendix

This Chapter provides details on the standard operating, standard shut-down and emergency shut-down procedures that need to be followed when using the different reactors employed for this work. Further details on the reactors used in the work presented in this Thesis can be found in Chapter 6.

7.1 Procedures of the Visible Light High-pressure Batch Reactor

The standard operating, standard shut-down and the emergency shut-down procedures are given below for the high-pressure visible light batch reactor. Details on the reactor itself are presented in Chapter 6.2.3.1. Extreme care must be taken when working with organic materials and oxygen in combination with elevated pressures and temperatures to minimise explosion risks.



Scheme 7-1 Representation of the batch photochemical reactor, adapted from the Thesis by J. Bellamy.[4] The labelling is as follows: CO_2 - delivered from a chilled Jasco™ PU-1580-CO_2 pump; O_2 – added via a Rheodyne dosage unit (DU); BPR - Jasco™ BP-1580-81 back pressure regulator; M - mixing chamber 15 cm 1/4" SS316 tubes at 50 °C, surrounded by an aluminium heating block; PT - pressure transducer (RDP Electronics); Cell- 5 mm path length (1.47 mL) with a LED block with 1 LED light; T1-7 - manual valve.

7.1.1 Standard Operating Procedure

- Ensure that all manual valves other than T1 and T4 are closed.
- Open the batch cell and carefully fill it with the required substrate, and photocatalyst. Close the cell tightly afterwards.
- If the addition of a co-solvent is required, remove the thermocouple from the batch cell and inject the co-solvent through this opening using a GC syringe. When finished, reattach the thermocouple to the top of the batch cell.

- Place the heating block around the batch cell and set the required temperature on the heater controller. A blast shield cover should be placed over this block.
- Set the desired temperature for mixing chamber M with the heater controller and allow the mixer to reach this temperature.
- Set the desired operating pressure at the BPR, start the CO_2 pump and open manual valve T2 to allow the system to reach pressure.
- Flush the system at the desired operating pressure with CO_2 for a minimum of 30 minutes.
- Test all the fittings in the reactor for leaks with Snoop® liquid leak detector.
- If leaks are found, reduce pressure to ambient (1 atm, 14 psi) and tighten the fitting.
- Confirm that the trip box is working and the pressure in the system is stable.
- Ensure that the pressure of oxygen in the cylinder is 20 bar greater than the operating pressure of the system.
- Set the switching rate of the Rheodyne® dosage unit and open T3.
- Continue to pump both the O_2 and CO_2 streams through the system for a minimum of 30 minutes.
- Partially open T5 followed by the very slow opening of T6. The gas mixture will now mix with the reagents in the batch cell. Monitor the pressure in the cell and ensure that this pressure increases by approximately 1 bar/s. Readjust T5 and T6 if the pressure increase is faster or slower than 1 bar/s.
- Once at the desired pressure, close T5 and T6 and monitor the pressure inside the batch cell to ensure that the pressure is maintained and no leaks are present.
- To start the photochemical reaction, remove the initial blast shield around the batch cell. Position the LED block in front of the window of the batch cell.
- Then turn the LED block on and place a large Lexan™ blast shields in front of the batch cell.
- While the photochemical reaction is taking place in the batch cell, the CO_2 and O_2 streams are no longer needed.

- Turn off the Rheodyne® dosage unit and the heater controller for mixing chamber M, and close T3 afterwards.
- Continue to pump CO_2 through the system for a minimum of 30 minutes to remove O_2 from the rig.
- After this time, turn off the CO_2 pump, close T2 and slowly depressurise the system by decreasing the set pressure value at the BPR.
- The batch cell can now be removed from the rest of the system by disconnecting the metal tubing from the inlet of T5 on the left-hand side.

7.1.2 Standard Shut-down Procedure

- Turn off the LED light.
- Depressurise the batch cell by opening T7 very slowly in order to prevent material leaving the cell through this outlet.

7.1.3 Emergency Shut-down Procedure

Press the red emergency shut-down button on the trip box. This will turn off power to the LEDs, the heaters and the oxygen dosage unit, while the pressure monitor and the BPR will remain on. The CO_2 pump will remain working as well to remove any oxygen from the system. If the system reaches the set pressure maximum, the CO_2 pump will switch off automatically.

7.1.4 Cleaning of the Reactor

The batch cell requires regular cleaning in order to prevent possible build-up of solid material. Typically isopropanol is used as the cleaning solvent. Note: do not use acetone as a cleaning solvent as acetone peroxides could be formed in the presence of oxygen.

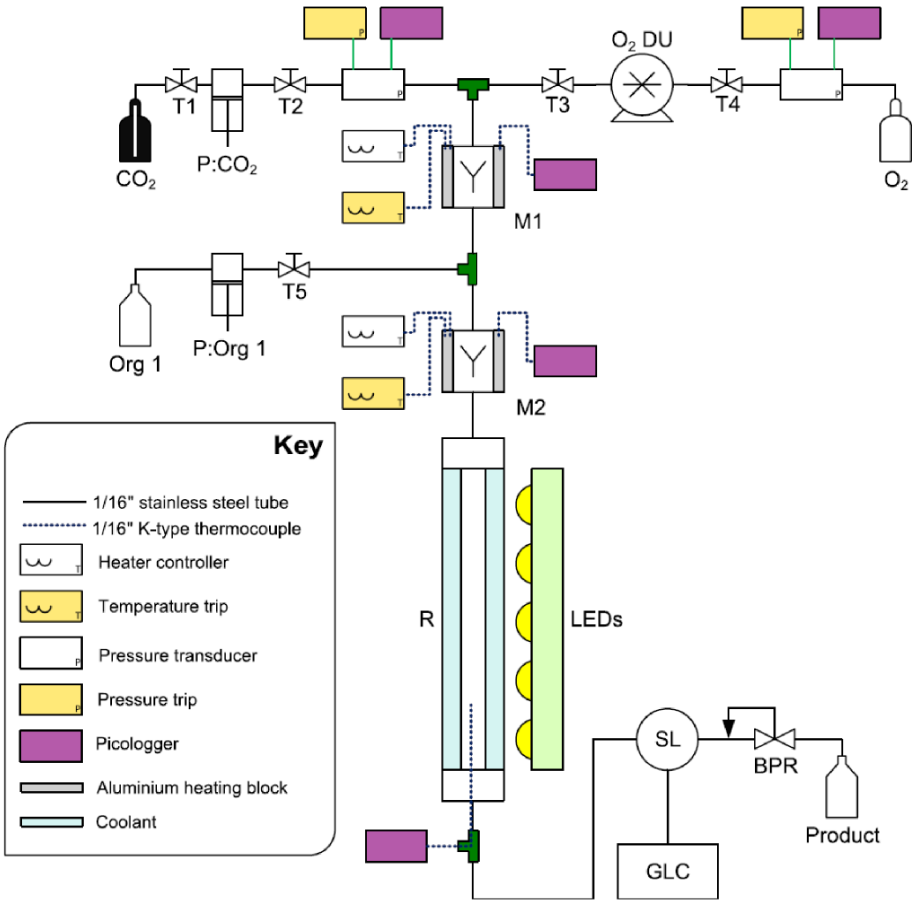
- Connect a HPLC pump to the batch cell at T5 and pump non-halogenated solvent (such as isopropanol) through the batch cell for a minimum of 30 minutes.
- Reconnect the batch cell to the original rig.
- Set the pressure at the BPR to 150 bar, start the CO_2 pump and open manual valve T2 to allow the system to reach pressure.
- Open T5-T7 and flush the system with CO_2 for a minimum of 30 minutes to eliminate any organic cleaning solvent from the system.
- Turn off the CO_2 pump, close T2 and slowly depressurise the system by decreasing the set pressure value at the BPR.

If this is not sufficient to clean the system:

- Clean the inside of the batch cell and the surrounding metal fittings with cotton sticks and isopropanol.

7.2 Procedures of the Visible Light High-pressure Flow Reactor

The standard operating, standard shut-down and emergency shut-down procedures are given below for visible light based photoreactions employing a flow reactor.



Scheme 7-2 Representation of the high-pressure continuous flow reactor, adapted from the Thesis by J. Bellamy.[4] The labelling is as follows: CO_2 - delivered from a chilled Jasco™ PU-1580-CO_2 pump; O_2 – added via a Rheodyne® dosage unit (DU); T1-5 - manual valve; BPR - Jasco™ BP-1580-81 back pressure regulator; M1/M2 - mixing chamber 15 cm 1/4" SS316 tubes at 50 °C, surrounded by an aluminium heating block; Org 1 - reaction mixture containing the photocatalyst, reductive quencher and substrate, dissolved in the required solvent system, which is pumped by P:Org 1 (Jasco™ PU-980 HPLC pump); R - sapphire tube reactor, which is temperature controlled via a recirculating water/ethylene glycol bath (1:1 v/v); LEDs - light source (3 × 5 × Citizen Electronics Co. Ltd CL-L233-C13N1-C mounted on water cooled stainless steel blocks); SL - high-pressure sample loop to allow for in-line GC sampling of the reaction mixture; GLC - Shimadzu GC-17A gas chromatograph

Reactions both with and without $scCO_2$ as a co-solvent were conducted. Reactions with solvents other than $scCO_2$ should follow the same procedure as outlined below, omitting the steps involving the heating of the mixing chambers and the CO_2 pump. Details on the reactors are presented in Chapter 6.2.3.2 and Chapter 6.2.3.3.

7.2.1 Standard Operating Procedure

- Ensure that all manual valves other than T1 and T4 are closed.
- Flush the reactor with isopropanol for at least 30 minutes at 5 mL/min for cleaning purposes.
- While checking for leaks using paper towel, increase the value on the back pressure regulator gradually until the required pressure is reached. Lexan™ blast shields should be in front of the sapphire tube reactor when the pressure is above ambient.
- If leaks are found, reduce pressure to ambient (1 atm, 14 psi) and tighten the leaking fitting.
- Confirm that the trip box is working and the pressure on the system is stable.
- Once at required pressure, check pump operation efficiency (at 1 mL/min) by recording the time taken to collect a volume of 10 mL of solvent from system outlet (>90 % efficiency required).
- Depressurise the system by reducing the set pressure on the BPR.
- Set the desired temperature for the mixing chambers M1 and M2 on the heater controllers.
- Flush the system with the solvent of the reaction for 20 minutes at 5 mL/min.
- Set the desired temperature at the recirculating bath for cooling the reactor and LEDs, start the recirculation and check for leakage in the reactor.
- Put the LED blocks around the sapphire tube reactor.
- Place Lexan™ blast shields in front of the sapphire tube reactor.
- Set the desired operating pressure at the BPR, start the CO_2 pump and open manual valve T2 to allow the system to reach pressure.
- Flush the system at the desired operating pressure with CO_2 for a minimum of 30 minutes.
- Ensure that the pressure of oxygen in the cylinder is 20 bar greater than the operating pressure of the system.
- Set the switching rate of the Rheodyne® dosage unit, start the oxygen dosing and open T3.

- Continue to pump both the O_2 and CO_2 streams through the system for a minimum of 30 minutes.
- Prepare the reagent mixture and connect this to the inlet of the organic pump.
- Set the organic pump to the required flow rate for the experiment and prime pump with required reagents.
- Start the organic pump and open T5 to combine the gas mixture with the organic mixture.
- Once liquid is observed at the end of the outlet tube after the BPR, turn the LED lights on to start the photochemical reaction.

7.2.2 Standard Shut-down Procedure

- Turn off the Rheodyne® dosage unit, the LEDs and the organic pump.
- Continue to pump CO_2 through the system for a minimum of 30 minutes to remove O_2 from the rig.
- Turn the CO_2 pump off and flush the system with isopropanol or the co-solvent using the organics pump at 5 mL/min for 45 minutes.
- Pump $scCO_2$ through the reactor at 1 mL/min, 180 bar and 40 °C to remove any solvent residues.
- Turn of the heating for M1 and M2.
- Once the temperature measured inside the reactor is below 25 °C, turn the recirculating bath off.
- With T2,T3,T5 and T6 closed, depressurise the system by slowly decreasing the set pressure on the BPR.
- In case the system will not be used for 12 hours, flush the system through with air to prevent oxidation of any metal rig parts.

7.2.3 Emergency Shut-down Procedure

Turn off the power switch on the trip box. This will turn off power to the LEDs, the heaters, the oxygen dosage unit and the organic pump, while the pressure

monitor, the recirculating bath and the BPR will remain on. The CO_2 pump will remain working as well to flush any organic material and oxygen from the system. If the system reaches the set pressure maximum, the CO_2 pump will switch off automatically.

7.2.4 Cleaning of the Reactor

The rig requires regular cleaning in order to prevent possible build-up of solid material. Typically isopropanol is used as a cleaning solvent. Note: do not use acetone as a cleaning solvent as acetone peroxides could be formed in the presence of oxygen.

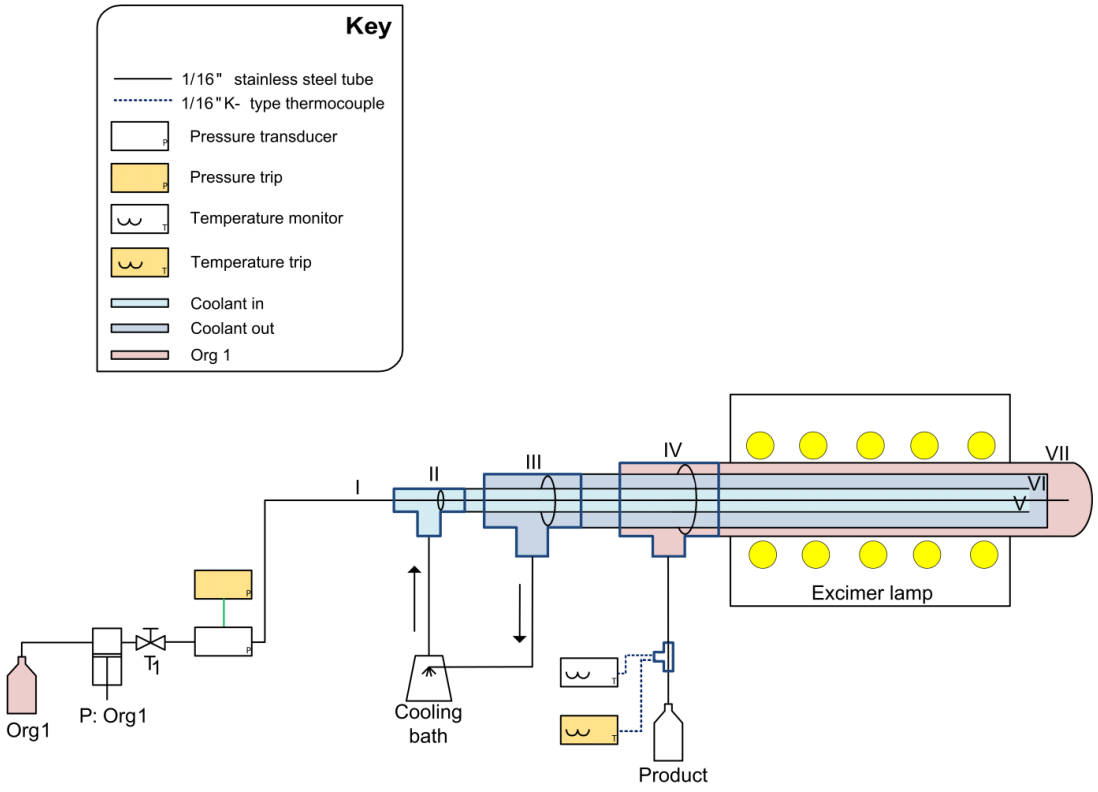
- Pump cleaning solution through system at 5-10 mL/min for at least 2 hours.

If this is not sufficient to clean the system:

- Take check valves out of pump head and sonicate them in isopropanol for 1 hour.
- Meanwhile: clean the other pump head parts with cotton sticks and isopropanol.
- Take reactor apart and clean the sapphire tube with isopropanol and clean connections. Replace O-rings if necessary (EPDM material).

7.3 Procedures of the UV Light Flow Reactor

The standard operating, standard shut-down and emergency shut-down procedures are given below for UV based photoreactions employing the reactor as described in Chapter 6.3.4. Care must be taken when working with ultraviolet light. The safety procedures detailed below must be strictly adhered to.



Scheme 7-3 Schematic of UV photochemistry rig; I) 1/16" stainless steel tubing; II) Swagelok™ T-piece, drilled through in house on left side opening; III) Swagelok™ T-piece, drilled through in-house on left side opening; IV) Bola GL 32 PTFE T-Piece; V) 1/4" stainless steel tubing; VI) 12 mm stainless steel tubing, welded closed at the bottom; VII) Quartz tube, sealed in-house; P: Org1 - Jasco™ PU-986 HPLC Pump; Cooling Bath - recirculating bath model Julabo® F32-HE, T1 - manual valve.

7.3.1 Standard Operating Procedure

- Ensure that the UV lamp is switched off at the lamp.
- Switch on the power to the system and reset the trip.
- Deoxygenate 250 mL of the solvent used in the photochemical reaction and pump this through the rig at a rate of at least 5.0 mL/min to clean the rig.
- At the same time, check all joints and fittings for leaks using paper towel.
- Prepare the reagent solution in an appropriate sized round bottom flask and deoxygenate by bubbling Argon through it for at least 10 minutes.
- Turn on the recirculating bath and set the desired temperature (Between -20 °C and 100 °C depending on the freezing and boiling point of the solvent). Allow the reactor to reach within 2 °C of the set temperature.
- Connect the deoxygenated reaction mixture to the organic pump inlet.
- Set the desired flow rate and start pump.
- Switch on the UV lamp using the power switch on the lamp box.
- Allow for equilibration time (typically 2 full system volumes).
- Take samples or collect reaction output, wearing gloves when the Lexan™ fume hood box is opened.

7.3.2 Standard Shut-down Procedure

- Stop the lamp and the organic pump using the emergency trip box.
- Set the lamp power switch to the off position.
- Turn the organic pump back on using the reset button.
- Pump 200 mL of clean solvent through the rig at a rate of 5.0 mL/min.
- Turn off the pump.
- Turn off the recirculating bath.
- Partially slide reactor outside of the lamp and check for fouling of the inner quartz surface. If it appears dirty proceed with the cleaning procedure.

7.3.3 Emergency Shut-down Procedure

Stop power to the UV lamp and organic pump by pressing the emergency stop button. Recirculating bath, temperature and pressure monitors will stay switched on. In the case of a solvent or coolant leak, all electronics should be switched off.

7.3.4 Cleaning of the Reactor and Changing Excimer Lamp

- With lamp pump and cooling bath off, unclamp the reactor.
- Carefully turn the turntable so that the end of the reactor is facing out of the fume cupboard.
- Carefully, completely slide the reactor out of the lamp and securely clamp vertically.
- Visually inspect for fouling.
- If necessary flush reactor with dimethyl sulfoxide (DMSO) at 5.0 mL/min until fouling is visibly removed. Then pump 200 mL of clean reaction solvent at a rate of at least 5.0 mL/min to remove DMSO from the system. Turn off the pump.
- If it is necessary carefully change the lamps, taking care that the lamp is replaced evenly on the turntable such that it does not fall.
- Slide the reactor back into the lamp. Reposition the turntable such that the fume cupboard can be closed. Clamp the reactor securely into position.

7.3.5 Safety

The excimer lamps are contained within a shrouding metal box. However, adequate protection against UV light should be taken. The University of Nottingham School of Chemistry standard operating procedures for the use of UV lamps for chemical reactions should be strictly adhered to. While the lamp is in operation, the Lexan™ fume-box doors should remain closed unless absolutely

necessary. Samples should be taken as quickly as possible and all skin must be covered by wearing gloves to ensure the minimum of exposure.